Sustainable Photochemical Approaches: Dual Iron-Photocatalysis and Transformations under Continuous Photo-Flow Conditions

Dissertation

Zur Erlangung des Doktorgrades der Naturwissenschaften

(Dr. rer. nat.)

An der Fakultät für Chemie und Pharmazie der Universität Regensburg

vorgelegt von

Viktor Klöpfer

aus

Chromtau, Kasachstan

Regensburg, Oktober 2025

Diese Arbeit wurde angeleitet von:		Prof. Dr. Oliver Reiser
Promotionsgesuch eingereicht am:		01.10.2025
Prüfungsausschuss:	Vorsitz:	Prof. Dr. Alkwin Slenczka
	1. Gutachter:	Prof. Dr. Oliver Reiser
	2. Gutachterin:	Prof. Dr. Julia Rehbein
	3. Gutachter:	Prof. Dr. Frank-Michael Matysik

Ort, Datum

Unterschrift Viktor Klöpfer

Der experimentelle Teil der vorliegenden Arbeit wurde in der Zeit von Juni 2021 bis Februar 2025 unter der Leitung von Herrn Prof. Dr. Oliver Reiser am Institut für Organische Chemie der Universität Regensburg angefertigt.

Mein besonderer Dank gilt Herrn Prof. Dr. Oliver Reiser für die Aufnahme in seinen Arbeitskreis, die Überlassung der interessanten Forschungsthemen, die anregenden Diskussionen und die stete Unterstützung.

Für meine liebende Familie und Klara…

„Wir sind gleichsam Zwerge, die auf den Schultern von Riesen sitzen, um mehr und Entfernteres als diese sehen zu können - freilich nicht dank eigener Sehkraft oder Körpergröße, sondern weil die Größe der Riesen uns zu Hilfe kommt und uns emporhebt.“

– Bernhard von Chartres

Danksagung

An dieser Stelle möchte ich mich zunächst bei all denjenigen bedanken, die mich im Laufe dieser Doktorarbeit begleitet und unterstützt haben:

Mein besonderer Dank gilt Herrn *Prof. Dr. Oliver Reiser* für die Aufnahme in seinen Arbeitskreis, das Vertrauen in meine Person, die hervorragenden Arbeitsbedingungen am Lehrstuhl und das Überlassen der interessanten Forschungsthemen. Ich bedanke mich für die gegebene Möglichkeit meine Arbeit im Rahmen eines Forschungsaufenthaltes auch am Indian Institute of Technology Indore, Indien voranzutreiben. Ich möchte mich auch besonders bei Frau *Prof. Dr. Julia Rehbein*, Herrn *Prof. Dr. Frank-Michael Matysik* und Herrn *Prof. Dr. Alkwin Slenczka* für die Bereitschaft den Prüfungsausschuss zu komplettieren und für die aufgebrachte Zeit bedanken.

Mein Dank gilt ebenfalls dem gesamten Arbeitskreis; insbesondere, *Andreas Ratzenböck* und *Sebastian Fischer* für den Bledschmatz im Labor und außerhalb, für die unzähligen Abende in der Stadt sowie die gemeinsame Zeit auf dem Fußballplatz, *Caro Nagel* für die Fürsorge, die Tennisstunden sowie den Einsatz als Ultra an jedem Fußballplatz in Regensburg; an der ein hervorragendes Mitglied des AK Reisers verloren ging; *Anurag Chinchole*, who was always up for a conversation and from whom I learned so much about chemistry, life and everything else; *Lea Minus Joy Großkopf* für ihren Namen und Ihr sowie *Manuel Kobras*, die die Aufgaben ihrer Vorgänger nahtlos übernahmen und das tägliche Leben im Labor durch viel Schwachsinn und Durst angenehmer machten. Bedanken möchte ich mich desweitern bei *all meinen Forschungs- und Bachelor-Studierenden*, die durch Ihre Arbeit mir eine große Hilfe im Labor waren und darüber hinaus zu guten Freunden geworden sind. Ganz besonders gilt dieser Dank *Ludwig Rüther*, *Leonie Roithmeier* und *Dominic Heilmann*.

Zuletzt will ich mich bei meinen Liebsten bedanken:

Meiner Freundin Klara, die mich seit der Bachelorarbeit begleitet und unterstützt – nicht nur während meiner Ausbildung, sondern in jeder Lebenssituation; die mich immer versteht, berät sowie ergänzt und die ich sehr schätze.

Meinem Bruder Kevin, der mir immer ein guter Gegenpol in vielen Situationen ist und der mich immer unterstützt.

Meinen Eltern, die für mich und meinem Bruder immer alles gegeben haben; die auch in schwierigen Situationen immer zuerst auf uns geachtet haben; bei denen man immer

gemerkt hat, dass sie stolz auf uns sind. Es ist nicht selbstverständlich, dass man auswandert, eine neue Sprache erlernt, sich in einem komplett neuen Umfeld wiederfindet und trotzdem den Kindern alles ermöglicht. Diese Doktorarbeit ist auch für euch. Ohne euch an meiner Seite hätte ich es nicht so weit schaffen können!

Table of Contents

List of Abbreviations

(V)LIH ..... (Visible) Light Induced Homolysis
ATRA..... Atom Transfer Radical Addition
BDE ..... Bond Dissociation Energy
BPR..... Back Pressure Regulator
C ..... Conversion
CF..... Continous Flow
DCA 9,10-Dicyanoanthracene
DMC ..... Dimethyl Carbonate
DoE ..... Design of Experiment
DPA 1,10-diphenylanthracene
EDG ..... Electron Donating Group
E_{Ox}..... Oxidation Potential
E_{Red}..... Reduction Potential
EWG ..... Electron Withdrawing Group
FCC ..... Face-Centered Central Composite
HAT ..... Hydrogen Atom Transfer
IL..... Light Intensity
iPr_2NEt ..... N,N-Diisopropylethylamine
k_{diff}..... Diffusion Rate Constant k
LED..... Light Emitting Diode
LMCT ..... Ligand-to-Metal Charge Transfer
L_{Me} ..... Ligand of Metal
MBH ..... Morita-Baylis-Hillman
MLCT ..... Metal-to-Ligand Charge Transfer
NIS ..... N-Iodosuccinimide
OFAT ..... One-Factor-at-a-Time
P ..... Productivity
PASAM..... *p*-Toluene Sulfonamide
Q ..... Flow Rate
S ..... Selectivity
SBLCT ..... σ-Bond-to-Ligand Charge Transfer
SCE ..... Standard Calomel Electrode
SET ..... Single Electron Transfer
T ..... Temperature
TBACl..... Tetrabutylammonium chloride
TEMPO ..... (2,2,6,6-Tetramethylpiperidin-1-yl)oxyl
TFA ..... 2,2,2-Triflouroacetic acid
TFF..... Two-Level Full Factorial
TOF ..... Turnover Frequency
t_R ..... Residence Time
TRIP 2,4,6-Triisopropylphenyl
UV..... Ultraviolet
VIS ..... Visible Light
Y ..... Yield

Chapter 1 - Introduction

1 Dual Catalytic Approaches in Sustainable Iron Photocatalysis

1.1 Transition Metal Photocatalysis & Modern Challenges

In all sectors of life, including chemistry, modern society is confronted with the issues of unsustainable processes harming the environment and contributing to global warming. Besides other principles of green chemistry, contemporary organic transformations that form carbon-carbon and carbon-heteroatom bonds depend on catalysts to increase sustainability effectively.[1] Furthermore, transition metal catalysis has proven to be an essential methodology for organic chemists, resulting in various Nobel-Prize-winning transformations, including palladium-catalyzed cross-coupling reactions, ruthenium-catalyzed metathesis, and others.[2]

Moreover, over the past three decades, ruthenium and iridium complexes have emerged as the photoredox catalysts of choice due to their efficiency in catalyzing reactions.[3,4] In the context of bimolecular, outer-sphere electron transfer between a photocatalyst and a substrate, key features of efficient photoredox catalysis include matching redox potentials, high extinction coefficient ε, and sufficiently long excited-state lifetimes in the microsecond range – adequate for diffusion through the solvent ($k_{diff} \sim 10^{10}$ M^{-1} s^{-1}) prior to encountering a ground state quencher.[3,5–8] However, despite their prevalent use, these 4d and 5d transition metals are among the rarest elements on Earth (Figure 1-1)[9], leading to diminishing economic and ecological efficiency of the photochemical processes involving iridium and ruthenium, respectively. In contrast, organic dyes offer a more affordable alternative in photochemical transformations, they often exhibit limited photostability.[10-13]

Additionally, earth-abundant 3d transition metal and lanthanide complexes present a more sustainable option (Figure 1-1)[9], but their ultrashort excited-state lifetimes in the nanosecond to picosecond range[14] render them unsuitable for catalyzing bimolecular, diffusion-controlled organic reactions by photo-initiated single electron transfer (SET)[5], although notable exceptions exist[15]. Ligand-to-metal charge transfer (LMCT) processes provide an alternative mechanistic approach to address this issue. By means of LMCT, an

electron is transferred from a filled orbital located on the ligand to an empty orbital on the metal center of a metal-ligand complex in an inner-sphere mechanism.[5]

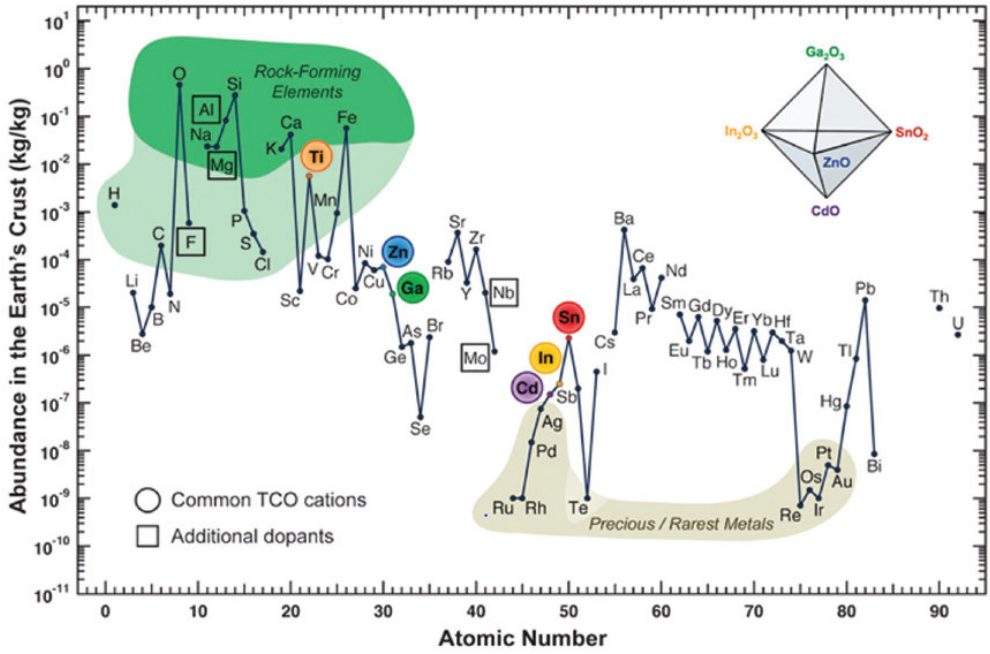

Figure 1-1. Abundance (atom fraction) of the chemical elements in Earth's upper continental crust as a function of atomic number. (Figure adapted from Ref. [9], © Creative Commons, public domain)

In this sense, two fundamental criteria need to be fulfilled: i) an easily accessible, low-energy empty d* orbital of the metal center, as observed typically in 3d transition metals such as Ni^{II}, Cu^{II}, Fe^{III}, and Ti^{IV}, and ii) σ or σ+π donating, electron-rich ligands to act as an internal source of electrons. Usually, (pseudo-)halide, alkoxide, or carboxylate groups as ligands have been observed to exhibit LMCT transition states. Upon light irradiation, the electron density increases on the antibonding orbital (d*/dσ*) of the metal center at the expense of the bonding orbital of the ligand (p/π). This electron density redistribution reduces the bond order of the metal-ligand bond, facilitating its homolytic bond cleavage and finally the generation of chemically reactive radicals. Consequently, the radical precursor functions as the substrate, and as a result, ultra-short, excited-state lifetimes and diffusion limitations become irrelevant as the substrate is directly coordinated to the metal center (Scheme 1-1,a).[5]

Interestingly, while a bimolecular outer-sphere electron transfer between a catalyst and a substrate requires a negative Gibbs free energy ΔG to be feasible, inner-sphere electron transfer – as observed in LMCT processes – does not depend on matching redox potentials.[5] This enables radical generation from substrates with high oxidation

potentials (E_{ox}), even with metal catalysts with low reduction potentials (E_{red}), regardless of the Gibbs free energy DG (Scheme 1-1,b).[16] The implementation of this strategy enhances the viability of using 3d transition metals or lanthanides in photocatalytic organic reactions, thereby benefiting both economic and ecological aspects.[5,17] As a result, 3d transition metal photocatalysis moved into focus for developing sustainable methods in organic chemistry.[5]

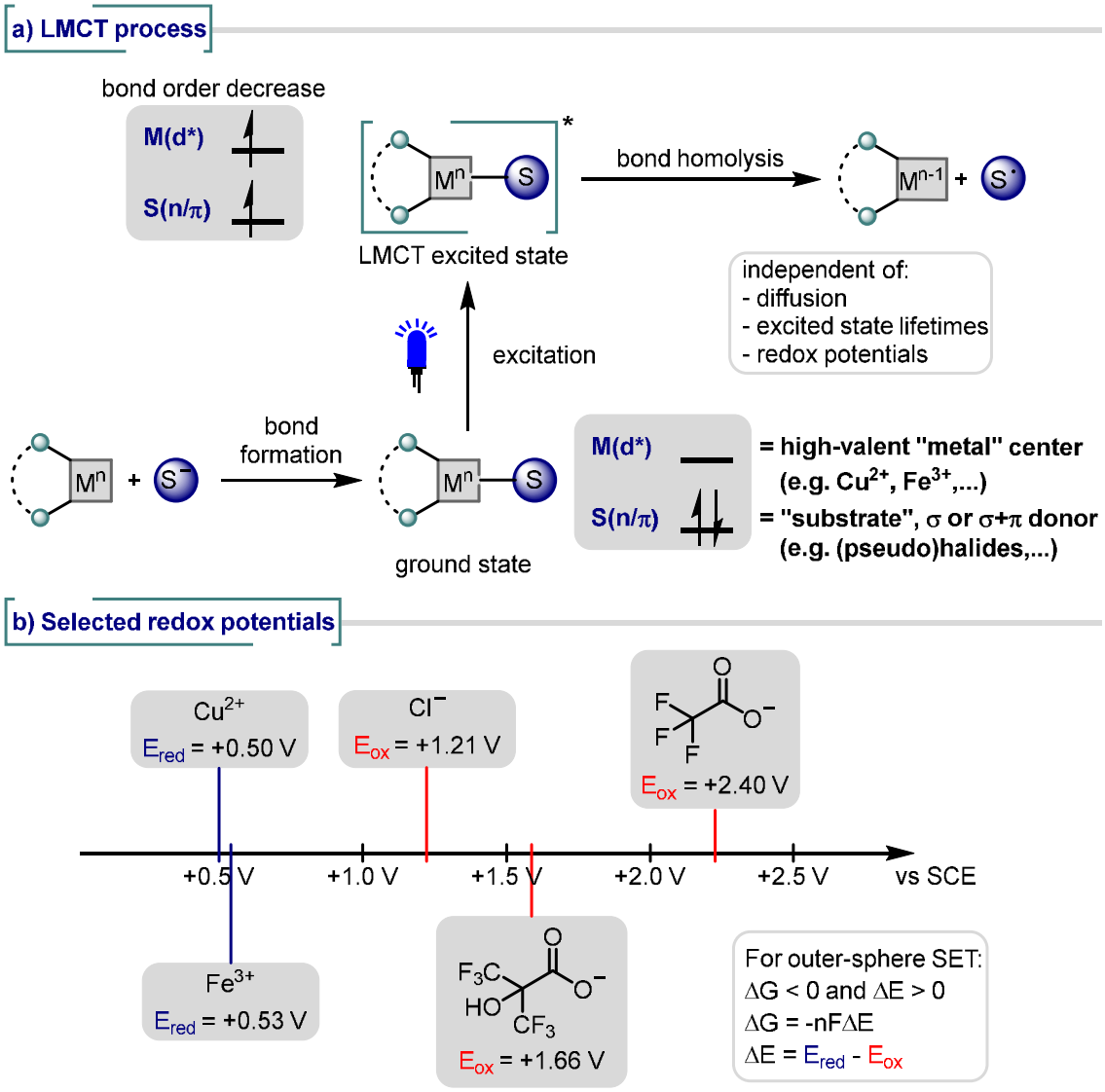

Scheme 1-1. a) Insights of LMCT processes in accordance with *Julia's* publication[5] and b) selected redox potentials vs saturated calomel electrode (SCE)[16,24–26] as illustration why outer-sphere SET processes are not feasible with 3d transition metals like Cu or Fe.

Notably, not all LMCT processes lead to homolysis[18,19] and there are also other charge transfer steps leading to bond dissociation of the ligand-metal bond, e.g., metal-to-ligand charge transfer (MLCT)[20] or σ-bond-to-ligand charge transfer (SBLCT).[21–23] However,

the present chapter will focus on LMCT-initiated homolysis utilizing sustainable metal complexes as photocatalysts.

1.2 Fe^{III} Dual Catalytic Strategies in Photoinitiated LMCT Processes of Earth-Abundant Transition Metals

Recently, first-row transition metals and lanthanides have proven to be sustainable photocatalysts in organic chemistry, developing various reaction types.[17] This chapter comprehensively summarizes the literature on redox-neutral, dual catalytic strategies involving iron photocatalysis, wherein light-mediated LMCT induces homolytic bond cleavage.

In the late 1960s, Imoto *et al*. first reported the photooxidation of organic molecules – 1,2-glycols, ethers, and toluene – using $FeCl_3$.[27–29] Although the mechanism of the transformation was not provided and most likely not known at this period, it marked the initial report on chlorine radical photogeneration from iron salts *via* LMCT in organic chemistry. Subsequent studies on the photooxidative functionalization of organic compounds driven by the formation of chlorine radicals from iron salts were carried out more systematically, clarifying the mechanistic steps of this approach.[30–37] In the late 20th century, Sugimori and coworkers published their procedure on the decarboxylative alkylation of 4-methylquinoline.[38] The proposed mechanism is based on the production of carboxyl radicals by the preceding formation of a Fe^{III}-OOCR complex and its (visible) light-induced homolysis ((V)LIH). These preliminary efforts subsequently facilitated the development of modern iron photolysis strategies.

This field of research has recently experienced a resurgence, accompanied by substantial advancements following the publications by Rovis[39,40] and Duan[25] in 2021. While contemporary work often relies on stoichiometric amounts of external oxidants[41–43] or oxygen[44,45] to complete the catalytic cycle of Fe^{III}/Fe^{II}, or on stoichiometric amounts of iron salts[46], dual catalytic approaches promise sustainability and novel synthetic routes, albeit less explored.[5,24,47] Consequently, this chapter aims to summarize dual catalytic strategies in iron photocatalysis based on LMCT-involved mechanistic steps. The literature will be organized according to the types of radicals generated by the LMCT of Fe^{III} complexes.

Alkoxy radical formation by (V)LIH of iron(III) complexes

Alkoxy radicals can be generated either directly or through prefunctionalization. These O-centered radicals are capable of undergoing various reactions, notably β-scission, hydrogen atom transfer (HAT) reactions, and addition to other moieties.[17] However, the direct formation of alkoxy radicals from hydroxy groups is challenging due to the relatively high bond dissociation energy (BDE) of O–H bonds (~105 kcal/mol) compared to that of C–H bonds (< 100 kcal/mol), leading to selectivity issues.[48,49]

While iron-catalyzed alkoxy radical formation has been reported *via* hydrogen atom transfer (HAT) with chlorine radicals (see more details below)[49], Amgoune *et al.* excluded, based on mechanistic investigations, the formation of chlorine radicals by LMCT in their procedure.[50] Instead, they identified Fe-alkoxide complex **5** as LMCT-active species in their trial photocatalytic cross-coupling of alcohols **2** with aryl halides **1** (Scheme 1-2). Notably, the in situ formed iron complex **5** remained active even in the absence of chloride ions in the reaction solution. The group enabled the reaction by synergistic iron LMCT and nickel catalysis, both in combination with an appropriate ligand (L_{Fe} and L_{Ni}), using 1,10-diphenylanthracene (DPA) as an electron shuttle between the metal catalysts. For iron catalysis, a benzoate-based, sterically demanding ligand was utilized to significantly enhance the reaction, likely due to increased stability of the Fe^{III} complexes **4-6**, improved protection of low-valent iron species from degradation to Fe^0, and better interaction of the metal center with the alcohol substrate. Conversely, the nickel ligand had a less pronounced effect on the reaction outcome.

The researchers proposed the following mechanism: First, the excited DPA oxidizes $Fe^{II}(L_{Fe})_n$ **6** to the corresponding Fe^{III} complex **4**. Upon complexation of the metal catalyst **4** with the alcohol **2** and formation of the LMCT active complex **5**, light irradiation cleaves the Fe^{III}–O bond, releasing the alkoxy radical **11** and regenerating the Fe^{II} catalyst **6**. The electrophilic radical **11** undergoes *β*-scission, forming the nucleophilic C-centered radical **12**.[51] Simultaneously, oxidative addition of the aryl bromide **1** to the $Ni^I(L_{Ni})X$ complex **7** leads to the formation of **8**, which is reduced by the DPA radical anion – previously formed by the oxidation of iron – to the Ni^{II}-species **8**. Trapping of the radical **12** generates the Ni^{III} complex **9**, which subsequently undergoes reductive elimination to form the desired product **3**, thus closing the nickel catalytic cycle by regeneration of Ni^I catalyst **7**.

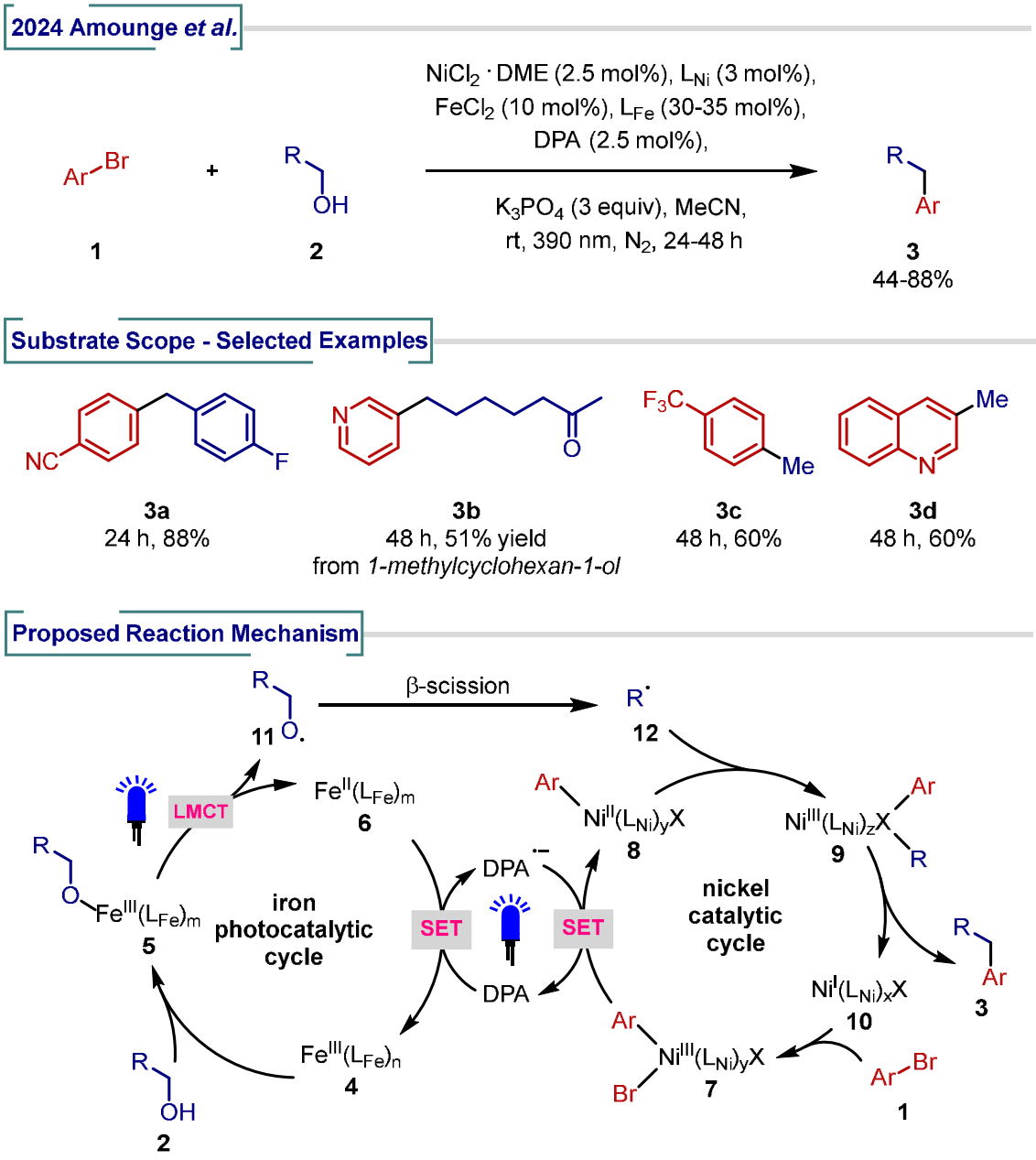

Scheme 1-2. Trial ironphotocatalyzed cross-coupling of alcohols **2** with aryl halides **1** using nickel and DPA as co-catalysts reported by Amgounge *et al.*

The cross-coupling reaction worked with moderate to excellent yield, including i) dehydroxymethylative arylation of aliphatic alcohols **2** to synthesize products of the type of **3a**, ii) ring-opening arylation of cyclic, tertiary alcohols **2** to yield alkyl ketones like **3b**, and iii) methylation of aryl halides **1** using tertiary alcohols **2** as methyl radical precursors to obtain **3c** and **3d**, representatively. The Amgoune group observed high tolerance for electron-poor and electron-rich aryl bromides **1** – including biologically relevant heteroaryl bromides **1** – and for sensitive moieties, such as –BPin or –SO_2Me groups in all three types of reactions. However, in the case of the dehydroxymethylative

arylation, alkoxy radical precursors **2,** forming radicals **12** of low stability, resulted in diminished yields. Additionally, no desired product was obtained with tertiary alkyl radicals as a well-known limitation of nickel/photoredox catalysis[52].

Carboxyl radical formation by (V)LIH of iron(III) complexes

Another class of O-centered radicals can be generated by LMCT active metal complex containing carboxylate ligands as substrates. (V)LIH leads to the formation of carboxyl radicals, which have been documented in the photocatalysis research of Cu^{II}, Ce^{IV}, and Fe^{III} salts.[5,53] Likewise alkoxy radicals, carboxyl radicals participate in various types of reactions. While the occurrence of additions to unsaturated bonds[53] and HAT reactions[54] depends on carboxyl radicals, which decarboxylate slowly, the most prominent reaction is the facile fragmentation of the carboxyl radical to CO_2 and alkyl radicals. An increase in entropy drives this process. In iron dual-photocatalyzed systems, this transformation represents the exclusive reactivity of carboxyl radical intermediates.[5]

In 2022, the Xia group reported a decarboxylative ring-opening strategy for tertiary, cyclic carboxylic acids **13,** enabled by mono catalytic iron LMCT under oxygen, obtaining 1,*n*-dicarbonyl compounds (Scheme 1-3).[44] The group identified the formation of an alkyl radical **19** upon decarboxylation of the corresponding carboxyl radical **18** as a key step in their transformation. While the reaction resulted in ring-opened products under oxygen, the group additionally envisioned capturing the carbon-centered radical intermediate with Co^{II}. By using established cobaloxime-catalysis[55] under N_2-atmosphere, the researchers obtained unsaturated products *via* the following postulated, dual catalytic mechanistic pathway:

Initially, the ligand exchange on the $Fe(acac)_3$ **15** with the deprotonated substrate **13** forms the Fe^{III} carboxylate **16**, which is identified as the productive, LMCT-active species. Light irradiation at 390 nm induces (V)LIH, resulting in $Fe(acac)_2$ **17** and carboxyl radical **18**. Subsequent decarboxylation provides nucleophilic, alkyl radical intermediate **19,**[51] which is trapped by the present cobaloxime-catalyst (Co^{II}) **20** – a persistent 17-electron metalloradical[56]. β-H elimination facilitates the generation of the desired decarboxylated, unsaturated product **14** and Co^{III} catalyst **23**. Finally, both metal catalysis cycles were closed by the redox reaction of the Co^{III}–H **23** and $Fe(acac)_2$ **17,** forming the original

metal species. Notably, there is an ongoing debate about the herein postulated *β*-H elimination step[57–59]:

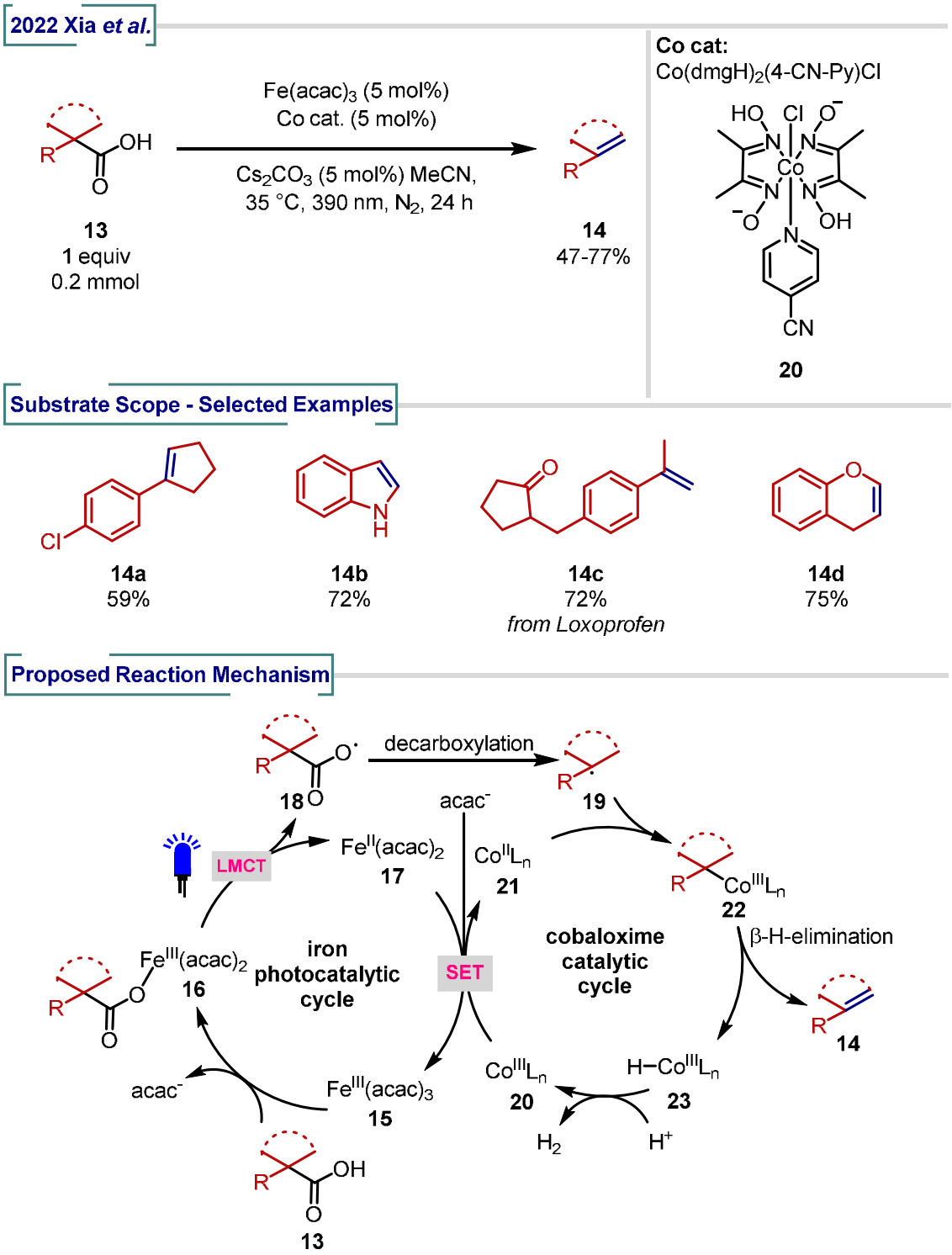

Scheme 1-3. Decarboxylative desaturation enabled by synergistic cobaloxime and photoinduced iron LMCT catalysis, as published by the Xia group.

The precise mechanistic pathway leading to the formation of the unsaturated product remains uncertain. It is yet to be determined whether the transformation proceeds *via* a

concerted β-hydride elimination mechanism or involves a second homolytic cleavage of the Co^{III}–C bond, initiated by a LMCT process. In the latter scenario, LMCT would generate an electrophilic and persistent Co^{II} radical species, which could facilitate a subsequent HAT from the β-sp^3 C–H bond of the alkyl radical intermediate (BDE < 30 kcal mol^{-1}), thereby affording the desired product **14**.[60] Nonetheless, both mechanistic pathways result the formation of the unsaturated product **14** along with a Co(III)–H species **23**.

The reaction yielded moderate to good results for eight cyclic carboxylic acids **13**. Interestingly, while the alternative mono catalytic ring-opening reaction under oxygen (described above) was successful only with tertiary carboxylic acids **13**, the formation of unsaturated products **14** using the reported dual catalytic approach also succeeded with secondary, cyclic alkyl radical precursors **13** (e.g. product **14b-d**).

Numerous articles on the dual catalytic application of iron salts in synergism with a HAT catalyst, in particular 2,4,6-triisopropylphenyl thiol (TRIP or its dimer TRIP disulfide), were published between 2023 and 2025.[16,26,61–63] In this context, West and coworkers have introduced two dual catalytic procedures: decarboxylative protonation[61] and decarboxylative hydrofluoroalkylation[16].

Fragmentating protonation of carboxyl radicals has been extensively studied in the past, for instance by Nicewicz *et al.* using Fukuzumi catalyst[64], but revealed certain limitations concerning the substrate scope. Their underlying outer-sphere mechanism-based approach presupposes strong oxidative photocatalysis, in which aryl carboxylic acids with electron-rich arene groups are unsuitable as the key radical intermediate is not formed due to oxidation of the aromatic moiety. The same applies to electron-rich olefin moieties and non-electron-poor amines present in carboxylic acids. West and collaborators overcame this issue by implementing an inner-sphere mechanism *via* LMCT of Fe^{III}-carboxylate complexes **28**, combined with TRIP disulfide as HAT catalyst (Scheme 1-4). The reaction yielded moderate to excellent results with primary, secondary, and tertiary carboxylic acids **24**, as well as electron-rich arenes and olefins containing various functionalities, e.g. halides (representative product **25a**) and alkynes (representative product **25b**). Additionally, late-stage functionalization of pharmaceuticals and natural products was successfully achieved under small-scale and gram-scale conditions, e.g. product **25c-d**).[61]

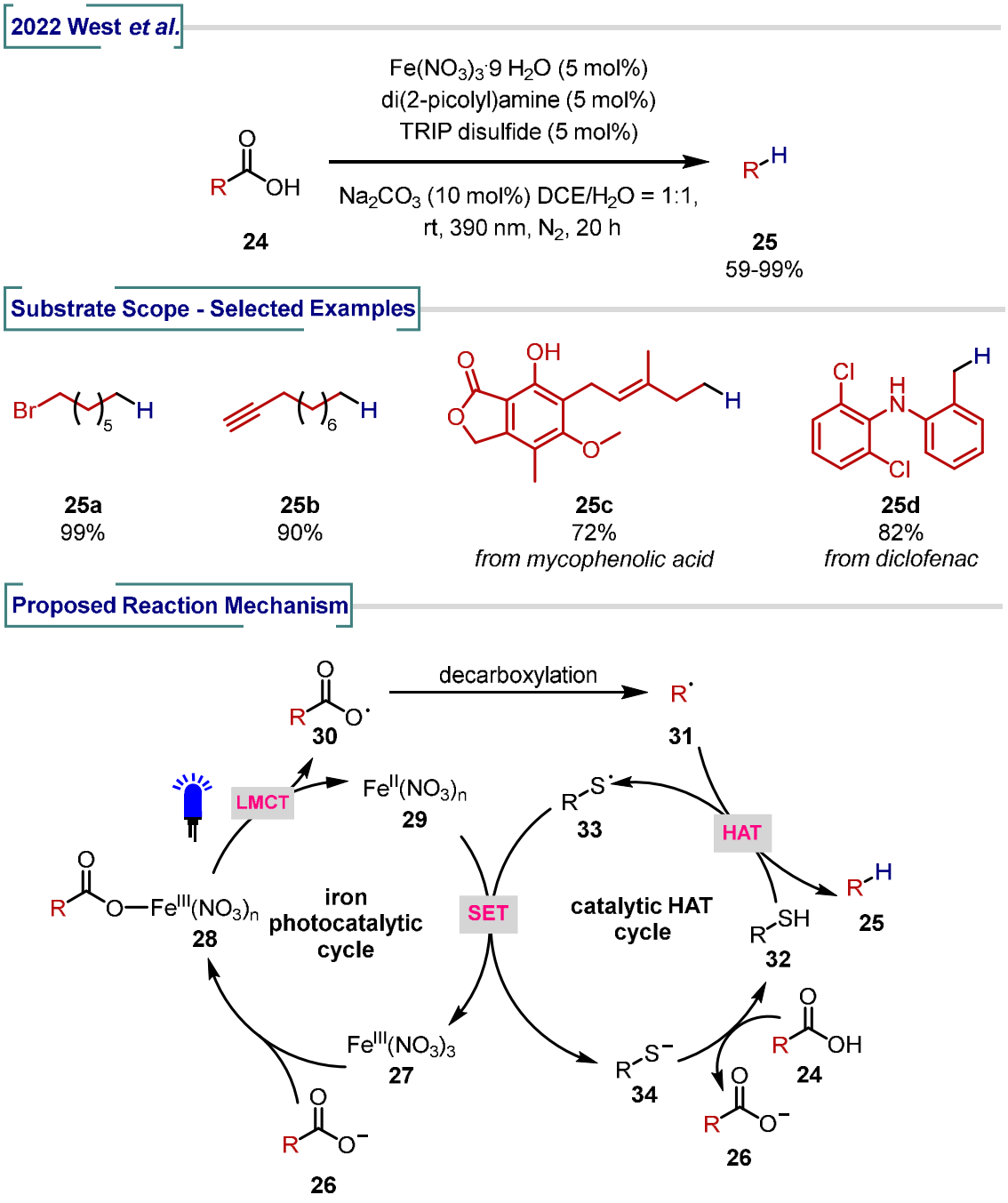

Scheme 1-4. Decarboxylative protonation of carboxylic acids **24,** utilizing iron LMCT catalysis synergistically with HAT catalysis; published by the West group.

The mechanism involves the formation of substrate-metal complex **28** between the deprotonated carboxylic acid **26** and the Fe^{III}-di(2-pinolyl)amine complex **27** through ligand exchange. Upon irradiation with LEDs at 390 nm, (V)LIH occurs, forming the Fe^{II}-species **29** and the corresponding carboxylic radical **30**. This radical **30** rapidly undergoes decarboxylation to produce the nucleophilic C-centered radical intermediate **31**,[51] which participates in a HAT reaction with catalyst **32**, leading to the

formation of the desired product **25** and thionyl radical **33**. SET from complex **29** to the S-centered radical **34** completes both catalytic cycles.

At the same time, the group also reported the decarboxylative hydroflouroalkylation of alkenes **36** with s similar dual catalytic approach, utilizing fluorinated carboxylic acids **35** as radical precursors.[16] Again, West *et al*. successfully overcame the issues associated with alternative outer-sphere SET strategies: Due to its extremely high E_{Ox} (> +2.24 V vs. SCE[65]), the direct CF_3 radical generation from 2,2,2-triflouroacetic acid (TFA, **35a**) remained highly challenging. It limits the scope of outer-sphere SET-based transformations, as numerous organic functional groups undergo oxidation at such forcing potentials.[66] In contrast, the formation of an LMCT active iron-TFA complex **39** and subsequent (V)LIH appeared to be an attractive alternative route, circumventing the high oxidation potential of TFA (**35a**) (see Figure 1-1,b).

The group successfully achieved hydrotrifluoromethylation, -difluoromethyl-ation, -monofluoromethylation, and -(polyfluoro)alkylation of alkenes **36** through LMCT of the corresponding iron complexes **39**. The reactive fluorinated radicals **42** were generated upon homolytic cleavage of the Fe–O bond (Scheme 1-5). The reaction proceeded with moderate to very good yields and tolerated oxidatively labile moieties, including sulfides and alcohols, offering a notable advantage compared to previous protocols relying on outer-sphere SET. The study highlights a highly group-tolerant fluorination reaction, offering substantial interest in synthesizing pharmaceutical compounds and late-stage functionalization.

Analogously to their decarboxylative protonation (Scheme 1-4), West and coworkers postulate the formation of complex **39**, which, upon exposure to UV-light, undergoes homolytic bond cleavage, resulting in an Fe^{II} complex **40** and the initial carboxyl radical **41**. Rapid decarboxylation leads to CO_2-extrusion and the formation of fluoroalkyl radical **42**. The latter adds to olefine **36,** and the resulting radical intermediate **43** reacts with the co-catalyst thiophenol **32** to form the desired product **37** and the corresponding thionyl radical **33**. **33** oxidizes the Fe^{II} complex **40** to conclude both cycles after protonation of the thiolate **34** ($Fe^{2+} \rightarrow Fe^{3+}$, E_{ox} = –0.53 V vs SCE and $RS^{\bullet} \rightarrow RS^{-}$, E_{Red} = +0.16 V vs SCE[67]). Concurrently, Xia and coworkers published a similar approach for the difluoromethylation of alkenes using $Fe(acac)_3$ as LMCT catalyst and TRIP as synergistic HAT catalyst, proposing a similar mechanism.[62]

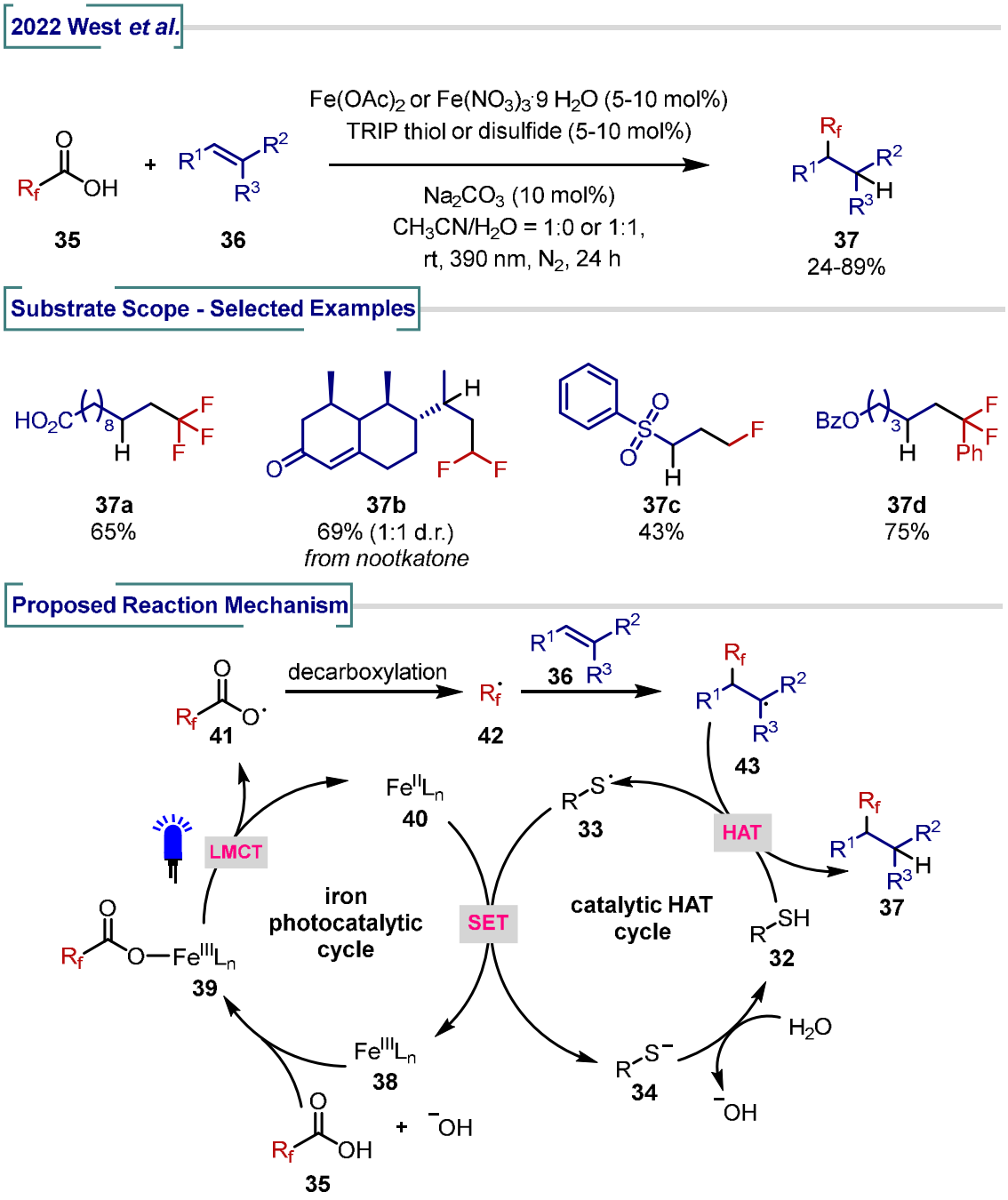

Scheme 1-5. Dual catalyzed iron LMCT enabled hydrofluoroalkylation of alkenes **36** with carboxylic acids **35** as reported by West *et al.*

In addition, Weix and Ackerman-Biegasiewicz *et al.* successfully achieved the dual-catalytic cross-coupling of decarboxylated carboxylic acids **43** with aryl halides **44** through the synergistic action of iron and nickel catalysis (Scheme 1-6).[68] This contrasts with the cross-coupling of alcohols with aryl bromides by the Amgoune group[50], which was dependent on the effective electron-shifting capability of DPA as an additional third catalyst (see Scheme 1-2).

Under optimized conditions, the reaction tolerated both electron-poor and electron-rich aryl halides **44**, including those that are typically challenging in outer-sphere metallophotoredox approaches, with good selectivity for the C–I bond over C–Br, C–Cl, and C–OTf. Notably, in the absence of any C–I bond, the reaction also proceeds selectively with C–Br. Heterocyclic iodides **44** also reacted smoothly, yielding the desired products **45** with yields up to 73% (e.g. **45b**). In contrast, vinyl iodides, alkyl iodides, and benzyl iodides were not tolerated under the reported reaction conditions. For carboxylic acids **43**, α- and β-heteroatom containing as well as benzylic carboxylic acids performed efficiently, obtaining the coupling product **45** in good to very good yields (e.g. **45a-c**). However, the standard reaction conditions could not be extended generally to unactivated carboxylic acids **43**. Changing the base to *i*Pr$_2$NEt or adding a ligand for the iron catalyst **46** furnished cross-coupled products **45** in up to 68% yield (e.g. **45d**). The conditions were also applied to tertiary amine group bearing carboxylic acids **43**, which are susceptible to oxidation by photocatalysis, resulting in the corresponding coupling product **45** with a yield of 40%. Driven by the huge functional group tolerance, the researchers also performed the derivatization of more complex compounds successfully. However, activation of sp^2-carboxylic acids remained challenging.

The group postulated a synergic Fe^{II}/Fe^{III}-$Ni^{I}/Ni^{II}/Ni^{III}$ catalytic mechanism: Ligand exchange on the Fe^{III} catalyst precursor **46** leads to the formation of species **47**, which – upon irradiation – subsequently fragmentates to the carboxylic radical intermediate **53** and Fe^{II} **48**. Facile decarboxylation of **53** results in C-centered radical **54**, which is trapped by the Ni^{I} species **52** present in solution, forming the Ni^{II}-alkyl intermediate **49**. By oxidizing Fe^{II} complex **48** and thus completing the iron catalytic cycle, the Ni^{II} complex **49** is reduced to **50**. A sequence of oxidative addition of the aryl halide **44** to generate **51** and reductive elimination leads to the release of the desired product **45** and closure of the nickel catalytic cycle.

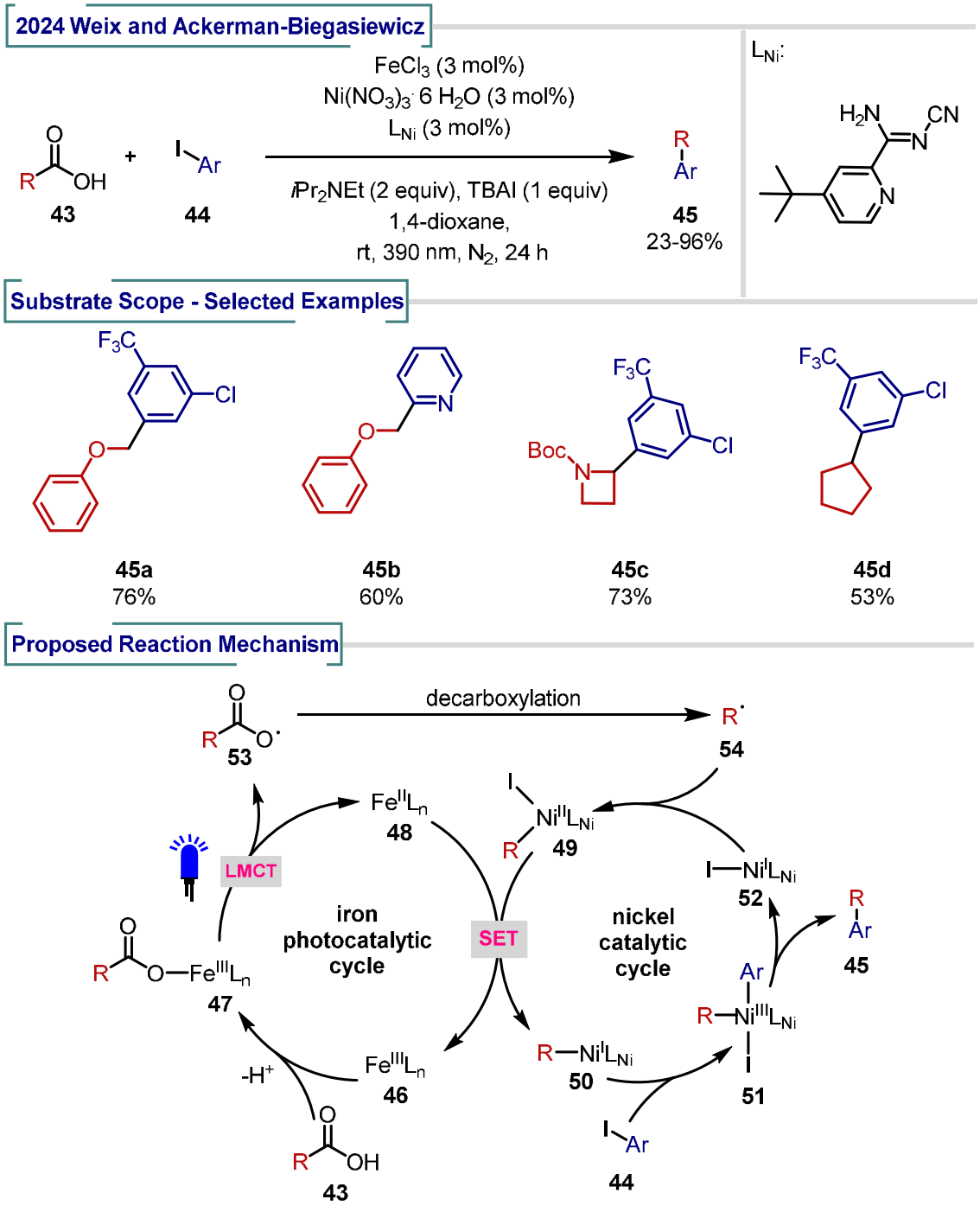

Scheme 1-6. Decarboxylative cross-coupling utilizing iron and nickel in a dual catalytic approach synergistically – published by Weix and Ackerman-Biegasiewicz *et al*.

In 2024, the Xu group developed a dual catalytic method for decarboxylative hydro(bistrifluoromethyl)carbinolation of alkenes **56** realized by the synergistic use of $Fe(OTf)_3$ and the dimer of 2,6-dimethylthiophenol **32** (Scheme 1-7).[26] Motivated by pharmaceutical relevance of bis(trifluoromethyl)carbinolation mimicking *tert*-butylalcohol or carboxylic acids[69,70], the group successfully addressed the issues arising with previously reported approaches – such as the use of toxic hexafluoroacetone,

substrate-based regioselectivity or synthetic inefficiency as for the incorporation of trifluoromethylated ketones prior to nucleophilic attack of CF_3^- – by implementing a process based on LMCT.[71–76] Herein, the iron-catalyzed, LMCT-based strategy circumvents again the challenge of outer-sphere oxidation surrendered by the relatively high oxidative potential of deprotonated **55** (1.66 V vs SCE[26]).

The reaction provided the corresponding bis(trifluoromethyl)carbinols of various differently substituted styrene **56a**, pyridines **56b** and **56d**, as well as Michael Acceptors **56c**. Notably, electron-rich and electron-neutral styrenes **56** worked smoothly but failed in other radical bis(trifluoromethyl)carbinolations.[74–78] While the reaction tolerated a broad scope of functional groups like ferrocene, thioethers, and halides, the conversion of internal or unactivated alkenes proved to be challenging with this approach, most likely due to poor electrophilicity or steric hindrance. In addition, the researchers envisioned expanding the substrate scope for other alkyl trifluoromethylcarbinols **55** by replacing one CF_3-group with a CH_3-group and hydrogen, respectively, resulting in the desired products with yields of 43-72%, e.g. **57d**. Notably, copper salts didn't perform under otherwise identical conditions, although they are known to catalyze decarboxylations analogously.[5]

Based on investigations, Xu *et al.* described the following mechanism: Upon deprotonation of **55** and ligand exchange on the metal center, complex **60** was formed. Irradiation leads to excitation, charge transfer from the ligand to the metal, and homolytic bond cleavage, resulting in Fe^{II}-species **61** and carboxyl radical **62**. Fragmentation of the radical **62** forms the C-centered radical **63** and extrudes CO_2. After addition of radical **63** to alkene **56**, a consecutive HAT reaction with thiophenol catalyst **32** provides the desired product **57** and thionyl radical **33**, which concludes both catalytic cycles by redox reaction with **61**.

Akondi *et al.* have reported a dual catalytic strategy for the decarboxylative alkylation of Morita–Baylis–Hillman (MBH) acetates **66**, introducing a $Fe(OTf)_2$/2,4,6-collidine dual catalytic system (Scheme 1-8).[79]

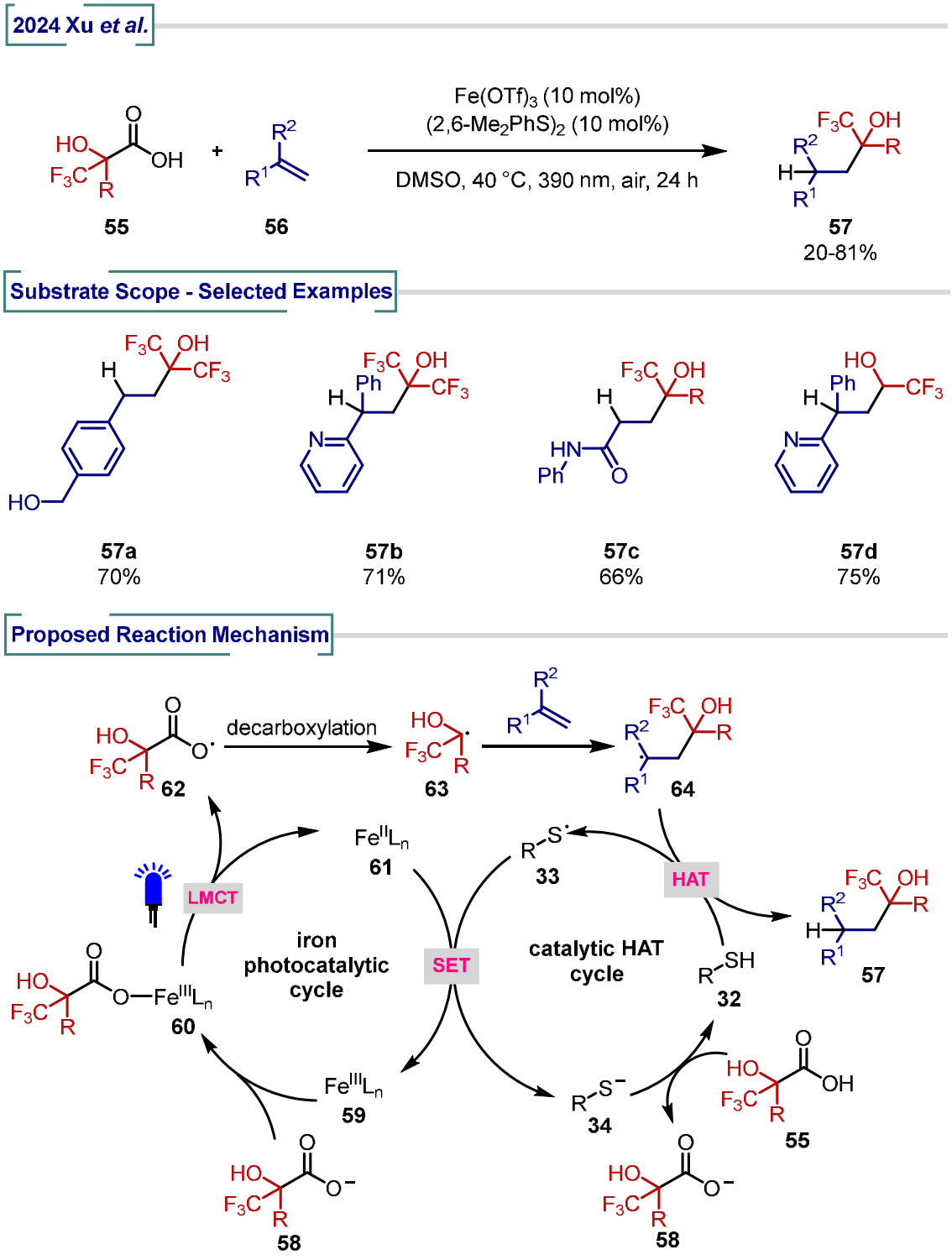

Scheme 1-7. Dual catalyzed, Fe-LMCT enabled synthesis of alkyl bis(trifluoromethyl)carbinols **57** by Xu *et al.*

The group obtained complex trisubstituted olefines **67** from easily synthesized MBH acetates **66** and readily available carboxylic acids **65** in a redox-neutral process using biodegradable dimethyl carbonate as solvent. The reaction produced various substituted cinnamates **67**, tolerating electron-withdrawing and electron-donating substituents on the

benzene ring and heteroaromatic analogs, with yields ranging from 26% to 93%. Additionally, MHB acetates **66** derived from aliphatic aldehydes and MHB acetates **66** containing different substituted esters gave the desired products in good yields. Other MHB acceptors **66** bearing a ketone, nitrile, and sulfone group (e.g. product **67b**), respectively, also performed smoothly. Additionally, the alkylation was conducted with various carboxylic acids **65**, obtaining the desired products **67** from 3^0-, 2^0-, or more challenging 1^0-alkyl[80] carboxylic acids **65** and tolerating functionalities like ethers, protected amines (e.g. **67c**), and fluorinated substituents. In contrast to the report of West *et al.*[16], the reaction didn't succeed using TFA (**35a**) as radical precursor. Notably, the *E*-isomer was formed predominantly with all substrates, except for MBH nitrile (*E:Z* = 1:10) and MBH acetates with a *para*-NO_2 substitution on the benzyl group (*E:Z* = 1:1), respectively.

The following mechanism was postulated by the researchers: After formation of allyl ammonium salt **73** by reaction of MBH acceptor **66** and 2,4,6-collidine (**72**), SET between salt **73** and Fe^{II} complex **71** results in the generation of iron(III) salt **69**, allylic radical **74** and the release of 2,4,6-collidine (**72**). Complexation of deprotonated carboxylic acid **65** with **72** and subsequent excitation leads to LMCT and homolytic bond cleavage, providing carboxyl radical **75** and regenerating Fe^{II} salt **71**. The radical **75** undergoes decarboxylation, forming the alkyl radical intermediate **76**. Finally, radical-radical combination leads to the formation of the desired product **67**.

The Vederas group conducted a study comparing decarboxylative, radical alkylation of Seebach-Beckwith dehydroalanine towards optically pure unnatural amino acids using iron, nickel, iridium, and eosin Y, respectively, as catalysts.[63] While the method with iron is based on an inner-sphere oxidation of the substrate *via* LMCT in combination with sterically demanding thiophenol as co-catalyst, the other catalysts rely on a mono-catalytic, outer-sphere oxidation mechanism. After optimization of the iron-catalyzed reaction, the group concluded that their Ir-photocatalyzed protocol was the most advantageous system for resonance-stabilized radicals in a head-to-head comparison. However, in cases of 3^0-alkyl carboxylic acids as radical precursor, the dual catalytic iron/thiophenol system performed efficiently and with very good yields, offering a promising alternative to more expensive, unsustainable Ir-catalysis. In contrast, iron catalysis performed poorly with 2^0- or 1^0-alkyl radical precursors under the reported conditions. However, Eosin Y and Ni complex, respectively, outperformed the iridium

catalytic system in this transformation, but both strategies rely on external reductants, and organophotocatalysts are known to decompose under prolonged irradiation times.[10–13]

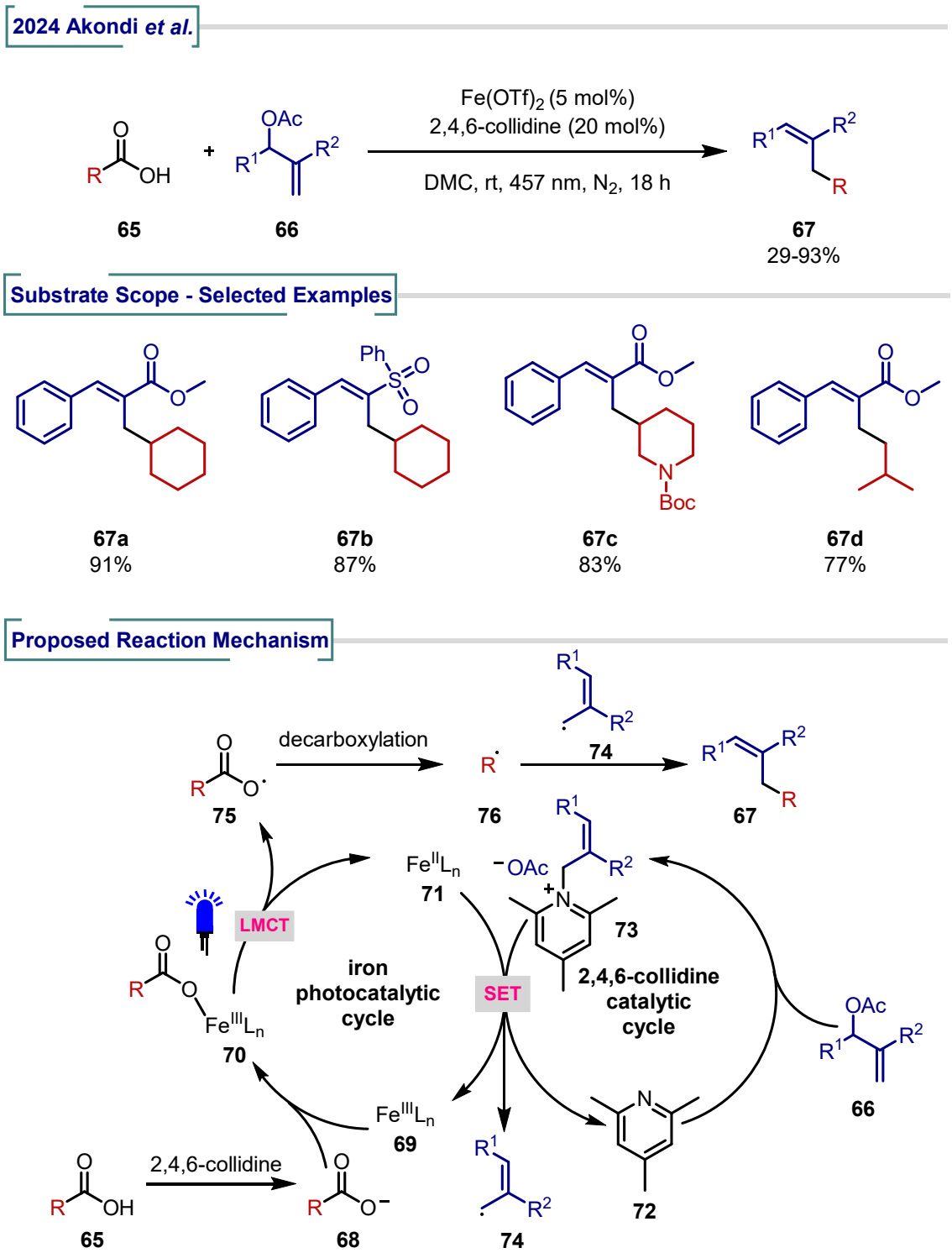

Scheme 1-8. Alkylation of Morita-Baylis-Hillman acetates **66** *via* decarboxylation initiated by VLIH in a dual catalytic fashion using both $Fe(OTf)_2$ **71** and 2,4,6-collidine (**72**) as catalysts, published by Akondi *et al.*

Chlorine radical formation by (V)LIH of iron(III) complexes

As noted earlier, the photochemical generation of chlorine radicals from iron chloride salts has been known since the 1960s[27–29] and has also been observed with other earth-abundant metal salts, such as copper[81] and nickel[82]. These radicals are characterized by high reactivity but at the same time low selectivity, e.g. in HAT reactions. Despite their common use – either for addition to sp^2-carbon atoms or for direct HAT – their utilization in dual catalytic approaches based on iron complex LMCT remains relatively unexplored.[5]

The Hu group developed a photocatalytic iron-catalyzed procedure for C-C bond cleavage of alcohols **77**.[49] Herein, chlorine radicals **82** lead to the generation of alkoxy radicals **83** that in turn triggers *ß*-scission (Scheme 1-9). Under blue light irradiation and in the presence of 2,4,6-collidine **72**, the researchers successfully transformed primary, secondary, and tertiary alcohols. Notably, the reaction was performed with both strained cyclic and unstrained alcohols **77**, achieving moderate to good yields while tolerating various functional groups such as halides, (thio-)ethers, and carbamates. It was also conducted for late-stage functionalization of natural products.

Mechanistic investigations provided the following insights: UV-VIS spectra of the reactants and reagents in various combinations were measured, displaying the typical $[FeCl_4]^-$ **79** absorption peak when tetrabutylammonium chloride and iron salt were present in the solution.[39,83] The peak decreases after prolonged irradiation, suggesting an LMCT process forming chlorine radicals and $[FeCl_3]^-$ **81** and ruling out Fe-alkoxy species formation under these conditions. Considering the selectivity issues associated with chlorine radicals **82** and the high BDE energies of O–H bonds, the transformation's selectivity must be derived from elsewhere. Therefore, a series of experiments were conducted as a competition study between toluene and 1-adamantanylmethanol. Although the benzylic C-H bond of toluene exhibits a lower BDE and is more likely to undergo a HAT reaction than the O-H bond of the 1-adamantanylmethanol, the conversion of toluene was progressively suppressed with increasing amounts of the alcohol present in the solution.[48,49] Therefore, the authors assumed the formation of a radical adduct involving chlorine radicals **82**, collidine **72**, and the hydroxy group. Consequently, the chlorine radical **82** selectively abstracts the hydrogen atom from the OH-group. This observation aligns with the study of Schelter *et al.*, which reported similar results with $CeCl_3$ photocatalysis.[84]

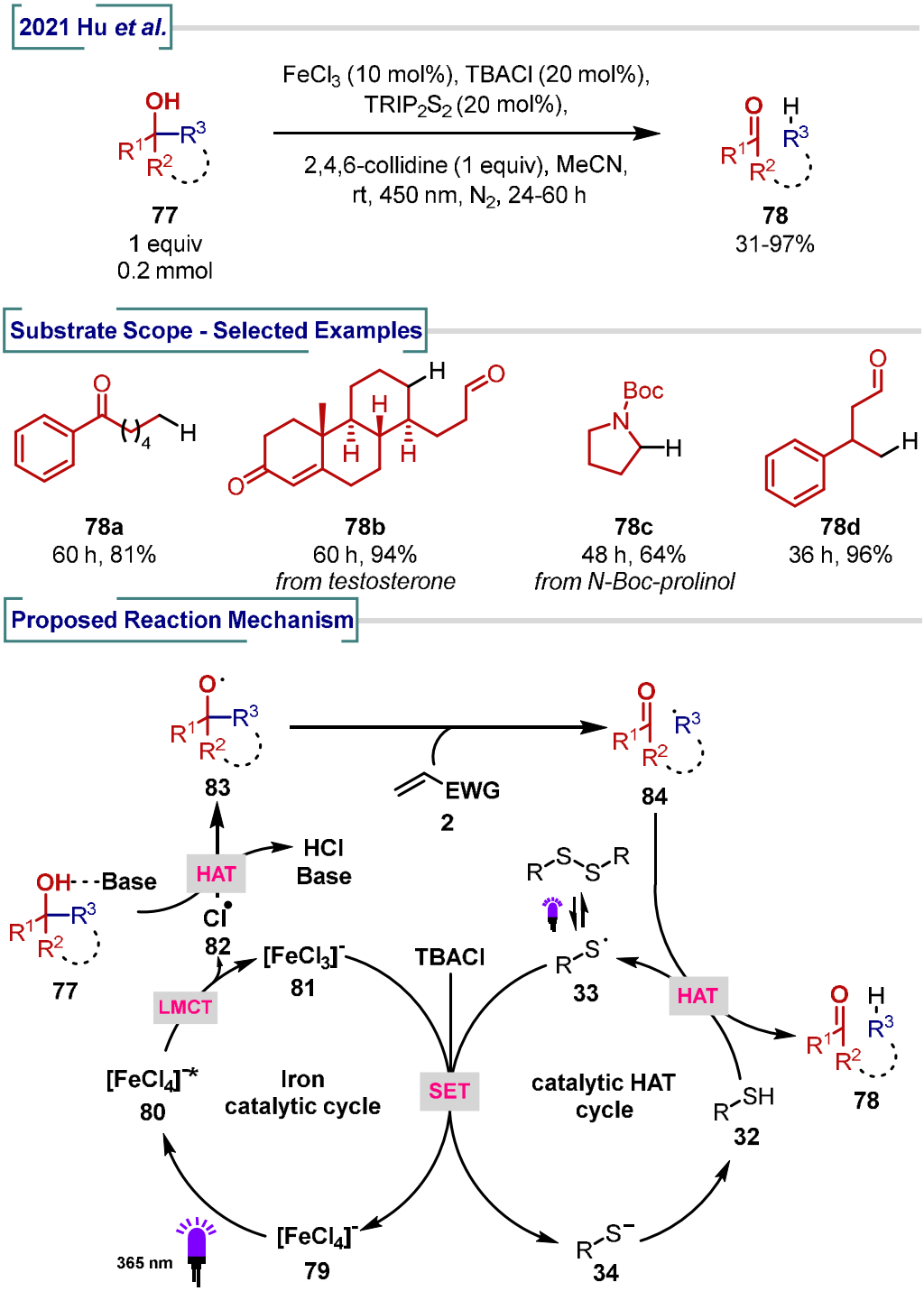

Scheme 1-9. Carbon-Carbon single bond cleavage enabled by dual catalytic use of $FeCl_3$ and $TRIP_2S_2$ reported by the Hu group.

The mechanistic proposal of the Hu group is based on the formation of the photoactive complex $[FeCl_4]^-$ **79** and its (V)LIH upon irradiation with blue light (450 nm), resulting in initial chlorine radical **82** and the corresponding Fe^{II} species **81**. After adduct formation of the chlorine radical **82**, 2,4,6-collidine **72,** and the substrate **77**, the halide radical **82** abstracts the hydrogen atom of the OH-group, leading to alkoxy radical **83**, which

subsequently undergoes *β*-scission. The newly formed, C-centered radical intermediate **84** undergoes a second HAT step from the HAT catalyst **32** present – TRIP disulfide – forming S-centered radical **33**. Redox reaction of thionyl radical **33** and iron(II) complex **81** concludes the iron and the HAT catalyst cycle, resulting in a dual catalytic process.

In 2022, Reiser *et al*. realized a photochemical, iron dual catalytic approach for hydroacylation of Michael acceptors **86** utilizing DPA as co-photocatalyst (Scheme 1-10).[85] As postulated by the group, the di-photonic transformation is based on the (V)LIH of a Fe^{III}–Cl bond upon irradiation with 365 nm at 30 °C. First, the formation of $[FeCl_4]^-$ **79** occurs in situ when iron(III) chloride, tetrabutylammonium chloride, $MgCl_2$, and HCl are combined. Irradiation with UV light leads to the homolytic cleavage of the metal halide bond, generating chlorine radicals **82** and Fe^{II} complex **81**. The catalytic cycle is closed by oxidation with excited-state DPA, forming the original Fe^{III} catalyst **79** and the radical anion of DPA. The chlorine radical **82** abstracts the carbonyl hydrogen atom of **85** to form HCl and acyl radical **88**. Nucleophilic in character, the acyl radical subsequently adds to electron-poor double bonds, forming radical intermediate **89**. Due to its position, α to the electron withdrawing group (EWG), the radical **89** undergoes reduction with the radical anion of DPA, which results in the closure of the catalytic cycle of DPA. Subsequent protonation yields the formation of the desired product **87**.

The reaction proceeded smoothly with yields ranging from 32% to 94% and tolerated several groups as substitution on the arene moiety of the acyl radical precursor **85**, including ortho substitution, halides, methoxy-, and cyano-groups. Regarding the alkene scope, the yields ranged from 30% to 83%. Most interestingly, the reaction also tolerated free carboxylic acid groups (e.g. product **87c**), which are known to be able to coordinate with iron to form a LMCT active species, too.[16,61,62,68,86] Furthermore, styrene and its derivatives were not feasible as radical-trapping partners, possibly due to chlorine radical **82** addition to the double bond[87].

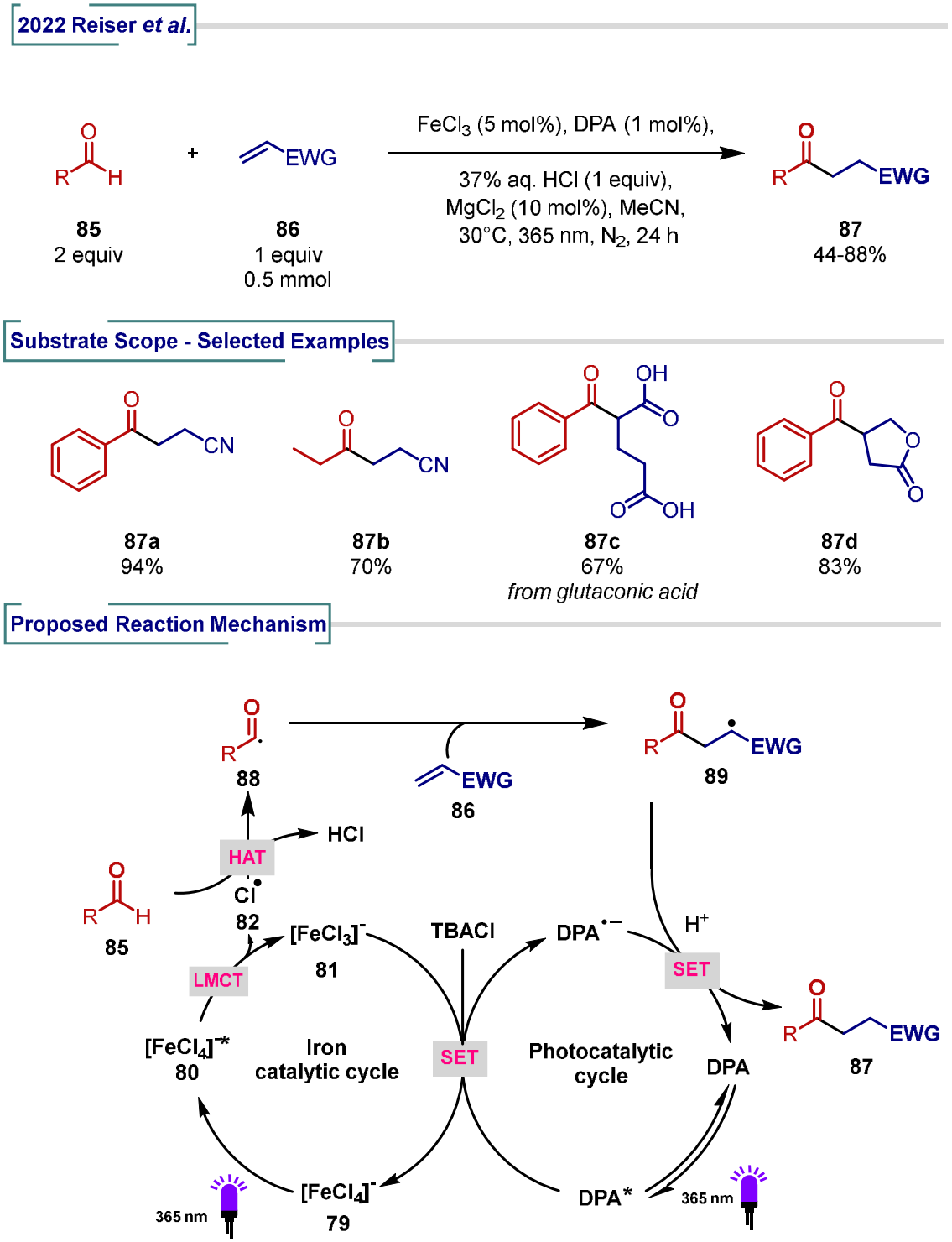

Scheme 1-10. Hydroacylation of Michel-acceptors **86** utilizing light-induced homolysis in a dual photocatalytic approach using Fe^{III} and DPA synergistically – published by Reiser and coworkers.

Contrary to the reports mentioned previously, in which the generated chlorine radical **82** performs a HAT reaction, West and coworkers achieved chlorine radical addition to numerous unsaturated C-C bonds using a dual catalytic approach relying on the formation

of an iron(III) based LMCT-active catalyst in conjunction with HAT catalysis (Scheme 1-11).[87]

Hereby, their LMCT-based, anti-Markovnikov hydro- and deuterochlorination addressed the issues of alternative direct, outer-sphere SET-based hydrochlorinations of C-C double bonds reported by Nicewicz[88,89] and Ritter[90], respectively. In particular, the acridinium-catalyzed anti-Markovnikov hydrochlorination reported by the Nicewicz group relies on the oxidation of styrene-type activated alkenes, forming a radical cation intermediate. However, the conversion of unactivated alkenes was unsuccessful due to their very high redox potentials (~2.8 V versus SCE[87]) and faced low regioselectivity with electron-rich aromatic alkenes as the arene moiety was oxidized rather than the alkene functionality. In addition, the method reported by the Ritter group was incompatible with tri- and 1,1-disubstituted cyclic alkenes, respectively, resulting in rearrangement or Markovnikov products as well as acid-sensitive functional groups weren't tolerated due to the use of HCl. By introducing a combination of iron(III) nitrate nonahydrate and TMSCl as catalytic system, forming the LMCT active species **93**, and thiophenol **32** as HAT catalyst, the West group was able to overcome these problems resulting in the formation of the desired anti-Markovnikov products **91** of activated, unactivated, electron-rich aromatic, tri- and 1,1-disubstituted as well as acid-sensitive groups bearing alkenes **90**. Furthermore, West *et al.* were able to convert alkynes **90** to the corresponding hydrochlorinated alkenes **91c** in good Z-selectivity. Notably, by substitution of H_2O by D_2O, the group was also able to obtain the corresponding deuterochlorinated products **91**. Interestingly, by performing the catalytic transformation with alkynes **90** in two consecutive steps under altered conditions – using either H_2O or D_2O as co-solvent – the group was able to generate vicinal dichlorides **91d** and isotopologues, respectively.

Based on mechanistic investigations, the researchers postulate the following mechanism: First, the catalytic species **93** is formed by combining aqueous $Fe(NO_3)_3$ **92** and TMSCl. Upon light irradiation, the excited catalyst undergoes LMCT, forming chlorine radical **82** and Fe^{II} complex **94**. Subsequently, radical **82** adds to the unsaturated C-C bond, resulting in a C-centered radical intermediate **95**, which abstracts a hydrogen atom from the HAT catalyst **32**, forming a thionyl radical **33** and the desired product **91**. Finally, the thionyl radical **32** undergoes oxidation of the Fe^{II} species **94** to form the original Fe^{III} complex **92** and gets protonated to re-form the HAT catalyst **32**, resulting in the conclusion of both catalytic cycles.

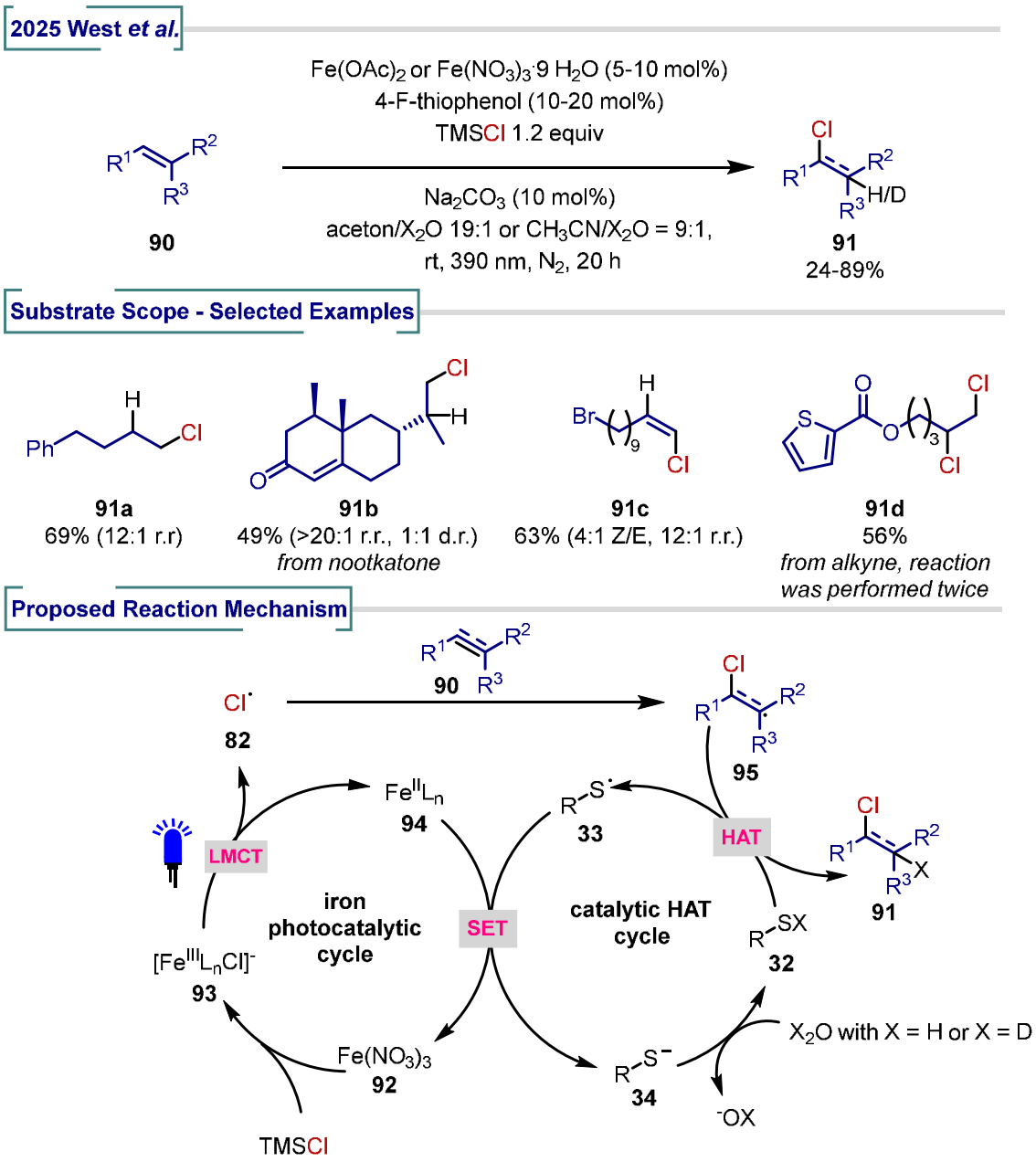

Scheme 1-11. Anti-Markovnikov hydro- and deuterochlorination of alkenes or alkynes **90** using iron photocatalysis and HAT catalysis synergistically.

1.3 Summary and Conclusion

Numerous first-row transition metal complexes exhibit LMCT excited states, which can be readily accessed by visible or UV light irradiation. These states are particularly prone to homolytic bond cleavage, enabling chemical reactivity even at ultrashort excited-state lifetimes.[14] Moreover, in contrast to well-established photoredox catalysis, LMCT-based photocatalysis operates *via* an inner-sphere oxidation mechanism. This eliminates reliance on diffusion and matching redox potentials, broadening the scope to include

substrates with high oxidation potentials, such as trifluoroacetic acid (TFA)[16], under mild conditions. Consequently, LMCT photocatalysis presents a more economical and ecologically sustainable alternative to well-established iridium- and ruthenium-based systems. Among the earth-abundant metals, iron complexes stand out as the most sustainable and cost-effective catalysts (Figure 1-1).

While mono iron-photocatalytic approaches showed various synthetically valuable transformations, they often required external oxidants to close the catalytic cycle.[5] In contrast, redox-neutral, dual iron-photocatalytic systems offer a more sustainable pathway, though they remain comparatively underexplored. This review has summarized recent research in dual iron-photocatalytic methodologies where (V)LIH of metal–substrate bonds generate reactive radical intermediates through LMCT. These include β-scission of alkoxy radicals[50], decarboxylative functionalizations[16,26,44,61–63,68,79], and HAT processes mediated by chlorine radicals[49,85,87]. While sterically demanding thiophenol derivatives have often served as co-catalysts[16,26,49,63,87], successful examples of synergistic catalysis with organic electron shuttles such as DPA[50,85], as well as other metal complexes like cobaloximes[44] and nickel species[50,68], illustrate the growing versatility of this approach. Interestingly, ligand exchange didn't interfere with the catalytic system when cobaloxime catalyst[44] or nickel complexes[50,68] were combined with the iron photocatalysts. Therefore, ligand tuning would offer the possibility of either diastereoselective desaturation reactions by cobaloxime catalysis[60] or asymmetric cross-coupling reactions by nickel catalysis[88,89] for future research.

Finally, while halogen- and oxygen-centered radicals are well represented in current LMCT photocatalysis[5], the application of other heteroatom-centered radicals, such as nitrogen- or pseudohalogen-based species (e.g., azide radicals), remains largely unexplored. The potential for innovation in sustainable synthetic chemistry through the expansion of the radical repertoire in iron LMCT catalysis is a compelling prospect for future research and development.

1.4 References

1 P. T. Anastas, J. C. Warner and J. C. Warner, *Green chemistry: theory and practice*, Oxford University Press, Oxford, 1. paperback., 2000.

2 H. Yorimitsu, M. Kotora and N. T. Patil, *Chem. Rec.*, 2021, **21**, 3335–3337.

3 C. K. Prier, D. A. Rankic and D. W. C. MacMillan, *Chem. Rev.*, 2013, **113**, 5322–5363.

4 D. Ravelli, S. Protti and M. Fagnoni, *Chem. Rev.*, 2016, **116**, 9850–9913.

5 F. Juliá, *ChemCatChem*, 2022, **14**, e202200916.

6 J. C. K. Chu and T. Rovis, *Nature*, 2016, **539**, 272–275.

7 J. L. Jeffrey, J. A. Terrett and D. W. C. MacMillan, *Science*, 2015, **349**, 1532–1536.

8 A. J. Musacchio, L. Q. Nguyen, G. H. Beard and R. R. Knowles, *J. Am. Chem. Soc.*, 2014, **136**, 12217–12220.

9 J. B. H. Gordon B. Haxel and Greta J. Orris, *Rare Earth Elements-Critical Resources for High Technology*, 2002.

10 N. A. Romero and D. A. Nicewicz, *Chem. Rev.*, 2016, **116**, 10075–10166.

11 D. Ravelli, A. Albini and M. Fagnoni, *Chem. Eur. J.*, 2011, **17**, 572–579.

12 D. P. Hari and B. König, *Chem. Commun.*, 2014, **50**, 6688–6699.

13 S. Fukuzumi and K. Ohkubo, *Org. Biomol. Chem.*, 2014, **12**, 6059–6071.

14 O. S. Wenger, *J. Am. Chem. Soc.*, 2018, **140**, 13522–13533.

15 A. Hossain, A. Vidyasagar, C. Eichinger, C. Lankes, J. Phan, J. Rehbein and O. Reiser, *Angew. Chem. Int. Ed.*, 2018, **57**, 8288–8292.

16 K.-J. Bian, Y.-C. Lu, D. Nemoto, S.-C. Kao, X. Chen and J. G. West, *Nat. Chem.*, 2023, **15**, 1683–1692.

17 Y. Abderrazak, A. Bhattacharyya and O. Reiser, *Angew. Chem. Int. Ed.*, 2021, **60**, 21100–21115.

18 K. S. Kjær, N. Kaul, O. Prakash, P. Chábera, N. W. Rosemann, A. Honarfar, O. Gordivska, L. A. Fredin, K.-E. Bergquist, L. Häggström, T. Ericsson, L. Lindh, A. Yartsev, S. Styring, P. Huang, J. Uhlig, J. Bendix, D. Strand, V. Sundström, P. Persson, R. Lomoth and K. Wärnmark, *Science*, 2019, **363**, 249–253.

19 A. K. Pal, C. Li, G. S. Hanan and E. Zysman-Colman, *Angew. Chem. Int. Ed.*, 2018, **57**, 8027–8031.

20 S. I. Ting, S. Garakyaraghi, C. M. Taliaferro, B. J. Shields, G. D. Scholes, F. N. Castellano and A. G. Doyle, *J. Am. Chem. Soc.*, 2020, **142**, 5800–5810.

21 B. D. Rossenaar, C. J. Kleverlaan, M. C. E. Van De Ven, D. J. Stufkens, A. Oskam, J. Fraanje and K. Goubitz, *J. Organomet. Chem.*, 1995, **493**, 153–162.

22 P. I. Djurovich and R. J. Watts, *J. Phys. Chem.*, 1994, **98**, 396–397.

23 P. I. Djurovich and R. J. Watts, *Inorg. Chem.*, 1993, **32**, 4681–4682.

24 S. M. Treacy and T. Rovis, *Synthesis*, 2024, **56**, 1967–1978.

25 Y. Jin, Q. Zhang, L. Wang, X. Wang, C. Meng and C. Duan, *Green Chem.*, 2021, **23**, 6984–6989.

26 H. Guo, W. Lai, J. Ni and P. Xu, *Org. Lett.*, 2024, **26**, 9568–9573.

27 H. Inoue, K. Tamaki, N. Komakine and E. Imoto, *Bull. Chem. Soc. Jpn.*, 1966, **39**, 1577–1582.

28 H. Inoue, K. Tamaki, N. Komakine and E. Imoto, *Bull. Chem. Soc. Jpn.*, 1967, **40**, 875–880.

29 H. Inoue, N. Komakine and E. Imoto, *Bull. Chem. Soc. Jpn.*, 1968, **41**, 2726–2733.

30 G. B. Shulpin and M. M. Kats, *React Kinet Catal Lett*, 1990, **41**, 239–243.

31 K. Takaki, J. Yamamoto, Y. Matsushita, H. Morii, T. Shishido and K. Takehira, *Bull. Chem. Soc. Jpn.*, 2003, **76**, 393–398.

32 K. Takaki, J. Yamamoto, K. Komeyama, T. Kawabata and K. Takehira, *Bull. Chem. Soc. Jpn.*, 2004, **77**, 2251–2255.

33 W. Wu, Z. Fu, X. Wen, Y. Wang, S. Zou, Y. Meng, Y. Liu, S. R. Kirk and D. Yin, *Appl. Catal. A Gen.*, 2014, **469**, 483–489.

34 W. Wu, X. He, Z. Fu, Y. Liu, Y. Wang, X. Gong, X. Deng, H. Wu, Y. Zou, N. Yu and D. Yin, *J. Catal.*, 2012, **286**, 6–12.

35 A. Kohda, K. Ueda and T. Sato, *J. Org. Chem.*, 1981, **46**, 509–515.

36 T. Sato, T. Oikawa and K. Kobayashi, *J. Org. Chem.*, 1985, **50**, 1646–1651.

37 M. Barbier, *Helv. Chim. Acta.*, 1984, **67**, 866–869.

38 A. Sugimori and T. Yamada, *Bull. Chem. Soc. Jpn.*, 1986, **59**, 3911–3915.

39 Y. C. Kang, S. M. Treacy and T. Rovis, *Synlett*, 2021, **32**, 1767–1771.

40 Y. C. Kang, S. M. Treacy and T. Rovis, *ACS Catal.*, 2021, **11**, 7442–7449.

41 J.-L. Tu, A.-M. Hu, L. Guo and W. Xia, *J. Am. Chem. Soc.*, 2023, **145**, 7600–7611.

42 Z. Li, X. Wang, S. Xia and J. Jin, *Org. Lett.*, 2019, **21**, 4259–4265.

43 N. Xiong, C. Zhou, S. Li, S. Wang, C. Ke, Z. Rong, Y. Li and R. Zeng, *Org. Lett.*, 2024, **26**, 2029–2033.

44 J.-L. Tu, H. Gao, M. Luo, L. Zhao, C. Yang, L. Guo and W. Xia, *Green Chem.*, 2022, **24**, 5553–5558.

45 Z. Zhang, G. Zhang, N. Xiong, T. Xue, J. Zhang, L. Bai, Q. Guo and R. Zeng, *Org. Lett.*, 2021, **23**, 2915–2920.

46 G. A. Lutovsky, S. N. Gockel, M. W. Bundesmann, S. W. Bagley and T. P. Yoon, *Chem.*, 2023, **9**, 1610–1621.

47 F. Glaser, A. Aydogan, B. Elias and L. Troian-Gautier, *Coord. Chem. Rev.*, 2024, **500**, 215522.

48 S. J. Blanksby and G. B. Ellison, *Acc. Chem. Res.*, 2003, **36**, 255–263.

49 W. Liu, Q. Wu, M. Wang, Y. Huang and P. Hu, *Org. Lett.*, 2021, **23**, 8413–8418.

50 M. Jaber, Y. Ozbay, E. Chefdeville, G. Tran and A. Amgoune, *ACS Catal.*, 2024, **14**, 12757–12768.

51 F. De Vleeschouwer, V. Van Speybroeck, M. Waroquier, P. Geerlings and F. De Proft, *Org. Lett.*, 2007, **9**, 2721–2724.

52 M. Yuan, Z. Song, S. O. Badir, G. A. Molander and O. Gutierrez, *J. Am. Chem. Soc.*, 2020, **142**, 7225–7234.

53 K. Wadekar, S. Aswale, V. R. Yatham, *Org. Biomol. Chem.*, 2020, **18**, 983–987.

54 S. Shirase, S. Tamaki, K. Shinohara, K. Hirosawa, H. Tsurugi, T. Satoh and K. Mashima, *J. Am. Chem. Soc.*, 2020, **142**, 5668–5675.

55 P. Dam, K. Zuo, L. M. Azofra and O. El-Sepelgy, *Angew. Chem. Int. Ed.*, 2024, **63**, e202405775.

56 B. P. Branchaud and G. X. Yu, *Organomet.*, 1993, **12**, 4262–4264.

57 K. C. Cartwright, A. M. Davies and J. A. Tunge, *Eur. J. Org. Chem.*, 2020, **2020**, 1245–1258.

58 D. C. Lacy, G. M. Roberts and J. C. Peters, *J. Am. Chem. Soc.*, 2015, **137**, 4860–4864.

59 D. P. Estes, D. C. Grills and J. R. Norton, *J. Am. Chem. Soc.*, 2014, **136**, 17362–17365.

60 H. Zhao, A. J. McMillan, T. Constantin, R. C. Mykura, F. Juliá and D. Leonori, *J. Am. Chem. Soc.*, 2021, **143**, 14806–14813.

61 Y. Lu and J. G. West, *Angew. Chem. Int. Ed.*, 2023, **62**, e202213055.

62 X.-K. Qi, L.-J. Yao, M.-J. Zheng, L. Zhao, C. Yang, L. Guo and W. Xia, *ACS Catal.*, 2024, **14**, 1300–1310.

63 I. Perov, K. F. Catenza, J. Jr. Abucay, Y.-T. Hsiao and J. C. Vederas, *Tetrahedron Lett.*, 2025, **159**, 155507.

64 J. D. Griffin, M. A. Zeller and D. A. Nicewicz, *J. Am. Chem. Soc.*, 2015, **137**, 11340–11348.

65 J. Lin, Z. Li, J. Kan, S. Huang, W. Su and Y. Li, *Nat. Commun.*, 2017, **8**, 14353.

66 H. Roth, N. Romero and D. Nicewicz, *Synlett*, 2016, **27**, 714–723.

67 P. D. Morse and D. A. Nicewicz, *Chem. Sci.*, 2015, **6**, 270–274.

68 R. Nsouli, S. Nayak, V. Balakrishnan, J.-Y. Lin, B. K. Chi, H. G. Ford, A. V. Tran, I. A. Guzei, J. Bacsa, N. R. Armada, F. Zenov, D. J. Weix and L. K. G. Ackerman-Biegasiewicz, *J. Am. Chem. Soc.*, 2024, **146**, 29551–29559.

69 E. L. Grimm, C. Brideau, N. Chauret, C.-C. Chan, D. Delorme, Y. Ducharme, D. Ethier, J.-P. Falgueyret, R. W. Friesen, J. Guay, P. Hamel, D. Riendeau, C. Soucy-Breau, P. Tagari and Y. Girard, *Bioorg. Med. Chem. Lett.*, 2006, **16**, 2528–2531.

70 M. P. Bourbeau, K. S. Ashton, J. Yan and D. J. St. Jean, *J. Org. Chem.*, 2014, **79**, 3684–3687.

71 T. Komata, K. Matsunaga, Y. Hirotsu, S. Akiba and K. Ogura, *J. Fluor. Chem.*, 2007, **128**, 902–909.

72 N. Marquet, E. Grunova, E. Kirillov, M. Bouyahyi, C. M. Thomas and J.-F. Carpentier, *Tetrahedron*, 2008, **64**, 75–83.

73 M. Sridhar, C. Narsaiah, B. C. Ramanaiah, V. M. Ankathi, R. B. Pawar and S. N. Asthana, *Tetrahedron Lett.*, 2009, **50**, 1777–1779.

74 Y. Zhang, M. Fujiu, H. Serizawa and K. Mikami, *J. Fluor. Chem.*, 2013, **156**, 367–371.

75 Y. Chang and C. Cai, *J. Fluor. Chem.*, 2005, **126**, 937–940.

76 L. A. Babadzhanova, N. V. Kirij, Yu. L. Yagupolskii, W. Tyrra and D. Naumann, *Tetrahedron*, 2005, **61**, 1813–1819.

77 J. B. Geri, M. M. Wade Wolfe and N. K. Szymczak, *Angew. Chem. Int. Ed.*, 2018, **57**, 1381–1385.

78 K. Domino, C. Veryser, B. A. Wahlqvist, C. Gaardbo, K. T. Neumann, K. Daasbjerg, W. M. De Borggraeve and T. Skrydstrup, *Angew. Chem. Int. Ed.*, 2018, **57**, 6858–6862.

79 D. Golagani, K. K. Prakash, S. Thapa, M. B. Sai Naik and S. M. Akondi, *Org. Lett.*, 2024, **26**, 8583–8588.

80 A. Reichle, H. Sterzel, P. Kreitmeier, R. Fayad, F. N. Castellano, J. Rehbein and O. Reiser, *Chem. Commun.*, 2022, **58**, 4456–4459.

81 J. K. Kochi, *J. Am. Chem. Soc.*, 1962, **84**, 2121–2127.

82 S. J. Hwang, D. C. Powers, A. G. Maher, B. L. Anderson, R. G. Hadt, S.-L. Zheng, Y.-S. Chen and D. G. Nocera, *J. Am. Chem. Soc.*, 2015, **137**, 6472–6475.

83 T. B. Swanson and V. W. Laurie, *J. Phys. Chem.*, 1965, **69**, 244–250.

84 Q. Yang, Y.-H. Wang, Y. Qiao, M. Gau, P. J. Carroll, P. J. Walsh and E. J. Schelter, *Science*, 2021, **372**, 847–852.

85 A. Chinchole, M. A. Henriquez, D. Cortes-Arriagada, A. R. Cabrera and O. Reiser, *ACS Catal.*, 2022, **12**, 13549–13554.

86 L.-J. Li, Y. Wei, Y.-L. Zhao, Y. Gao and X.-Q. Hu, *Org. Lett.*, 2024, **26**, 1110–1115.

87 K.-J. Bian, D. Nemoto, Y. Chen, Y.-C. Lu, S.-C. Kao, X.-W. Chen, A. A. Martí and J. G. West, *Nat. Synth.*, 2025, **4**, 314–326.

88 D. J. Wilger, J.-M. M. Grandjean, T. R. Lammert and D. A. Nicewicz, *Nat. Chem.*, 2014, **6**, 720–726.

89 K. A. Margrey and D. A. Nicewicz, *Acc. Chem. Res.*, 2016, **49**, 1997–2006.

90 J. Kim, X. Sun, B. A. Van Der Worp and T. Ritter, *Nat. Catal.*, 2023, **6**, 196–203.

Chapter 2

2 Dual Iron- and Organophotocatalyzed Hydroformylation, Hydroacylation and Hydrocarboxylation of Michael-Acceptors Utilizing 1,3,5-Trioxanes as C1-Synthone‡

2.1 Abstract

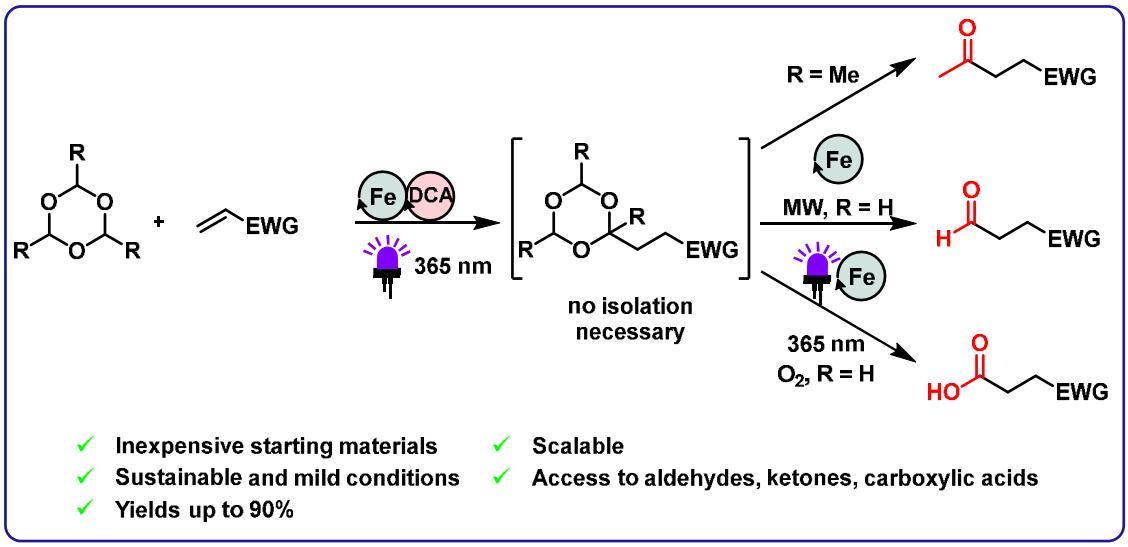

A protocol based on photocatalytic cycles of both iron(III)chloride and 9,10-dicyanoanthracene (DCA) is developed for the masked hydroformylation, hydroacylation, and hydrocarboxylation of Michael-Acceptors utilizing readily available 1,3,5-trioxanes. Initiated by the LMCT of $[FeCl_4]^-$ to generate chlorine radicals that promote hydrogen atom transfer (HAT) from the trioxanes, 9,10-dicyanoanthracene is used as co-photocatalyst to accelerate the formation of the desired products by facilitating the reoxidation of iron(II) to iron(III). The methodology is robust, allowing the generation of aldehydes, ketones, and carboxylic acids either by altering the trioxane and deprotection strategy or by subsequent photocatalyzed conversion of the initially obtained aldehydes.

‡ This chapter is based on: V. Klöpfer†, A. Chinchole†, O. Reiser, *Tetrahedron Chem.* 2024, **10**, 100073–100077. (†Authors contributed equally). All reactions and substrates in this chapter marked with * are performed and isolated by A. Chinchole during his experimental work for his Ph.D. thesis at the Institute of Organic Chemistry, University of Regensburg, Germany, under the supervision of Prof. Dr. Oliver Reiser between October 2019 and May 2023. O. Reiser was supervising this project.

2.2 Introduction

Aldehydes represent common moieties in both fine and bulk chemicals, as well as in biologically active compounds (Scheme 2-1).[1–3] Consequently, the introduction of this functional group into readily available starting materials is an active area of research. The transition-metal-catalyzed oxo-process has found extensive use for the hydroformylation of alkenes, which is applied in the industry on a million-ton scale. It is distinguished by effectiveness (turnover frequency (TOF) up to ~ 35000 h^{-1}) and high atom efficiency to the use of syngas as reagent. However, precisely designed ligands and elevated temperatures are essential for the transformation.[4–7] Thermal[8] or photochemical[1] alternatives *via* the formation of formyl anion or formyl radical have been developed but leave room for improvement concerning atom efficiency and non-noble photocatalysts, respectively.

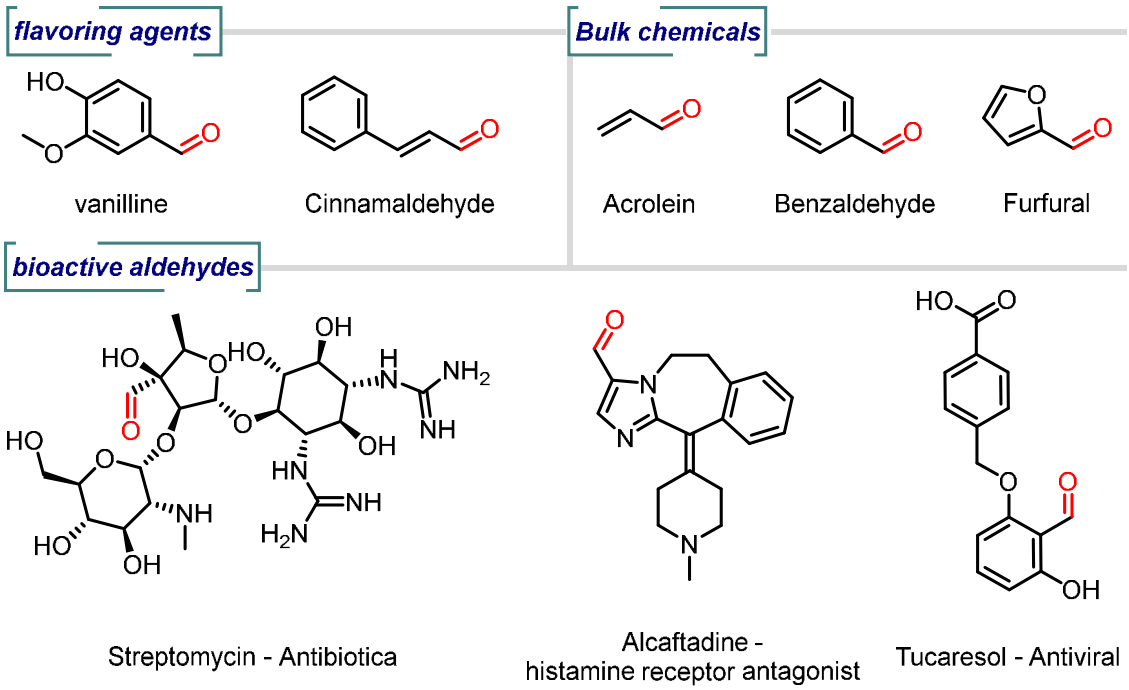

Scheme 2-1. Representative Aldehydes in bulk and fine chemicals as well as in bioactive compounds.

The indirect hydroformylation generating radicals from cyclic acetals for addition to alkenes appears to be promising to overcome the difficulties of direct formyl radical formation and its synthetic utilization.[9–12] Especially relevant for this study, several

photocatalytic approaches have been recently developed (Scheme 2-2).[13–20] Radical formation from cyclic acetals can be realized either by a HAT or a SET mechanism. While reactions via SET are characterized by perfect regioselectivity,[18,19] HAT-based procedures tend to be less selective resulting in the formation of regioisomers[13,14,16]. The emergence of isomers arises with 1,3-dioxalane due to multiple C–H bonds with small differences in bond dissociation energies (BDE = 86.8 kcal mol^{-1} for C2–H vs. 88.2 kcal mol^{-1} for C4/C5–H, Scheme 2-2).[16] However, the Doyle group successfully performed a HAT based reaction with good regioselectivity (Scheme 2-2, top).[16] Moreover, for this transformation the formation of regioisomers was circumvented for one example by using 1,3,5-trioxane as a radical precursor. However, while the hydrolysis of the 1,3-dioxolane products proceeds readily under acidic conditions[15,16], the deprotection of 1,3,5-trioxane analogs appeared to be more challenging[16].

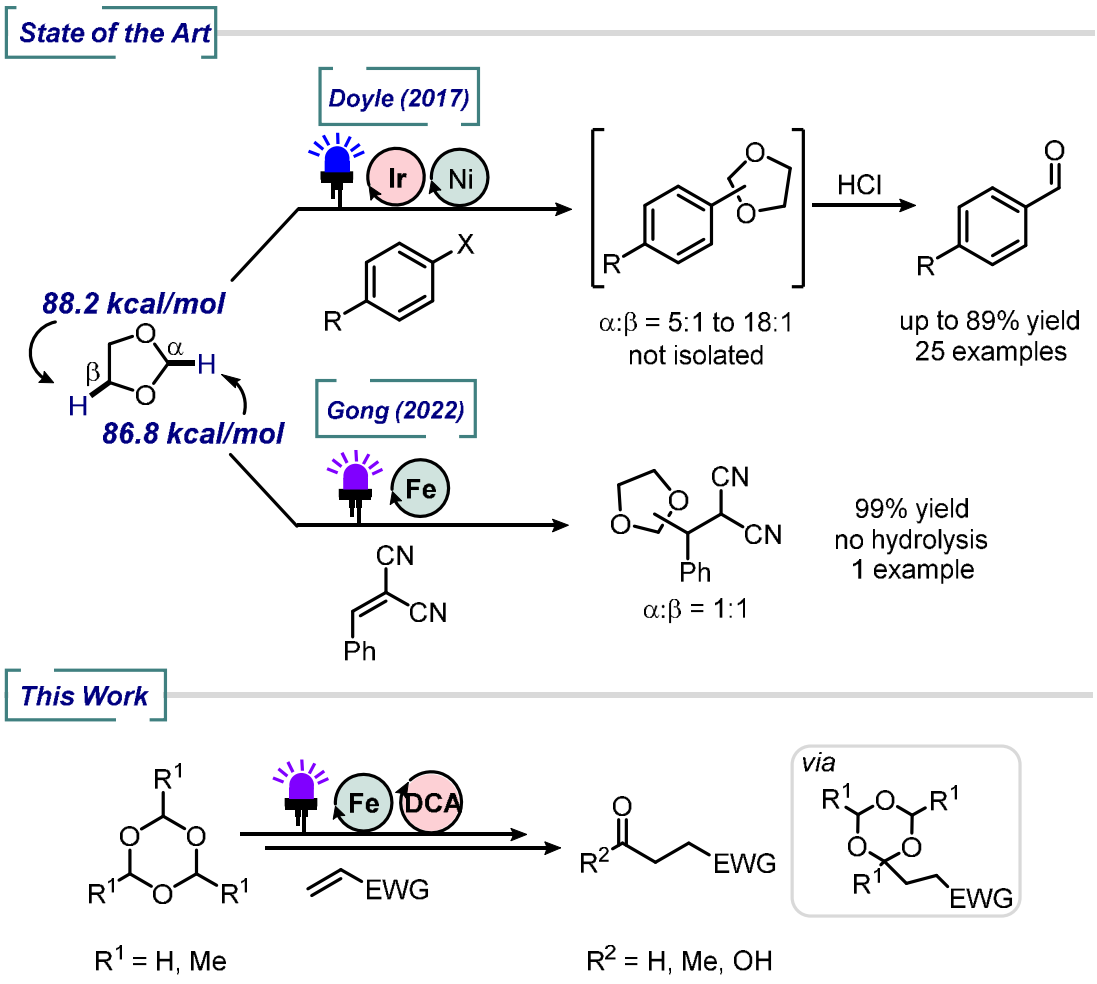

Scheme 2-2. State of the art: masked formylation of arenes and acetalization of Michael-acceptors. This work: indirect hydroformylation, -acylation, and -carboxylation of Michael-acceptors.

We demonstrate here the utilization of 1,3,5-trioxanes **1**, representing inexpensive feedstock chemicals, as masked formyl radical sources for the indirect functionalization of Michael acceptors **2** catalyzed by iron(III) chloride and 9,10-dicyanoantracene (DCA) in a dual-catalytic fashion. By varying the acetal and deprotection strategy, the corresponding aldehydes **4**, ketones **6**, and carboxylic acids **5** becomes accessible.

2.3 Results and Discussion

Table 2-1. Reaction Optimization.

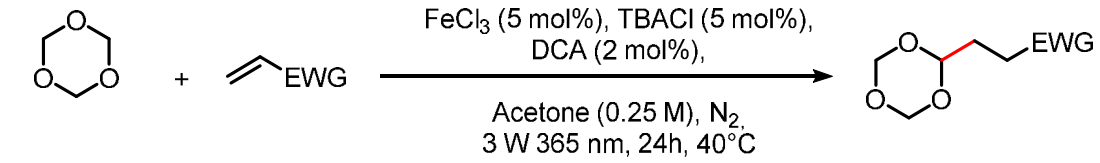

1a, 6 equiv **2a**, 1 equiv **3a**

Entry	Variation	Yield %[a]
1*	No variation	80
2[b]*	DPA (1 mol%), $MgCl_2$ (10 mol%), HCl (1 equiv), MeCN (0.25 M), **1a** (3 equiv)	Traces
3*	DPA (1 mol%), MeCN (0.25 M), **1a** (3 equiv), no additional Cl^- source	Traces
4*	DPA (1 mol%), **1a** (3 equiv), no additional Cl^- source	49
5*	DPA (2 mol%), **1a** (3 equiv), no additional Cl^- source	54
6*	3 equiv of **1a**, no additional Cl^- source	55
7*	3 equiv of **1a**	60
8	TBABr instead of TBACl	30 (at 400 nm)
9	Without DCA	46

[a]NMR yields using 1,1,2,2-tetrachlorethane as an internal standard. [b]Conditions reported in our previous work on the hydroacylation of alkenes.[21]

In our previous work, we capitalized on the LMCT of Fe(III)–Cl[22,23] in combination with 9,10-diphenylanthracene (DPA) as a co-catalyst for the C,H-functionalization of aldehydes with electron-deficient alkenes.[21] Reasoning that the C,H-functionalization of 1,3,5-trioxanes (**1**) can be achieved in an analogous way, we commenced our study by

irradiating 1,3,5-trioxane (**1a**) and acrylonitrile (**2a**) in acetonitrile in the presence of catalytic amounts of $FeCl_3$ and DPA (the complete optimization table is given in *2.7.3 Complete Reaction Optimization and Control Experiments*). However, only traces of the product **3a** were observed after 24 h (Table 2-1, entry 2). Subsequently, we removed all additional chloride sources and performed the reaction under otherwise identical conditions, which resulted again only in traces of product **3a** (Table 2-1, entry 3). It turned out that the solvent was a decisive factor for the transformation: Screening revealed that acetone is best, giving rise to **3a** in 49 % yield (Table 2-1, entry 4). The yield increased slightly with 2 mol% DPA (Table 2-1, entry 5); however, higher catalyst loading didn't lead to further improvement of the yield due to its limited solubility (for more details see SI). Evaluation of alternative photocatalysts showed a comparable performance between DPA and DCA (Table 2-1, entry 5–6), letting us choose the latter for economic reasons. Considering the key role of chlorine radicals as the HAT reagent, we screened several chloride sources as additives and found that tetrabutylammonium chloride (TBACl) was beneficial for this reaction, yielding **3a** in 60 % (Table 2-1, entry 7). Tetramethylammonium chloride showed poor solubility in acetone, resulting in low yields, moreover, HCl was found to be incompatible (for more details see *2.7.3 Complete Reaction Optimization and Control Experiments*). Notably, using tetrabutylammonium bromide induced a red shift in the metal complex (for more details and for UV/Vis spectra see *2.7.4 Experimental Mechanistic Investigations*), prompting us to explore near-visible light conditions (400 nm irradiation), but a diminished yield (30 %) was observed for **3a** (Table 2-1, entry 8). Finally, employing six equivalents of trioxane **1a** was found to be optimal, improving the yield of **3a** to 80 % (Table 2-1, entry 1). Control experiments confirmed that light and iron were crucial for the reaction to proceed. However, **3a** is still formed even without DCA as a co-catalyst albeit with a reduced yield (46 %, Table 2-1, entry 9), indicating that DCA accelerates the process by shuttling electrons between Fe(II) and the transient organic radicals that are formed (see *2.5 Mechanistic Investigation*).

2.4 Scope & Further Derivatization

Under the optimized conditions, a diverse range of electron-deficient alkenes could be coupled with **1a** (Scheme 2-3). Reflecting the nucleophilic nature of radical **A** (see *2.5 Mechanistic Investigation*, Scheme 2-5) derived from HAT of **1a**, α,β-unsaturated nitriles, carbonyl compounds, and vinyl sulfones proved to be amenable substrates giving rise to **3a-3i** in 68–90 % yield. Especially, the developed methodology proves effective for

functionalizing feedstock chemicals derived from renewable resources as demonstrated with the synthesis of **3c** and **3d**.

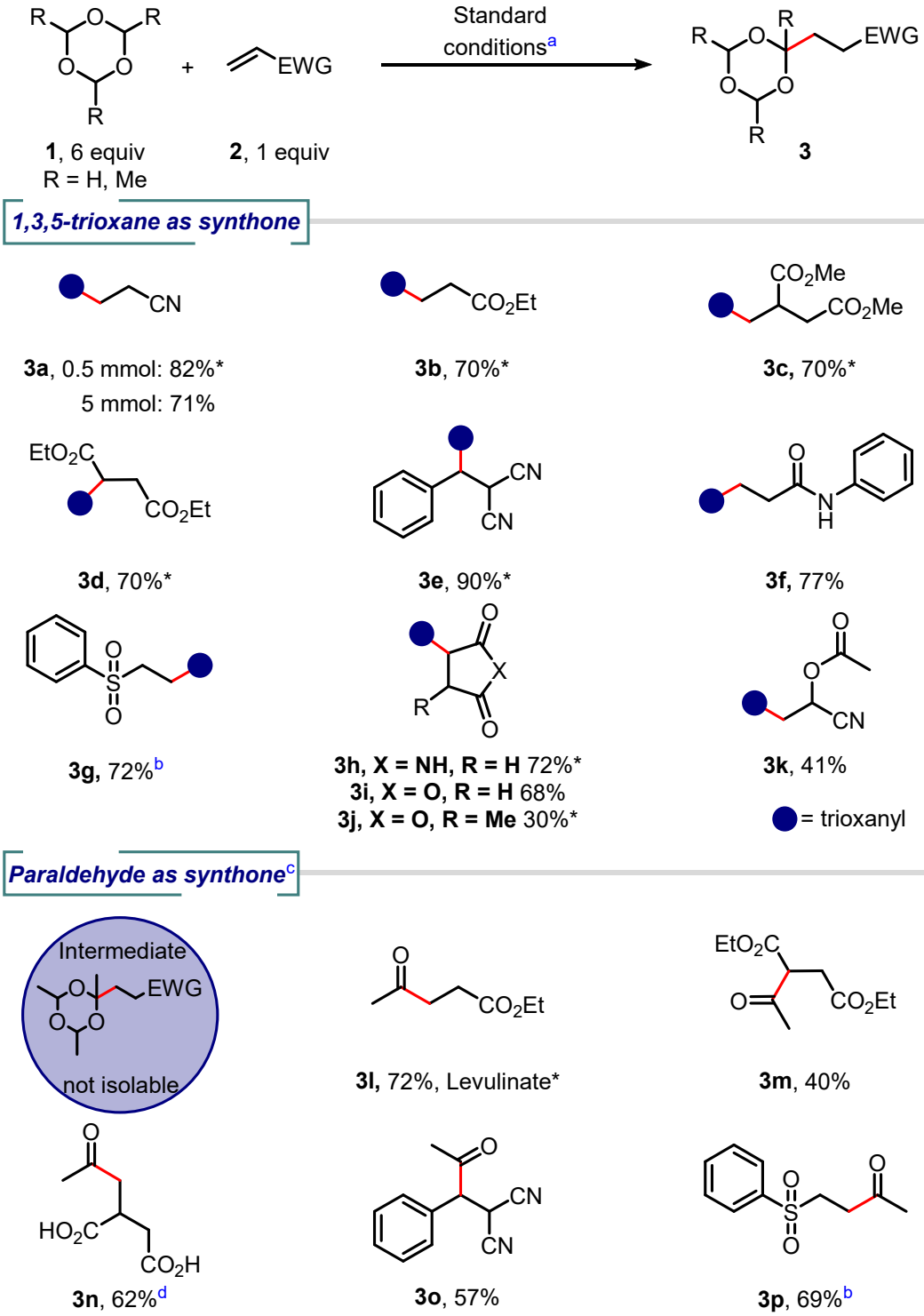

Scheme 2-3. Substrate scope of the masked hydroformylation of Michael-acceptors. [a]*Standard conditions*: 1 (3 mmol), 2 (0.5 mmol), Acetone (0.25 M), anhyd. $FeCl_3$ (5 mol%), TBACl (5 mol%), DCA (2 mol%), 40 °C, 24 h, 3W 365 nm LED, N_2. [b]36 h of reaction time. [c]15 equiv of paraldehyde. [d]Crude reaction mixture was transferred to a microwave vial and heated under microwave conditions (150 °C for 30 min) to obtain the product.

However, yields dropped with increased electron density of the double bond, resulting in moderate yields for **3j-3k**. Scale-up of the reaction was demonstrated for **3a** (71 % at a 5 mmol scale). Furthermore, we applied the standard conditions to styrene, 2,3,4,5,6-pentafluorostyrene, and 1- octene, respectively, however, these experiments proved unsuccessful, resulting in complex reaction mixtures. Since we did not observe multiple substitutions of trioxane **1a**, we attempted to convert isolated trioxane adduct **3a** to give the corresponding di- or trifunctionalized trioxanes, respectively. However, even after 48 h under irradiation, no significant conversion of **3a** was observed (see *2.7.5 Photochemical Procedure and Further Transformations*).

When trimethyl trioxane (**1b**) was subjected to the reaction conditions with various Michael-acceptors, the corresponding ketones were directly formed, obviating the need for hydrolysis of the trioxane moiety. Methyl ketones from acrylates **3l-3m**, α,β-unsaturated nitrile **3o**, and vinyl sulfones **3p** were successfully synthesized this way. Especially the synthesis of ethyl levulinate (**3l**), an essential precursor for value added products[24], was achieved in 72 % yield. Itaconic acid could also be converted successfully under the optimized conditions to **3n** in 62 % yield but required microwave heating of the crude product mixture to achieve complete hydrolysis of the trioxane moiety.

While paraldehyde **1b** gave rise directly to the deprotected ketones **3l-3p**, trioxanyl adducts **3a-3k** (Scheme 2-3) are stable under the reaction conditions allowing further diversification (Scheme 2-4). Simple microwave heating of the crude in 1,4-dioxane/water or pure 1,4-dioxane utilizing again $FeCl_3$ (5–20 mol%) but this time capitalizing on its Lewis acid properties to cleave the ketal moiety, resulted in aldehyde **4a-4c**. Alternatively, carrying out this deprotection step under aerobic conditions and UV-light irradiation leads to the corresponding carboxylic acids as demonstrated for **5a-5c**. Especially, the direct synthesis of 3-cyanopropanoic acid (**5a**) from acrylonitrile (**2a**) was achieved in high yields. **5a** is known as a building block of significant pharmaceutical relevance[25,26] but is challenging to synthesize given the low yields reported for alternative photochemical[27] and electrochemical[28] methodologies, which is also reflected by its high commercial price.

Furthermore, we envisioned that aldehyde **4c** could undergo another coupling reaction with electron poor alkenes to give rise to the unsymmetric ketones. Indeed, we were pleased to find that irradiation of **4c** in the presence of catalytic amounts of $FeCl_3$ initiated

a HAT process being selective for the aldehyde C,H (Scheme 2-4, c).[22] The resulting acyl radical smoothly underwent addition to acrylonitrile (**2a**) giving rise to 6 in 75 % yield.

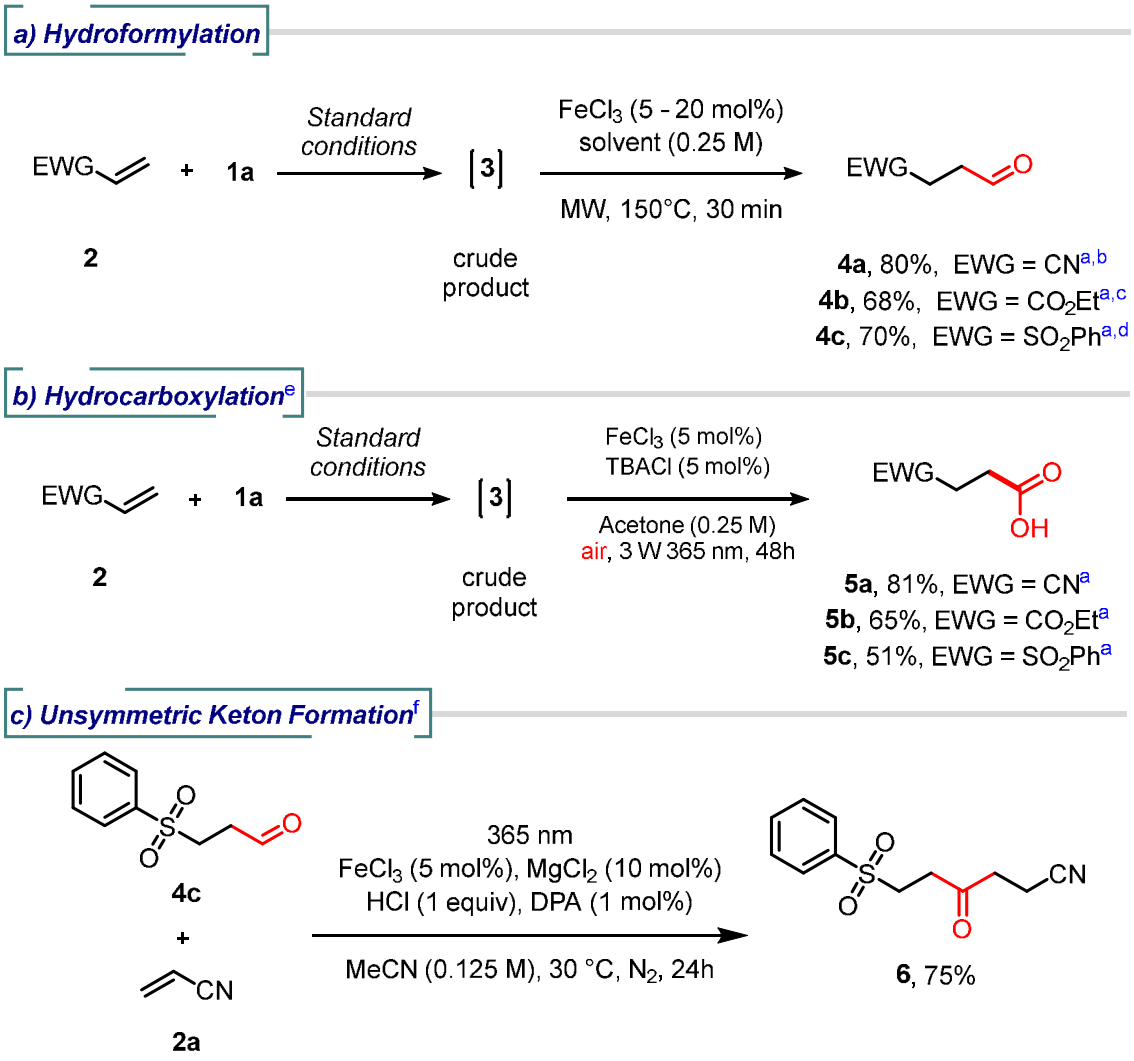

Scheme 2-4. Diversification of the obtained crude trioxane products and further conversion. Standard conditions: 1 (3 mmol), 2 (0.5 mmol), Acetone (0.25 M), anhyd. $FeCl_3$ (5 mol%), TBACl (5 mol%), DCA (2 mol%), 40 °C, 24 h, 3W 365 nm LED, N_2. [a]Isolated yields over two steps. [b]Conditions for second step: 3a (crude product, 0.5 mmol scale), anhyd. $FeCl_3$ (20 mol%), 1,4-dioxane/H2O 1:1 (0.25 M), MW, 150°C, 30 min. [c]Conditions for second step: 3b (crude product, 0.5 mmol scale), anhyd. $FeCl_3$ (20 mol%), 1,4-dioxane (0.25 M), MW, 100°C, 30 min. [d]Conditions for second step: 3g (crude product, 0.5 mmol scale), anhyd. $FeCl_3$ (5 mol%), 1,4-dioxane/H2O 1:1 (0.25 M), MW, 150°C, 30 min. [e]Conditions for second step: 3a, 3b or 3g (crude product, 0.5 mmol scale), Acetone (0.25 M), anhyd. $FeCl_3$ (5 mol%), TBACl (5 mol%), DCA (2 mol%) 40 °C, 48 h, 3W 365 nm LED, air. [f]Conditions: 4c (1 mmol); 2a (0.5 mmol), MeCN (0.25 M), $MgCl_2$ (10 mol %), 37% aq. HCl (1 equiv), anhyd. $FeCl_3$ (5 mol%), DPA (1 mol%), 30 °C, 24 h, 3 W 365 nm LED.

2.5 Mechanistic Investigations

Mechanistic studies conducted for the reaction of **1a** and **2a** revealed that in the presence of TEMPO (2 equiv) no product **3a** is formed while detection of both TEMPO adducts from radicals **A** and **B** by HR-MS was possible (Scheme 2-5, a). UV/Vis studies showed that $FeCl_3$ formed the photoactive complex $[FeCl_4]^-$ in solution even without an additional chloride source being present, which adsorbs in the near UV-light range with a maximum at 362 nm.[29,30] Addition of TBACl resulted in an enhanced absorption intensity, which confirmed that TBACl was not essential for the formation of $[FeCl_4]^-$ but beneficial for the reaction (see *2.3 Results and Discussion*, Table 2-1, entry 6–7). No indication of other interactions between the iron complex, DCA, and any reactants were seen (for more details see *2.7.4 Experimental Mechanistic Investigations*).

In combination with our previous findings[22] and other evidence from the literature[13], a plausible mechanism for the title transformation (Scheme 2-5, c) starts with the formation of the photochemical active complex $[FeCl_4]^-$. Light-induced homolysis initiated via LMCT forms Fe(II) and a chlorine radical which abstracts a hydrogen (HAT) from trioxane **1** to form the C-centered trioxanyl radical **A**. **A**, being nucleophilic in nature, adds to electron-deficient alkenes **2** to form radical **B**. To close the catalytic cycle, Fe(II) needs to be reoxidized to Fe(III), which goes along with the reduction of radical B followed by protonation to yield the product 3. This process is effectively mediated by DCA (**7**), which from its excited state **8** takes an electron from Fe(II) to form radical anion **9** followed by the reduction of **B**. Performing a Stern-Volmer experiment, in which the fluorescence of DCA was quenched successfully by $FeCl_2$, confirmed the role of DCA regarding the reoxidation of Fe(II) (Scheme 2-5, b). The emission decreased with an increasing amount of $FeCl_2$ being present in a solution of acetone (for more details see *2.7.4 Experimental Mechanistic Investigations*). Alternatively, as indicated by control experiments (see *2.3 Results and Discussion*, cf. Table 2-1, entry 9), Fe(II) can be reoxidized directly by radical **B**, resulting in the desired product and closure of the catalytic iron-cycle.

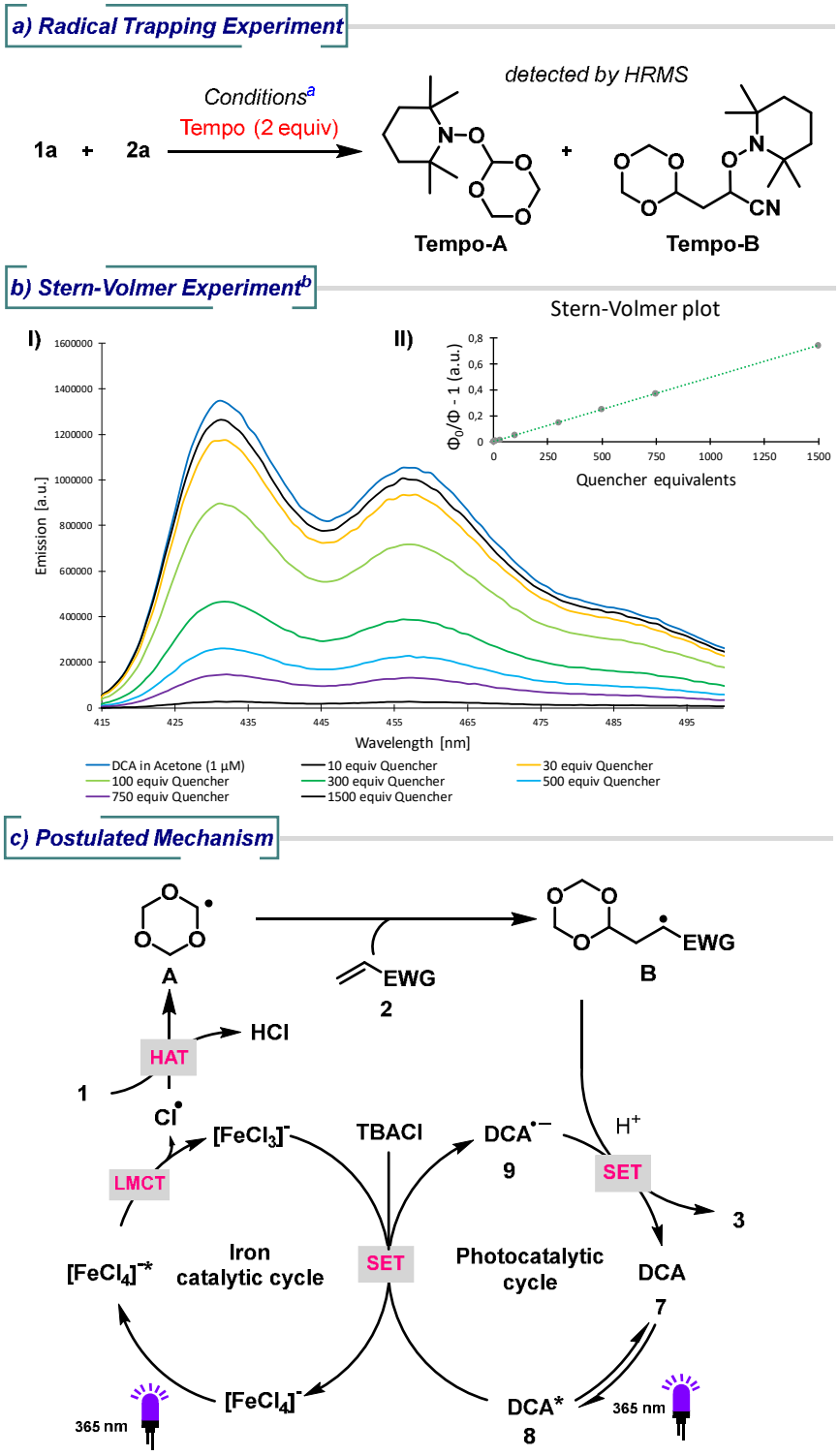

Scheme 2-5. Mechanistic investigation and plausible reaction mechanism for the masked hydroformylation. [a]Conditions: **1** (3 mmol), **2** (0.5 mmol), Acetone (0.25 M), anhyd. $FeCl_3$ (5 mol%), TBACl (5 mol%), DCA (2 mol%), TEMPO (1 mmol), 40 °C, 24 h, 3W 365 nm LED, N_2. [b]Stern-Volmer experiment: I) Fluorescence emissions spectra of DCA in Acetone (1 µM). Quencher = $FeCl_2$, the equivalents were increased gradually. Excitation at a wavelength of 400 nm. Emission spectra range from 415 nm to 600 nm. II) Stern-Volmer plot: linear correlation between quenching effect and quencher equivalents.

2.6 Conclusion

To conclude, we report the radical utilization of readily available trioxanes for the indirect hydroformylation, hydroacylation and hydrocarboxylation initiated by a HAT process. Combining two photocatalytic cycles, i.e. iron(III)-LMCT to generate chlorine radicals and reoxidation of Fe(II) to Fe(III) from excited state 9,10-dicyanoanthracene, we were able to obtain aldehydes **4**, ketones **3l-3p** and carboxylic acids **5**, respectively. Additionally, the initially formed aldehydes **4** can be converted to the unsymmetric ketone **6**, underscoring the potential of iron photocatalysis for sustainable synthesis.

2.7 Experimental Part

2.7.1 General Information

Commercially available chemical materials were purchased in high quality and were used without further purification. Thereby, weight was calculated based on purity mentioned on the container. All reactions were carried out in oven-dried glassware under atmospheric conditions unless otherwise stated. Reactions with moisture or oxygen sensitive reagents were performed in flame-dried glassware under an atmosphere of predried nitrogen. All photochemical reactions were carried out in flame-dried glassware applying three consecutive freeze-pump-thaw cycles. Reactions were monitored by thin layer chromatography (TLC). Anhydrous solvents were prepared by established laboratory procedures.[31] DCM, EtOAc, n-pentane and hexanes (40-60 °C) for chromatography were distilled prior to use. The reported yields are referred to isolated compounds unless otherwise stated.

Chromatography

Thin layer chromatography (TLC) was performed with TLC precoated aluminum sheets (Merck) Silica gel 60 F254, 0.2 mm layer thickness and visualized by a dual short ($\lambda = 254$ nm) / long ($\lambda = 366$ nm) wavelength UV lamp. Staining was done with Seebach`s Magic Stain (2.5 g phosphomolybdic acid, 1.0 g cerium(IV) sulfate tetrahydrate, 94.0 mL distilled water and 6.0 mL conc. sulfuric acid), vanillin (6.0 g vanillin, 100.0 mL ethanol (95%) and 1.0 mL conc. sulfuric acid) or potassium permanganate (1.0 g $KMnO_4$, 2.0 g Na_2CO_3 and 100.0 mL distilled water) followed by heating. Column chromatography was performed with silica gel (Merck, 0.063-0.200 mm particle size) and flash silica gel (Merck, 0.040-0.063 mm particle size).

NMR-Spectroscopy

^{1}H-NMR spectra were recorded on Bruker Avance 300 (300 MHz), Bruker Avance 400 (400 MHz) or Bruker Avance III 400 "Nanobay" (400 MHz) Spectrometer. Spectra were evaluated in first order and coupling constants *J* are reported in Hertz (Hz). Splitting patterns for the spin multiplicity of the signals in the spectra are given as the following: s = singlet, bs = broad singlet, d = doublet, t = triplet, q = quartet, p = pentet, sex = sextet, hept = heptet, m = multiplet and combinations thereof. Chemical shifts for ^{1}H-NMR were reported as δ, parts per million (ppm), relative to the signal of $CHCl_3$ at 7.26 ppm.

^{13}C-NMR spectra were recorded on Bruker Avance 300 (75 MHz), Bruker Avance 400 (101 MHz) or Bruker Avance III 400 "Nanobay" (101 MHz) Spectrometer. Chemical shifts for ^{13}C-NMR were reported as δ, parts per million (ppm), relative to the center line signal of the $CDCl_3$ triplet at 77.16 ppm.

IR-Spectroscopy

FTIR spectroscopy was carried out on a Cary 630 FTIR Spectrometer. Solid and liquid compounds were measured neatly, and the wave numbers are reported as cm^{-1}.

Mass Spectrometry

Mass spectra were recorded by the Central Analytic Department of the University of Regensburg using Jeol AccuTOF GCX and Agilent Q-TOF 6540 UHD Spectrometer. High-resolution mass spectra were measured using electron ionization (EI) or electrospray ionization (ESI) for ionisation.

Microwave Experiments

Microwave irradiation experiments were carried out using an Anton Paar Monowave 300 reactor. The size of the used vials was 5 mL, the reaction mixture was stirred with a magnetic stir bar. All reactions were performed in sealed reaction vessels. The temperature was monitored by internal probe type.

UV/Vis spectrophotometry

UV/Vis spectroscopy was carried out on an Analytik jena Specord® 200Plus. All compounds were measured in the solvent, which was used during the experiments in flow. Measurement range was from 190 nm to 1100 nm.

Stern Volmer Experiments

Fluorescence Quenching Interactions were investigated using a HORIBA Fluoromax-4 of the Horiba Scientific, using a High Precision Cell 117100F-10-40 quartz cuvette with screw cap (Hellma Analytics quartz cuvette, 10 x 10 mm, 3.5 mL). Measurement range was from 415 nm to 600 nm.

2.7.2 Photochemical Setup Photos:

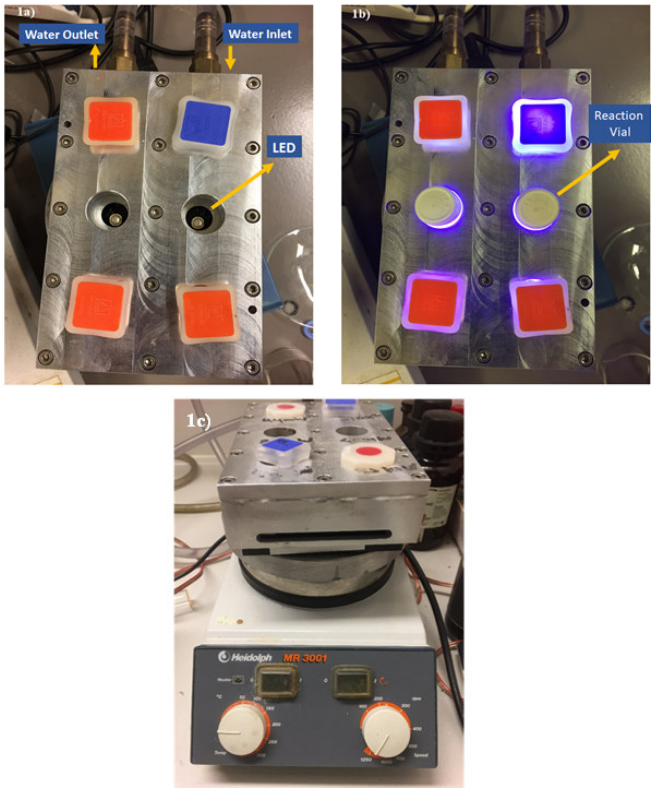

Figure 2-1. Photochemical reaction setup for hydrocarbonylation of alkenes. The irradiation was done using Inolux IN-C68QABTMU2 – UV LED (3.08 W electric power @700mA, λ = 365 nm).

2.7.3 Complete Reaction Optimization and Control Experiments

Table 2-2. Full optimization table for the iron-catalyzed masked hydroformylation of electron-deficient alkenes[a]

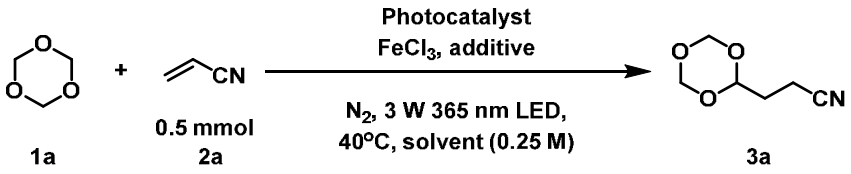

Entry	Conditions	Yield[b] [%]
1[c]*	$FeCl_3$ (5 mol%), DPA (1 mol%), $MgCl_2$ (10 mol%), HCl (1 equiv), MeCN (0.25 M), **1a** (3 equiv)	Traces
2[d]*	$FeCl_3$ (0.05 mol%), HCl (1 mol%), MeCN (0.2 M), **1a** (10 equiv), 3 W 390 nm LED, 40 °C	No reaction
3*	$FeCl_3$ (5 mol%), DPA (1 mol%), MeCN (0.25 M), **1a** (3 equiv)	Traces
4*	$FeCl_3$ (5 mol%), DPA (1 mol%), EA (0.25 M), **1a** (3 equiv)	Traces
5*	$FeCl_3$ (5 mol%), DPA (1 mol%), dimethyl carbonate (0.25 M), **1a** (3 equiv)	Traces
6*	$FeCl_3$ (5 mol%), DPA (1 mol%), DCE (0.25 M), **1a** (3 equiv)	13
7*	$FeCl_3$ (5 mol%), DPA (1 mol%), Aceton (0.25 M), **1a** (3 equiv)	49
8*	$FeCl_3$ (5 mol%), DPA (2 mol%), Aceton (0.25 M), **1a** (3 equiv)	54
9*	$FeCl_3$ (5 mol%), DCA (1 mol%), Aceton (0.25 M), **1a** (3 equiv)	48
10*	$FeCl_3$ (5 mol%), DCA (2 mol%), Aceton (0.25 M), **1a** (3 equiv)	55
11*	$FeCl_3$ (5 mol%), DCA (5 mol%), Aceton (0.25 M), **1a** (3 equiv)	55
12*	$FeCl_3$ (5 mol%), TBACl (5 mol%), DCA (2 mol%), Aceton (0.25 M), **1a** (3 equiv)	60
13	$FeCl_3$ (5 mol%), TBACl (20 mol%), DCA (2 mol%), Aceton (0.25 M), **1a** (3 equiv)	42
14*	$FeCl_3$ (5 mol%), $Me_4N^+Cl^-$ (5 mol%), DCA (2 mol%), Aceton (0.25 M), **1a** (3 equiv)	Traces
15*	$FeCl_3$ (5 mol%), $Et_4N^+Cl^-$ (5 mol%), DCA (2 mol%), Aceton (0.25 M), **1a** (3 equiv)	Traces
16*	$FeCl_3$ (5 mol%), $PhMe_3N^+Cl^-$ (5 mol%), DCA (2 mol%), Aceton (0.25 M), **1a** (3 equiv)	Traces

17	$FeCl_3$ (5 mol%), TBABr (20 mol%), DCA (2 mol%), Aceton (0.25 M), **1a** (3 equiv)	30 (at 400 nm)
18*	$FeCl_3$ (5 mol%), TBACl (20 mol%), DCA (2 mol%), Aceton (0.25 M), **1a** (2 equiv)	40
19*	**$FeCl_3$ (5 mol%), TBACl (20 mol%), DCA (2 mol%), Aceton (0.25 M), 1a (6 equiv)**	**80**
20*	$FeCl_3$ (5 mol%), TBACl (20 mol%), DCA (2 mol%), Aceton (0.25 M), **1a** (10 equiv)	80
21*	$FeCl_3$ (5 mol%), TBACl (20 mol%), DPA (1 mol%), Aceton (0.25 M), **1a** (6 equiv)	76
22	$FeCl_3$ (5 mol%), TBACl (20 mol%), DCA (2 mol%), Aceton (0.25 M), **1a** (6 equiv)	no reaction[e]
23	$FeCl_3$ (5 mol%), TBACl (20 mol%), Aceton (0.25 M), **1a** (6 equiv)	46%
24	$FeCl_3$ (5 mol%), TBACl (20 mol%), DCA (2 mol%), Aceton (0.25 M), **1a** (6 equiv), air	crm[f]
25	DCA (2 mol%), Aceton (0.25 M), **1a** (6 equiv)	no reaction[g]

DPA = 9,10-Diphenylanthracene, DCA = 9,10-Dicyanoanthracene, TBACl = Tetrabutylammonium chloride, TBABr = Tetrabutylammonium bromide, EA = ethyl acetate. [a]*Reaction conditions:* **1a** (indicated equivalents)**, 2a** (0.5 mmol, 1 equiv), $FeCl_3$ (indicated equivalents), additive (indicated equivalents) and Photocatalyst (indicated equivalents) in solvent (degassed, 0.25 M); irradiation with 365 nm (3W LED) under a N_2 atmosphere for 24h as 40°C. [b]NMR yields using 1,1,2,2-Tetrachlorethane as an internal standard. [c]Conditions reported previously in our recent work.[21] [d]Conditions reported similarly by Gong *et al.*[13] [e]No irradiation. [f]Irradiation under air. [g]Reaction without $FeCl_3$ as a catalyst.

2.7.4 Experimental Mechanistic Investigations

UV/Vis Studies

As the masked hydroformylation was perfomed at 365 nm, Figure 2-2 shows spectra ranging from 325 nm to 525 nm. Upon dissolution of $FeCl_3$ in acetone, a new peak emerged, exhibiting a maximum at 362 nm, which is attributed to the photoactive complex $[FeCl_4]^-$.[29,30] After addition of TBACl, the absorbances within this range notably increased. Moreover, the spectra obtained in the presence of DCA, 1,3,5-trioxane (**1a**), and acrylonitrile (**2a**) reveals the overlapping of individual spectra, indicating no interactions between the compounds and the iron-chloride complex.

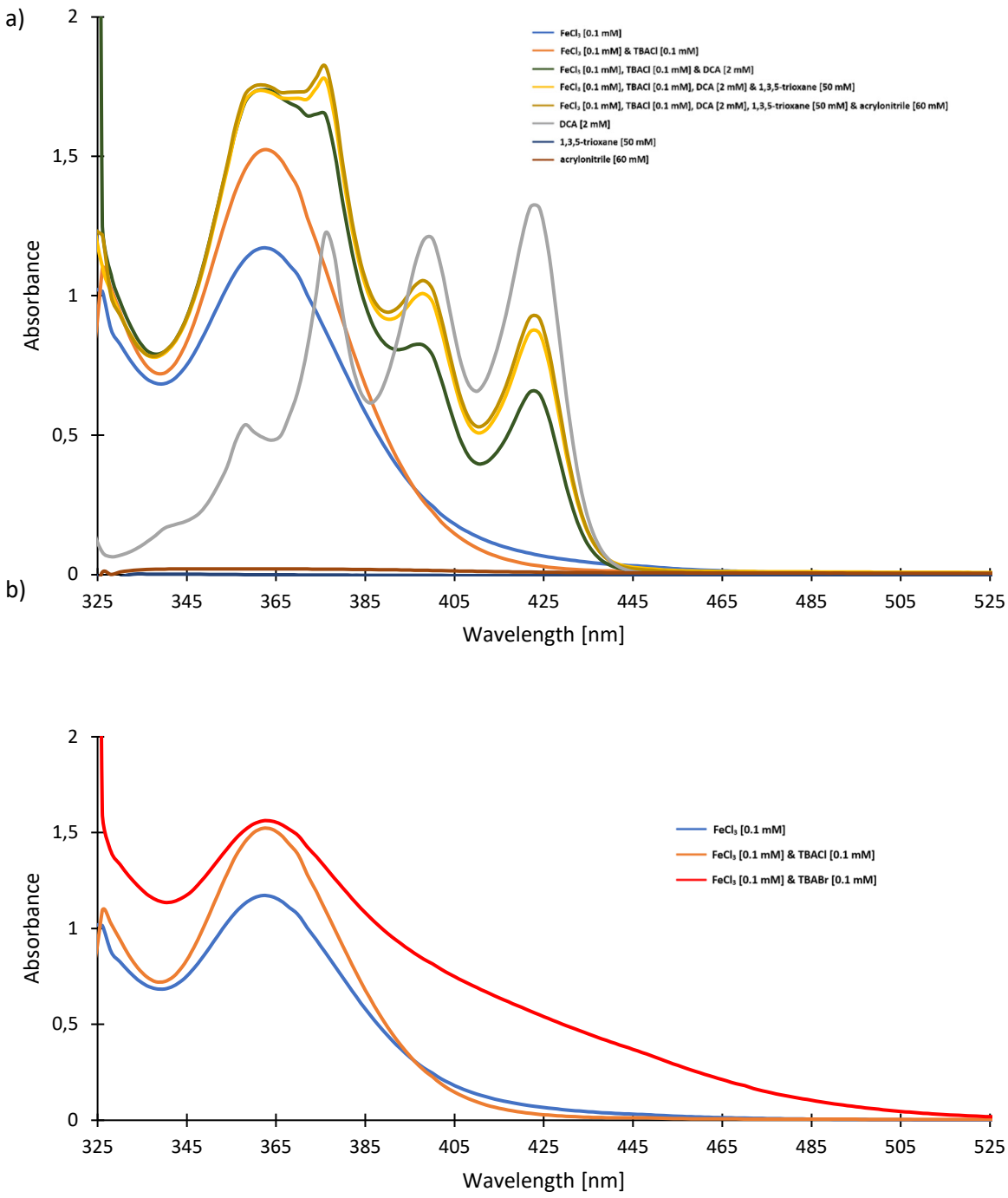

Figure 2-2. UV/Vis spectra for mechanistic investigations, all spectra were measured using acetone as solvent. a) Mechanistic investigations using UV/VIS Studies to identify interactions of reagents. b) Comparison of the UV/VIS Spectra of $FeCl_3$ + TBACl (tetrabutylammonium chloride) and $FeCl_3$ + TBABr (tetrabutylammonium bromide). TBABr leads to a bathochromic shift of the absorption.

Stern-Volmer Experiment

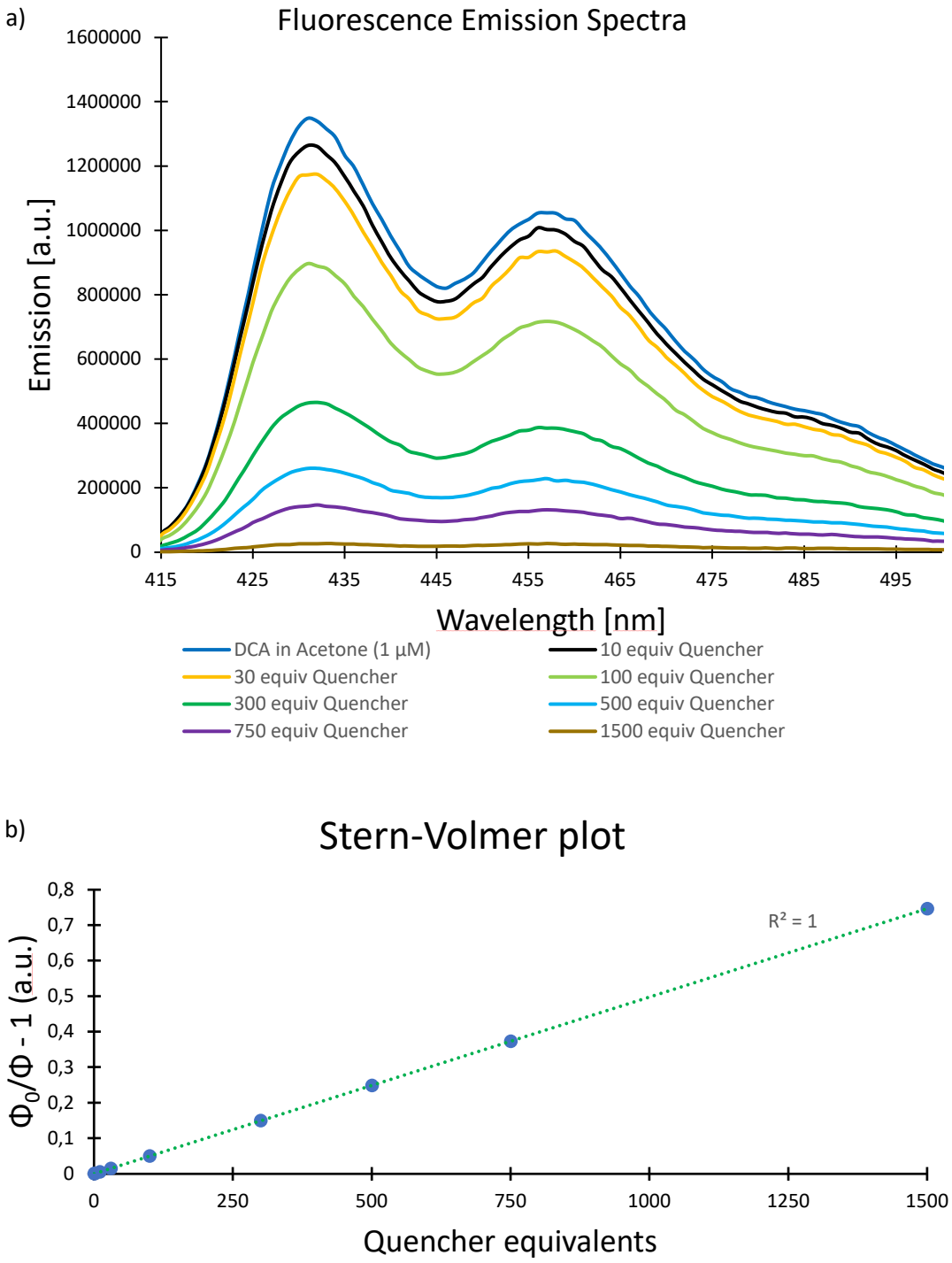

Figure 2-3. Stern-Volmer experiment for mechanistic investigations.a) Fluorescence emissions spectra of DCA in Acetone (1 µM) and in presence of $FeCl_2$ as quencher (excitation with 400 nm light). With increasing amount of the quencher (10 – 1500 equivalents) the fluorescence decreased. b) Stern-Volmer plot for validation; proving the linear correlation of quencher equivaltens ($FeCl_2$) and fluorescence quenching.

A solution of DCA in Acetone (2 mL, 1 µM) was prepared in a cuvette with a screw cap and degassed by purging with N_2 for 10 min. Furthermore, a solution of $FeCl_2$ in Acetone (5 mL, 1 mM) was prepared in a vial, sealed with a rubber septum and degassed by purging with N_2 for 10 min. After the original fluorescence emissions spectra of DCA in acetone (1 µM) was measured, 10, 30, 100, 300, 500, 750 and 1500 equivalents of $FeCl_2$ was added subsequently to the original solution in the cuvette and the fluorescence emissions spectra was measured with different amounts of $FeCl_2$ present. Excitation proceeded with light of 400 nm in each measurement. As a result, we observed that $FeCl_2$ quenched the fluorescence emission of DCA. With an increasing amount of $FeCl_2$ present in the solution, the fluorescence emission gradually decreased, suggesting the oxidation of Fe(II) to Fe(III). The quenching effect was confirmed through the Stern-Volmer plot, which exhibited linearity, thereby validating the experiment.

Radical Trapping Experiment with TEMPO:

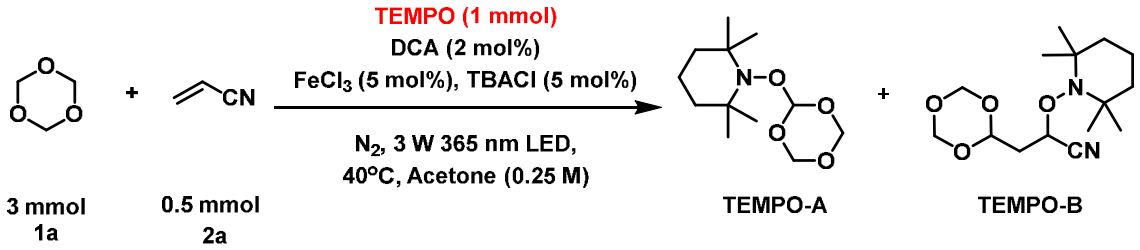

An oven-dried glass vial (4 mL size) equipped with a stirring bar was charged with dicyanoanthracene (2.3 mg, 2 mol%, 0.02 equiv), 1,3,5-trioxane (**1a**) (270 mg, 3 mmol, 6 equiv), TEMPO (156 mg, 1mmol, 2 equiv) followed by the addition of acetone (2 mL) to the reaction vessel. Then $FeCl_3$ (100µL of 0.5M anhydrous $FeCl_3$ solution in acetone) and TBACl (100 µL of 0.5M anhydrous TBACl solution in acetone) was added to the reaction mixture. The reaction vessel was then sealed with a rubber septum, and the mixture was degassed by sparging nitrogen gas for 10 min. Afterwards alkene **2a** (32.7 µL, 0.5 mmol, 1 equiv) were added sequentially. The reaction mixture was then irradiated at 365 nm for 24 h. Later, the reaction mixture was transferred to a round bottom flask and concentrated *in vacuo*. The crude mixture was analyzed by HRMS to detect the two different TEMPO adducts **TEMPO-A** and **TEMPO-B**.

HRMS (ESI) for TEMPO-A: exact m/z calculated for $C_{12}H_{23}NO_4$ (M+H+) 246.17; Found 246.1698.

HRMS (ESI) for TEMPO-B: exact m/z calculated for $C_{15}H_{26}N_2O_4$ (M+H+) 299.1965 ; Found 299.1964.

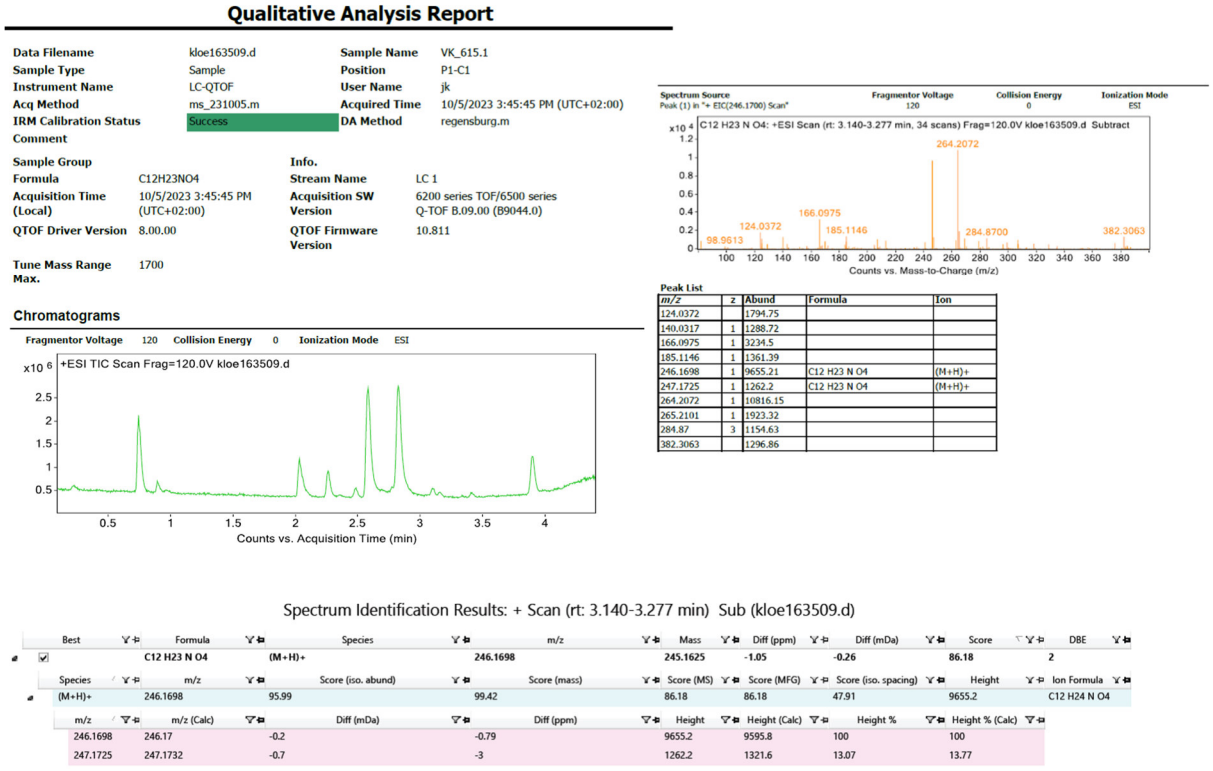

Figure 2-4. Original mass spectroscopy data for the detection of the tempo adduct TEMPO-A.

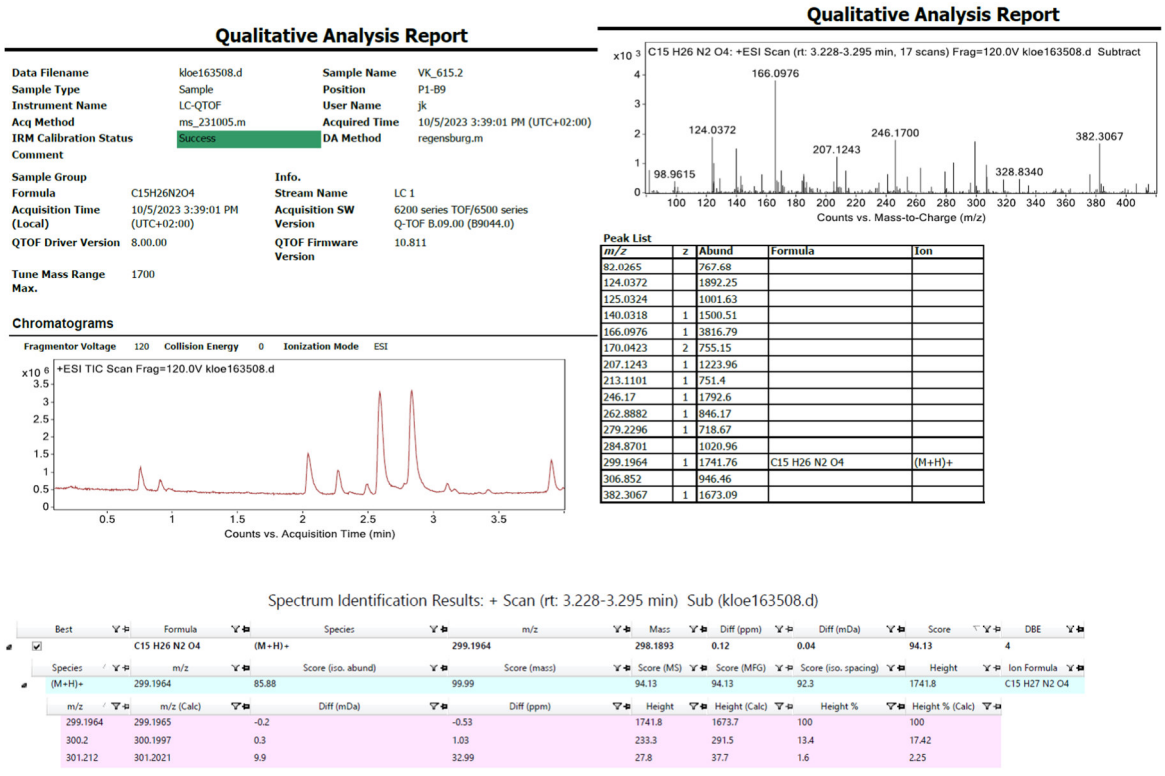

Figure 2-5. Original mass spectroscopy data for the detection of the tempo adduct TEMPO-B.

2.7.5 Photochemical Procedure and Further Transformations

General Procedure for Photocatalytic Hydroformylation of alkenes:

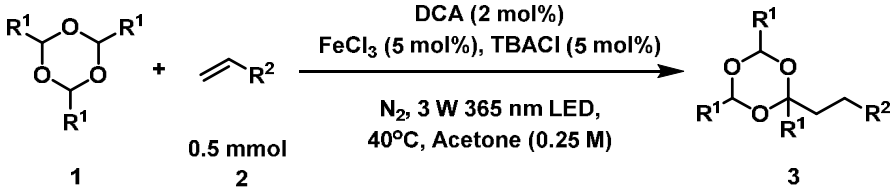

An oven-dried glass vial (4 mL size) equipped with a stirring bar was charged with dicyanoanthracene (DCA) (2.3 mg, 2 mol%, 0.02 equiv), trioxane **1** (6 equiv or 15 equiv), followed by the addition of acetone (2 mL or 1 mL) to the reaction vessel. Then $FeCl_3$ (100µL of 0.5 M anhydrous $FeCl_3$ stock solution in acetone, 5 mol%) and TBACl (100 µL of 0.5 M anhydrous TBACl stock solution in acetone, 5 mol%) was added to the reaction mixture. The reaction vial was then sealed with a rubber septum, and the mixture was degassed by sparging nitrogen gas for 10 min. Afterwards alkene **2** (0.5 mmol, 1 equiv) were added sequentially. The reaction mixture was then irradiated at 365 nm for 24 h. Later, the reaction mixture was transferred to a round bottom flask and concentrated *in vacuo*. The crude mixture was purified using chromatography using hexanes and ethyl acetate to afford the pure product **3**.

Note: *In the case of solid alkenes, they were charged in the reaction vial before degassing the reaction mixture.*

3-(1,3,5-trioxan-2-yl)propanenitrile (**3a**)*

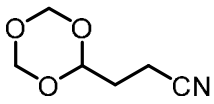

Following GP, **3a** was prepared from 1,3,5-trioxane (**1a**) (270 mg, 3 mmol, 6 equiv) and acrylonitrile (**2a**) (32.7 µL, 0.5 mmol, 1 equiv). The crude mixture was purified by column chromatography (Hexanes:EtOAc- 3:1, R_f = 0.3) to afford **3a** as colourless oil (59 mg, 82%).

^{1}H NMR (300 MHz, Chloroform-*d*) δ 5.26 – 5.20 (m, 2H), 5.14 – 5.03 (m, 3H), 2.53 (t, *J* = 7.4 Hz, 2H), 2.04 (td, *J* = 7.4, 4.7 Hz, 2H **^{13}C NMR (75 MHz, Chloroform-*d*)** δ 119.25, 99.18, 93.28, 30.10, 11.37. **HRMS (ESI):** exact m/z calculated for $C_6H_{13}N_2O_3$ ($M+NH_4+$) 161.0921; Found 161.0923 **IR (cm^{-1}):** 752, 805, 946, 1028, 1107, 1166, 1259, 1367, 1457, 1539, 1733, 2855, 2926

Ethyl 3-(1,3,5-trioxan-2-yl)propanoate (**3b**)*

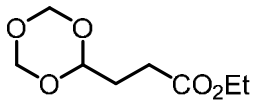

Following GP, **3b** was prepared from 1,3,5-trioxane (**1a**) (270 mg, 3 mmol, 6 equiv) and ethyl acrylate (**2b**) (53.2 µL, 0.5 mmol, 1 equiv). The crude mixture was purified by column chromatography (Hexanes:EtOAc- 1:1, R_f = 0.6) to afford **3b** as colourless oil (66.5 mg, 70%).

^{1}H NMR (400 MHz, Chloroform-*d*) δ 5.18 – 5.15 (m, 2H), 5.06 – 5.03 (m, 2H), 4.97 (t, *J* = 5.0 Hz, 1H), 4.11 (q, *J* = 7.1 Hz, 2H), 2.43 (t, *J* = 7.4 Hz, 2H), 1.98 (td, *J* = 7.4, 5.0 Hz, 2H), 1.23 (t, *J* = 7.2 Hz, 3H). **^{13}C NMR (101 MHz, Chloroform-*d*)** δ 173.03, 100.78, 93.31, 60.55, 29.50, 27.94, 14.28. **HRMS (ESI):** exact m/z calculated for $C_8H_{15}O$ (M+H+) 191.0914; Found 191.0916 **IR (cm^{-1}):** 700, 760, 812, 890, 950, 1066, 1162, 1259, 1371, 1446, 1729, 2870, 2981.

Dimethyl 2-((1,3,5-trioxan-2-yl)methyl)succinate (**3c**)*

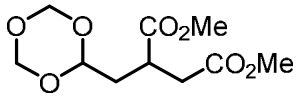

Following GP, **3c** was prepared from 1,3,5-trioxane (**1a**) (270 mg, 3 mmol, 6 equiv) and dimethylitaconate (**2c**) (70 µL, 0.5 mmol, 1 equiv). The crude mixture was purified by column chromatography (Hexanes:EtOAc- 1:1, R_f = 0.45) to afford **3c** as colourless oil (87 mg, 70%).

^{1}H NMR (400 MHz, Chloroform-d) δ 5.15 (dq, J = 5.5, 2.0 Hz, 2H), 5.03 (dd, J = 5.8, 3.9 Hz, 2H), 4.98 (q, J = 4.8 Hz, 1H), 3.69 – 3.60 (m, 7H), 3.09 – 2.98 (m, 1H), 2.76 – 2.66 (m, 1H), 2.64 – 2.52 (m, 1H), 2.09 (dtd, J = 13.9, 6.6, 4.3 Hz, 1H), 1.85 (dt, J = 14.2, 5.9 Hz, 1H). **^{13}C NMR (101 MHz, Chloroform-*d*)** δ 174.55, 172.07, 100.23, 93.27, 93.24, 52.14, 51.85, 36.23, 35.93, 35.75. **HRMS (ESI):** exact m/z calculated for $C_{10}H_2NO_7$ (M+NH_4+) 266.1234; Found 266.1237. **IR (cm^{-1}):** 735, 849, 890, 943, 998, 1051, 1159, 1263, 1367, 1438, 1725, 2113, 2858, 2955

Diethyl 2-(1,3,5-trioxan-2-yl)succinate (**3d**)*

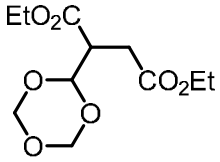

Following GP, **3d** was prepared from 1,3,5-trioxane (**1a**) (270 mg, 3 mmol, 6 equiv) and diethylmaleate (**2d**) (81 µL, 0.5 mmol, 1 equiv). The crude mixture was purified by column chromatography (Hexanes:EtOAc- 1:1, R_f = 0.45) to afford **3d** as colourless oil (92 mg, 70%).

^{1}H NMR (300 MHz, Chloroform-*d*) δ 5.27 (d, *J* = 4.3 Hz, 1H), 5.18 (ddd, *J* = 6.2, 3.6, 1.2 Hz, 2H), 5.07 (dd, *J* = 10.9, 6.3 Hz, 2H), 4.15 (dq, *J* = 14.2, 7.1 Hz, 4H), 3.21 (dt, *J* = 9.1, 4.5 Hz, 1H), 2.88 – 2.70 (m, 2H), 1.24 (td, *J* = 7.1, 3.3 Hz, 6H). **^{13}C NMR (75 MHz, Chloroform-*d*)** δ 172.02, 170.38, 100.30, 93.30, 93.28, 61.39, 60.82, 46.21, 30.25, 14.28, 14.19. **HRMS (ESI):** exact m/z calculated for $C_{11}H_{22}NO_7$ ($M+NH_4^+$) 280.1391; Found 280.1392 **.IR (cm^{-1}):** 805, 849, 954, 1028, 1095, 1267, 1371, 1461, 1729, 1777, 2981, 3435.

2-(phenyl(1,3,5-trioxan-2-yl)methyl)malononitrile (**3e**)*

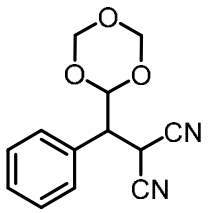

Following GP, **3e** was prepared from 1,3,5-trioxane (**1a)** (270 mg, 3 mmol, 6 equiv) and benzylidene malononitrile (**2e**) (77 mg, 0.5 mmol, 1 equiv). The crude mixture was purified by column chromatography (Hexanes:EtOAc- 1:1, R_f = 0.5) to afford **3e** as colourless oil (110 mg, 90%).

^{1}H NMR (400 MHz, Chloroform-*d*) δ 7.44 (m, 5h), 5.38 (d, *J* = 5.0 Hz, 1H), 5.33 (dd, *J* = 6.3, 1.2 Hz, 1H), 5.23 (dd, *J* = 6.3, 1.3 Hz, 1H), 5.16 (d, *J* = 6.3 Hz, 1H), 5.09 (d, *J* = 6.4 Hz, 1H), 4.45 (d, *J* = 5.6 Hz, 1H), 3.47 (t, *J* = 5.2 Hz, 1H). **^{13}C NMR (101 MHz, Chloroform-*d*)** δ132.31, 129.69, 129.40, 129.06, 111.91, 111.62, 99.94, 93.33, 93.28, 49.86, 24.82. **HRMS (ESI):** exact m/z calculated for $C_{13}H_{16}N_3O_3$ ($M+NH_4^+$) 262.1186;

Found 262.1186 **IR (cm^{-1}):** 700, 879, 946, 984,1058, 1125, 1166, 1215, 1267, 1394, 1457, 1498, 1602, 1707, 2870.

N-phenly-3-(1.3.5-trioxan-2-yl)propanamide (**3f**)

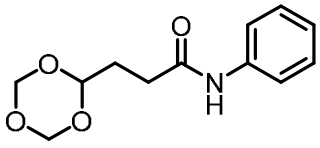

Following GP, **3f** was prepared from 1,3,5-trioxane (**1a**) (270 mg, 3 mmol, 6 equiv) and N-phenyl acrylamide (**2f**) (74 mg, 0.5 mmol, 1 equiv). The crude mixture was purified by column chromatography (Hexanes:EtOAc- 1:1, R_f = 0.2) to afford **3f** as a white solid (91 mg, 77%).

^{1}H NMR (300 MHz, Chloroform-*d*) δ 7.78 (s, 1H), 7.51 – 7.49 (m, 2H), 7.31 – 7.29 (m, 2H), 7.11 – 7.05 (m, 1H), 5.19 (d, *J* = 6.7 Hz, 2H), 5.08 – 5.04 (m, 3H), 2.52 (t, *J* = 7.2 Hz, 2H), 2.10 (td, *J* = 7.1, 4.7 Hz, 2H). **^{13}C NMR (75 MHz, Chloroform-*d*)** δ 170.80, 138.04, 129.03, 124.29, 119.96, 100.82, 93.31, 30.75, 29.73. **HRMS (ESI):** exact m/z calculated for $C_{12}H_{15}NO_4$ (M+H+) 238.1074; Found 238.1076. **IR (cm^{-1}): 693,** 753, 893, 954, 984, 1047, 1163, 1375, 1443, 1528, 1599, 1655, 2870, 3288. **m. p.** 136 – 137 °C

2-(2-(phenylsulfonyl)ethyl)-1,3,5-trioxane (**3g**)

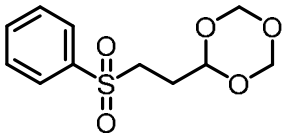

Following GP, **3g** was prepared from 1,3,5-trioxane (**1a**) (270 mg, 3 mmol, 6 equiv) and phenyl vinylsulfone (**2g**) (84 mg, 0.5 mmol, 1 equiv). The crude mixture was purified by column chromatography (Hexanes:EtOAc- 1:1, R_f = 0.5) to afford **3g** as colourless oil (93 mg, 72%).

^{1}H NMR (400 MHz, Chloroform-*d*) δ 7.94 – 7.87 (m, 2H), 7.69 – 7.63 (m, 1H), 7.57 (dd, *J* = 8.3, 6.9 Hz, 2H), 5.14 (d, *J* = 6.7 Hz, 2H), 5.06 (t, *J* = 4.5 Hz, 1H), 5.03 (d, *J* = 6.8 Hz, 2H), 3.32 – 3.23 (m, 2H), 2.15 – 2.05 (m, 2H). **^{13}C NMR (101 MHz, Chloroform-*d*)** δ 138.99, 133.94, 129.47, 128.15, 99.15, 93.20, 50.43, 27.81. **HRMS**

(ESI): exact m/z calculated for $C_{11}H_{18}NO_5S$ (M+NH_4+) 276.0902; Found 276.0902. **IR (cm^{-1}):** 690, 723, 746, 880, 932, 1051, 1088, 1148, 1390, 1450, 2855, 2922.

3-(1,3,5-trioxan-2-yl)pyrrolidine-2,5-dione (**3h**)*

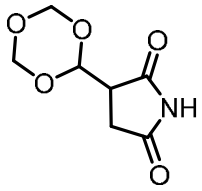

Following GP, **3h** was prepared from 1,3,5-trioxane (**1a**) (270 mg, 3 mmol, 6 equiv) and maleimide (**2h**) (48 mg, 0.5 mmol, 1 equiv). The crude mixture was purified by column chromatography (Hexanes:EtOAc- 3:1, R_f = 0.4) to afford **3h** as colourless oil (67 mg, 72%).

^{1}H NMR (300 MHz, DMSO-*d*$_6$) δ 5.42 (d, *J* = 2.7 Hz, 1H), 5.14 (t, *J* = 5.4 Hz, 4H), 3.21 (ddd, *J* = 7.7, 6.0, 2.6 Hz, 1H), 2.69 (d, *J* = 2.5 Hz, 1H), 2.66 (s, 1H). **^{13}C NMR (75 MHz, DMSO-*d*$_6$)** δ 178.53, 177.23, 98.86, 93.01, 92.76, 46.08, 30.50. **HRMS (ESI):** exact m/z calculated for $C_7H_{13}NO_5$ (M+NH_4+) 205.0819; Found 220.0822 **IR (cm^{-1}):** 767, 823, 864, 939, 995, 1032, 1066, 1125, 1177, 1289, 1356, 1394, 1476, 1498, 1699, 1774, 2094, 2780, 3063.

3-(1,3,5-trioxan-2-yl)dihydrofuran-2,5-dione (**3i**)

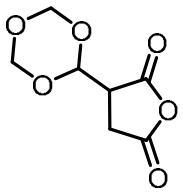

Following GP, **3i** was prepared from 1,3,5-trioxane (**1a**) (270 mg, 3 mmol, 6 equiv) and maleic anhydride (**2i**) (49 mg, 0.5 mmol, 1 equiv). The crude mixture was purified by column chromatography (Hexanes:EtOAc- 3:1, R_f = 0.35) to afford **3i** as colourless oil (64 mg, 68%).

^{1}H NMR (300 MHz, Acetone-*d*$_6$) δ 5.55 (d, *J* = 2.7 Hz, 1H), 5.28 – 5.19 (m, 4H), 3.67 (td, *J* = 7.3, 2.8 Hz, 1H), 3.20 (d, *J* = 7.1 Hz, 2H). **^{13}C NMR (75 MHz, Acetone-*d*$_6$)** δ 171.45, 170.81, 99.06, 93.81, 93.62, 46.79, 29.90. **HRMS (ESI):** exact m/z calculated for $C_7H_{12}NO_6$ (M+NH_4+) 206.0659; Found 206.0658 **IR (cm^{-1}):** 805, 849, 954, 1028, 1095, 1267, 1371, 1461, 1729, 1777, 2981, 3435

3-methyl-4-(1,3,5-trioxan-2-yl)dihydrofuran-2,5-dione (**3j**)*

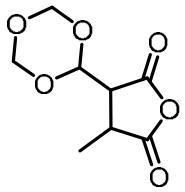

Following GP, **3j** was prepared from 1,3,5-trioxane **1a** (270 mg, 3 mmol, 6 equiv) and citraconic anhydride (**2j**) (45 µL, 0.5 mmol, 1 equiv). The crude mixture was purified by column chromatography (Hexanes:EtOAc- 1:1, R_f = 0.4) to afford **3j** as colourless oil (30 mg, 30%).

^{1}H NMR (400 MHz, Chloroform-*d*) δ 5.35 (d, *J* = 2.3 Hz, 1H), 5.28 – 5.21 (m, 3H), 5.09 – 5.05 (m, 2H), 3.37 – 3.24 (m, 2H), 1.57 (d, *J* = 6.9 Hz, 3H). **^{13}C NMR (101 MHz, Chloroform-*d*)** δ 173.18, 168.58, 98.58, 93.30, 93.27, 48.51, 37.70, 10.35. **HRMS (ESI):** exact m/z calculated for $C_8H_{14}NO_6$ (M+NH_4+) 220.0816; Found 220.0816 **IR (cm^{-1}):** 700, 909, 1069, 1166, 1125, 1192, 1271, 1304, 1401, 1353, 1453, 1699, 2102, 2937.

1-cyano-2-(1,3,5-trioxan-2yl)ethyl acetate (**3k**)

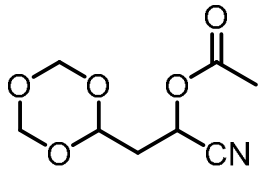

Following GP, **3k** was prepared from 1,3,5-trioxane (**1a**) (270 mg, 3 mmol, 6 equiv) and 1-cyanovinyl acetate (**2k**) (52.3 µL, 0.5 mmol, 1 equiv). The crude mixture was purified by column chromatography (Hexanes:EtOAc 3:1, R_f = 0.3) to afford **3k** as colourless oil (47 mg, 41%).

^{1}H NMR (300 MHz, Chloroform-*d*) δ 5.49 (t, *J* = 7.1 Hz, 1H), 5.23 – 5.20 (m, 2H), 5.13 -5.07 (m, 3H), 2.33 (dd, *J* = 7.2, 5.1 Hz, 2H), 2.15 (s, 3H). **^{13}C NMR (75 MHz, Chloroform-*d*)** δ 168.92, 116.50, 97.56, 93.29, 56.79, 37.02, 20.49. **HRMS (APCI):** exact m/z calculated for $C_8H_{11}NO_5$ (M+NH_4+) 219.0975; Found 219.0975 **IR (cm^{-1}):** 943, 1040, 1137, 1163, 1215, 372, 1409, 1752, 2870.

Ethyl 4-oxopentanoate (**3l**)*

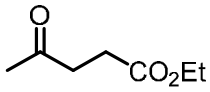

Following GP, **3l** was prepared from paraldehyde (**1b**) (1 mL, 15 equiv) and ethyl acrylate (**2b**) (53.2 µL, 0.5 mmol, 1 equiv), dissolved in Acetone (1 mL). The crude mixture was purified by column chromatography (Hexanes:EtOAc- 1:1, R_f = 0.7) to afford **3l** as colourless oil (53 mg, 72%).

^{1}H NMR (400 MHz, Chloroform-*d*) δ 4.10 (q, *J* = 7.1 Hz, 2H), 2.73 (t, *J* = 6.6 Hz, 2H), 2.54 (t, *J* = 6.5 Hz, 2H), 2.17 (s, 3H), 1.23 (t, *J* = 7.1 Hz, 3H). **^{13}C NMR (101 MHz, Chloroform-*d*)** δ 206.81, 172.84, 60.72, 38.05, 29.98, 28.12, 14.26.
Analytical data is in accoradance to the literature.[32]

Diethyl 2-acetylsuccinate (**3m**)

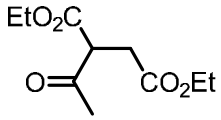

Following GP, **3m** was prepared from paraldehyde (**1b**) (1 mL, 15 equiv) and diethylmaleate (**2d**) (81 µL, 0.5 mmol, 1 equiv), dissolved in Acetone (1 mL). The crude mixture was purified by column chromatography (Hexanes:EtOAc- 1:1, R_f = 0.6) to afford **3m** as colourless oil (44 mg, 40%).

^{1}H NMR (300 MHz, Chloroform-*d*) δ 4.20 (q, *J* = 7.1 Hz, 2H), 4.12 (q, *J* = 7.1 Hz, 2H), 3.97 (dd, *J* = 8.1, 6.4 Hz, 1H), 2.96 (dd, *J* = 17.5, 8.1 Hz, 1H), 2.81 (dd, *J* = 17.5, 6.4 Hz, 1H), 2.35 (s, 3H), 1.29 – 1.26 (m, 3H), 1.25 – 1.22 (m, 3H). **^{13}C NMR (75 MHz, Chloroform-*d*)** δ 201.87, 171.46, 168.52, 61.93, 61.12, 54.80, 32.51, 30.05, 14.24, 14.15.
Analytical data is in accoradance to the literature.[33]

2-(2-oxopropyl)succinic acid (**3n**)

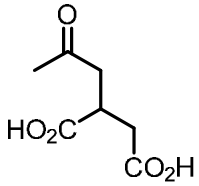

Following GP, **3n** was prepared from paraldehyde (**1b**) (1 mL, 15 equiv) and itaconic acid (**2l**) (48 mg, 0.5 mmol, 1 equiv), dissolved in Acetone (1 mL). The excess paraldehyde was evaporated on rotatory evaporator. Then, the residue was dissolved in a mixture of 1,4-dioxane 1:1 H_2O (2 mL) and transferred to a microwave vial (10 mL), the vial was equipped with a magnetic stir bar, closed with a cap and placed in the microwave reactor. After a reaction time of 30 min at 150 °C, till completion (monitored by TLC, product: Hexanes:EtOAc:Formic Acid 3:1:0.1, R_f = 0.2), the crude product was transferred to a round bottom flask and the solvent was evaporated. Addition of 2 mL of DCM led to the crystallisation, the crystals were filtered and washed with cold DCM (2 mL) to obtain a the desired product **3n** as a white solid (54 mg, 62%).

^{1}H NMR (400 MHz, DMSO-*d*$_6$) δ 12.25 (br, 2H), 3.03-2.94 (m, 1H), 2.82 (dd, *J* = 17.8, 7.0 Hz, 1H), 2.61 (dd, *J* = 17.8, 6.0 Hz, 1H), 2.54-2.45 (m, 1H), 2.36 (dd, *J* = 16.7, 6.0 Hz, 1H), 2.09 (s, 3H). **^{13}C NMR (101 MHz, DMSO-*d*$_6$)** δ 206.51, 175.04, 172.89, 43.73, 36.05, 35.12, 29.84. **HRMS (ESI):** exact m/z calculated for $C_7H_{10}O_5$ $(M–H)^-$ 173.0455; Found 173.046. **IR (cm^{-1}):** 731, 764, 828, 999, 1021, 1218, 1364, 1714, 3444, 3485.

2-(2-oxo-1-phenylpropyl)malononitrile (**3o**)

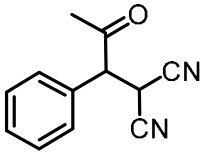

Following GP, **3o** was prepared from paraldehyd (**1b**) (1 mL, 15 equiv) and benzylidene malononitrile (**2e**) (77 mg, 0.5 mmol, 1 equiv), dissolved in Acetone (1 mL). The crude mixture was purified by column chromatography (Hexanes:EtOAc- 1:1, R_f = 0.5) to afford **3o** as colourless oil (56 mg, 57%).

^{1}H NMR (300 MHz, Chloroform-*d*) δ 7.49 – 7.47 (m, 3H), 7.29 – 7.25 (m, 2H) 4.36 (d, *J* = 8.4 Hz, 1H), 4.26 (d, *J* = 8.4 Hz, 1H), 2.18 (s, 3H). **^{13}C NMR (75 MHz, Chloroform-*d*)** δ 201.51, 131.15, 130.28, 130.21, 128.82, 112.05, 111.41, 59.15, 28.41, 25.62.

Analytical data is in accoradance to the literature.[34]

4-(phenylsulfonyl)butan-2-one (**3p**)

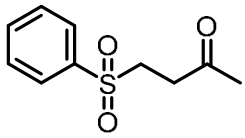

Following GP, **3p** was prepared from paraldehyde (**1b**) (1 mL, 15 equiv) and phenyl vinylsulfone (**2g**) (84 mg, 0.5 mmol, 1 equiv), dissolved in Acetone (1 mL). The crude mixture was purified by column chromatography (Hexanes:EtOAc- 1:1, R_f = 0.6) to afford **3p** as colourless oil (104 mg, 69%).

^{1}H NMR (400 MHz, Chloroform-*d*) δ 7.89 (d, *J* = 7.1 Hz, 2H), 7.66 (t, *J* = 7.4 Hz, 1H), 7.56 (t, *J* = 7.6 Hz ,3H), 3.36 (t, *J* = 7.5 Hz, 2H), 2.91 (t, *J* = 7.5 Hz, 2H), 2.16 (s, 3H). **^{13}C NMR (101 MHz, Chloroform-*d*)** δ 203.78, 139.03, 134.04, 129.51, 128.04, 50.63, 35.96, 29.97.
Analytical data is in accoradance to the literature [34].

5 mmol Scale Reaction

3-(1,3,5-trioxan-2-yl)propanenitrile (**3a**)

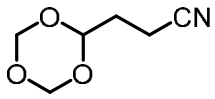

Up-scaling to 5 mmol scale was carried out according to general procedure GP in a flame-dried Schlenk tube (30.0 mL size) using 1,3,5-trioxane (**1a**) (2.7 g, 30 mmol, 6 equiv), acrylonitrile (**2a**) (327.6 µL, 5 mmol, 1 equiv), DCA (22.83 mg, 100 µmol, 2 mol%), $FeCl_3$ (5 mol%, 500µL of 0.5M anhydrous $FeCl_3$ stock solution in acetone) and TBACl (5 mol%, 500 µL of 0.5M anhydrous TBACl stock solution in acetone) dissolved in

acetone (19 mL, total colume 20 mL) to afford **3a** as colourless oil (501 mg, 70%) after chromatography purification on silica gel (Hexanes:EtOAc- 9:1 to 3:1).

Accurate temperature control is crucial for a high yield. We cooled the reaction vial with a ventilator from a distance of 10 cm and kept the light source 3 cm away from the vial. As light source we used two identical LED plates (same plates as shown in Figure 2-1*).*

Unsuccessful Reactions*

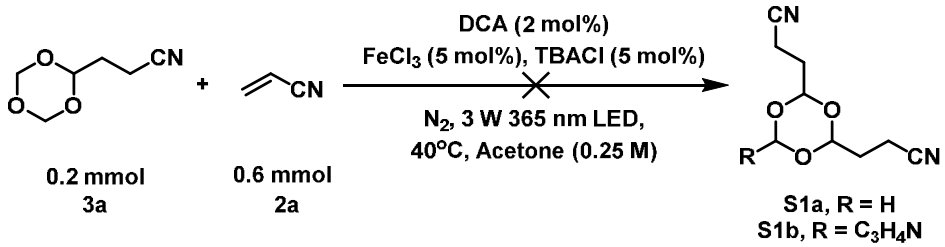

An oven-dried glass vial (4 mL size) equipped with a stirring bar was charged with dicyanoanthracene (DCA) (0.913 mg, 2 mol%, 0.02 equiv), trioxane adduct **3a** (29 mg, 0.2 mmol, 1 equiv), followed by the addition of acetone (0.8 mL) to the reaction vessel. Then $FeCl_3$ (40µL of 0.5 M anhydrous $FeCl_3$ stock solution in acetone, 5 mol%) and TBACl (40 µL of 0.5 M anhydrous TBACl stock solution in acetone, 5 mol%) was added to the reaction mixture. The reaction vial was then sealed with a rubber septum, and the mixture was degassed by sparging nitrogen gas for 10 min. Afterwards alkene **2a** (39 µL, 0.6 mmol, 3 equiv) was added sequentially. The reaction mixture was then irradiated at 365 nm for 48 h. Later, the reaction mixture was transferred to a round bottom flask and concentrated *in vacuo* and analyzed by quantitative NMR using 1,1,2,2-tetrachlorethane as internal standard. No significant conversion was observed.

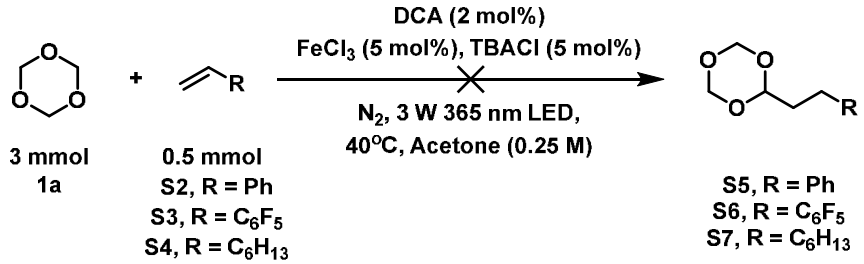

An oven-dried glass vial (4 mL size) equipped with a stirring bar was charged with dicyanoanthracene (DCA) (2.3 mg, 2 mol%, 0.02 equiv), trioxane (**1**) (6 equiv or 15 equiv), followed by the addition of acetone (2 mL or 1 mL) to the reaction vessel. Then $FeCl_3$ (100µL

of 0.5 M anhydrous $FeCl_3$ stock solution in acetone, 5 mol%) and TBACl (100 µL of 0.5 M anhydrous TBACl stock solution in acetone, 5 mol%) was added to the reaction mixture. The reaction vial was then sealed with a rubber septum, and the mixture was degassed by sparging nitrogen gas for 10 min. Afterwards styrene (**S2**), 2,3,4,5,6-pentafluorostyrene (**S3**) or 1-octene (**S4**) (0.5 mmol, 1 equiv) were added sequentially. The reaction mixture was then irradiated at 365 nm for 24 h. Later, the reaction mixture was transferred to a round bottom flask, concentrated *in vacuo* and transferred to a NMR tube for analysis (after removing $FeCl_3$ by silica gel short plug filtration). The experiments resulted in a complex reactions mixture with no product formation (NMR analysis).

Deprotection and Further Tranformations

4-oxobutanenitrile (**4a**)

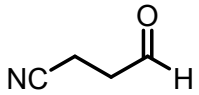

Following GP, **3a** was prepared from 1,3,5-trioxane (**1a**) (270 mg, 3 mmol, 6 equiv) and acrylonitrile (**2a**) (32.7 µL, 0.5 mmol, 1 equiv). The crude reaction solution was transferred to a round bottle flask. After evaporation of the solvent on the rotavap, the residue was dissolved in 1 mL 1,4-dioxane and the solution was transferred to a microwave vial (10 mL). After adding 1 mL of destilled water (total concentration: 0.25 M) and 12.15 mg $FeCl_3$ (= 15 mol%, total cat loading: 20 mol% as 4.05 mg (5 mol%) remained from the first step) the vial was equipped with a magnetic stir bar, closed with a cap and placed in the microwave reactor. After a reaction time of 30 min at 150 °C, the starting material was completely consumed (monitored by TLC). The crude mixture was purified by column chromatography (Hexanes:EtOAc- 3:1, R_f = 0.2) to afford **4a** as colourless oil (33 mg, 80%).

^{1}H NMR (300 MHz, Chloroform-*d*) δ 9.79 (s, 1H), 2.91 (t, *J* = 7.2 Hz, 2H), 2.63 (t, *J* = 7.1 Hz, 2H). **^{13}C NMR (75 MHz, Chloroform-*d*)** δ 197.06, 118.60, 39.09, 10.14.
Analytical data is in accordance to the literature.[35]

Ethyl 4-oxobutanoate (**4b**)

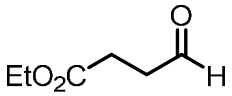

Following GP, **3b** was prepared from 1,3,5-trioxane (**1a**) (270 mg, 3 mmol, 6 equiv) and ethyl acrylate (**2b**) (53.2 µL, 0.5 mmol, 1 equiv). The crude reaction solution was transferred to a round bottle flask. After evaporation of the solvent on the rotavap, the residue was dissolved in 2 mL 1,4-dioxane (total concentration: 0.25 M) and the solution was transferred to a microwave vial (10 mL). After adding 12.15 mg $FeCl_3$ (= 15 mol%, total cat loading: 20 mol% as 4.05 mg (5 mol%) remained from the first step), the vial was equipped with a magnetic stir bar, closed with a cap and placed in the microwave reactor. After a reaction time of 30 min at 100 °C, the starting material was completely consumed (monitored by TLC). The crude mixture was purified by column chromatography (Hexanes:EtOAc- 3:1, R_f = 0.45) to afford **4b** as yellowish oil (44 mg, 68%).

^{1}H NMR (300 MHz, Chloroform-*d*) δ 9.81 (t, *J* = 0.7 Hz, 1H), 4.14 (q, *J* = 7.1 Hz, 2H), 2.82 – 2.77 (m, 2H), 2.64 – 2.59 (m, 2H), 1.26 (t, *J* = 7.1, 3H). **^{13}C NMR (75 MHz, Chloroform-*d*)** δ 200.20, 172.38, 60.97, 38.69, 26.74, 14.30.
Analytical data is in accordance to the literature.[36]

3-(phenylsulfonyl)propanal (**4c**)

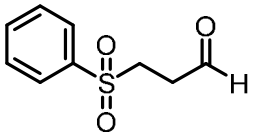

Following GP, **3g** was prepared from 1,3,5-trioxane (**1a**) (270 mg, 3 mmol, 6 equiv) and phenyl vinylsulfone (**2g**) (84 mg, 0.5 mmol, 1 equiv). The crude reaction solution was transferred to a round bottle flask. After evaporation of the solvent on the rotavap, the residue was dissolved in 1 mL 1,4-dioxane and the solution was transferred to a microwave vial (10 mL). After adding 1 mL of destilled water (total concentration: 0.25 M; 5 mol% $FeCl_3$ was still present from the first step and no additional $FeCl_3$ was added), the vial was equipped with a magnetic stir bar, closed with a cap and placed in the microwave reactor. After a reaction time of 30 min at 150 °C, the starting material was

completely consumed (monitored by TLC). The crude mixture was purified by column chromatography (Hexanes:EtOAc- 3:1, R_f = 0.3) to afford **4c** as yellowish oil (70 mg, 70%).

^{1}H NMR (300 MHz, Chloroform-*d*) δ 9.74 (s, 1H), 7.92 – 7.89 (m, 2H), 7.68 – 7.65 (m, 1H), 7.61 – 7.56 (m 2H), 3.41 (t, *J* = 7.4 Hz, 2H), 2.97 (t, *J* = 7.4 Hz, 2H). **^{13}C NMR (75 MHz, Chloroform-*d*)** δ 197.01, 138.72, 134.23, 129.62, 128.15, 49.20, 36.64.
Analytical data is in accordance to the literature.[1]

3-cyanopropanoic acid (**5a**)

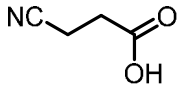

Following GP, **3a** was prepared from 1,3,5-trioxane (**1a**) (270 mg, 3 mmol, 6 equiv) and acrylonitrile (**2a**) (32.7 µL, 0.5 mmol, 1 equiv). The crude reaction solution was transferred to a round bottom flask. After the excess of the trioxane was removed by sublimation by rotary evaporator, the crude reaction mixture was dissolved in acetone (2 mL) and irradiated open to air with UV light (365 nm) for additional 48 h. After completion (monitored by TLC) the reaction mixture was transferred to a round bottom flask and concentrated *in vacuo*. The crude product was purified by short plug silica gel chromatography (Dichlormethan:EtOAc 1:0 to 0:1, R_f = 0.2 with Hexanes:EtOAc:Formic Acid 1:1:0.1) to obtain the desired product **5a** as colourless solid (40 mg, 81%)

^{1}H NMR (300 MHz, Chloroform-*d*) δ 2.78-2.74 (m, 2H), 2.69-2.65 (m 2H). **^{13}C NMR (75 MHz, Chloroform-*d*)** δ 175.29, 118.34, 29.80, 12.87.
Analytical data is in accordance to the literature.[37]

4-ethoxy-4-oxobutanoic acid (5**b**)

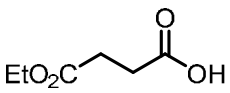

Following GP, **3g** was prepared from 1,3,5-trioxane (**1a**) (270 mg, 3 mmol, 6 equiv) and ethyl acrylate (**2b**) (53.2 µL, 0.5 mmol, 1 equiv). The crude reaction solution was

transferred to a round bottom flask. After the excess of the trioxane was removed by sublimation by rotavap, the crude reaction mixture was dissolved in acetone (2 mL) and irradiated open to air with UV light (365 nm) for additional 48 h. After completion (judged by TLC) the reaction mixture was transferred to a round bottom flask and concentrated *in vacuo*. The crude product was purified by silica gel chromatography (Hexanes:EtOAc 3:1 to 1:1, R_f = 0.3 with Hexanes:EtOAc:Formic Acid- 1:1:0.1) and subsequently extracted under basic and acidic conditions to obtain the desired product **5b** as colourless solid (58 mg, 65%)

^{1}H NMR (400 MHz, Chloroform-*d*) δ 4.16 (q, *J* = 7.2, 2H), 2.70 – 2.67 (m, 2H), 2.64 – 2.60 (m, 2H),1.26 (t, *J* = 7.2 Hz, 2H). **^{13}C NMR (101 MHz, Chloroform-*d*)** δ 178.12, 172.39, 61.02, 29.04, 29.02, 14.24.
Analytical data is in accordance to the literature.[38]

3-(phenylsulfonyl)propanoic acid (**5c**)

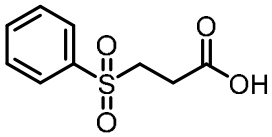

Following GP, **3g** was prepared from 1,3,5-trioxane (**1a**) (270 mg, 3 mmol, 6 equiv) and phenyl vinylsulfone (**2g**) (84 mg, 0.5 mmol, 1 equiv). The crude reaction solution was transferred to a round bottom flask. After the excess of the trioxane was removed by sublimation by rotavap, the crude reaction mixture was dissolved in acetone (2 mL) and irradiated open to air with UV light (365 nm) for additional 48 h. After completion (judged by TLC) the reaction mixture was transferred to a round bottom flask and concentrated *in vacuo*. The crude product was purified by silica gel chromatography (Hexanes:EtOAc 3:1 to 1:1, R_f = 0.4 with Hexanes:EtOAc:Formic Acid- 1:1:0.1) and subsequently extracted under basic and acidic conditions to obtain the desired product **5c** as colourless solid (55 mg, 50%)

^{1}H NMR (300 MHz, Chloroform-*d*) δ 7.93-7.90 (m, 2H), 7.71-7.66 (m, 1H), 7.61-7.56 (m, 2H), 3.42 (t, *J* = 7.6 Hz, 2H), 2.79 (t, *J* = 7.6 Hz, 2H). **^{13}C NMR (75 MHz, Chloroform-*d*)** δ 175.16, 138.38, 134.31, 129.63, 128.28, 51.31, 27.68.
Analytical data is in accordance to the literature.[39]

4-oxo-6-(phenylsulfonyl)hexanenitrile (**6**)

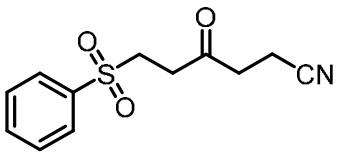

An oven-dried glass vial (4 mL size) equipped with a stirring bar was charged with aldehyde **4c** (99 mg, 0.5 mmol, 2 equiv), diphenylanthracene (0.83 mg, 1 mol%, 0.01 equiv) and magnesium chloride (2.38 mg, 10 mol%, 0.1 equiv). Followed by the addition of dry MeCN (2mL) to the reaction vessel. Then $FeCl_3$ (50 µL of 0.25M anhydrous $FeCl_3$ solution in dry MeCN) was added to the reaction mixture. The reaction vessel was then sealed with a rubber septum and the mixture was then degassed by sparging nitrogen gas for 10 min. Afterwards, hydrochloric acid (25 µL of 37% aqueous HCl) and acrylonitrile (**2a**) (16 µL, 0.25 mmol, 1 equiv) were added sequentially under nitrogen flow. The reaction mixture was then irradiated at 365 nm for 24 h. Later, the reaction mixture was transferred to a round bottom flask and concentrated in vacuo. The crude mixture was purified using chromatography (Hexanes:EtOAc- 7:3, to 3:2, R_f = 0.3 for Hexanes:EtOAc- 1:1) to afford **6** as yellowish oil (47 mg, 75%).

^{1}H NMR (400 MHz, Chloroform-*d*) δ 7.92 – 7.87 (m, 2H), 7.74 – 7.65 (m, 1H), 7.62 – 7.55 (m, 2H), 3.42 (t, *J* = 7.3 Hz, 2H), 2.94 (t, *J* = 7.3 Hz, 2H), 2.86 (t, *J* = 7.0 Hz, 2H), 2.57 (t, *J* = 7.0 Hz, 2H). **^{13}C NMR (101 MHz, $CDCl_3$)** δ 201.89, 138.86, 134.26, 134.20, 129.65, 128.08, 118.65, 50.50, 50.47, 38.01, 34.89, 11.46. **HRMS (ESI):** exact m/z calculated for $C_{12}H_{13}NO_3S$ (M+H+) 252.0689; Found 252.0694 **IR (cm^{-1}):** 690, 746, 1085, 1144, 1304, 1413, 1446, 1722, 2251, 2933.

2.7.6 NMR Spectra

3-(1,3,5-trioxan-2-yl)propanenitrile (**3a**)

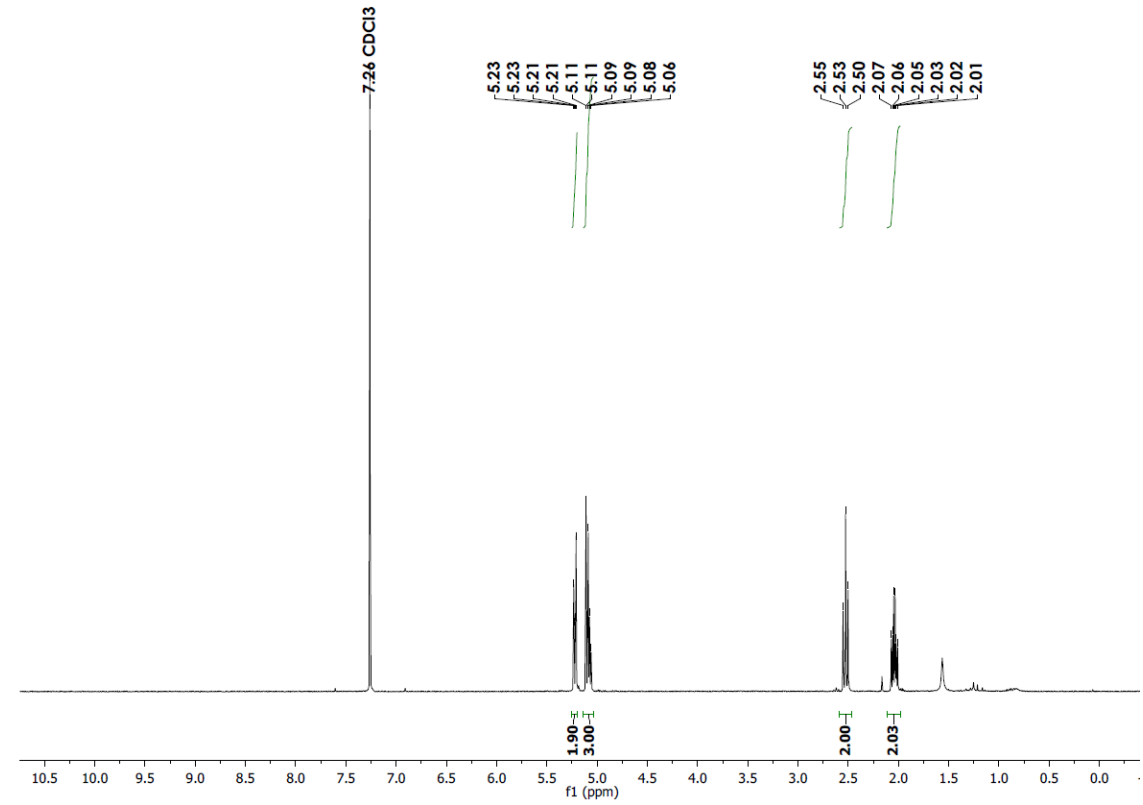

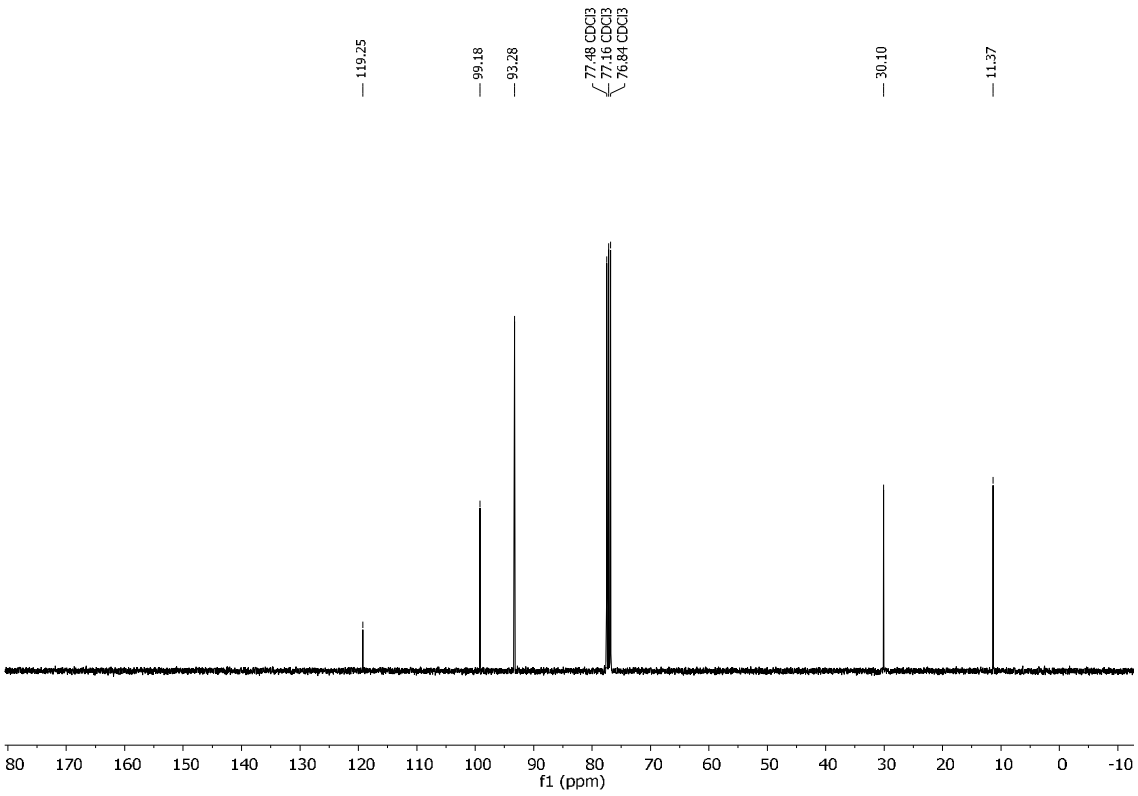

Ethyl 3-(1,3,5-trioxan-2-yl)propanoate (**3b**)

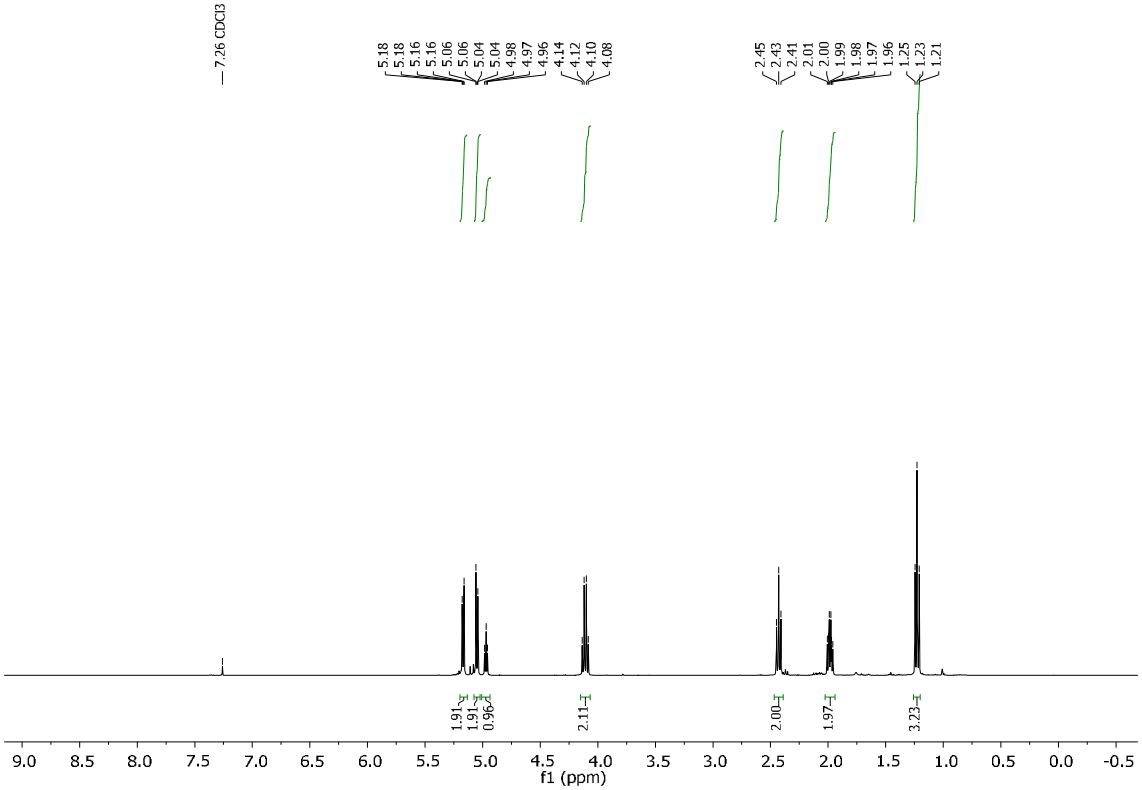

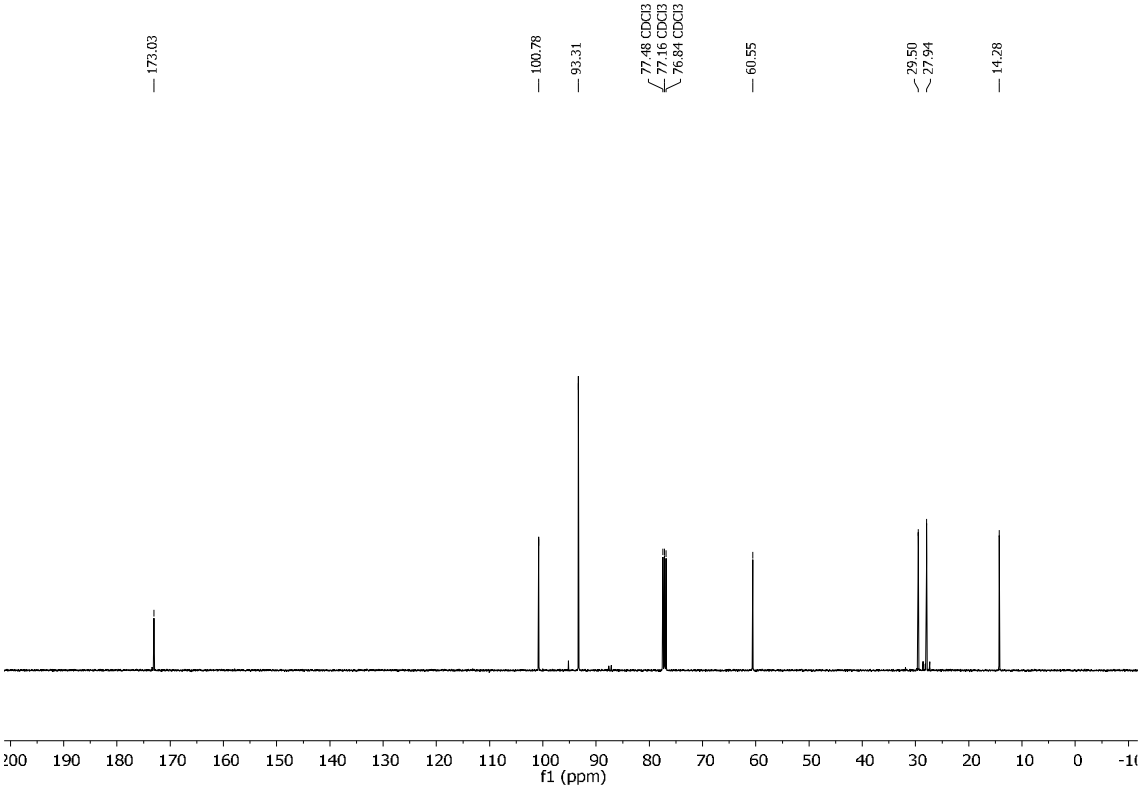

Dimethyl 2-(1,3,5-trioxan-2-yl)methyl)succinate (**3c**)

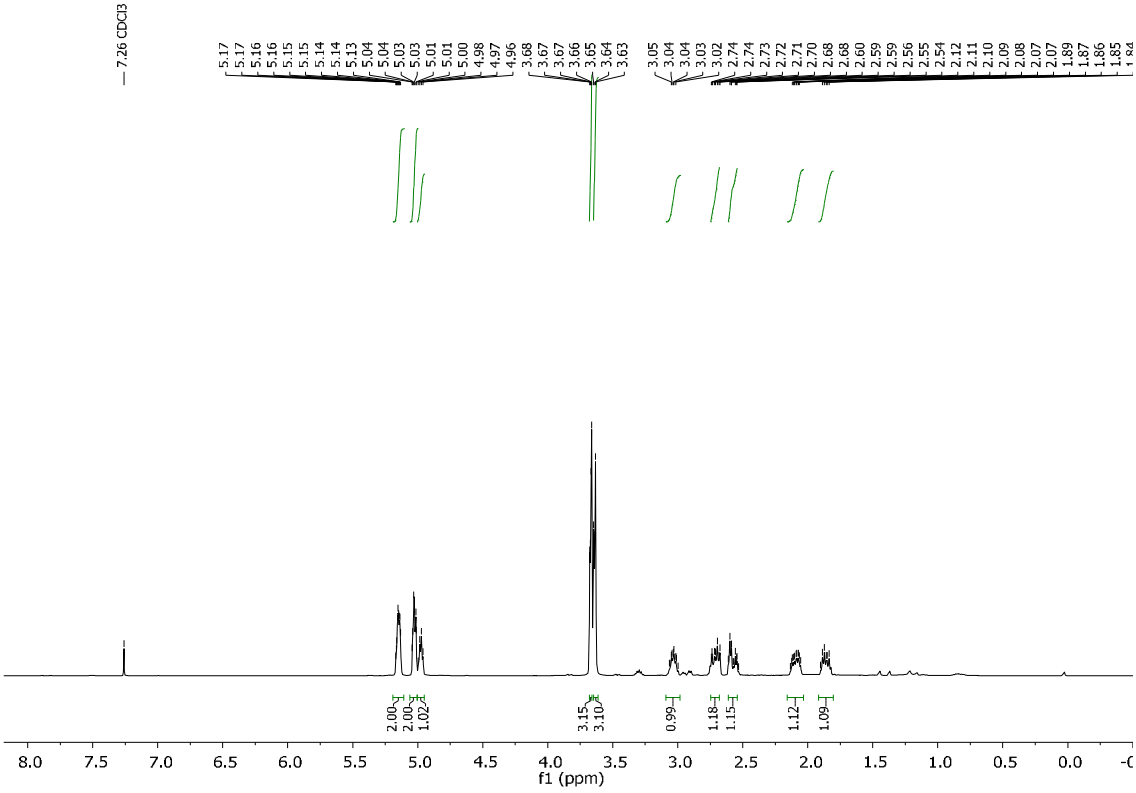

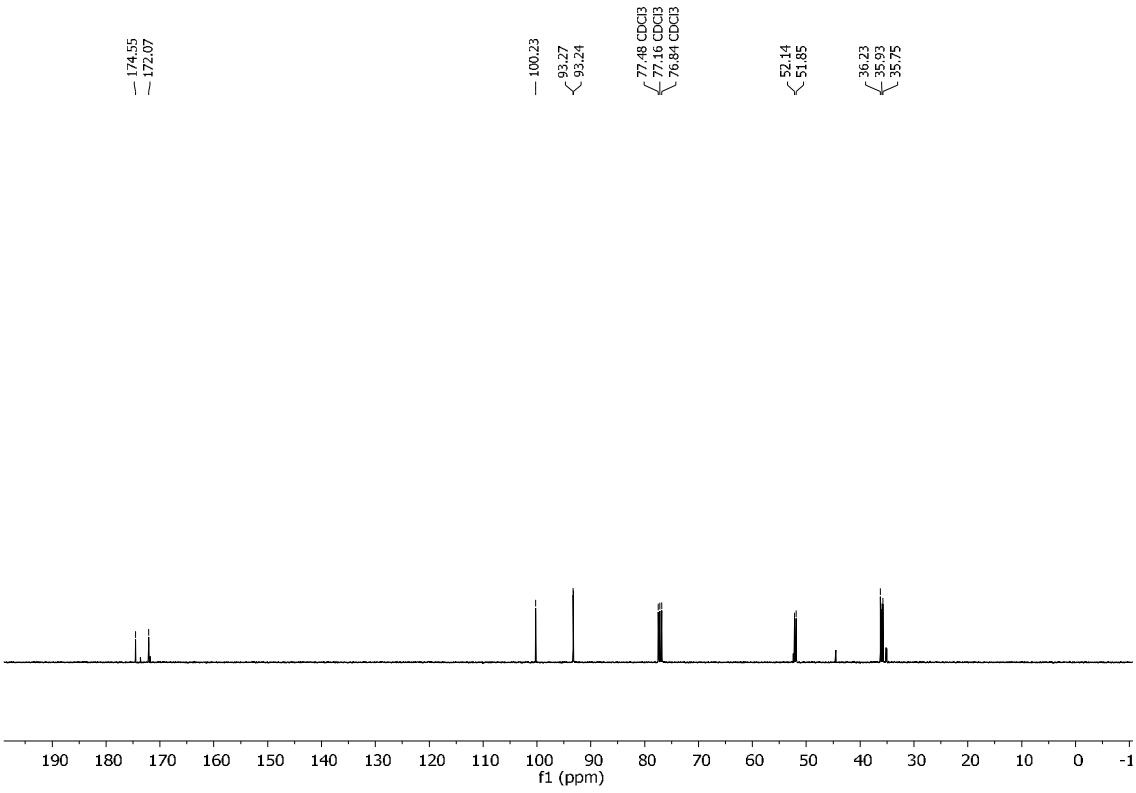

Diethyl 2-(1,3,5-trioxan-2-yl)succinate (**3d**)

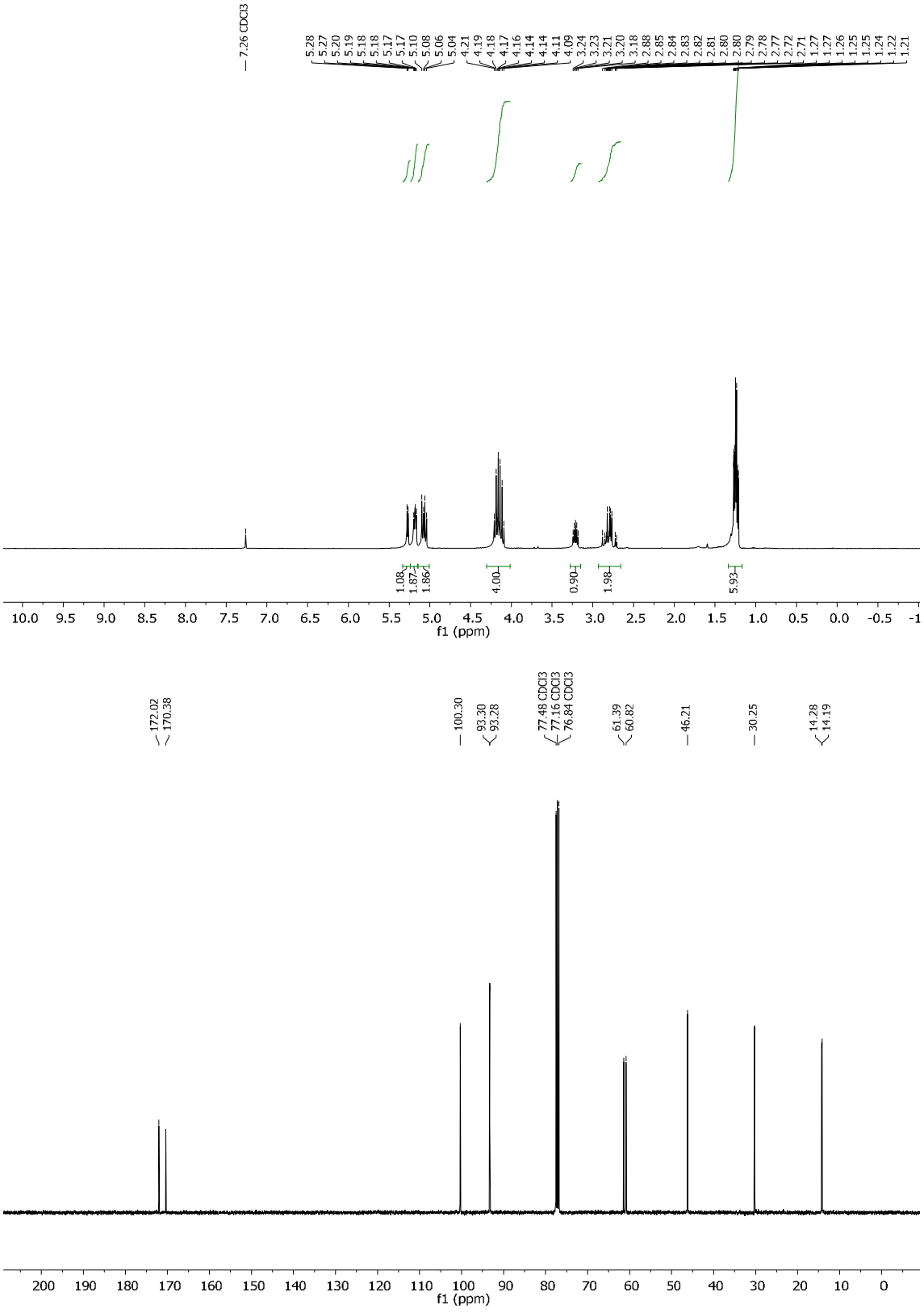

2-(phenyl(1,3,5-trioxan-2-yl)methyl)malononitrile (**3e**)

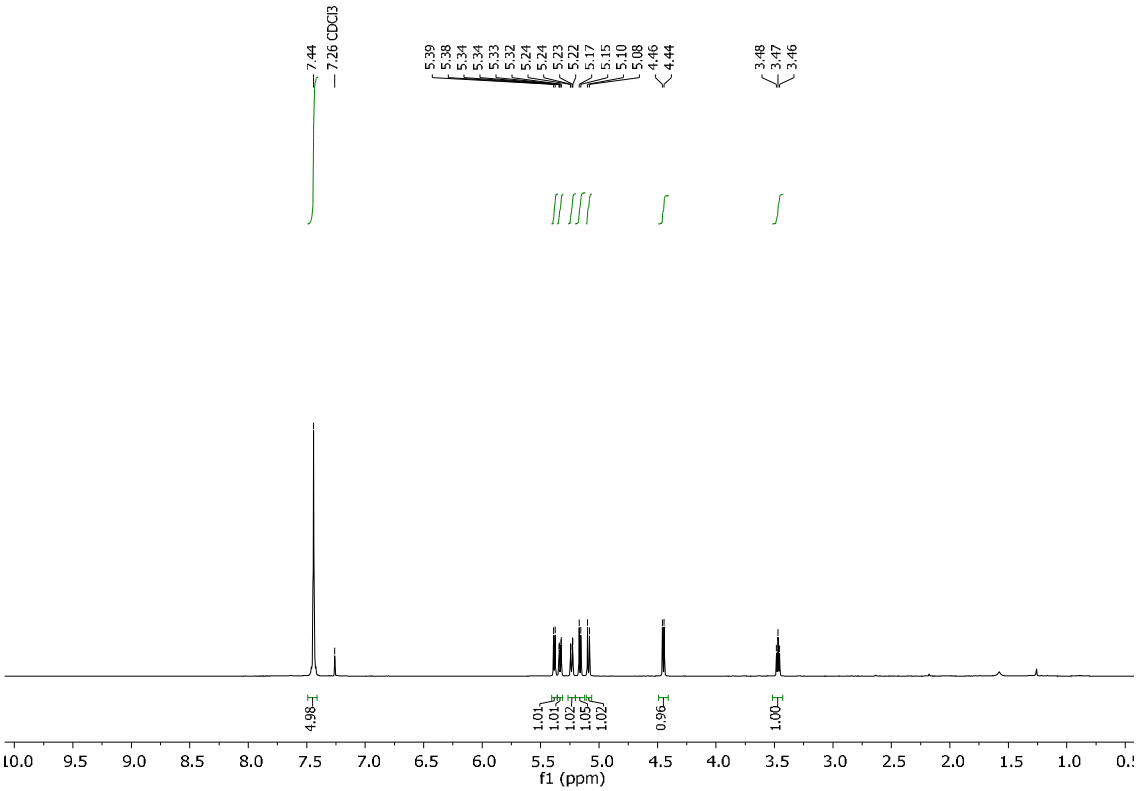

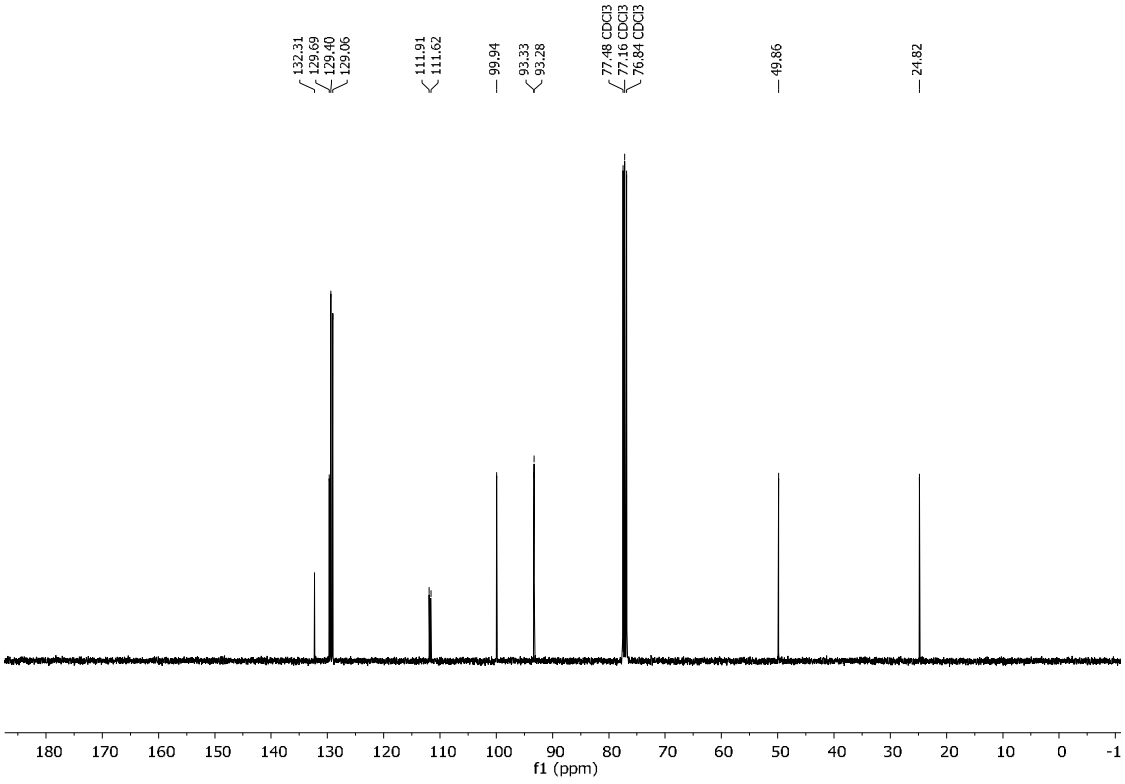

N-phenly-3-(1.3.5-trioxan-2-yl)propanamide (**3f**)

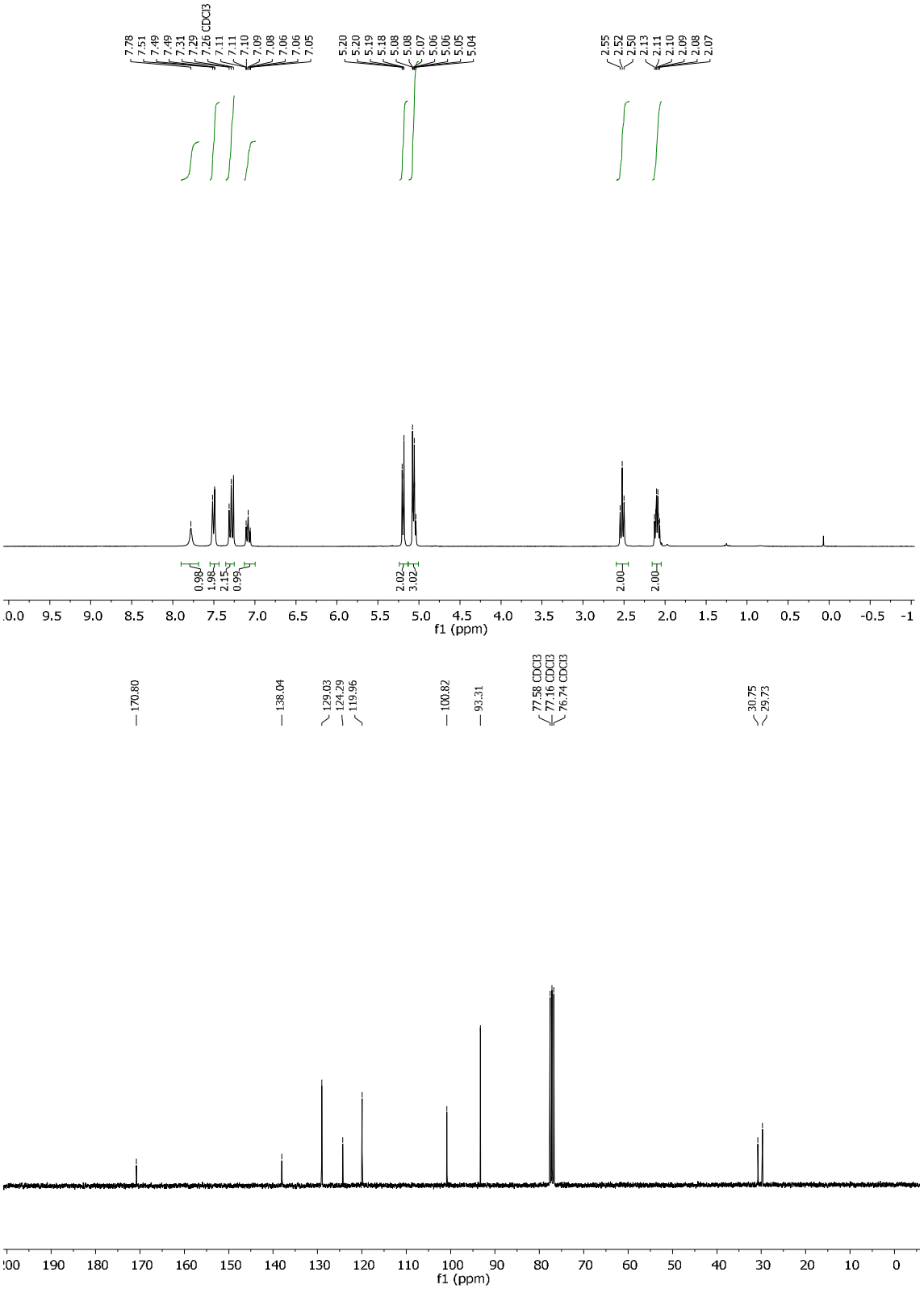

2-(2-phenylsulfonyl)ethyl)-1,3,5-trioxane (**3g**)

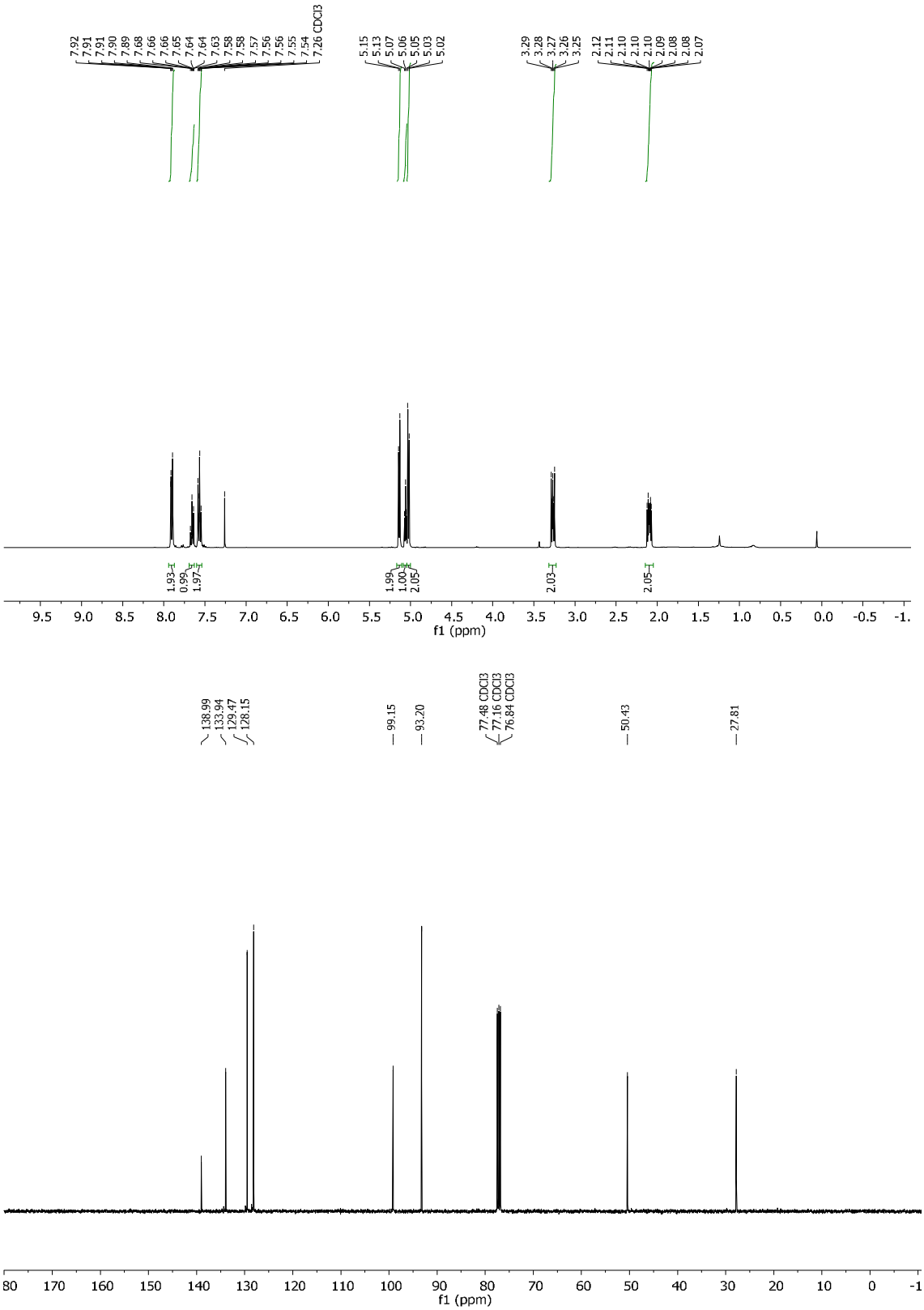

3-(1,3,5-trioxan-2-yl)pyrrolidine-2,5-dione (**3h**)

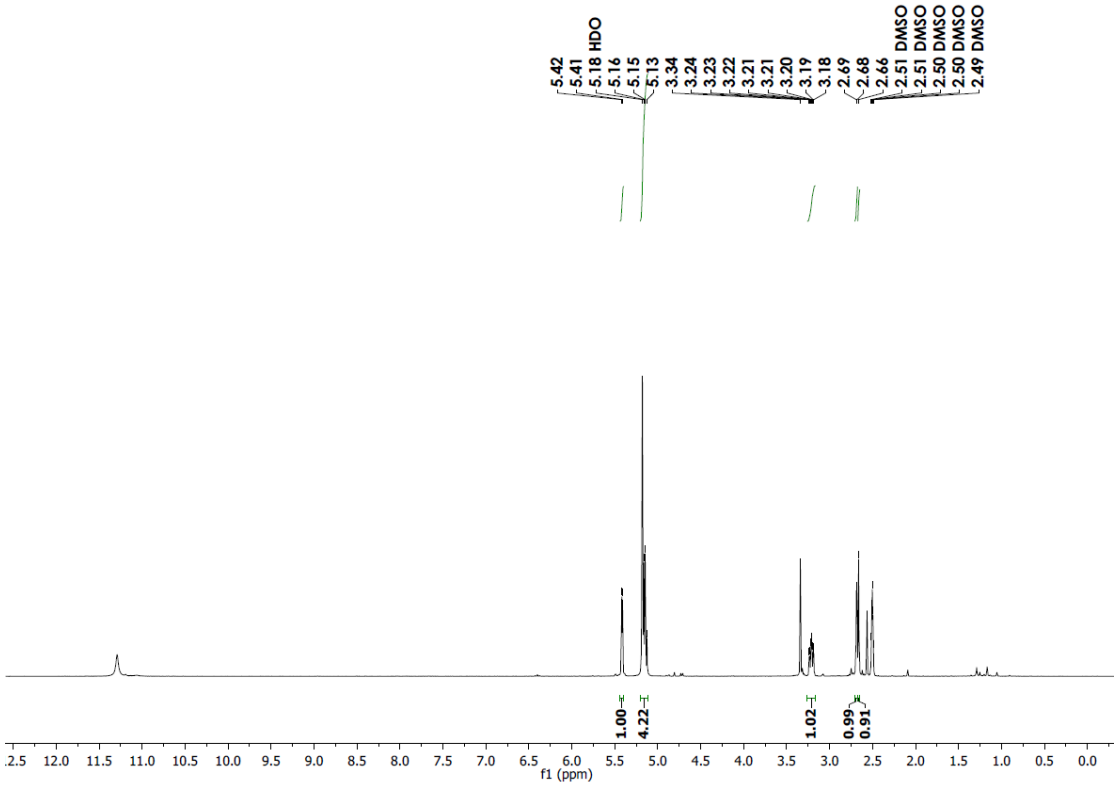

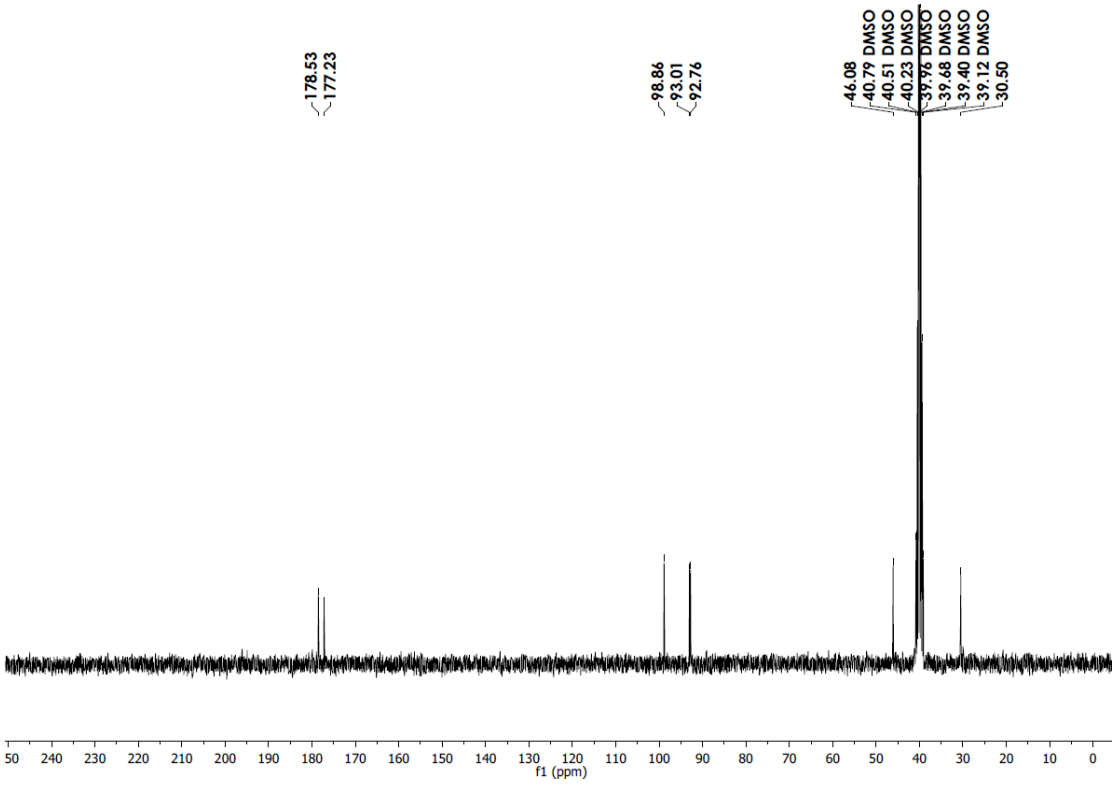

3-(1,3,5-trioxan-2-yl)dihydrofuran-2,5-dione (**3i**)

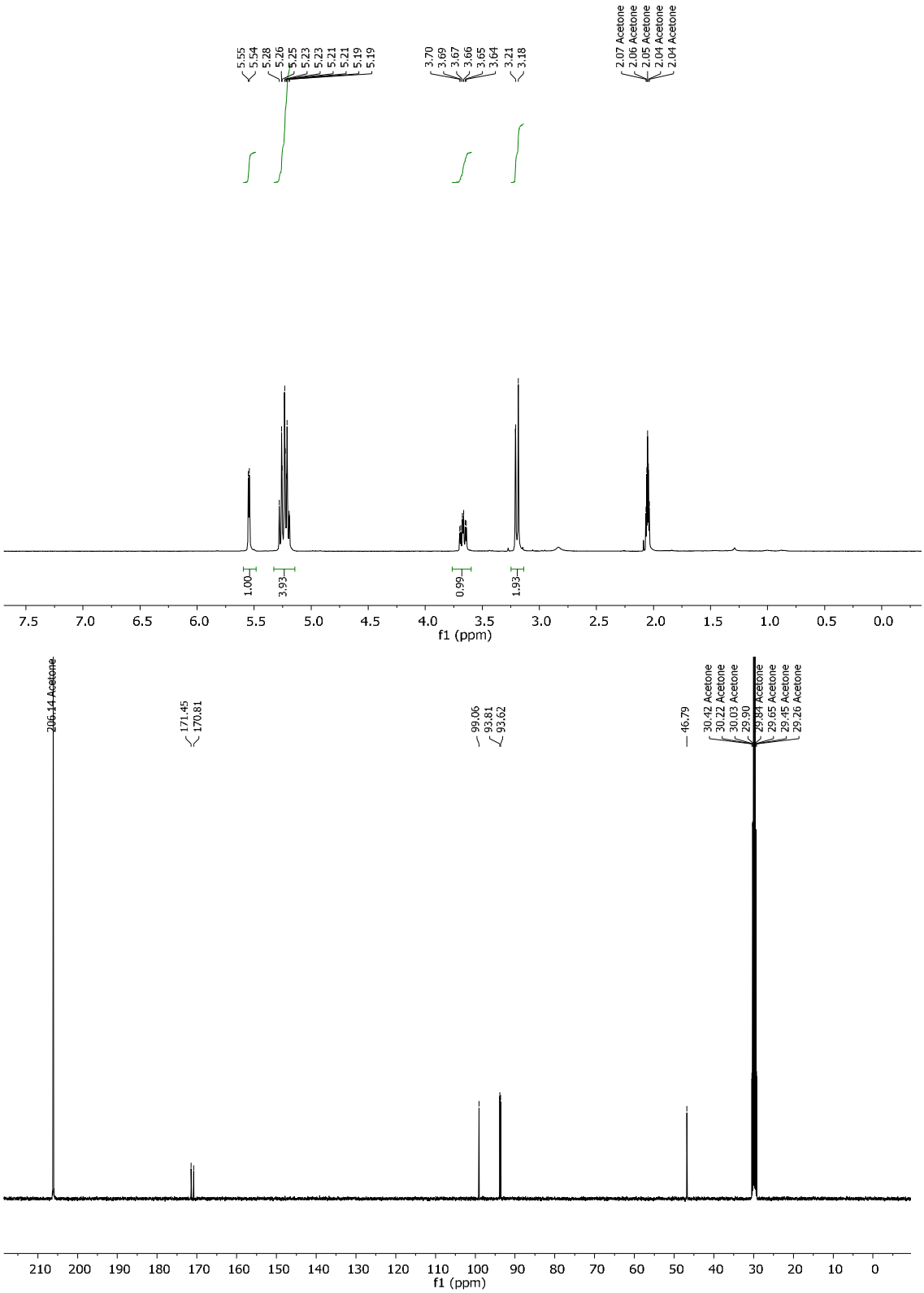

3-methyl-4-(1,3,5-trioxan-2-yl)dihydrofuran-2,5-dione (**3j**)

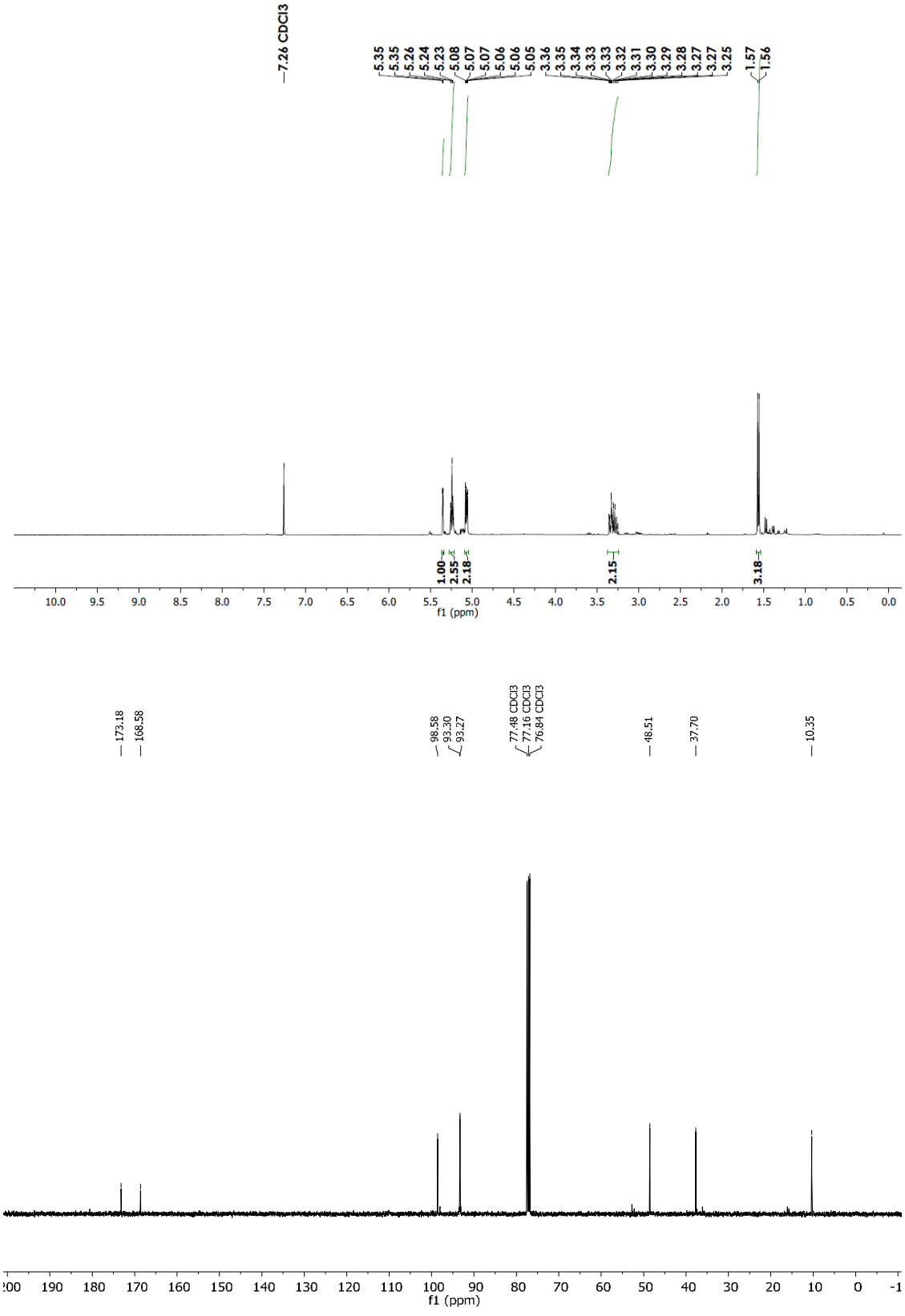

1-cyano-2-(1,3,5-trioxan-2-yl)ethyl acetate (**3k**)

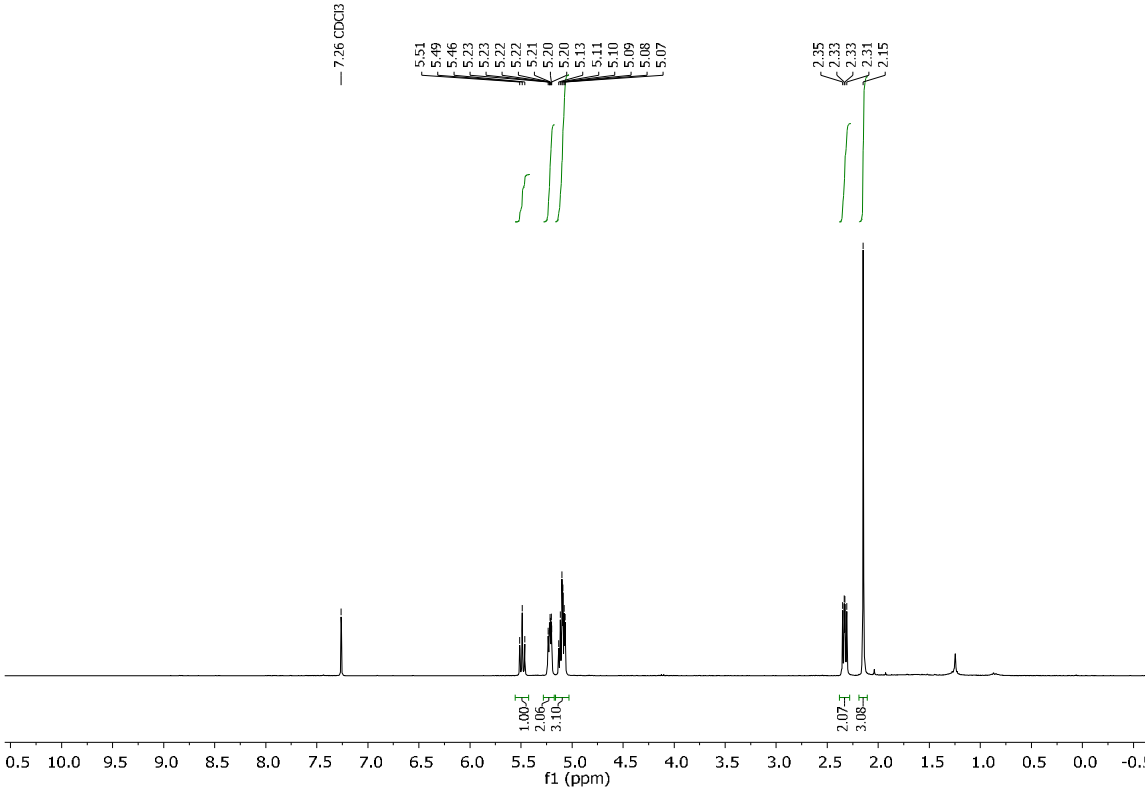

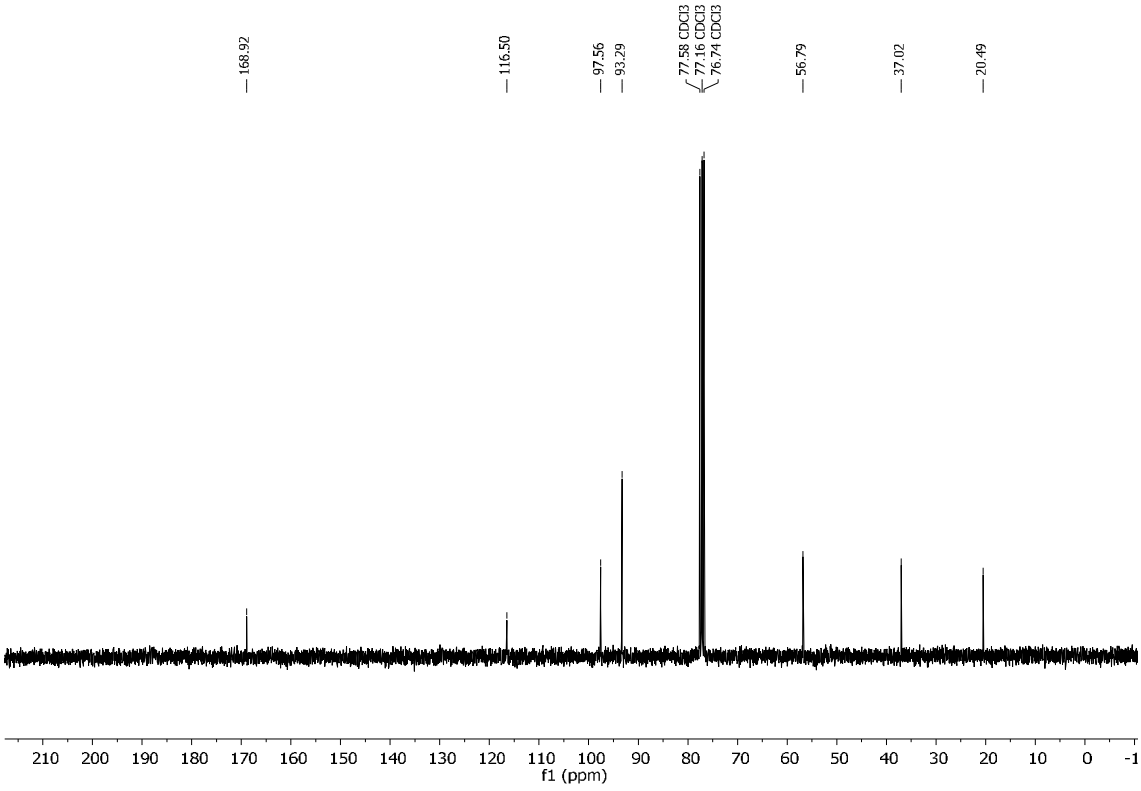

Ethyl 3-oxopentanoate (**3l**)

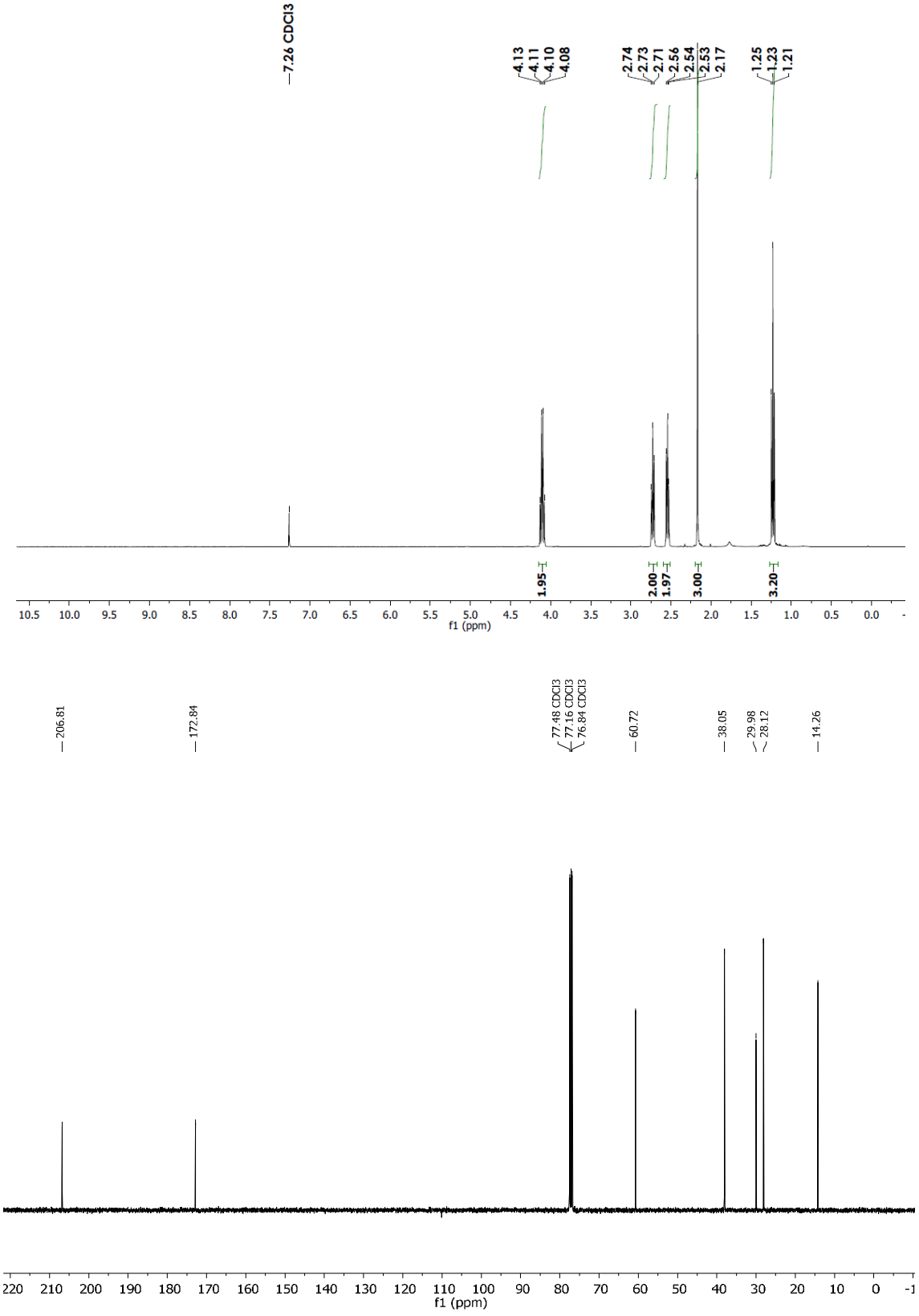

Diethyl 2-acetylsuccinate (**3m**)

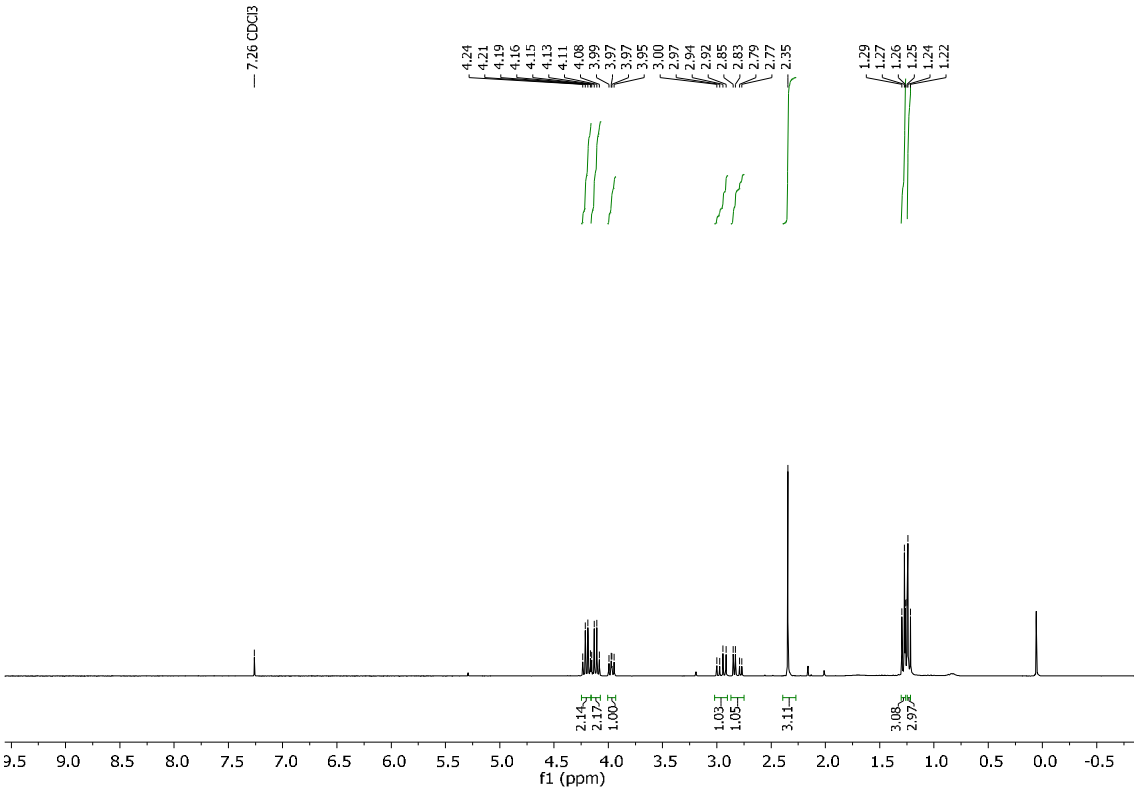

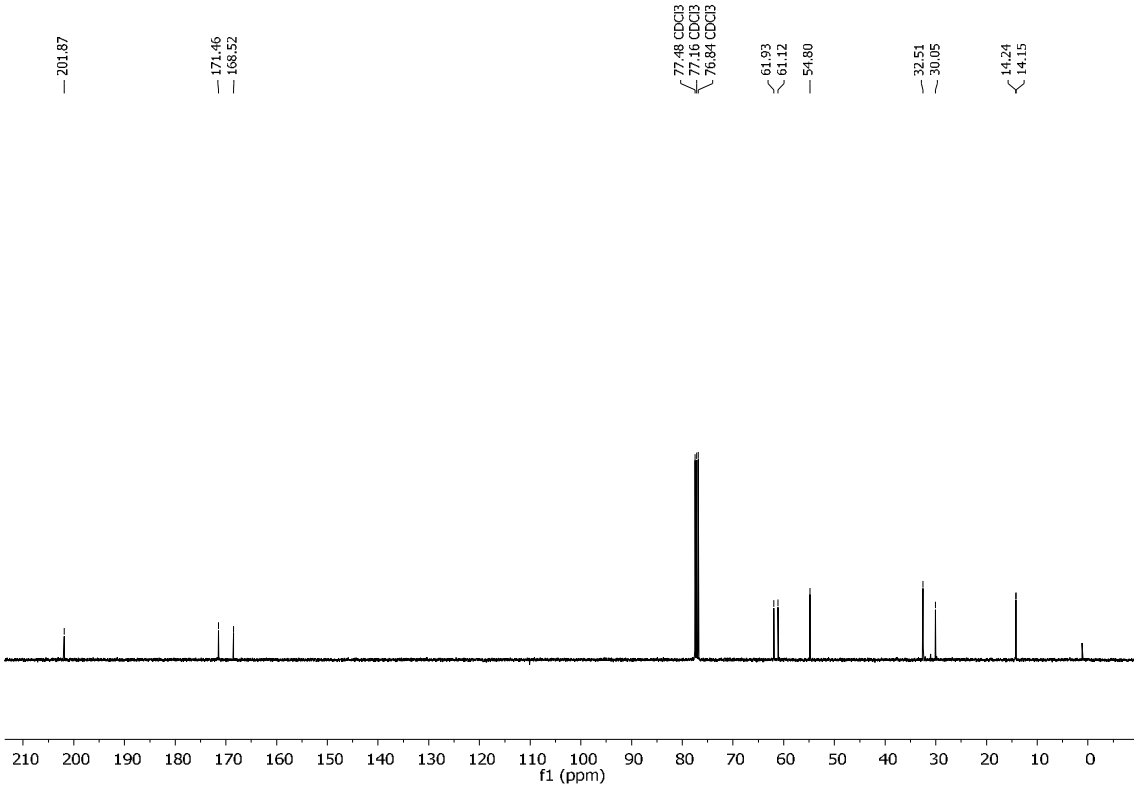

2-(2-oxopropyl)succinic acid (**3n**)

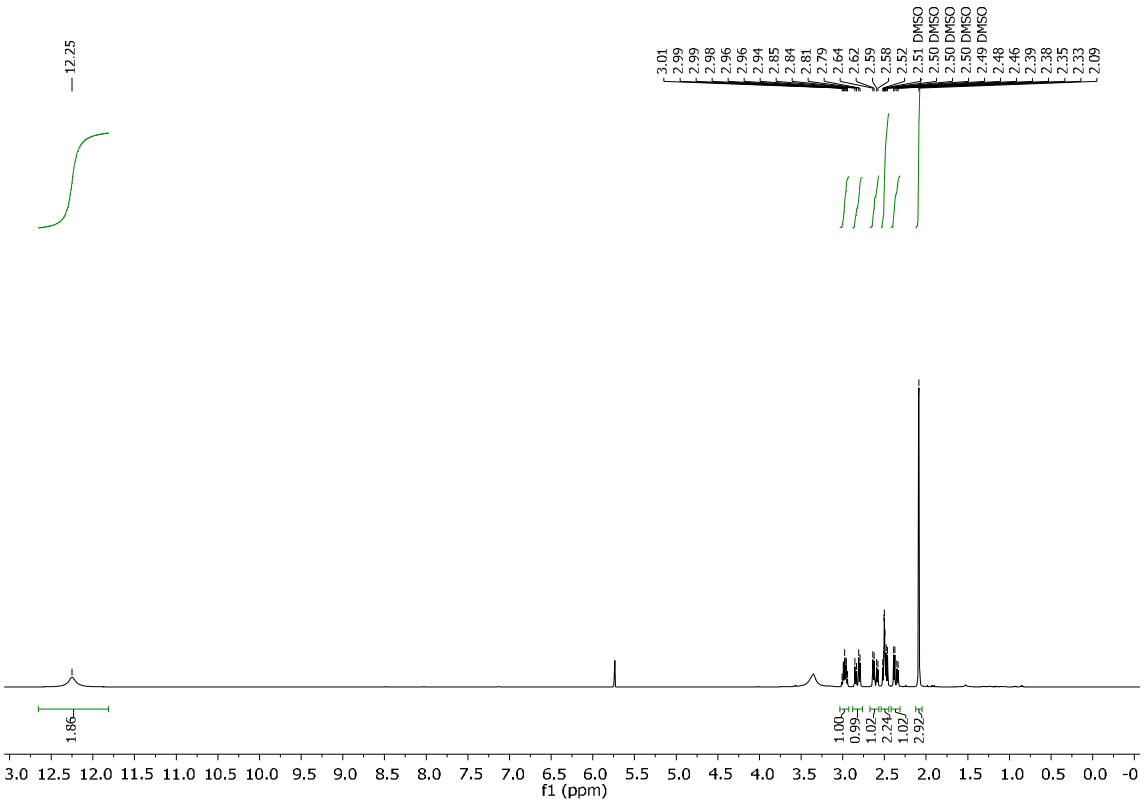

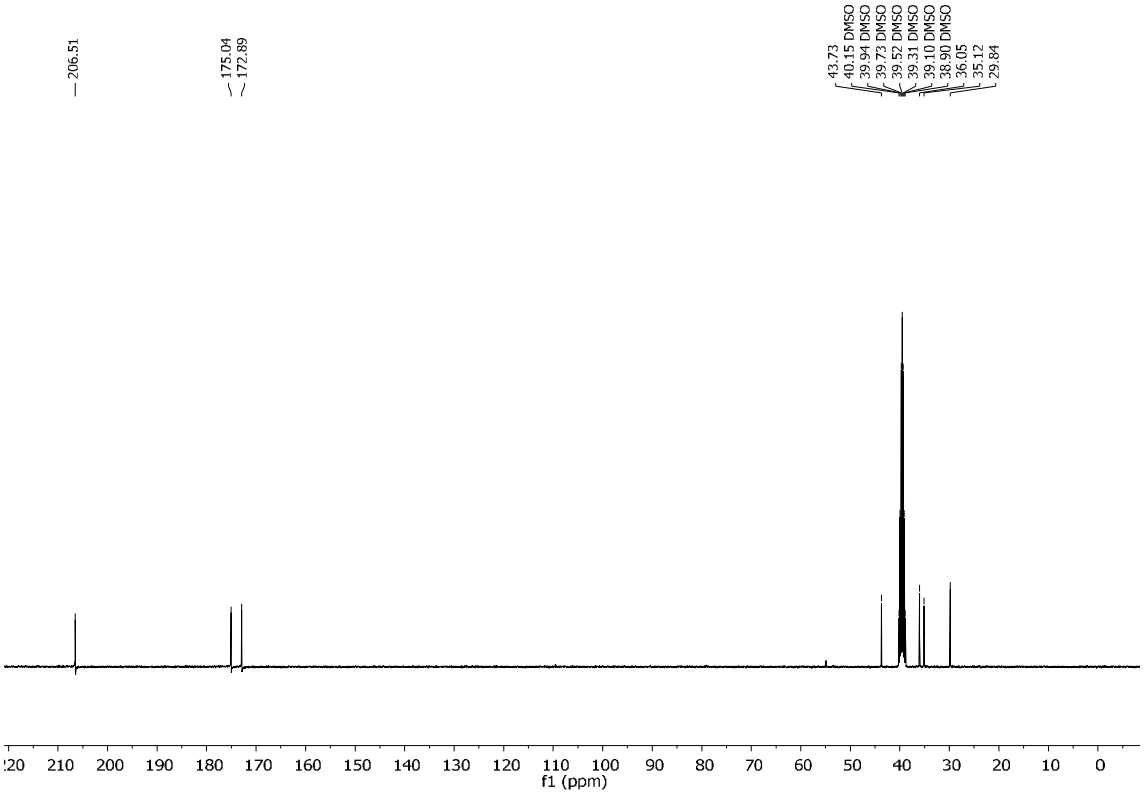

2-(2-oxo-1-phenylpropyl)malononitrile (**3o**)

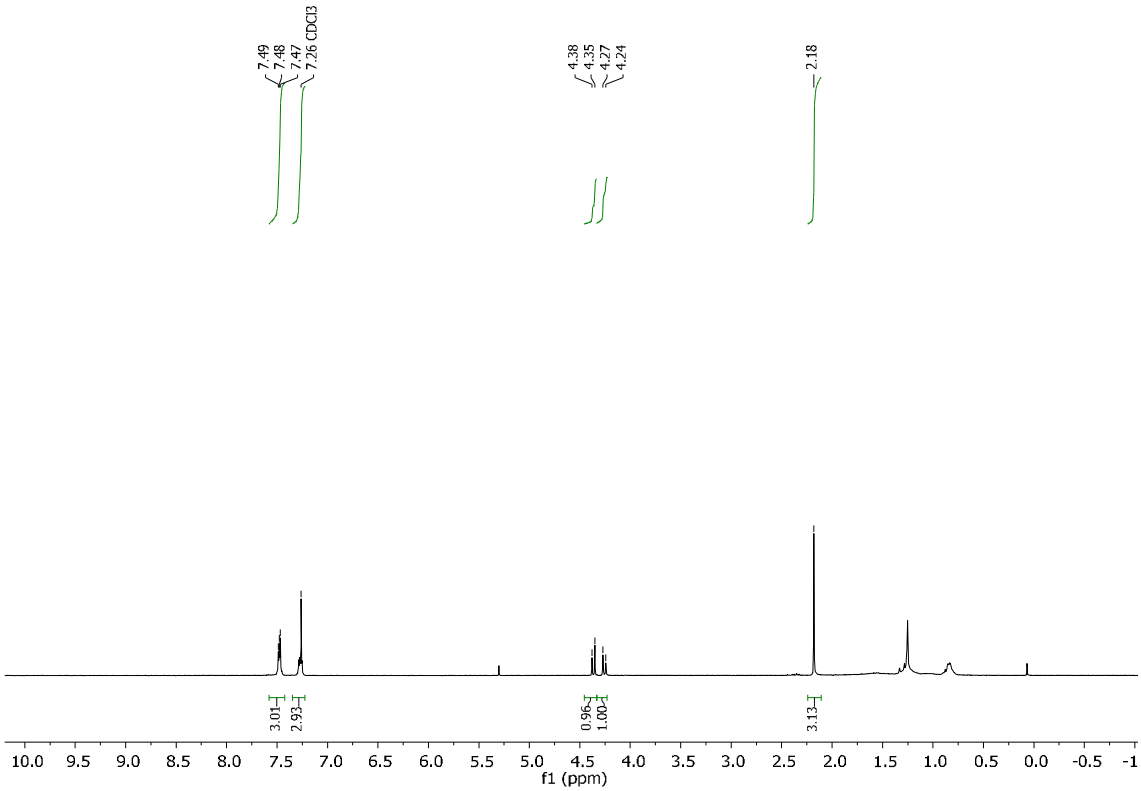

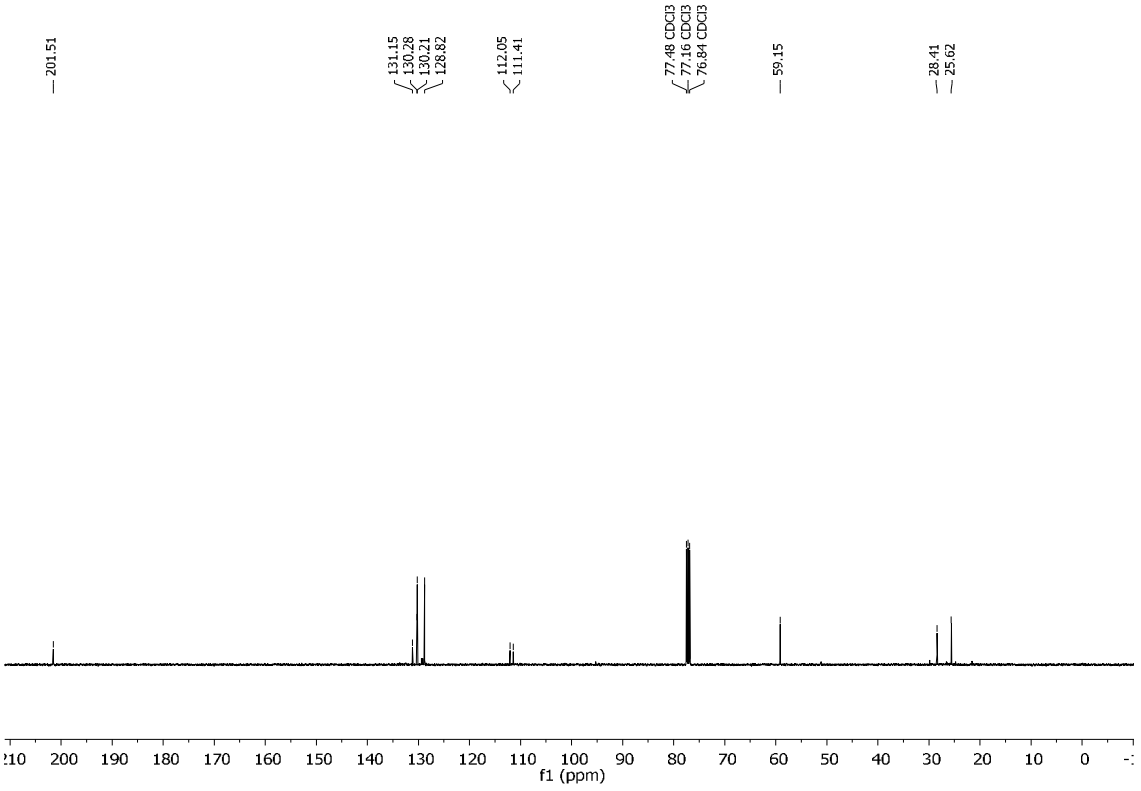

4-(phenylsulfonyl)butan-2-one (**3p**)

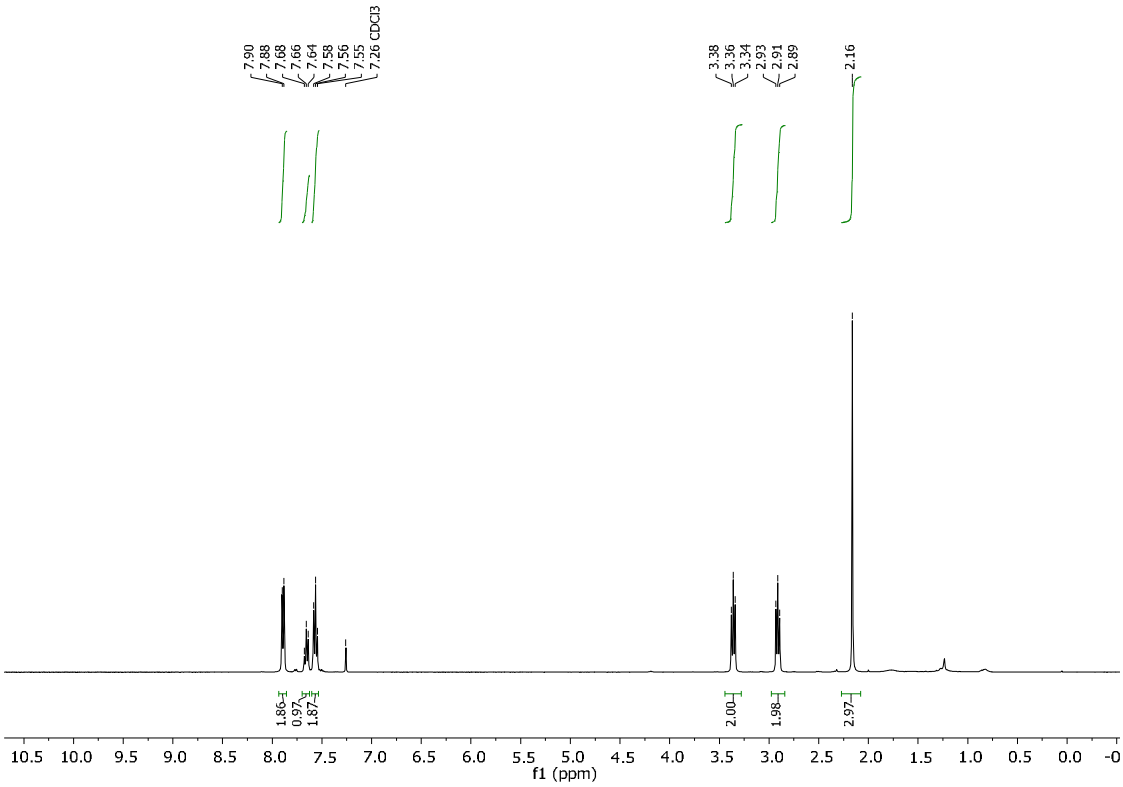

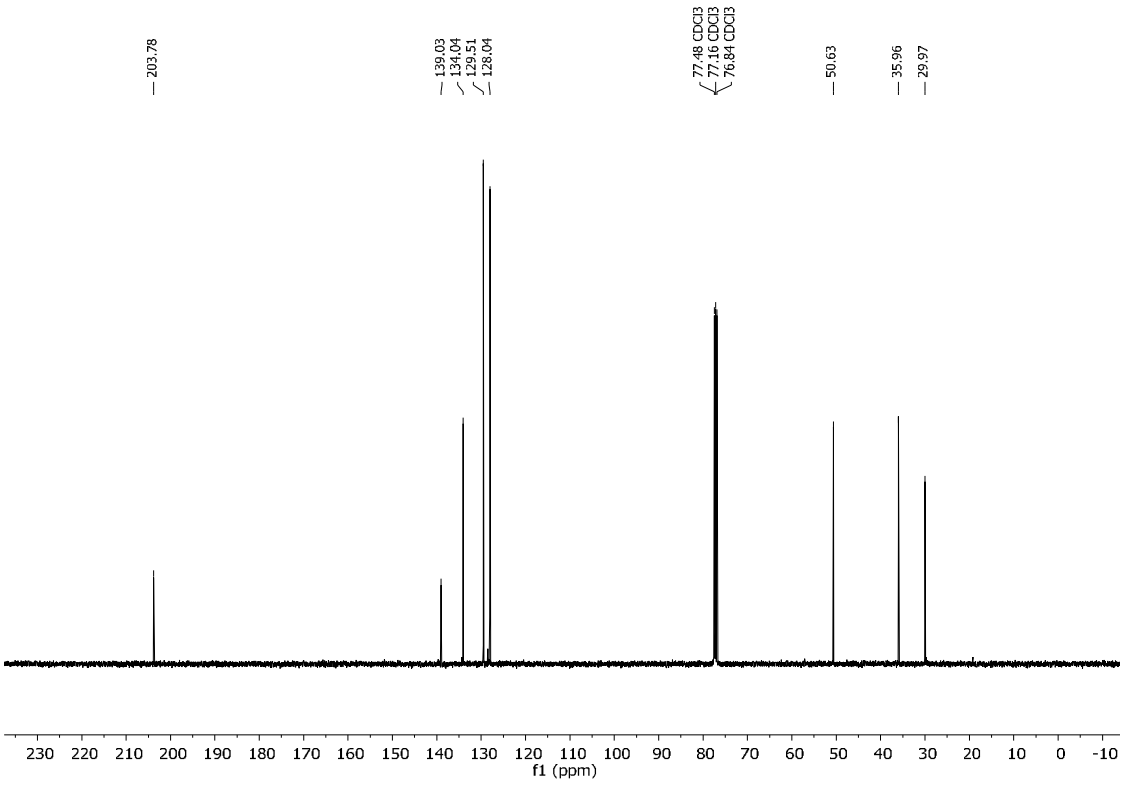

4-oxobutanenitrile (**4a**)

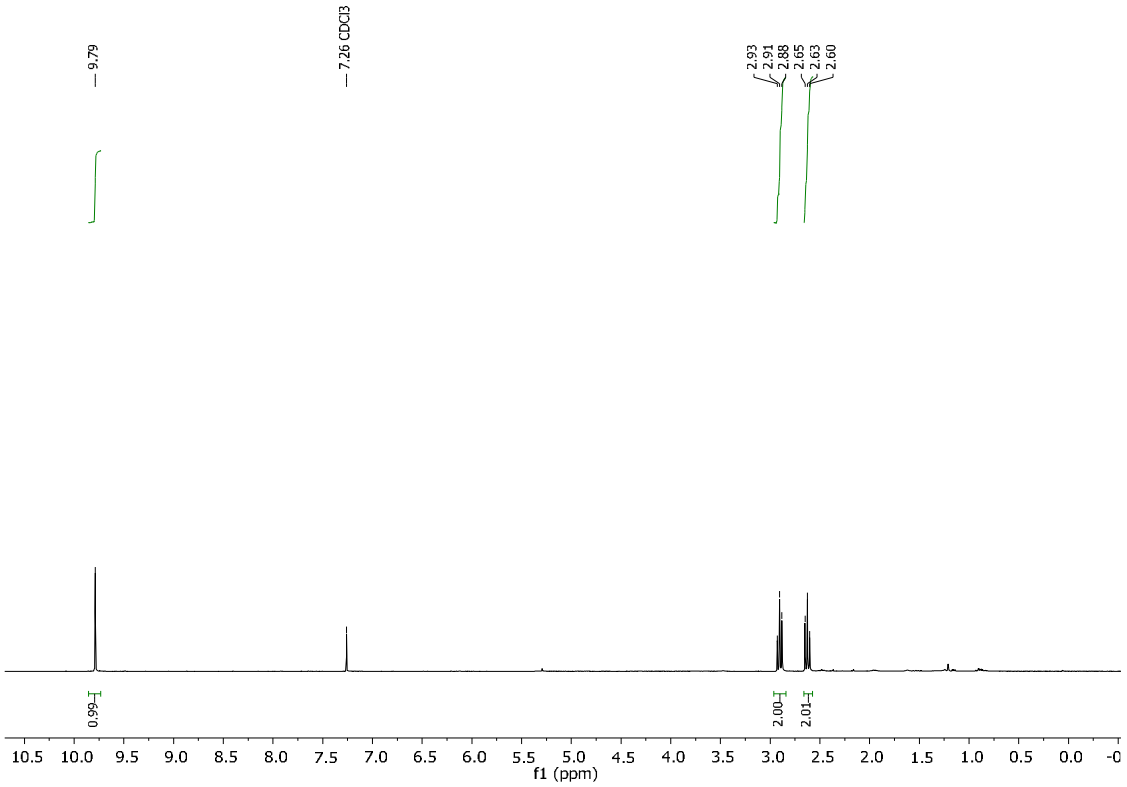

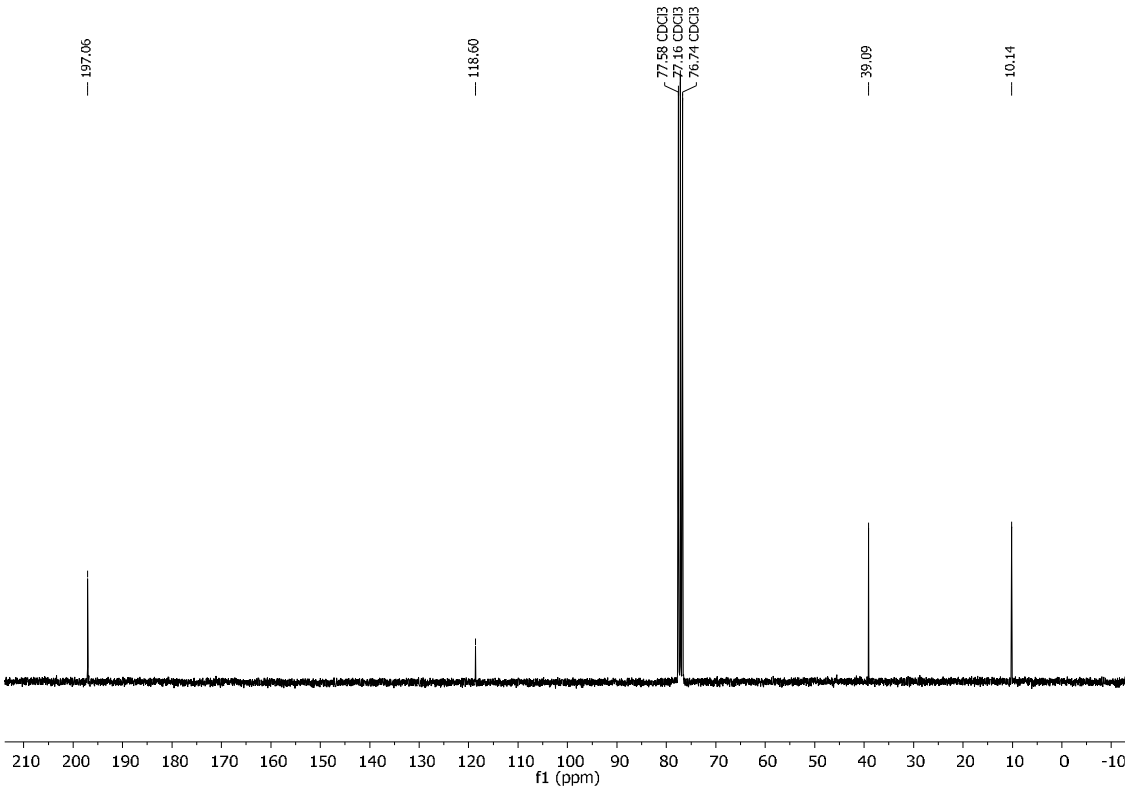

Ethyl 4-oxobutanoate (**4b**)

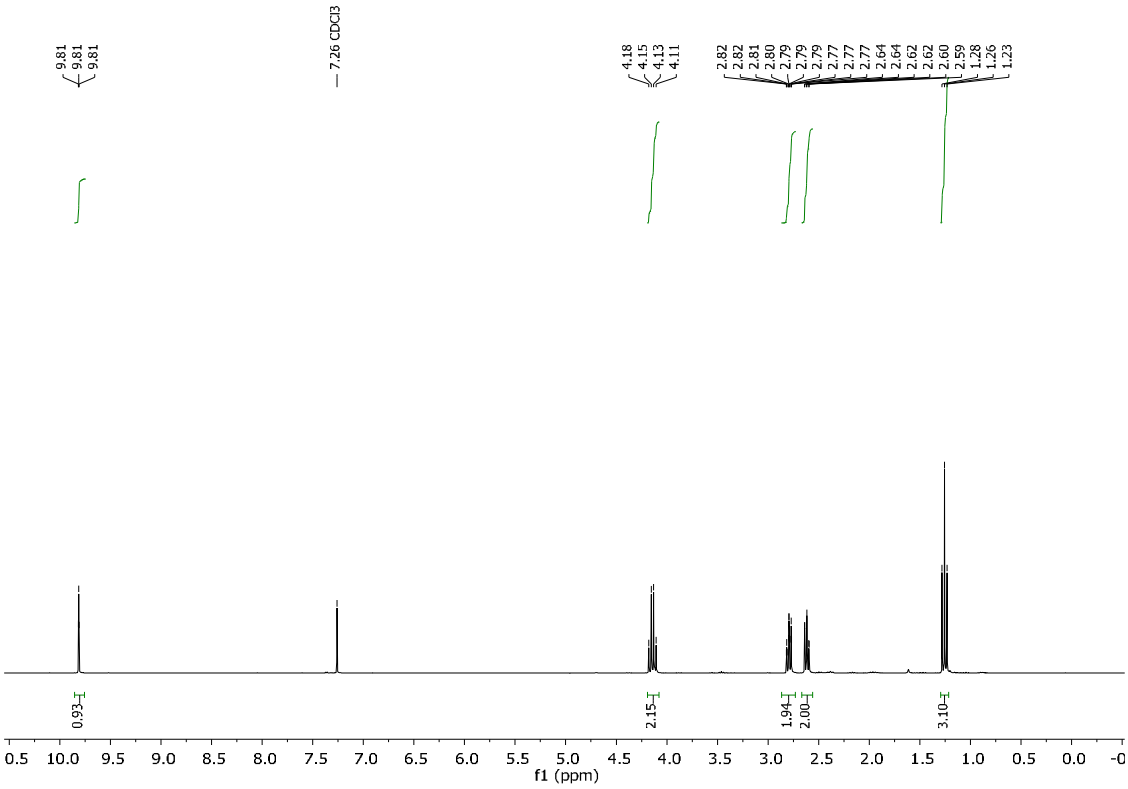

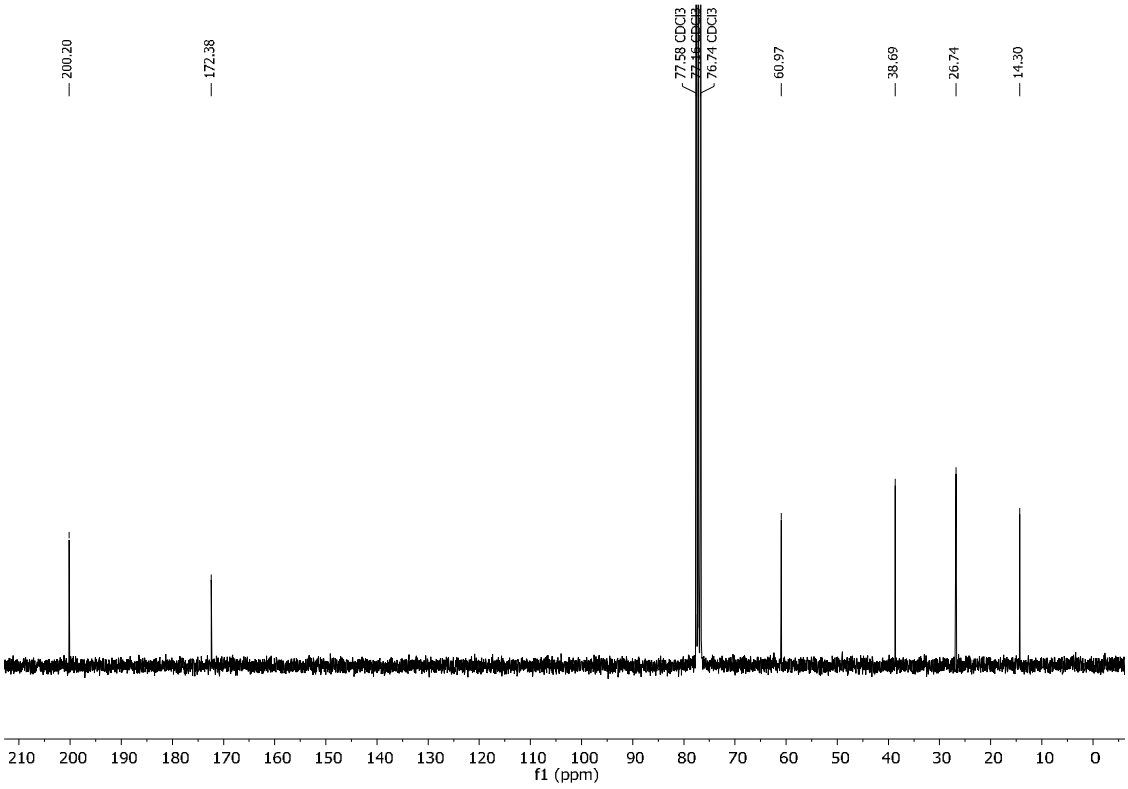

3-(phenylsulfonyl)propanal (**4c**)

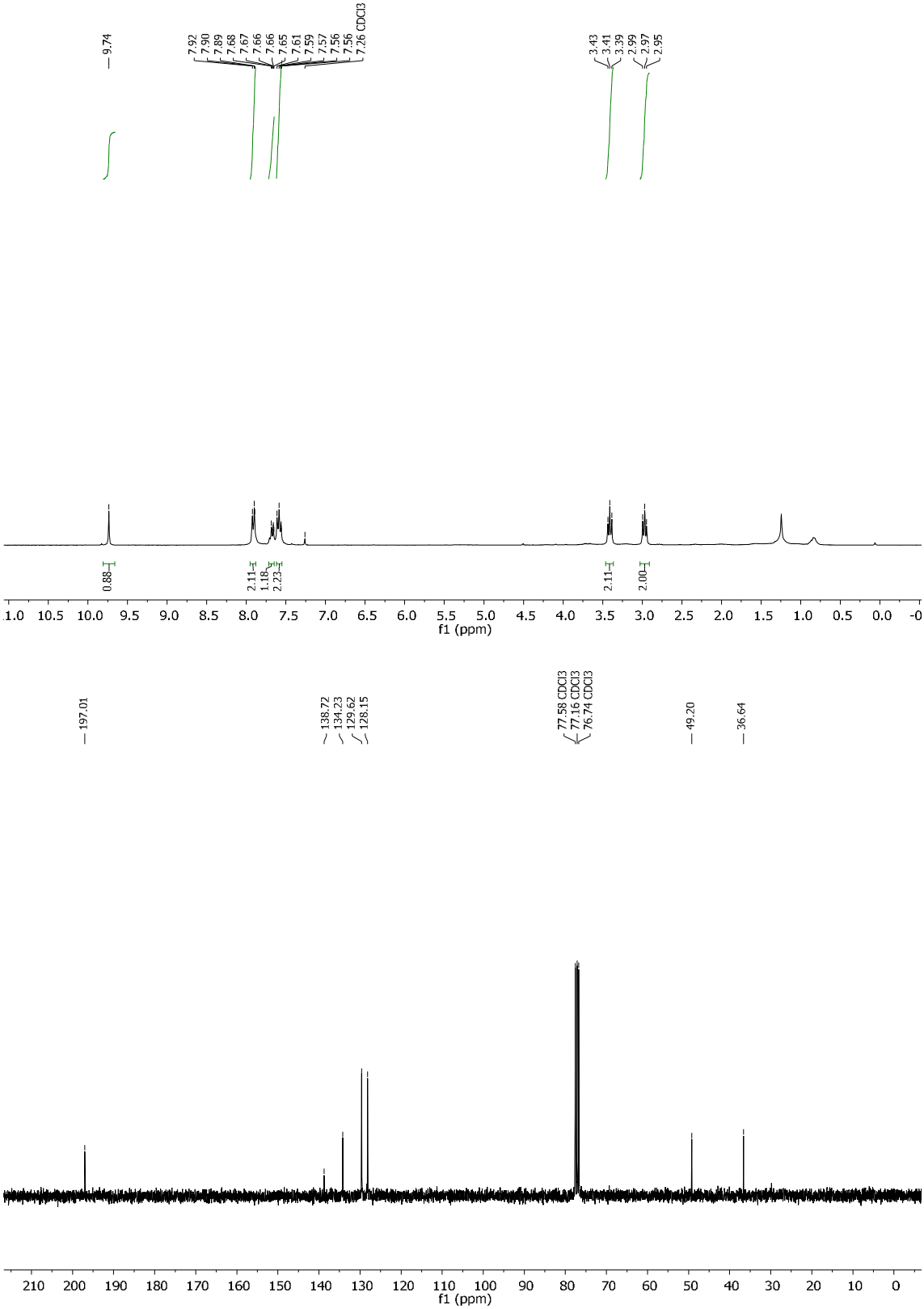

3-cyanopropanoic acid (**5a**)

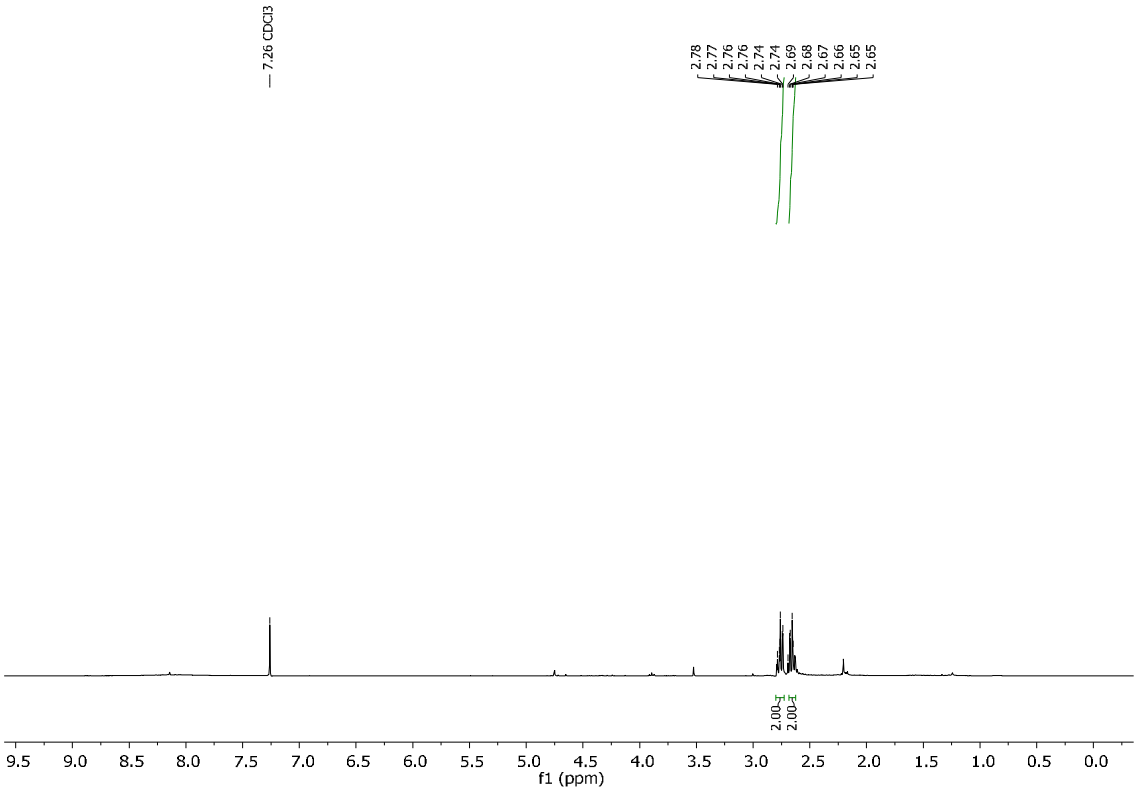

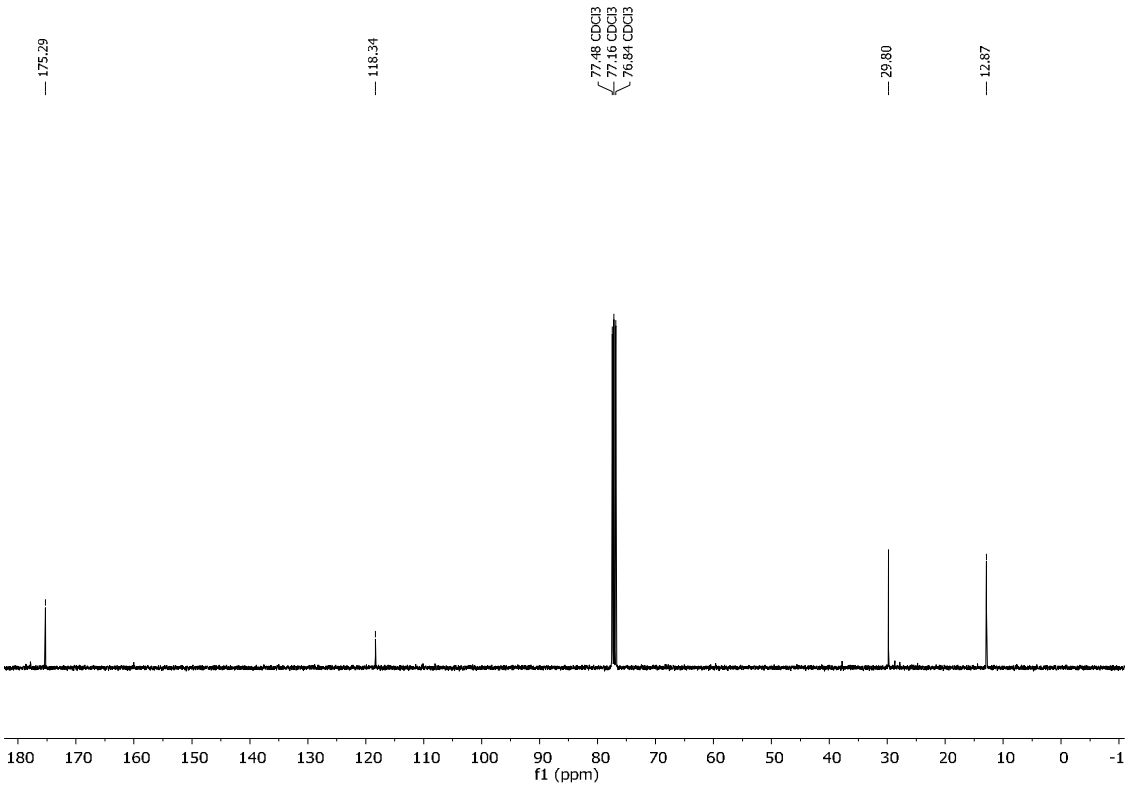

4-ethoxy-4-oxobutanoic acid (**5b**)

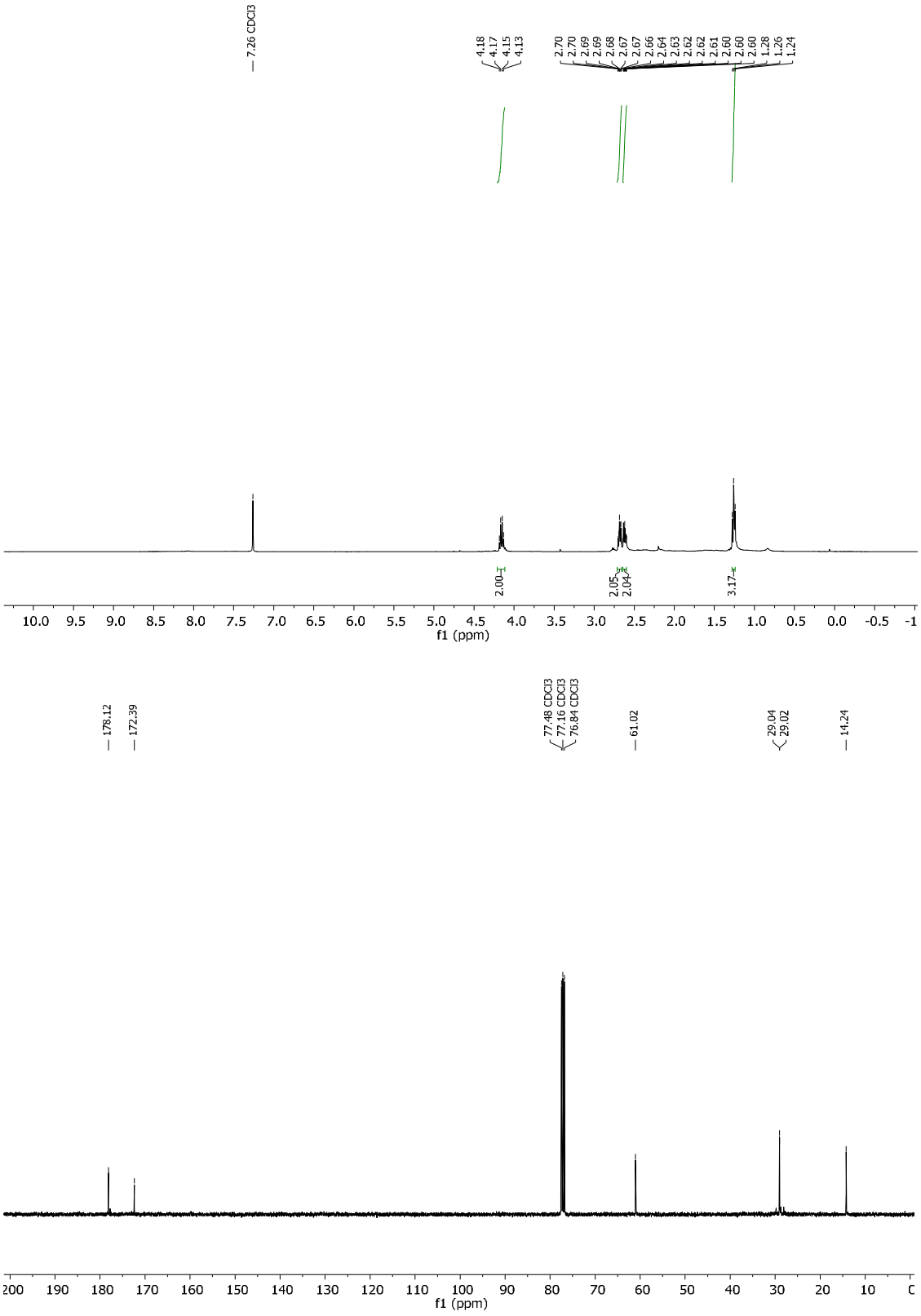

3-(phenylsulfonyl)propanoic acid (**5c**)

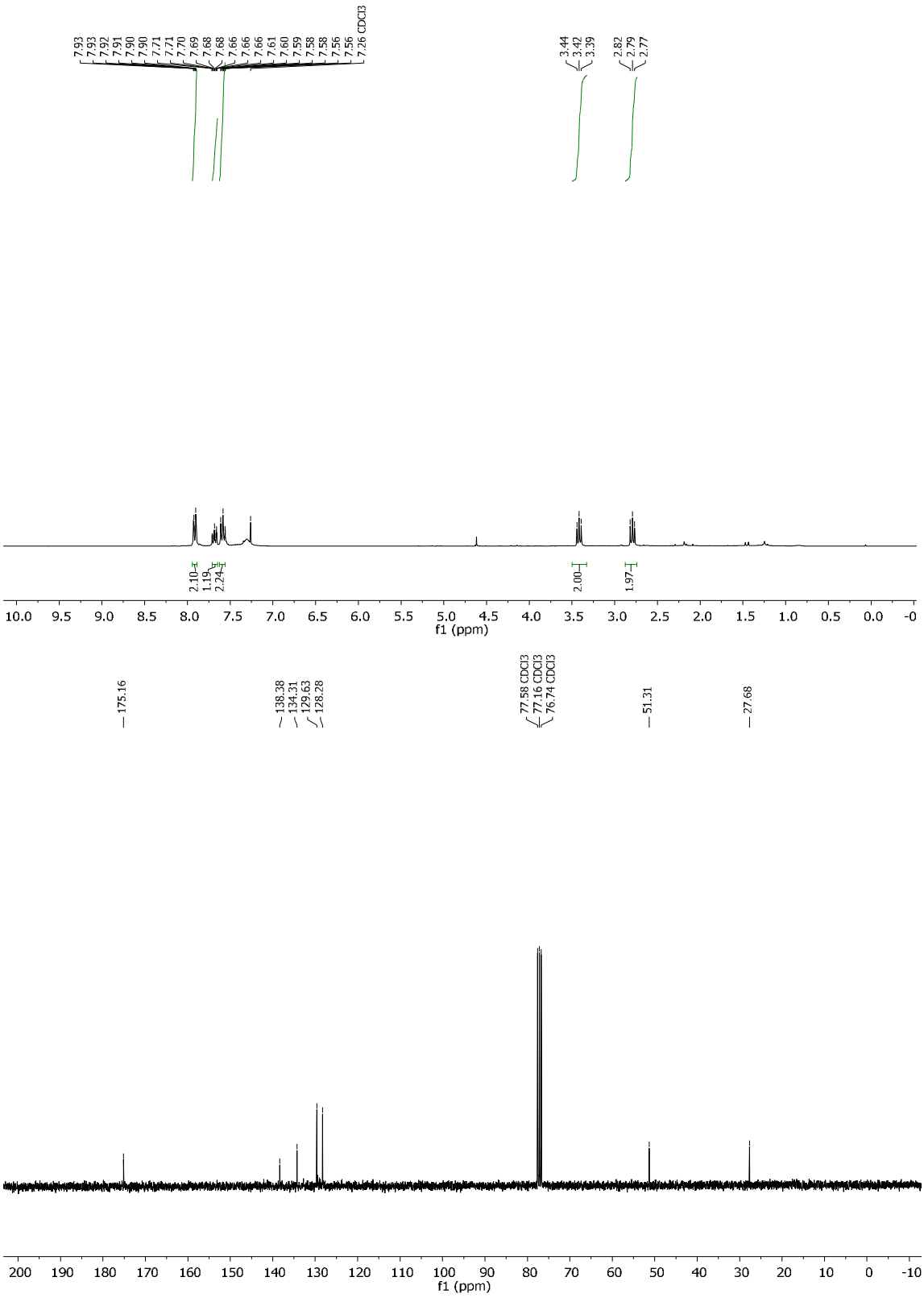

4-oxo-6-(phenylsulfonyl)hexanenitrile (**6**)

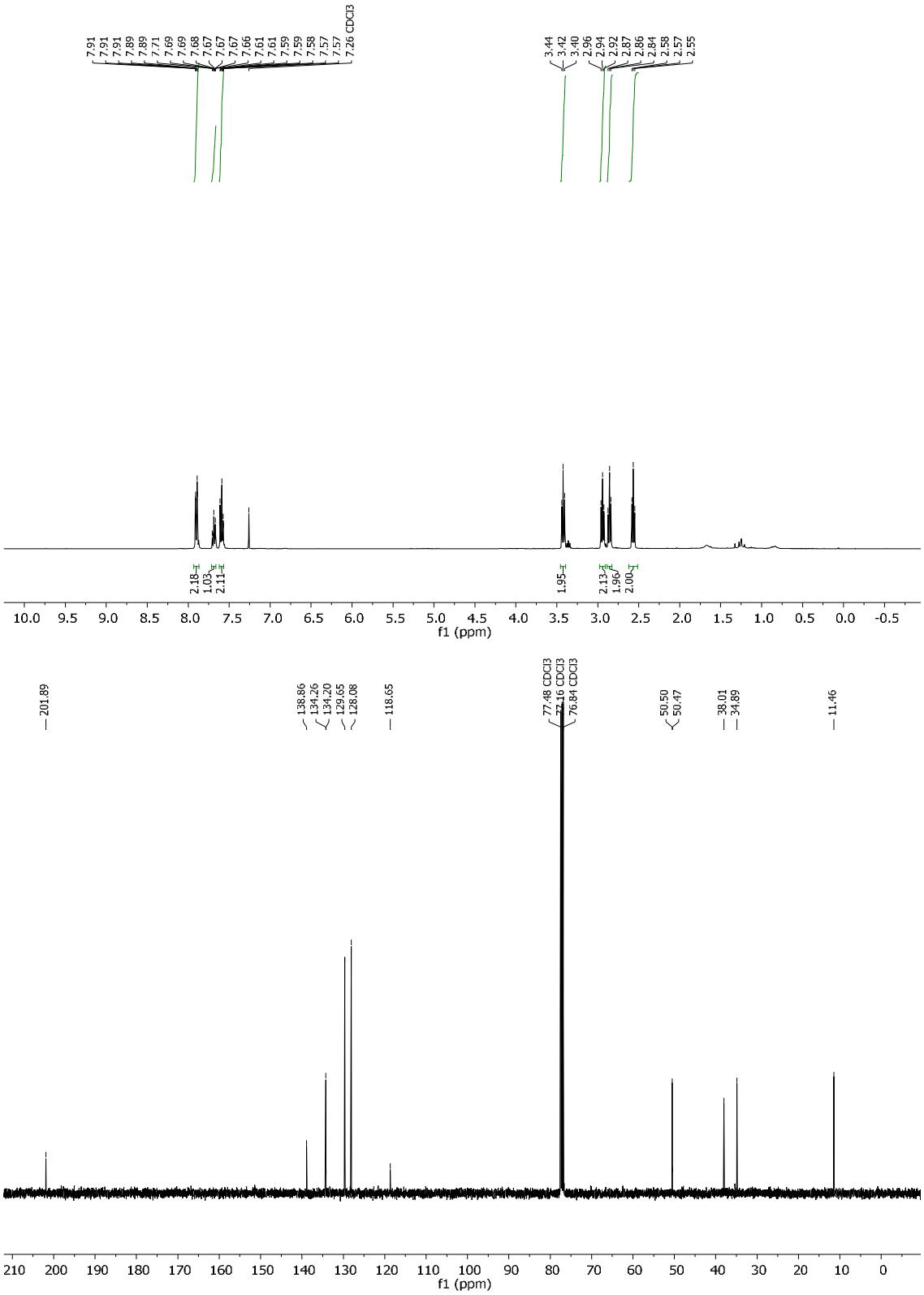

2.8 References

1 D. Liu, K. Yang, D. Fang, S. Li, Y. Lan and Y. Chen, *Angew. Chem. Int. Ed.*, 2023, **62**, e202213686.

2 H. Geng, X. Chen, J. Gui, Y. Zhang, Z. Shen, P. Qian, J. Chen, S. Zhang and W. Wang, *Nat. Catal.*, 2019, **2**, 1071–1077.

3 S. He, X. Chen, F. Zeng, P. Lu, Y. Peng, L. Qu and B. Yu, *Chin. J. Chem.*, 2020, **31**, 1863–1867.

4 R. Franke, D. Selent and A. Börner, *Chem. Rev.*, 2012, **112**, 5675–5732.

5 J. Pospech, I. Fleischer, R. Franke, S. Buchholz and M. Beller, *Angew. Chem. Int. Ed.*, 2013, **52**, 2852–2872.

6 B. Zhang, D. Peña Fuentes and A. Börner, *ChemTexts*, 2022, **8**, 2.

7 D. M. Hood, R. A. Johnson, A. E. Carpenter, J. M. Younker, D. J. Vinyard and G. G. Stanley, *Science*, 2020, **367**, 542–548.

8 J. Zhang, C. Xing, B. Tiwari and Y. R. Chi, *J. Am. Chem. Soc.*, 2013, **135**, 8113–8116.

9 J. G. Calvert, *J. Chem. Phys.*, 1958, **29**, 954–955.

10 J. E. Baggott, H. M. Frey, P. D. Lightfoot and R. Walsh, *Chem. Phys. Lett.*, 1986, **132**, 225–230.

11 J. E. Baggott, H. M. Frey, P. D. Lightfoot and R. Walsh, *J. Phys. Chem.*, 1987, **91**, 3386–3393.

12 S. K. Jensen, S. R. Keiding and J. Thøgersen, *Phys. Chem. Chem. Phys.*, 2010, **12**, 8926.

13 Z.-Y. Dai, S.-Q. Zhang, X. Hong, P.-S. Wang and L.-Z. Gong, *Chem. Catal.*, 2022, **2**, 1211–1222.

14 J. Jin and D. W. C. MacMillan, *Angew. Chem. Int. Ed.*, 2015, **54**, 1565–1569.

15 W. Ou, G. Zhang, J. Wu and C. Su, *ACS Catal.*, 2019, **9**, 5178–5183.

16 M. K. Nielsen, B. J. Shields, J. Liu, M. J. Williams, M. J. Zacuto and A. G. Doyle, *Angew. Chem. Int. Ed.*, 2017, **56**, 7191–7194.

17 D. Ravelli, A. Albini and M. Fagnoni, *Chem. Eur. J.*, 2011, **17**, 572–579.

18 V. C. Gerken and E. M. Carreira, *ACS Catal.*, 2022, **12**, 10787–10792.

19 C. Ma, H. Meng, J. Li, X. Yang, Y. Jiang and B. Yu, *Chin. J. Chem.*, 2022, **40**, 2655–2662.

20 Y. Wang, X.-F. Liu and W.-M. He, *Org. Chem. Front.*, 2023, **10**, 4198–4210.

21 A. Chinchole, M. A. Henriquez, D. Cortes-Arriagada, A. R. Cabrera and O. Reiser, *ACS Catal.*, 2022, **12**, 13549–13554.

22 X.-Y. Yuan, C.-C. Wang and B. Yu, *Chin. Chem. Lett.*, 2024, 109517.

23 L. H. M. De Groot, A. Ilic, J. Schwarz and K. Wärnmark, *J. Am. Chem. Soc.*, 2023, **145**, 9369–9388.

24 F. D. Pileidis and M. Titirici, *ChemSusChem*, 2016, **9**, 562–582.

25 R. E. Trout, A. Zulli, E. Mesaros, R. W. Jackson, S. Boyd, B. Liu, J. Hamrick, D. Daigle, C. L. Chatwin, K. John, L. McLaughlin, S. M. Cusick, W. J. Weiss, M. E. Pulse, D. C. Pevear, G. Moeck, L. Xerri and C. J. Burns, *J. Med. Chem.*, 2021, **64**, 10155–10166.

26 D. He, J. Ma, X. Shi, C. Zhao, M. Hou, Q. Guo, S. Ma, X. Li, P. Zhao, W. Liu, Z. Yang, J. Mou, P. Song, Y. Zhang and J. Li, *Chem. Pharm. Bull.*, 2014, **62**, 967–978.

27 Y. Huang, J. Hou, L.-W. Zhan, Q. Zhang, W.-Y. Tang and B.-D. Li, *ACS Catal.*, 2021, **11**, 15004–15012.

28 A. M. Sheta, A. Alkayal, M. A. Mashaly, S. B. Said, S. S. Elmorsy, A. V. Malkov and B. R. Buckley, *Angew. Chem. Int. Ed.*, 2021, **60**, 21832–21837.

29 T. B. Swanson and V. W. Laurie, *J. Phys. Chem.*, 1965, **69**, 244–250.

30 Y. C. Kang, S. M. Treacy and T. Rovis, *Synlett*, 2021, **32**, 1767–1771.

31 W. L. F. Armarego, *Purification of laboratory chemicals*, Butterworth-Heinemann, Kidlington, Oxford, 8th ed., 2017.

32 A. V. Nakhate and G. D. Yadav, *ACS Sustain. Chem. Eng.*, 2016, **4**, 1963–1973.

33 W. Dong, P. Yao, Y. Wang, Q. Wu and D. Zhu, *ChemCatChem*, 2020, **12**, 6311–6316.

34 L. Capaldo, R. Riccardi, D. Ravelli and M. Fagnoni, *ACS Catal.*, 2018, **8**, 304–309.

35 Y. Zhou, A. K. Gupta, M. Mukherjee, L. Zheng and W. D. Wulff, *J. Org. Chem.*, 2017, **82**, 13121–13140.

36 P. V. Ramachandran, W. Mitsuhashi and B. Biswas, *Org. Chem. Front.*, 2015, **2**, 885–889.

37 D. Zhu, C. Mukherjee, E. R. Biehl and L. Hua, *Adv. Synth. Catal.*, 2007, **349**, 1667–1670.

38 D. Hidasová and T. Slanina, *J. Org. Chem.*, 2023, **88**, 6932–6938.

39 C. I. Grove, M. J. Di Maso, F. A. Jaipuri, M. B. Kim and J. T. Shaw, *Org. Lett.*, 2012, **14**, 4338–4341.

Chapter 3

3 Catalyst-Free, Scalable Heterocyclic Flow Photocyclopropanation‡

3.1 Abstract

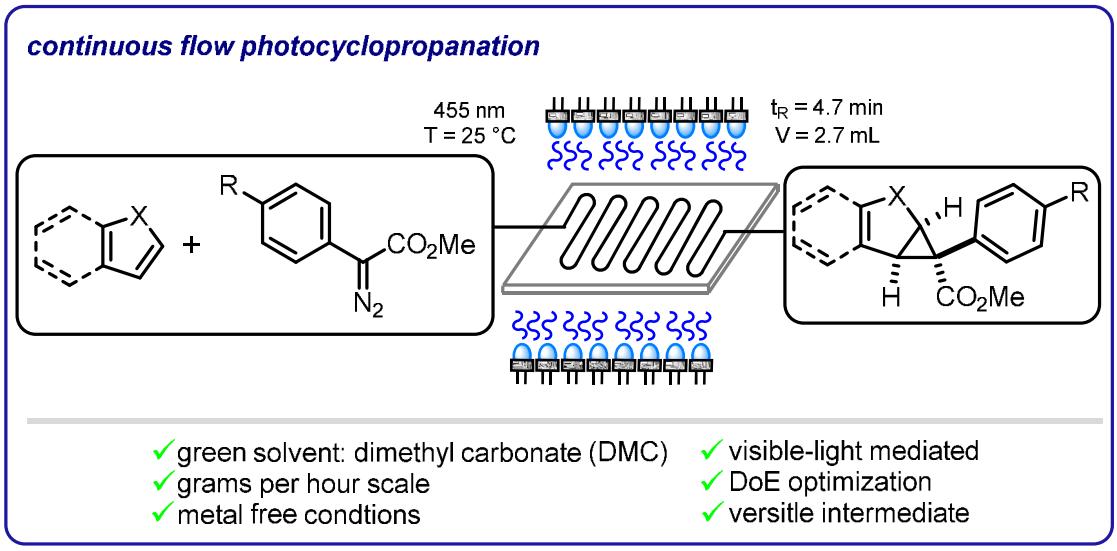

Industrial process development is driven by several factors, including safety, cost, robustness, and environmental aspects. However, attempts to establish aryl diazo esters – which are highly valued in academic research for their reactivity as carbene precursors – in the chemical industry have been limited by their explosivity and toxicity. Their catalyst-free photolysis in continuous flow improves safety, sustainability and scalability compared to batch reactions. Herein, we report the continuous flow catalyst-free photocyclopropanation of heterocycles in up to grams per h productivity in a non-chlorinated, biodegradable solvent. Highly functionalized cyclopropanated products are key intermediates in the synthesis of drugs and pharmaceutically relevant compounds. Optimal conditions and process understanding were obtained by a Design of Experiments

‡ This chapter is based on: V. Klöpfer, R. Eckl, J. Floß, P. M. C. Roth, O. Reiser, J. P. Barham, *Green Chem* **2021**, *23*, 6366–6372. The work was mostly processed during my Master's Thesis, but finalized and published during my Ph.D. In this manner, the substrate scope was extended and finalized during my Ph.D.; all substrates marked with * were not yet reported in my Master Thesis. The entire project was documented here for completeness and as a starting point for the following work. R. Eckl performed the big scale batch reaction with DCM as solvent. J. Floß performed all melting point measurements for the compounds of this chapter and synthesized TsN_3 and **2a-2d**. P.M.C Roth provided technical support for the Corning® Advanced-FlowTM Lab Photo Reactor. O. Reiser and J. P. Barham were supervising this project.

approach. In comparison with a large-scale batch experiment, continuous flow conditions improved yield, productivity, and process safety.

3.2 Introduction

Since the first syntheses of diazo compounds by Griess in 1858,[1] they have risen to become one of the most versatile reagents in the toolbox of organic synthesis. Their applications include X H insertions (X = C, O, N, S), ylide formations, cycloadditions, and cyclopropanations.[2] In particular, the latter has proven an efficient method to access heavily-functionalized intermediates that are readily converted into pharmaceutically-relevant compounds and drugs.[3] For example, (-)-desoxyeseroline,[4] pyrrolo[3,2-e]indoles,[5] LY2140023,[6] tropanes,[7] arglabine™,[8] polycyclic endoperoxides,[9] paraconic acid derivates[10] or (S)-vigabatrin[11] are all readily accessible from a functionalized cyclopropanated heteroarene core (Scheme 3-1). While diazo compounds are highly valued in academic research, their industrial applications are rare due to the toxicity and explosivity of these reactants.[12] One of the infrequent industrial utilizations of ethyl diazoacetate was reported in 2008 by Bristol-Myers Squibb in the synthesis of a selective serotonin reuptake inhibitor on a kilogram scale.[13,14] With the vision of applying these important yet hazardous diazo compounds in large-scale syntheses, a trend in both academic and industrial research has emerged in recent years utilizing continuous flow (CF) technology to handle them in a safe and controlled manner.[15] In general, the larger surface-area-to-volume ratio in CF reactors provides better heat transfer rates compared to batch reactions (avoiding adiabatic conditions). The risk of thermal runaways is suppressed, and the overall hazard mitigated by much smaller amounts of reactants within the reactor at any given time compared to a similarly productive batch process. Therefore, CF reactors represent a markedly safer alternative than traditional batch reactors for handling high-energy chemical processes.[16] Specifically for the handling of diazo compounds, the comparatively smaller volume of CF reactors and their ability to handle gas-evolving reactions under back-pressure are highly attractive. Since 2010, an increasing number of publications have disclosed the synthesis as well as the conversion of diazo compounds in CF. Decomposition of the diazo to carbene species was mostly metal-catalyzed - as in batch. Common methods rely on homogeneous or immobilized complexes based on Cu^{I}, Cu^{II} and Rh^{II}. Chiral ligands have enabled enantioselective reactions.[17–24]

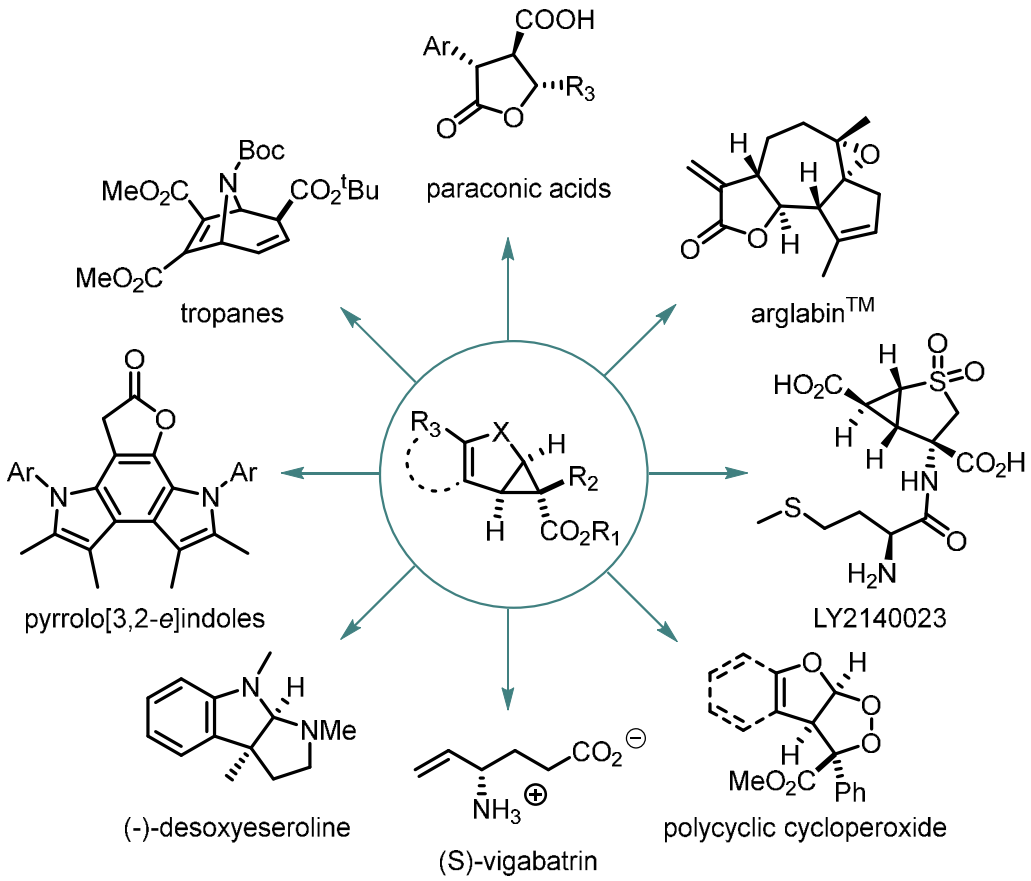

Scheme 3-1. Examples of pharmaceutically-relevant compounds and drugs derived from cyclopropanated heteroarenes.

In addition to safety, the cost, productivity, yield, purity, robustness, and environmental aspects contribute considerably to decision-making processes in industrial applications.[16] Visible light photons are a clean, non-contaminating energy source that can be used to power chemical reactions under ambient conditions. Photochemistry and CF make for an attractive match, complementing the increased safety of CF in terms of cost, atom efficiency and sustainability. The typical issue of poor scalability of photochemical batch reactions due to logarithmical dependence of transmitted light with path length (Lambert-Beer's law) is addressed by CF photochemistry. The constant distance of the solution to the light source and defined layer thickness enables continuous photo-flow reactors to be highly efficient and easily scalable.[25–28] Koenigs *et al.* contributed seminally to the utilization of diazo compounds **2** in CF photoreactors (Scheme 3-2, b). Inspired by the work of Davies *et al.* on the photolysis of aryl diazoacetate **2** by low-energy visible light to give cyclopropanated hetereoarenes **3** (Scheme 3-2, a),[29] the Koenigs group successfully cyclopropanated phenylacetylene **4b** *via* photolysis of methyl 2-diazo-2-phenylacetate **2a** in a simple glass CF microreactor. Compared to batch

photocyclopropanations, reaction time was decreased, and productivity increased. However, the yield of **5b** decreased from 97% to 72% under the most productive conditions. Recent work by the same group complemented their previous study with the cyclopropanation of styrene (**4a**). Under the best conditions, **5a** was obtained in 83% following quantitative conversion of **4a** at a residence time of 1 h.[30–32]

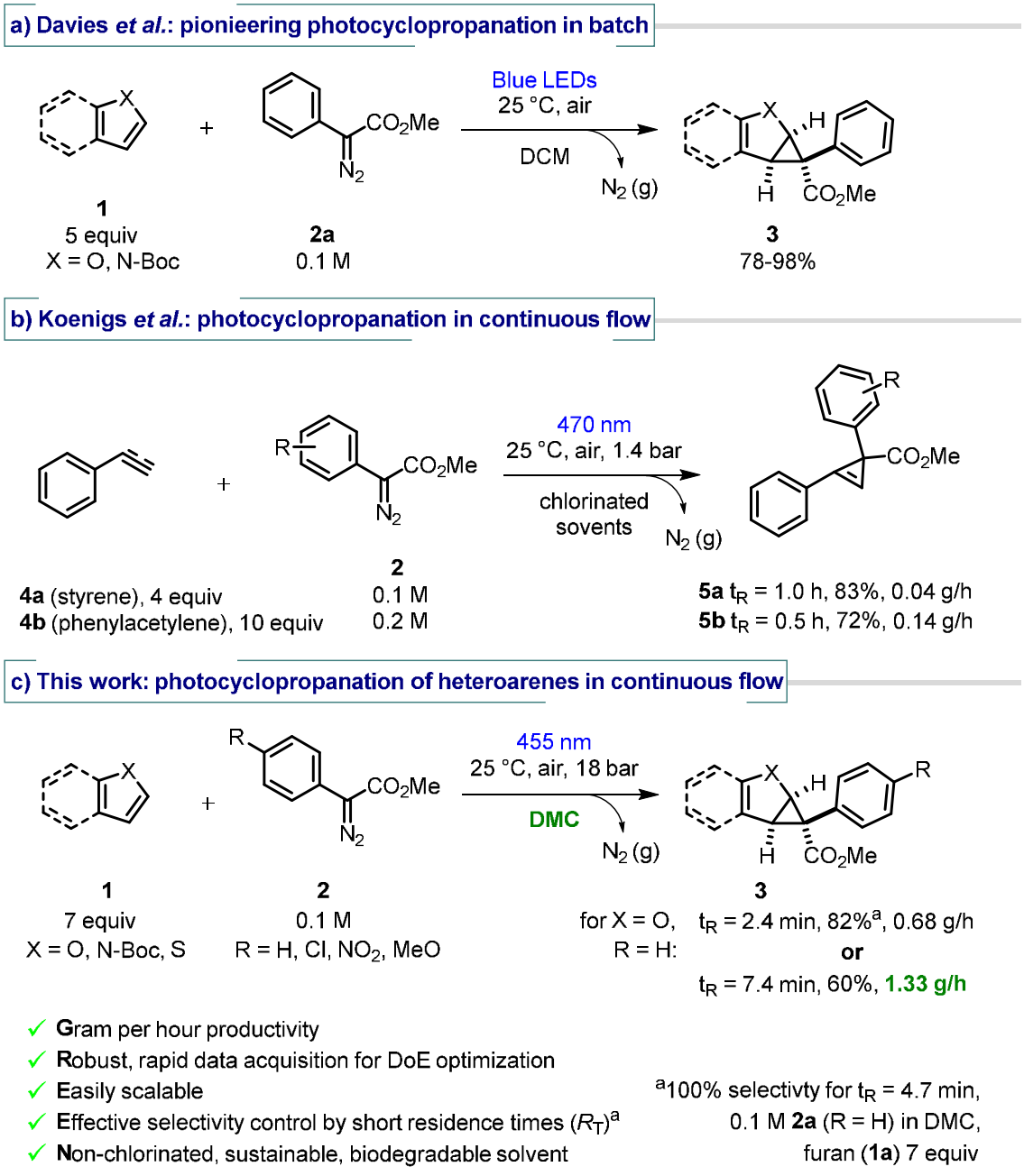

Scheme 3-2. a). Photolysis of **2a** by Davies and co-workers,[29] b). Previous flow photocyclopropanations of styrene (**4a**)[32] and phenylacetylene (**4b**)[30] Koenigs and co-workers. C). This work: Safe, scalable, sustainable flow photocyclopropanation of heteroarenes **1** in biodegradable solvent in up to g h^{-1}.

From a processability perspective, the replacement of chlorinated solvents with 'green' solvents is highly desirable.[33] Low-boiling solvents such as dichloromethane and chloroform as used in previous reports are non-ideal for CF reactions as they readily cavitate in pump manifolds designed to deliver higher flow rates and throughput. Furthermore, chlorinated solvents are in general (i) carcinogenic, (ii) costly to transport and manipulate in large volumes due to high density and (iii) are environmentally unsustainable. Moreover, a key advantage of CF is the ability to control selectivity *via* residence time control, since the product can be removed from the reaction conditions before it undergoes subsequent reactions (like di-additions).[34–36] In the cited studies, residence times are relatively long (30-60 min), increasing risk of by-products. On the other hand, long residence times restrict productivity, a characteristic response that assumes superior importance in CF processes – especially in industry.

Herein, we report a safe, scalable, and sustainable photocyclopropanation of various heteroarenes **1** under ambient conditions (Scheme 3-2, c). Biodegradable (higher-boiling), non-toxic solvent dimethyl carbonate (DMC)[37] not only replaced chlorinated solvents, it gave superior results. Robustness of the CF photoreactor allowed rapid data acquisition for rapid optimization with software-assisted Design of Experiments (DoE). Optimal conditions were identified for selectivity (up to 100% selectivity, 82% yield) and productivity (up to 1.3 g h^{-1}) using a compact (2.7 mL) CF reactor. Superiority of the photo CF process over its batch equivalent was demonstrated by comparisons of productivity and yield.

3.3 Results and Discussion

3.3.1 Transfer of Photocyclopropanation into Continuous Flow

In this study, a commercial CF photoreactor (Lab Flow Photoreactor©, 2017 Corning Incorporated) was employed (schematic depiction in Figure 3-1). Reactions were performed by pumping a single cooled feedstock solution from a reservoir into a 2.7 mL microfluidic module sandwiched between two light intensity-controllable LED panels and irradiated with 455 nm. A back pressure regulator (BPR) was set at 10-18 bars to solubilize nitrogen evolved from diazo photolysis and ensure a consistent liquid flow rate. Reaction mixtures were collected in a measuring cylinder and responses determined by off-line quantitative NMR analysis using an inert internal standard. We selected yield (Y)

of **3aa** [%], conversion (C) of **2a** [%], selectivity (S) towards **3aa** [%] and productivity (P) of **3aa** [mg/min] as the responses. Initial experiments focused on transferring batch conditions to flow. Due to its low boiling point and associated risk of cavitation, DCM was poorly processible and was initially substituted with (non-ideal) solvent dichloroethane in the initial one-factor-at-a-time (OFAT) optimization (Table 3-1). DCE as solvent allowed stable flow rates and allowed the effect of various factors on the reaction to be evaluated. Temperature (T), concentration of diazo **2a** (the molar ratio of **2a** : **1a** was kept constant at 1 : 5), residence time (t_R) (as a function of the flow rate) and light intensity (I_L) were varied. While temperature did not appreciably affect the results of the experiments (Table 3-1, entries 1-3), all other factors were crucial for the reaction (Table 3-1, entries 4-7). An increased backpressure (from 10 to 18 bar) was required for runs with a higher concentration (Table 3-1, entry 7) to prevent gas evolution in the microfluidic path and ensure stable flow rates. Performing the reaction in DMC resulted in improved yield, selectivity, and productivity (Table 3-1, entries 6 vs 8). For completeness, a control reaction conducted in DCE without light confirmed the photochemical nature of the reaction and the recovery of diazo **2a** (Table 3-1, entry 9).

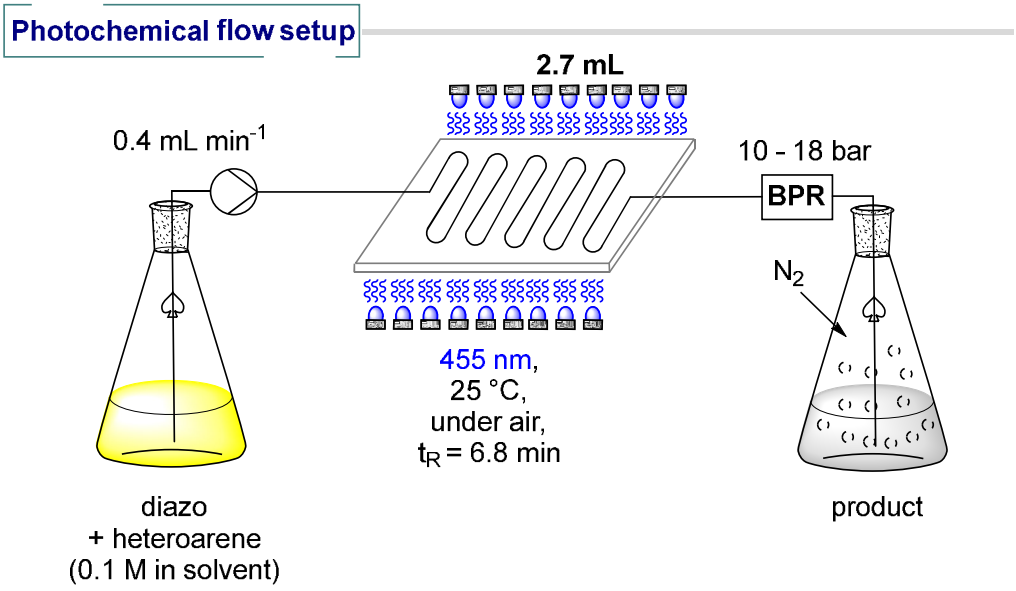

Figure 3-1. Configuration of the photochemical flow reactor with feedstock solution, dual-piston pump, microfluidic module (2.7 mL), BPR and collection flask.

Table 3-1. Selected results from the initial experiments according to OFAT changing temperature, t_R, I_L, overall concentration, and solvent at a back pressure of 10 bars.

Entry	Solvent	Conc. **2a** [M]	**tR** [min]	I_L [%]	*T* [°C]	C[a] of **2a** [%]	Y[a] of **3aa** [%]	S[a] to **3aa** [%]	P[a] of **3aa** [mg h-1]
1	DCE	0.1	6.8	100	5	88	67	76	348
2	DCE	0.1	6.8	100	25	91	67	74	348
3	DCE	0.1	6.8	100	40	93	66	71	340
4	DCE	0.1	3.9	100	25	79	56	71	509
5	DCE	0.03	6.8	100	25	95	54	57	85
6	DCE	0.1	6.8	50	25	66	47	72	246
7[b]	DCE	0.3	6.8	100	25	71	53	75	831
8[b]	**DMC**	**0.1**	**6.8**	**100**	**25**	**89**	**77**	**87**	**400**
9	DCE	0.1	6.8	0	25	0	0	0	0

[a]determined by quantitative NMR analysis by addition of 1,3,5-trimethoxybenzene as an internal standard before running the experiments, estimated error ±5 %. [b]performance at 18 bars of backpressure.

3.3.2 DoE Optimization Study

Recently, the synthetic community has realized that CF is a powerful tool to rapidly acquire data for statistical optimization methods that expediate the identification of optimal conditions.[38–41] Using the conditions of entry 8 (Table 3-1) as a starting point, and with confidence in the robustness of the system to rapidly acquire highly reproducible data, a DoE-assisted optimization was performed to find the optimal reaction conditions within the processable limits of the system. I_L, equivalents of heteroarene partner and flow rate (f_R) were defined as factors. We chose the ratio of diazo : heteroarene over the overall concentration with the view to identify the most sustainable conditions as possible and to experimentally substantiate any requirement for an excess of heteroarene **1**. To investigate significant (a = 0.05) effects of the singular factors as well as the possible presence of multifactor interactions on responses, a "two-level full factorial" design (TFF) was employed (for more details see *3.4.3 Software-Supported Optimization by Design of Experiment (DoE)*), costing 8 experiments and several center points for error validation. A mathematical model was fitted to the data according to which model gave the best statistical fit according to ANOVA (analysis of variance). It could be seen that none of the four responses were influenced by multifactor interactions. Conversion was influenced only by two factors; f_R had a negative influence while I_L had a positive influence, as expected.[42] Yield was influenced by all three factors, where only f_R had a negative effect. Selectivity was influenced neither by f_R nor I_L, but was heavily influenced by the ratio of **2a** : **1a**. This justified the use of an excess of furan (**1a**), presumably necessary to intercept the carbene intermediate from **2a** before its dimerization or further

degradation. Productivity was the only response positively influenced by all three factors, as expected. We sought to identify the optimal conditions within this design space. While the TFF design could sufficiently compare relative influences effects of different experimental factors, it was inappropriate for accurate result predictions due to the inability to model data curvature. Therefore, a face-centered central composite design (FCC) was employed to obtain a more accurate response surface (Figure 3-2). FCC response surfaces for both selectivity and productivity gave maxima in the studied design space. In the case of yield and conversion, response surfaces indicated that longer t_R could improve responses further. However, preliminary experiments showed that slower flow rates led to instability of the flow and larger errors in t_R. The requirement for excess furan to achieve high yield, selectivity and productivity was evident from all response surfaces. The response surfaces were validated by performing three experiments at selected points on the surface (Table 3-2). While two of these were for simple validation, the third experiment aimed to predict the optimal conditions according to 'desirability'. Selectivity was assigned the highest desirability, yield and productivity the second highest, and conversion the lowest. A highly productive and effective process would be economically more attractive than a process at quantitative conversion but lower efficiency, especially in this reaction, in which the unconsumed substrates are easily recoverable. Actual values of conversion (Table 3-2, entries 1-3), yields as well as the productivities of entry 1 and 3 were just outside the calculated space, but agreement was deemed acceptable taking into account quantitative NMR analytics subject of an error of ±5% (for more details see *3.4.3 Software-Supported Optimization by Design of Experiment (DoE)*). Due to the control and robustness of the CF system, together with the salient benefit of CF in rapid screening of conditions from a single feedstock, the full dataset for the DoE optimization was collected in just two afternoons. The optimum conditions were exploited to afford 1.5 g of isolated **3aa** after 2.4 h runtime.

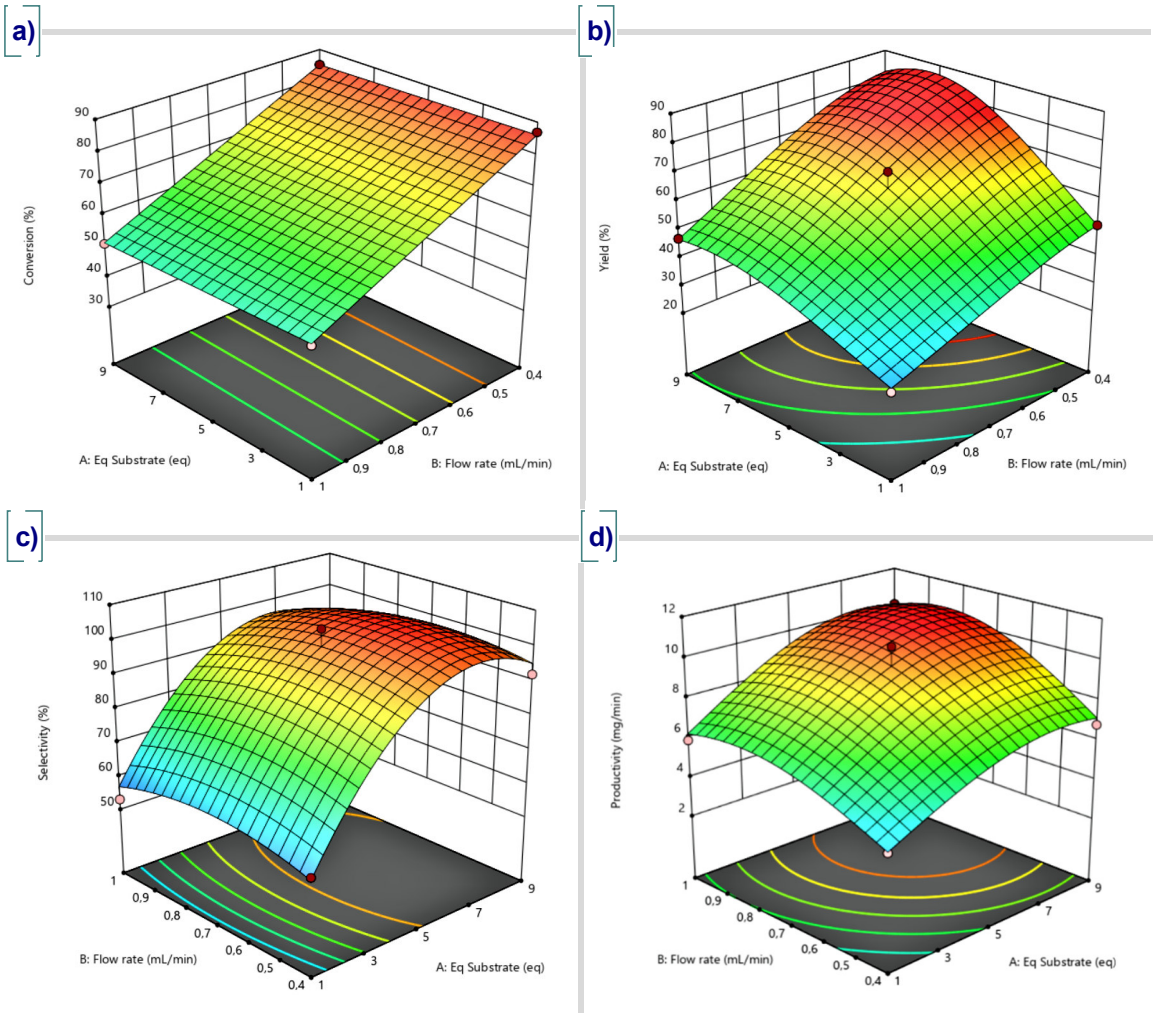

Figure 3-2. Statistically calculated 3-dimensional response surface for a) conversion, b) yield, c) selectivity and d) productivity. All shown curves are for I_L = 100 %. Low and high values of the responses are symbolized by cold and warm areas on the curves.

Table 3-2. Model confirming results.

Entry	Solvent	Ratio	t_R [min]	I_L [%]	C[a] of **2a** [%]	Y[a] of **3aa** [%]	S[a] to **3aa** [%]	P[a] of **3aa** [mg h^{-1}]
1	DMC	4	3.4	80	62 (58)[b],[c]	55 (50)[b],[c]	90 (86)[d]	594 (542)[b],[c]
2	**DMC**	**7**	**4.7**	**100**	**84 (79)**[b],[c]	**82 (87)**[c]	**98 (99)**[d]	**606 (602)**[c]
3	DMC	8	6.0	60	76 (68)[b],[c]	74 (69)[b],[c]	96 (92)[d]	464 (389)[b],[c]

Predicted results are given in parentheses as mean, upper or lower 95% confidence limits, for more details see *3.4.3 Software-Supported Optimization by Design of Experiment (DoE)*. [a]determined by quantitative NMR analysis by addition of 1,3,5-trimethoxybenzene as an internal standard before running the experiments, estimated error ±5%. [b]In these cases, the actual value was not within the calculated range, but taking into account the standard errors of design and the analytical method together, predicted and measured values were in reasonable agreement. [c]The upper limit of prediction is shown. [d]The lower limit of prediction is shown.

3.3.3 Gram-Scale Experiment

Increasing the overall concentration of the optimal conditions defined by our desirability from 0.1 M to 0.3 M (diazo **2a**) more than doubled productivity of **3aa** from 0.61 g h^{-1} to 1.34 g h^{-1}. Under these conditions, 9.9 g of **3aa** were isolated after 7.4 h runtime (Scheme 3-3).

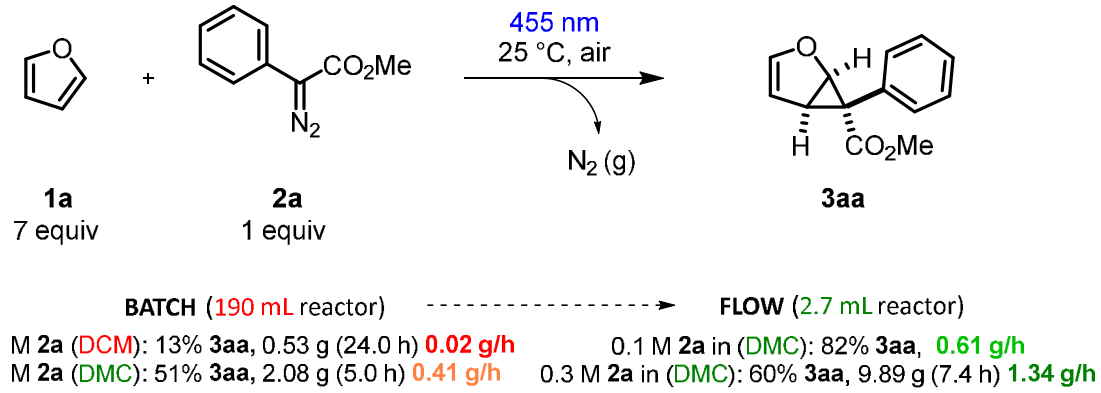

Scheme 3-3. Comparison of large-scale batch reaction in DCM and DMC, respectively, with the long-term continuous flow reaction under optimal and more productive conditions, respectively.

Under the most productive CF conditions, yield was lower than the optimal conditions due to a decrease in conversion. In all cases, the unconverted substrates were easily recovered by distillation (**1a**) and column chromatography (**2a**), respectively. A large-scale batch reaction was performed under analogous conditions to the optimal flow reaction (Scheme 3-3). A 0.1 M solution of **2a** (190 mL) in DMC were irradiated in a large-scale batch laboratory reactor at a wavelength of 455 nm (Figure 3-4). After 5 h, the reaction had completed and 2.0 g (yield 51%) of **3aa** were isolated (a nominal productivity of 0.40 g h^{-1}) This result clearly underlined the advantage in efficiency of performing the photocyclopropanation in CF compared with a large-scale batch reactor, likely due to the continuous removal of **3aa** from the reaction conditions which mitigates against the product undergoing cyclopropanation (di-adduct) or decomposition pathways. The overall size-footprint and hazard of the CF reactor is much lower, due to the reactor volume of irradiated diazo **2a** being 70x smaller than the large-scale batch reactor. Compared to a gram-scale reaction in DCM, the benefit of DMC as a green solvent was also apparent in batch, increasing the yield from 13% to 51% on a larger scale.

3.3.4 Substrate Scope

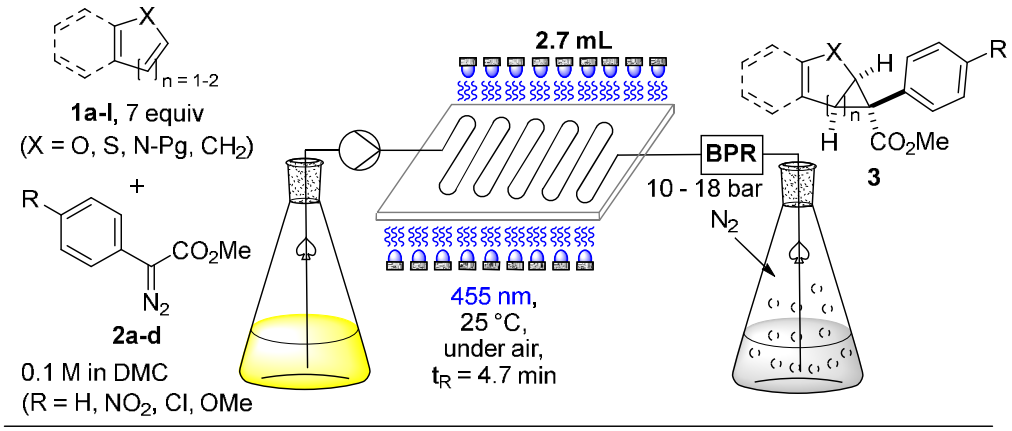

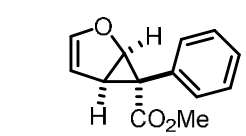

3aa
82%, **608 mg/h**

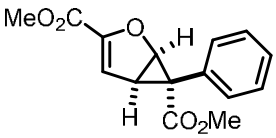

3ba
52%, **384 mg/h**

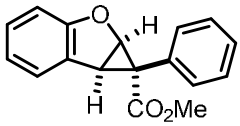

3ca
49%, **362 mg/h**

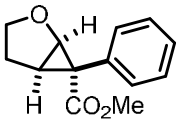

3da*
61%, **451 mg/h**

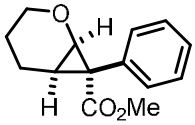

3ea*
52%, **385 mg/h**

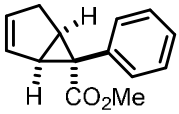

3fa*
71%, **525 mg/h**

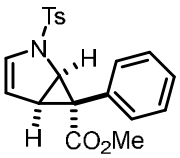

3ga*
51%, **377 mg/h**

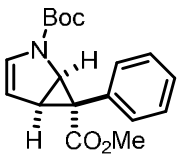

3ha
51%, **377 mg/h**

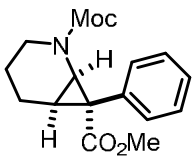

3ia*
57%, **422 mg/h**

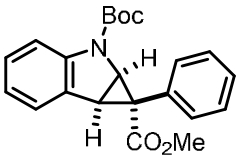

3ja
56%, **414 mg/h**

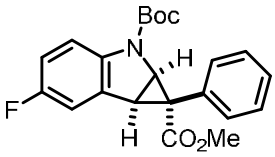

3ka*
57%, **422 mg/h**

3la
29%, **214 mg/h**

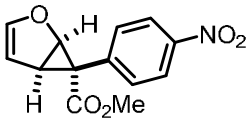

3ab[a]
27%, **140 mg/h**

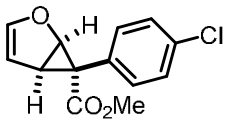

3ac[a]
48%, **249 mg/h**

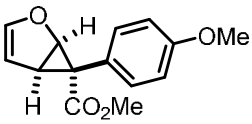

3ad
69%, **510 mg/h**

Scheme 3-4. Substrate scope under the optimized conditions. [a]A longer residence time (t_R = 6.8 min) was employed due to lower conversion of electron-poor diazo compounds.

With optimal conditions in hand, several arenes **1a–l** as well as diazo compounds **2a–d** were converted under optimized conditions in flow (Scheme 3-4). Unsurprisingly, results were the best using the model substrates of the optimization study furan **1a** and diazo acetate 2a. While the yields of **3ba**–**3ka** and **3ac**–**3ad** were good to very good (ca. 50–70%), the yields of **3la** and **3ab** were lower. In the reactions of most heteroarenes and hetero-/carbocycles the conversion of diazo acetate **2a** was in the same range as expected. In the case of the methyl 2-(4-nitrophenyl)-2-diazoacetate (**2b**) and methyl 2-(4-chlorophenyl)-2-diazoacetate (**2c**) the conversion of the diazo compound was low at a 4.7 min residence time. Even at longer residence times (t_R = 6.8 min) the conversion only reached 69% for **2b** and 77% for **2c**. Lower conversion was rationalized by the absorbance of diazoesters at ca. λ = 450 nm light being negatively affected by the substitution at the *para*-position of the aryl group. Thereby, conversion to the reactive carbene intermediate is decreased. Lower product yields of **3ab** and **3ac** may be rationalized by the lower concentrations of carbene intermediate at a given time in the reactor, which may be prone to competing pathways if the reaction rate with the heterocycle is not sufficiently fast. In contrast, an electron-donating group (EDG) at the same position (in **2d**) increased absorbance at ca. λ = 450 nm, resulting in more consumption of the diazo compound **2d** (for UV/Vis spectra of diazo compounds, see Figure 3-10). These results consisted with previous small-scale batch results in our group, where **3ab** and **3ad** were obtained in 40% and 73%, respectively, similar to the selectivity observed herein had the reactions of **2c** and **2d** reached full conversion in CF. An analogous observation on the importance of *para*-substitution at the aryl diazoester was made in a blue light-induced [4 + 1]-annulation under batch conditions.[43] Koenigs *et al.* described the photocyclopropanation of styrenes in CF *via* the photolysis (λ = 470 nm) of various aryl diazoesters **2** with EWGs and EDGs. However, in their report diazo compounds were fully consumed to their carbene equivalents, likely due to the long residence times employed (t_R = 1 h), thus reactivity differences of substitution on the aryl ring were not identified.[32]

In addition to the differences in conversion, selectivity was influenced by substitution on the aryl group of **2**.[44–47] Decreases in yield and selectivity when a *para*-EDG was present in the aryl diazoester were previously attributed to the less electrophilic character of the singlet carbene derived from **2d**.[46] Herein, photolysis of diazoacetate **1a** always resulted in a selectivity of ca. 60% or more (except in the synthesis of **3la**), somewhat lower than in described batch reactions.[29,48] This was attributed to performing the optimization study with furan (**1a**) as the model substrate. Cyclopropanations of benzothiophene (**1l**) and

thiophene have rarely been described before by a metal catalyzed approach.[6,48–50] In general, cyclopropanation of sulfur-containing heteroarenes are rare, challenging reactions. In the case of the synthesis of compound **3la**, the selectivity of 39% accorded with a published small scale batch reaction, in which a 43% selectivity was reported.[48] The low yield (and selectivity) of **3la** could be rationalized by ylid formation.[51] The structure of the cyclopropanes was confirmed using cyclopropanated benzothiophene (**3la**) as an example by X-ray crystallography (structure is shown in *3.4.4 Synthesis and analytical Data*). Despite inferior results of some substrates, in all cases, the CF photocyclopropanation successfully delivers several hundred mg of products per hour as useful, highly-functionalized intermediates for further synthetic applications. Thus, our conditions serve as an efficient platform to rapidly provide useful quantities of cyclopropanated intermediates in the context of their uses in drug discovery or reaction discovery.

3.3.5 Conclusion

In conclusion, we report a highly efficient, selective and catalyst- free visible light photocyclopropanation of both heteroarenes and hetero-/carbocycles in continuous flow. Hazards associated with the explosivity of diazo compounds and their evolution of N_2 upon reaction are safely contained by back pressure in a microfluidic module and by a small volume of reaction mixture exposed to the reaction conditions at any given time. The robustness of the reactor system allowed rapid identification of optimal conditions *via* Design of Experiment analysis, which in turn demonstrated the key importance of heterocycle stoichiometry on high selectivity and yields. The reaction is amenable to a variety of heterocyclic cores and diazoesters and can be easily scaled to gram per hour productivities in dimethyl carbonate as a non-toxic, biodegradable ‘green’ solvent.

3.4 Experimental Part

3.4.1 General Information

Reagents, Solvents and Working Methods

Commercially available chemical materials were purchased in high quality and were used without further purification. Solvents for reaction mixtures were used in p.a. quality or dried according to common procedures.[52] EtOAc and hexanes (40-60 °C) for chromatography were distilled prior to use. The reported yields are referred to isolated compounds unless otherwise stated. Reactions were monitored by thin layer chromatography (TLC).

Nuclear Magnetic Resonance Spectroscopy (NMR)

NMR spectra were recorded using a Bruker Avance 400 (^{1}H: 400 MHz, ^{13}C: 101 MHz, T = 298 K) instrument. All chemical shifts are reported in δ[ppm] (multiplicity, coupling constant *J*, number of protons, assignment of proton) relative to the solvent residual peak as the internal standard. All spectra were recorded in $CDCl_3$ (δ = 7.26 ppm in ^{1}H NMR, δ = 77.16 ppm in ^{13}C NMR). The spectra were analyzed by first order and coupling constants *J* are given in Hertz [Hz] and are uncorrected. Abbreviations used for ^{1}H NMR signal multiplicity: s = singlet, br. s = broad singlet, d = doublet, dd = doublet of a doublet, ddd = doublet of a doublet of a doublet, ddt = doublet of a doublet of a triplet, t = triplet, q = quartet, m = multiplet, b = broad.

Chromatography

Thin-layer chromatography (TLC) was performed with TLC precoated aluminum sheets (Machery-Nagel TLC sheets ALUGRAM Xtra SIL G/UV254, thickness 0.2 mm). Visualization was accomplished by a dual short (λ = 254 nm) / long (λ = 366 nm) wavelength UV lamp. Where necessary, staining was done with a vanillin (6.0 g vanillin in 100 mL ethanol) or potassium permanganate (1.0 g $KMnO_4$ and 2.0 g $Na_{2c}O_3$ in 100 mL water) solution. Column chromatography was performed using silica gel (Merck Geduran Si 60, 0.063-0.200 nm particle size) and/or flash silica gel 60 (Merck Geduran Si 60, 0.040-0.063 nm particle size) as the stationary phase in glass columns with either G2 or G3 frits. 4

UV/Vis Spectroscopy

UV/Vis spectroscopy was carried out on an Analytik jena Specord® 200Plus. All compounds were measured at 10 µM in dimethylcarbonate in a 10 x 10 mm quartz cuvette; the solvent used for their preparative flow reactions. Measurement range was from 190 nm to 1100 nm.

Mass Spectrometry

Mass spectrometry was performed in the Central Analytical Department of the University of Regensburg on an Agilent Technologies 6540 UHD Accurate-Mass Q-TOF LC/MS. Masses observed are accurate to within ±5 ppm. The Ionization method is noted at the analytical data of each compound (ESI = electrospray ionization, EI = electron ionization).

IR Spectroscopy

ATR-IR spectroscopy was carried out on a Biorad Excalibur FTS 3000 MX, equipped with a Specac Golden Gate Diamond Single Reflection ATR-System or on an Agilent Technologies Cary 630 FTIR. Solid and liquid compounds were measured neat as a thin film.

X-Ray Crystallography

X-ray crystallographic analysis was performed by the Central Analytic Department of the University of Regensburg using an Agilent Technologies SuperNova, Single clear colourless block-shaped crystals of **3la** were used as supplied. A suitable crystal with dimensions 0.14 × 0.13 × 0.11 mm^3 was selected and mounted on a MITIGEN holder oil on a XtaLAB Synergy R, DW system, HyPix-Arc 150 diffractometer. The crystal was kept at a steady T = 123.00(10) K during data collection. The structure was solved with the ShelXT 2018/2 (Sheldrick, 2018) solution program using dual methods and by using Olex2 1.3-alpha (Dolomanov *et al.*, 2009) as the graphical interface. The model was refined with ShelXL 2018/3 (Sheldrick, 2015) using full matrix least squares minimisation on F^2.

Melting point measurements

Melting points were recorded on Stanford Research Systems OptiMelt MPA 100 Automated Melting Point System.

3.4.2 Setup of the Photochemical Reactors

Photochemical Flow Reactor

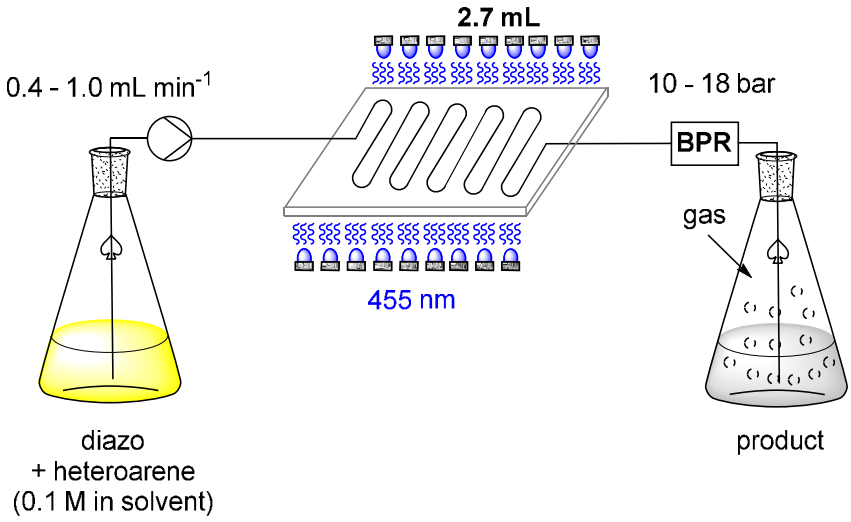

Figure 3-3. Schematic of the flow reactor set-up including reaction mixture feedstock, pump, fluidic module (2.7 mL), BPR and collection flask.

All flow reactions were performed in a *Corning® Advanced-FlowTM Lab Photo Reactor*. The reactor comprised of one fluidic module type G1 LF (glass) for low flow rates, two LED panels composed of 6 x 20 LED each (20 LEDs of each wavelength on each panel, irradiation from both sides, radient power of each LED at 100%: 1360 mW (700 mA), therefore 27.2 W input power for each panel), a dual piston pump with a metal free Teflon pump head, an adjustable back pressure regulator (BPR) and two thermostat units (for controlling temperature of LEDs and for controlling the user specified temperature of the fluidic module). Settable wavelengths of the LEDs were 340, 375, 395, 420, 450 and 530 nm; 450 nm was used throughout this study as guided by the UV/Vis spectra of diazoesters. The fluidic module was designed for the mixture of one or two flow paths and had a total reactor volume of 2.7 mL. To mitigate background photodegradation or evaporation of arene substrate, pre-prepared reaction mixture feedstocks were maintained in an ice bath and in the dark before pumping into the reactor system *via* the dual piston pump. Depending on the reaction mixture concentration, the adjustable back pressure regulator was set between 1018 bars (0.1 M = 10 bars, 0.3 M = 18 bars) to keep nitrogen – which evolved during photolysis of the diazoesters – in solution and thus to ensure a constant flow rate. The pressure in the reactor was monitored by a pressure sensor integrated into the pump module. For safety and to maintain integrity of the fluidic

module, the maximal allowed pressure was set to 18 bar on the pump sensor such that exceeding 18 bar pressure ceased the flow. A schematic is depicted in Figure 3-3.

Photochemical Big-Scale Batch Reactor

Figure 3-4. Large-scale batch photo-reactor.

3.4.3 Software-Supported Optimization by Design of Experiment (DoE)

A design space for optimization was chosen by the reliable operational limits of the factors of interest as well as prior knowledge of the system:

Flow rate "f_R" = 0.4 (lowest precise flow rate of the pump module under the conditions of back-pressure) → 1.0 mL/min {poor conversion due to too short residence time};

Llight intensity "I_L" = 0 → 100% (as defined by the reactor system);

equivalents of **1a** from 1 → 9 (aiming for the compromise of lowest possible equivalents of **1a** while prioritizing highest possible selectivity and yield).

Experiments at the extremes of the design space were investigated, along with replicate center points to model a 3-dimensional response surface and predict the optimal conditions or to predict the next iteration of design space based by statistical software analysis. The software *Design Expert Version 12* by *StatEase®* was used to interpret the results and to build a statistical model to fit the experimental data (by ANOVA). During the DoE, a "two-level full factorial" (TFF) design and subsequent face-centered central composite (FCC) design was carried out. For TFF, M^n experiments were required, where M is the number of levels and n is the number of factors. In this case, 8 (= 2^3) experiments were performed without counting center points or replicates (Figure 3-5, a). FCC design contains an embedded factorial design with center points that are amplified with a group of star points at the center of each face of the factorial space, for curvature modelling (Figure 3-5, b). TFF design results are in Table 3-3.

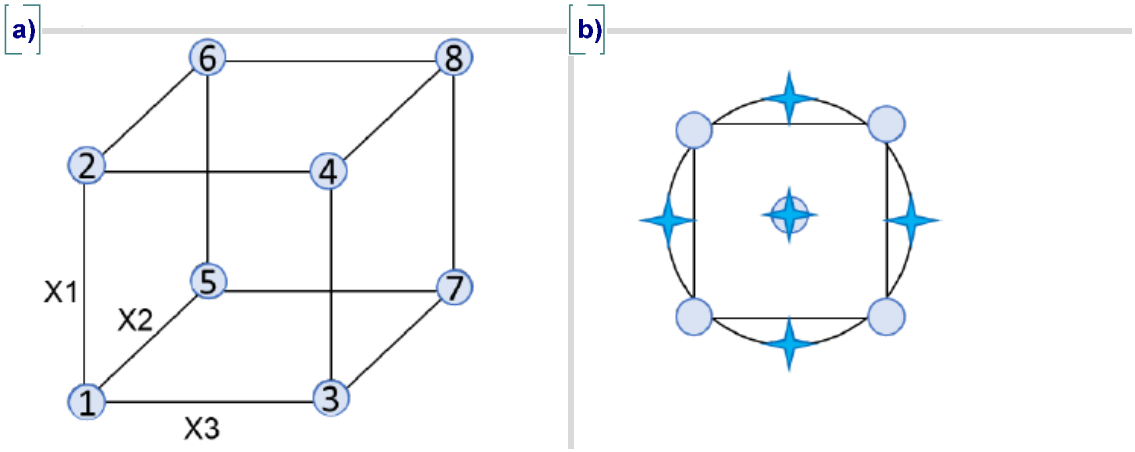

Figure 3-5. a) Two-level full factorial (TFF) design with three factors and b) 2-dimensional view of the 3-dimensional (cube) face-centered central composite (FCC) design for DoE study.

Table 3-3. Results of the Two-level Full Factorial (TFF) Design: Photoinduced Cyclopropanation of Furan (**1a**)

Std	Run	**A**: Substrate **1a** [equiv]	**B**: f_R [mL/min]	**C**: I_L [%]	C[a] of **2a** [%]	Y[a] of **3a** [%]	S[a] to **3a** [%]	P[a] of **3a** [mg h^{-1}]
6	1	9	0.4	100	85	79	92	408
11	2	5	0.7	75	55	53	96	483
4	3	9	1.0	50	34	30	90	396
3	4	1	1.0	50	33	20	62	265
9	5	5	0.7	75	57	53	92	478
1	6	1	0.4	50	68	36	52	185
2	7	9	0.4	50	63	59	94	308
10	8	5	0.7	75	57	52	92	475
7	9	1	1.0	100	52	27	53	352
8	10	9	1.0	100	51	47	91	608
12	11	5	0.7	75	62	61	98	557
5	12	1	0.4	100	87	51	58	263
13	13	5	0.7	75	61	58	96	527

[a]determined by quantitative NMR analysis by addition of 1,3,5-trimethoxybenzene as an internal standard before running the experiments, estimated error ±5%. P = productivity, Y = yield, C = conversion, S = selectivity.

For the analysis, the data were fitted into the model which gave the best statistical fit according to ANOVA (analysis of variance). For conversion and selectivity, a linear model was most suitable. In the case of yield and productivity, a decadic logarithmic model fitted most. From the TFF design analysis, half normal plots were obtained, which graphically identify whether or not factors and factor interactions had a significant effect on the given response and compare the degree of their influence qualitatively (Figure 3-6). The green triangles on each graph intersected by the red line represented the experimental error derived from replicates of the center data points. Factors close to the intersecting red line carried an insignificant effect, while the relative distance of the other factors from that line indicated their degree of influence. It could be seen that none of the four responses was influenced by an interaction. In the case of conversion, the factor f_R had a negative (longer t_R leading to higher conversion) while the factor I_L had a positive influence on the response (Figure 3-6, a). The yield was controlled by all three factors, with only f_R having a negative effect (Figure 3-6, b). Selectivity was not affected by either f_R or I_L, but the ratio between substrates was crucial for this response (Figure 3-6, c). Productivity was positively influenced by all three factors (Figure 3-6, d). While all the influences of the singular factors on each response were as expected, it could not be

assumed that no interactions between the factors affected the outcome of the runs. Thus, the results indicated a simple factor-response correlation.

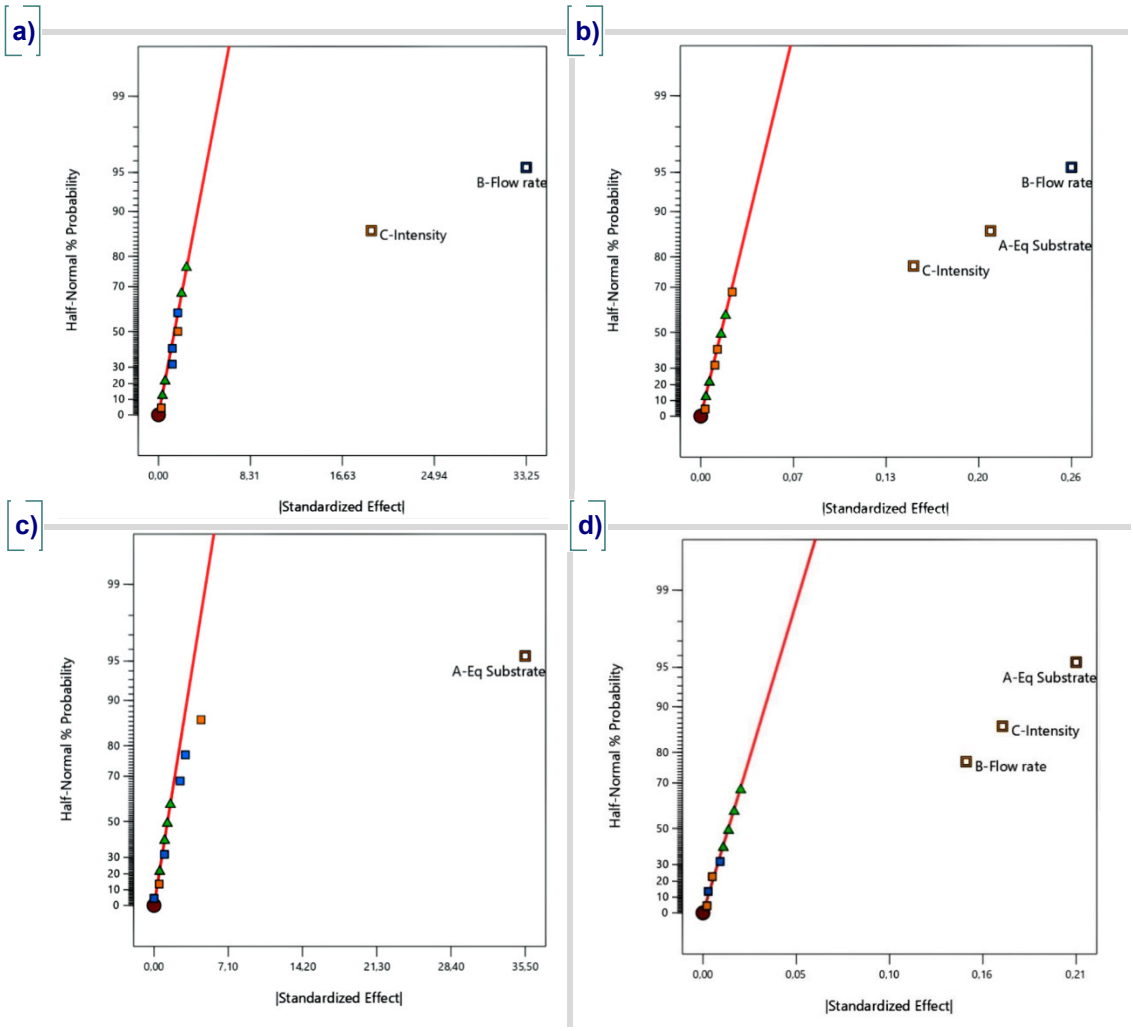

Figure 3-6. Evaluation of significant effects of the factors on each response by Shapiro test. Statistically based calculations with a = 0.05 showed the qualitative effect. Orange squares (■) symbolizing positive, blue squares (■) symbolizing a negative impact on the responses, the experimental error was symbolized by the green triangles (▲). a) conversion of 2a, b) yield of 3a, c) selectivity towards 3a and d) productivity of 3a. "Eq substrate" (A) stands for the equivalents of substrate **1a** in respect to 1 equiv of 2a. Flow rate (B = f_R) was given in mL/min. "Intensity" stands for relative light intensity (C = I_L).

While the TFF design could sufficiently compare the effects of different experimental factors, it is unable to model data curvature and was therefore inappropriate for accurate result predictions. This can be seen in the higher standard error of design moving in any direction away from the center points (Figure 3-7). Therefore, a face-centered central composite (FCC) design was employed to determine the optimized reaction conditions.

The TFF design was augmented with an additional six experiments (a “star design”). Usually, this star design employs data points outside of the TFF cube to minimize the standard error of design further, however longer t_R than 6.7 mL/min and more than 100% of I_L could not practically be achieved due to instability of flow rates at lower than 0.4 mL/min and other instrumental limits (negative intensity, flow rate and equivalents are impossible). Therefore, the star points of the FCC design were positioned on the faces of the cube (Figure 3-5, b). Its results are given in Table 3-4.

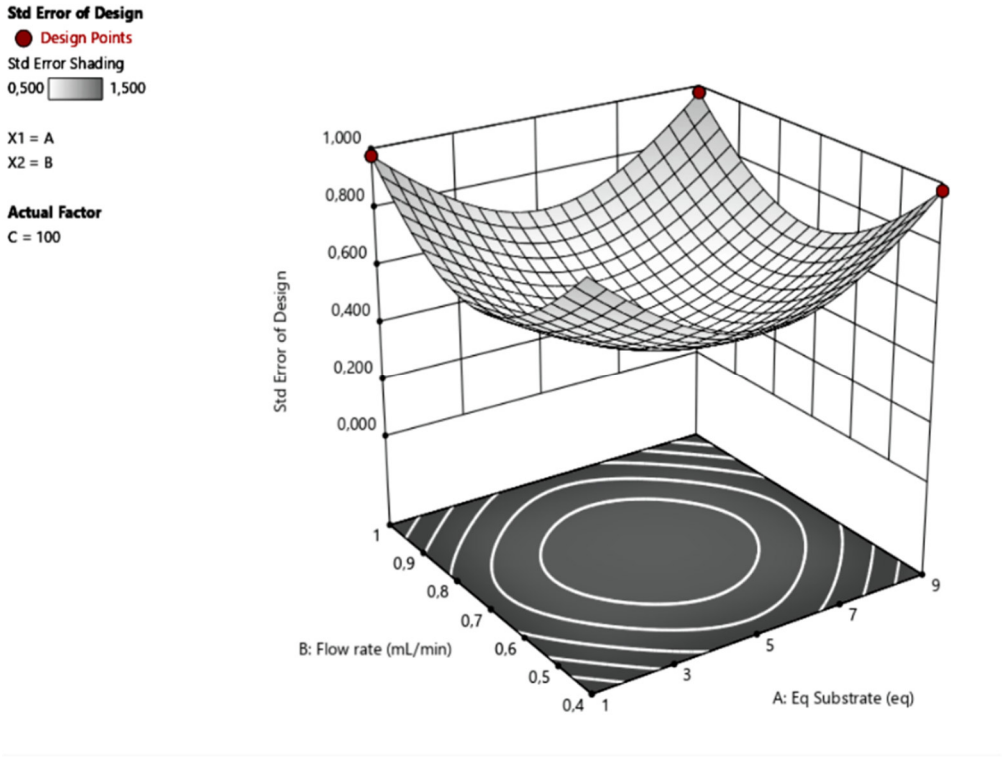

Figure 3-7. Statistical standard error for two-level full factorial (TFF) design.

Table 3-4. Results of the Face-Centered Central Composite Design : Cyclopropanation of Furan (**1a**)

Std	Run	**A**: Substrate **1a** [equiv]	**B**: f_R [mL/min]	**C**: I_L [%]	C[a] of **2a** [%]	Y[a] of **3a** [%]	S[a] to **3a** [%]	P[a] of **3a** [mg h^{-1}]
8	1	9	1.0	100	51	47	91	608
14	2	5	0.7	100	68	70	104	639
15	3	5	0.7	75	55	53	96	483
6	4	9	0.4	100	85	79	92	408
5	5	1	0.4	100	87	51	58	263
2	6	9	0.4	50	63	59	94	308
10	7	9	0.7	75	60	56	94	509
19	8	5	0.7	75	57	52	92	475
4	9	9	1.0	50	34	30	90	396
17	10	5	0.7	75	57	53	92	478
18	11	5	0.7	75	62	61	98	557
11	12	5	0.4	75	75	68	92	355
12	13	5	1.0	75	40	37	93	481
9	14	1	0.7	75	59	37	62	334
3	15	1	1.0	50	33	20	62	265
7	16	1	1.0	100	52	27	53	352
13	17	5	0.7	50	40	38	96	349
16	18	5	0.7	75	61	58	96	527
1	19	1	0.4	50	68	36	52	185

[a]determined by quantitative NMR analysis by addition of 1,3,5-trimethoxybenzene as an internal standard before running the experiments, estimated error ±5%. P = productivity, Y = yield, C = conversion, S = selectivity

The analysis of the FCC design led to the modeling of the curvatures for each response (Figure 3-8).

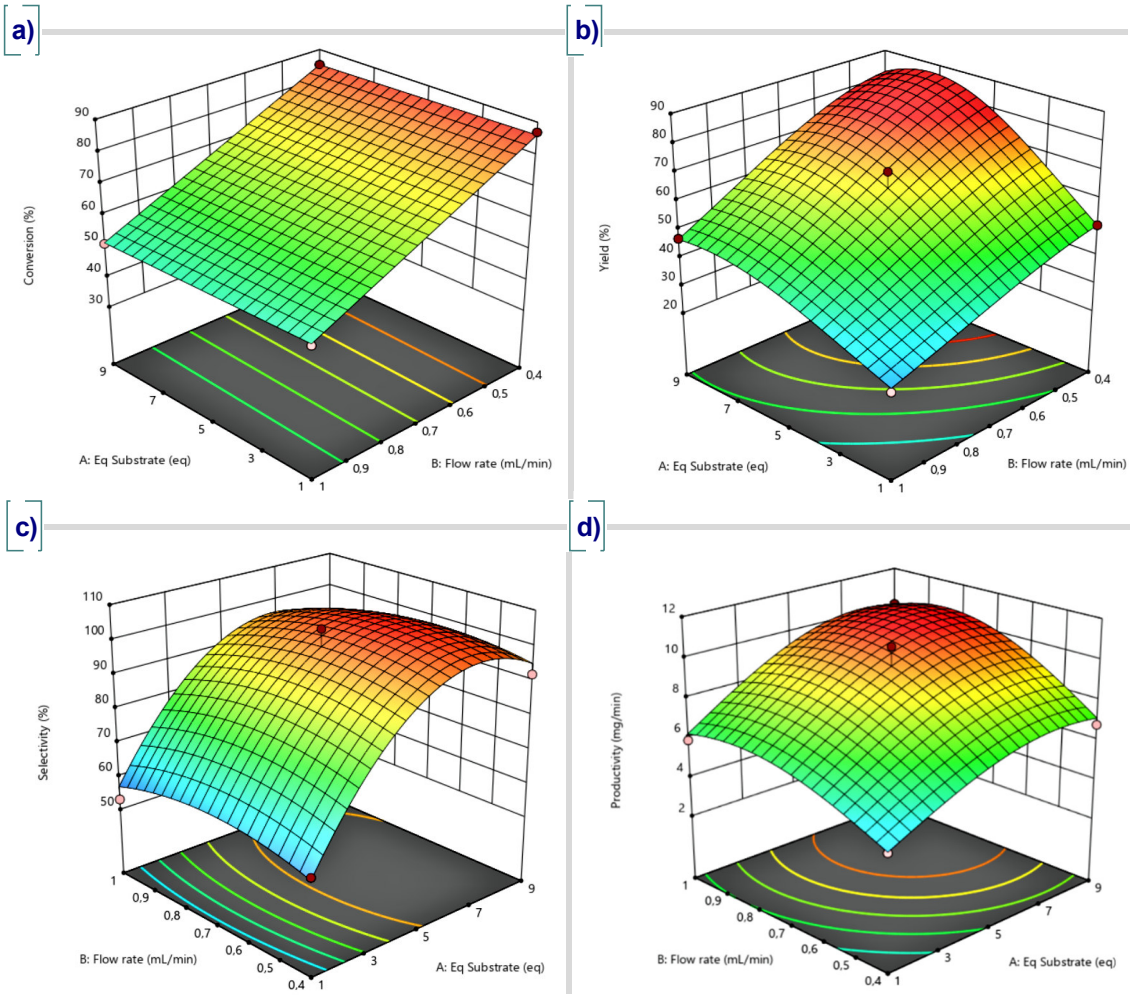

Figure 3-8. Statistically-calculated 3-dimensional response surface for a) conversion, b) yield, c) selectivity and d) productivity. All shown curves are for I_L = 100%. Low and high values of the responses are symbolized by cold and warm areas on the curves.

Conversion and selectivity followed a linear model, while for yield an inverse square root model and productivity a decadic logarithm model were most suitable. For all responses, the optimum lay in the investigated design space for the used reactor system. Both, the graph of productivity and the curve of selectivity showed their maximum in the studied range. In the case of yield and conversion, the curves indicated that with a longer t_R the results of both responses could be further improved. However, preliminary experiments showed that slower flow rates led to a larger error in the t_R and the outcome of the experiments became subject to a larger variation. In addition, it was evident from the response surfaces that an excess of furan was essential to maintain high yield, selectivity, and productivity. Unreacted furan (**1a**) was recovered easily by distillation.

The statistical models were confirmed by further validation experiments setting certain conditions and comparing the results predicted by the model and the experimental results. In this sense, the results of three new conditions were examined, which had not yet been performed during the DoE or OFAT study. While two experiments aimed only to validate the response surface, a third experiment aimed to both validate the response surface and to confirm the results of the predicted optimal conditions. To determine our 'optimal' conditions, the 'desirability' algorithm of the software was employed - selectivity was assigned the highest desirability, yield and productivity the second highest, and conversion the lowest desirability. A highly productive and effective process would be economically more attractive than a process at quantitative conversion but with lower efficiency, especially in this reaction, in which the unconsumed substrates are easily recovered. The results of the confirmation runs are summarized in Table 3-5. The means of the predicted results are given in parentheses. The comparison of the experimental and predicted values is based on statistical calculations. The software specified a range around the predicted value. If the value of the actual result lied within this calculated range, then it was valid with a confidence interval of 95% that the difference between the determined and the predicted result was insignificant. The error type I was therefore 5% (in summary for both sides of the Gaussian curve), i.e. the probability that an actual value, in reality, differed significantly from the predicted value, but this was not identified, was 5%. All experimental values of the conversion (entries 1-3), the measured values of the yields, as well as the productivity of entries 1 and 3 were just outside the calculated space, but the analytics by quantitative NMR was subject to an estimated error of $\pm$5%. Given the likely overlap of the analytical and DoE response surface errors, the agreement is overall reasonable. Since the predicted values of the other responses were confirmed, the response surface model was experimentally validated.

Table 3-5. Confirmation of the obtained model by performing of three runs three times . Conditions of entry 1: **2a** 1 equiv : 4 equiv **1a**, t_R = 3.4 min, I_L = 80%; entry 2: **2a** 1 equiv : 7 equiv **1a**, t_R = 4.7 min, I_L = 100%; entry 3: **2a** 1 equiv : 8 equiv **1a**, t_R = 6 min, I_L = 60%. The "Data Mean" has to lie within the space between "95% low" and "95% high". This space is calculated for an error type I of 5% (both sides of the Gaussian curve). The concentration was 0.1 M with respect to **2a** for all experiments.

Entry	Response	Predicted Mean	Std. Error	n	95% low	Data Mean[a]	95% high
1	Productivity [mg h^{-1}]	502.8756	39.18942	3	471.0546	**594.3594**	536.8458
	Yield	46.9422%	3.26076%	3	42.1041%	**55.2936%**	52.2631%
	Conversion	54.9132%	2.93467%	3	50.921%	**61.6667%**	58.9053%
	Selectivity	90.0486%	3.75104%	3	84.2236%	89.6667%	95.8736%
2	Productivity [mg h^{-1}]	558.762	43.5447	3	495.7536	605.9196	629.778
	Yield	79.4315%	7.16394%	3	66.3135%	81.6731%	95.5709%
	Conversion	75.7432%	2.93467%	3	71.1905%	**83.6667%**	80.2958%
	Selectivity	102.927%	3.75104%	3	95.3594%	97.6667%	110.494%
3	Productivity [mg h^{-1}]	361.2288	28.1508	3	325.5942	**463.8366**	400.764
	Yield	63.4598%	5.12046%	3	54.6024%	**74.2909%**	73.8756%
	Conversion	65.5132%	2.93467%	3	60.8841%	**76.0000%**	70.1422%
	Selectivity	95.2676%	3.75104%	3	88.2628%	96.3333%	102.272%

[a]determined by quantitative NMR analysis by addition of 1,3,5-trimethoxybenzene as an internal standard before running the experiments, estimated error ±5%.

Entry 2 represents the optimal conditions in the specified sense and the best results. It is noteworthy that, due to the position of the star designs on the faces of the cube, the errors on the prediction become larger at the edges of the design space (Figure 3-9).

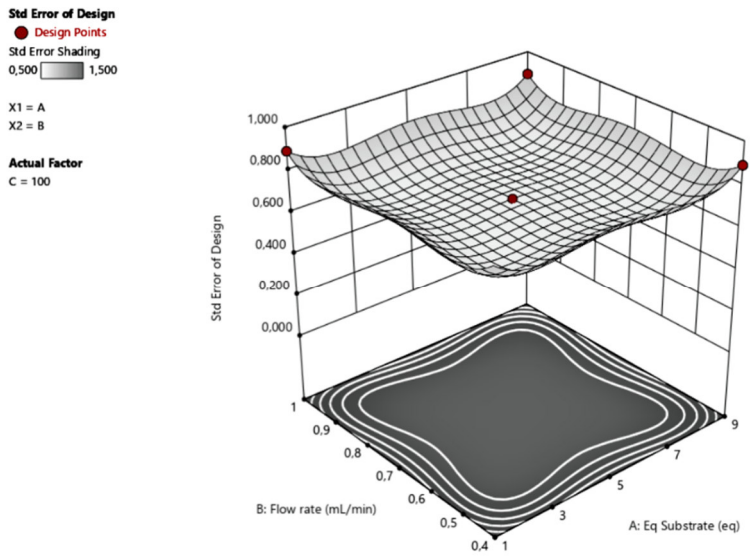

Figure 3-9. Statistical standard error for face-centered central (FCC) composite model.

3.4.4 UV/VIS Spectra of Diazoacetates

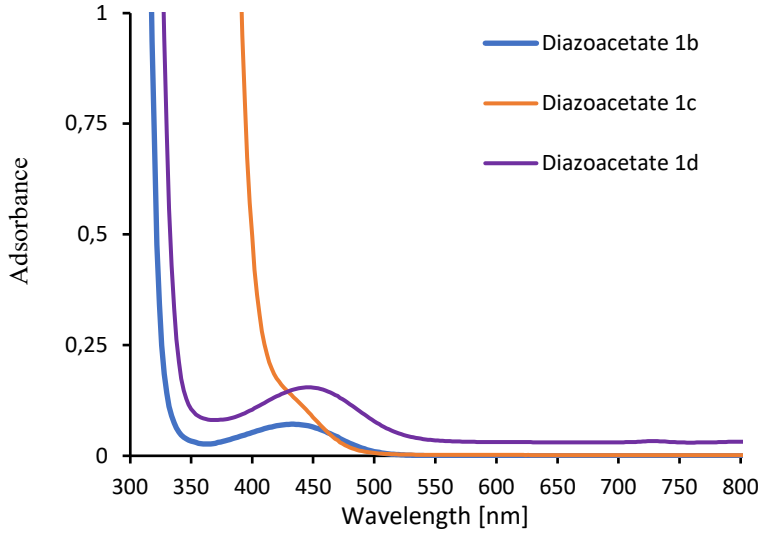

Figure 3-10. UV/Vis spectra of the synthesized aryl diazoacetates **2b-d**.The spectra of **2a** (50 µM) was reported by Davies *et al.*[29]

3.4.5 Synthesis and Analytical Data

Starting Material Synthesis

Heteroarenes **1a**, **1b, 1c**, **1d, 1e** and **1l** were purchased and used without further purification. Cyclopentadiene (**1f**) was freshly destilled from its dimere. Heteroarenes **1g-k** were readily available and synthesized according to the common procedures. Their analytical data are consistent with the literature.[4,53,54]

4-methylbenzenesulfonyl azide **(TsN_3)**

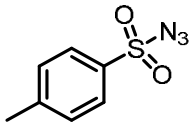

TsN_3

p-Toluenesulfonylchloride (36.2 g, 190 mmol, 1.0 equiv) was dissolved in acetone (200 mL) and water (200 mL). Then **NaN_3** (12.9 g, 199 mmol, 1.1 equiv) was added in portions at 0 °C and the mixture was stirred for 2.5 h at 0 °C. The reaction mixture was concentrated under reduced pressure to half of its volume. The aqueous phase was extracted with Et_2O (3 × 70 mL) and the combined organic phases were dried over

$MgSO_4$. Evaporation of the solvent yielded **TsN_3** (37.3 g, 181 mmol, > 99%) as a colorless oil.

^{1}H NMR (400 MHz, $CDCl_3$): δ = 7.84 (d, J = 8.4 Hz, 2H), 7.41 (d, *J* = 8.0 Hz, 2H), 2.48 (s, 3H).

The analytical data were consistent with the literature.[55]

*CAUTION: Tosyl azide (**TsN_3**), while one of the safer azides and whose utility in the preparation of diazo compounds is noted, thermally decomposes above 120 °C and should be handled at room temperature or below. It forms explosive azides with metals such as Cu, Pb, Hg, Ag, Au, and reacts with acids to form hydrazoic acid (HN_3) which is a toxic, spontaneously explosive gas. Chlorinated solvents should be avoided. All work with NaN_3 should be conducted behind a shield and in a fume hood. Excess NaN_3 is destroyed in a fume hood by oxidation with cerium(IV) ammonium nitrate.* → (a) G. G. Hazen, L. M. Weinstock, R. Connell, F. W. Bollinger, *Synth. Comm.* 1981, **11**, 947-956; (b) P. Cardillo, L. Gigante, A. Lunghi, A. Fraleoni-Morgera, P. Zanirato, *New. J. Chem.* 2008, **32**, 47-53; (c) Bretherick's Handbook of Reactive Chemical Hazards, P.G. UrbenElsevier, Amsterdam, 2007. (d) H. M. L. Davies, W.-h. Hu, D. Xing, Methyl Phenyldiazoacetate, *Encyclopedia of Reagents for Organic Synthesis*, 2015, Wiley.

methyl 2-diazo-2-phenylacetate **(2a)**

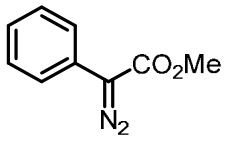

2a

*CAUTION: All aryl diazo esters in the following section were treated as per the title compound. The title compound (**2a**) is stable to storage at room temperature or below. No difficulty was experiences after several years of studying this compound. However, caution is exercised in handling this compound due to its explosive potential; especially heating should be avoided. It is recommended that all procedures using this compound be conducted behind a blast shield* → H. M. L. Davies, W.-h. Hu, D. Xing, Methyl Phenyldiazoacetate, *Encyclopedia of Reagents for Organic Synthesis*, 2015, Wiley.

DBU (29.81 g, 195.8 mmol, 1.5 equiv) was added dropwise to a solution of methyl 2-phenylacetate (16.60 g, 160.6 mmol, 1.0 equiv) and TsN_3 (38.62 g, 195.8 mmol, 1.5 equiv) in dry MeCN (150 mL) at room temperature under nitrogen atmosphere. After stirring for 24 h the mixture was diluted with water (50 mL) and the aqueous phase was extracted with Et_2O (5 x 150 mL). The combined organic layers were washed with brine (150 mL) and dried over $NaSO_4$. The solvent was evaporated and purification of the crude product by column chromatography (PE:EA = 95:5) yielded compound **2a** (21.14 g, 120.0 mmol, 92%) as a red-orange oil.

^{1}H NMR (400 MHz, $CDCl_3$): δ = 7.37 – 7.35 (m, 2H), 7.28 – 7.24 (m, 2H), 7.08 – 7.04 (m, 1H), 3.74 (s, 3H).

The analytical data were in accordance with the literature.[56]

methyl 2-diazo-2-(4-nitrophenyl)acetate **(2b)**

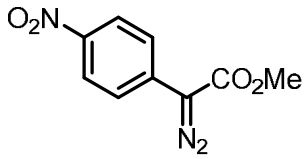

2b

DBU (3.51 g, 23.1 mmol, 1.5 equiv) was added dropwise to a solution of methyl 2-(4-nitrophenyl)acetate (3.00 g, 15.4 mmol, 1.0 equiv) and TsN_3 (4.55 g, 23.1 mmol, 1.5 equiv) in dry MeCN (150 mL) at room temperature under nitrogen atmosphere. After stirring for 24 h the mixture was diluted with water (50 mL) and the aqueous phase was extracted with Et_2O (3 x 50 mL). The combined organic layers were washed with brine (50 mL) and dried over $MgSO_4$. The solvent was evaporated and purification of the crude product by column chromatography (PE:EA = 95:5) yielded compound **2b** (3.00 g, 13.6 mmol, 88%) as a yellow solid.

^{1}H NMR (400 MHz, $CDCl_3$): δ = 8.24 – 8.21 (m, 2H), 7.67 – 7.65 (m, 2H), 3.90 (s, 3H).

The analytical data were in accordance with the literature.[57]

methyl 2-(4-chlorophenyl)-2-diazoacetate **(2c)**

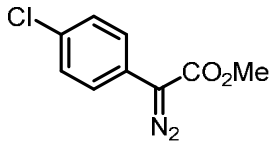

2c

DBU (3.41 g, 22.4 mmol, 1.5 equiv) was added dropwise to a solution of methyl 2-(4-chlorophenyl)acetate (2.75 g, 14.9 mmol, 1.0 equiv) and TsN_3 (4.42 g, 22.4 mmol, 1.5 equiv) in dry MeCN (150 mL) at room temperature under nitrogen atmosphere. After stirring for 24 h the mixture was diluted with water (50 mL) and the aqueous phase was extracted with Et_2O (3 x 50 mL). The combined organic layers were washed with brine (50 mL) and dried over $MgSO_4$. The solvent was evaporated and purification by chromatography (PE:EA = 95:5) yielded compound **2c** (2.73 g, 13.0 mmol, 87%) as an orange solid.

^{1}H NMR (400 MHz, $CDCl_3$): δ = 7.33 – 7.31 (m, 2H), 7.26 – 7.24 (m, 2H), 3.77 (s, 3H).

The analytical data were in accordance with the literature.[56]

methyl 2-diazo-2-(4-methoxyphenyl)acetate **(2d)**

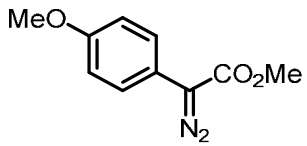

2d

DBU (4.69 g, 30.8 mmol, 1.5 equiv) was added dropwise to a solution of methyl 2-(4-methoxyphenyl)acetate (3.69 g, 20.5 mmol, 1.0 equiv) and TsN_3 (6.07 g, 30.8 mmol, 1.5 equiv) in dry MeCN (150 mL) at room temperature under nitrogen atmosphere. After stirring for 24 h the mixture was diluted with water (50 mL) and the aqueous phase was extracted with Et_2O (3 x 50 mL). The combined organic layers were washed with brine (50 mL) and dried over $MgSO_4$. The solvent was evaporated and purification by chromatography (PE:EA = 95:5) yielded compound **2d** (3.42 g, 16.6 mmol, 81%) as a red solid.

^{1}H NMR (400 MHz, $CDCl_3$): δ = 7.38 – 7.25 (m, 2H), 7.28 – 7.24 (m, 2H), 7.08 – 7.04 (m, 1H), 3.74 (s, 3H), 3.70 (s, 3H).

The analytical data were in accordance with the literature.[56]

General Procedure (GP) for the Photoinduced Cyclopropanation of Heteroarenes in Flow:

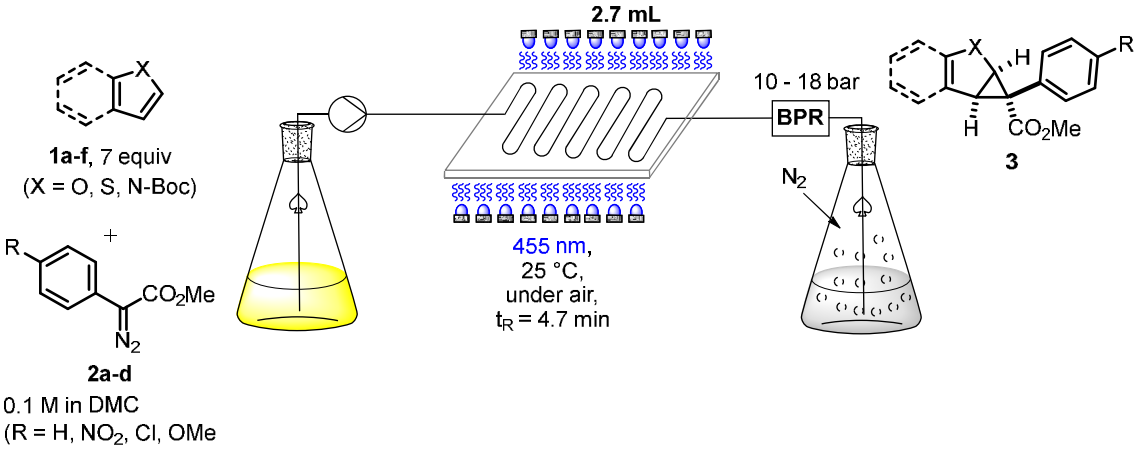

Under air, diazoacetate **2** (1 equiv, 0.1 M), 1,3,5-trimethoxybenzene (0.1 equiv, 0.01M, for quantitative NMR-analysis) and heteroarene **1** (from 7 equiv, 0.7 M) were dissolved in DMC (DCM and DCE during optimization) to form a homogenous feedstock. From this point, the feedstock was kept cool either in the fridge (for storage) or by an ice bath (during experiments) and kept in the dark with foil shielding. Before pumping the solution through the system, the reactor was flushed with the used solvent and the wavelength was set to 455 nm. Each sample was collected after conditioning the reactor to the set conditions (if not otherwise specified, under the optimal conditions as defined by the DoE study: t_R = 4.7 min, I_L = 100%, *T* = 25°C). The volume of each sample was measured and the solvent was evaporated under reduced pressure. Purification was performed by column chromatography using petroleum ether/ ethyl acetate (PE : EA = 19:1, 9:1 + 20% triethylamine) as eluent.

*As reactive intermediates for further synthetic transformations, the hazards of all compounds in family **3** are unknown and compounds should be treated as toxic until data are available.*

methyl (1S,5S,6R)-6-phenyl-2-oxabicyclo[3.1.0]hex-3-ene-6-carboxylate **(3aa)**

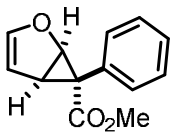

3aa

According to GP, methyl furan (**1a**) (836.8 mg, 6.6 mmol, 7 equiv) and methyl 2-diazo-2-phenylacetate (**2a**) (167 mg, 1 mmol, 1 equiv) were dissolved in DMC (10 mL). The solution was pumped through the reactor and collected. Purification *via* chromatography yielded 177.3 mg of the target compound **3aa** (0.82 mmol, 82%) as a colorless solid.

65 mmol scale run at higher productivity:

Under air, diazoacetate **2a** (14.0 g, 0.080 mol, 1 equiv) and furan (**1a**) (37.9 g ,0.556 mol, 7 equiv) were dissolved in 265 mL DMC to form a homogenous feedstock. From this point, the feedstock was kept cool either in the fridge (for storage) or by an ice bath (during experiments) and kept in the dark with foil shielding. Before pumping the solution through the system, the reactor was flushed with the used solvent. The sample was collected after conditioning the reactor to the set conditions (t_R = 4.7 min, I_L = 100%, *T* = 25°C). After running the experiment for 7.4 h (= after pumping 0.075 mol of the substrate through the reactor system), the volume was measured, the solvent evaporated and the product **3aa** was isolated by column chromatography using petroleum ether/ethyl acetate (PE : EA = 19:1, 9:1 + 20% triethylamine) as eluent to obtain 9.89 g (0.046 mol, 60%, 1331 mg h^{-1}).

Gram-scale batch reaction comparison

Under air, diazoacetate **2a** (3.3 g, 0.019 mol, 1 eq) and furan (**1a**) (9.1 g, 0.133 mol, 7 equiv) were dissolved in 180 mL DMC to form a homogenous solution. The solution was transferred into the large-scale batch reactor and was irradiated at 455 nm. After running the experiment for 5 h, the solvent was evaporated and the product **3aa** was isolated by column chromatography (PE : EA = 19:1, 9:1 + 20% triethylamine) to obtain 2.08 g (9.60 mmol, 51%).

R*f*: (PE:EA =5:1) = 0.35.

^{1}H NMR (400 MHz, $CDCl_3$): δ 7.28 – 7.24 (m, 3H), 7.19 – 7.17 (m, 2H), 5.91 (dd, *J* = 2.6, 0.8 Hz, 1H), 5.22 (t, *J* = 2.6, Hz, 1H), 5.13 (dd, *J* = 5.6, 0.8 Hz, 1H), 3.61 (s, 3H), 3.30 (dd, *J* = 5.6, 2.6 Hz, 1H)

^{13}C NMR (101 MHz, $CDCl_3$): δ = 174, 147.4, 132.8, 130.8, 127.9, 127.6, 104.1, 70.9, 52.6, 39.4, 27.9

The analytical data were in accordance with the literature.[10]

dimethyl (1S,5S,6R)-6-phenyl-2-oxabicyclo[3.1.0]hex-3-ene-3,6-dicarboxylate **(3ba)**

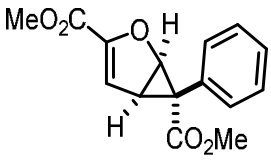

3ba

According to GP, methyl furan-2-carboxylate (**1b**) (836.8 mg, 6.6 mmol, 7 equiv) and methyl 2-diazo-2-phenylacetate (**2a**) (167 mg, 1 mmol, 1 equiv) were dissolved in DMC (10 mL). The solution was pumped through the reactor and collected. Purification *via* chromatography yielded 135.2 mg of the target compound **3ba** (0.52 mmol, 52%) as a colorless solid.

R_f(PE:EA = 5:1) = 0.25.

^{1}H NMR (400 MHz, $CDCl_3$): δ = δ 7.27 – 7.19 (m, 5H), 6.11 (d, *J* = 3.0 Hz, 1H), 5.23 (d, *J* = 5.4 Hz, 1H), 3.64 (s, 3H), 3.61 (s, 3H), 3.37 (dd, *J* = 5.4, 3.0 Hz, 1H);

^{13}C NMR (101 MHz, $CDCl_3$): δ = : δ 173.3, 159.0, 149.0 , 132.4, 129.7, 128.2, 127.9, 114.2, 71.2, 53.0, 52.2, 39.6, 28.7

The analytical data were in accordance with the literature.[10]

methyl (1R,1aS,6bS)-1-phenyl-1a,6b-dihydro-1H-cyclopropa[b]benzofuran-1-carboxylate **(3ca)**

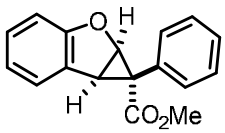

3ca

According to GP, 2,3-benzofuran (**1c**) (454.4 mg, 3.9 mmol, 7 equiv) and methyl 2-diazo-2-phenylacetate (**2a**) (96.8 mg, 0.6 mmol, 1 equiv) were dissolved in DMC (6 mL). The solution was pumped through the reactor and collected. Purification *via* chromatography yielded 71.7 mg of the target compound **3ca** (0.3 mmol, 49%) as a colorless solid.

R_f(PE:EA = 5:1) = 0.41.

^{1}H NMR (400 MHz, $CDCl_3$): δ = 7.35 (dd, *J* = 7.4 Hz, 1.4 Hz, 1H), 7.07 (s, 5H), 6.90 (td, *J* = 7.8 Hz, J = 1.4 Hz, 1H), 6.80 (td, *J* = 7.4 Hz, 1.0 Hz, 1H), 6.45 (d, *J* = 7.1 Hz, 1H), 5.36 (d, *J* = 5.5 Hz, 1H), 3.79 (d, *J* = 5.5 Hz, 1H), 3.67 (s, 3H).

^{13}C NMR (101 MHz, $CDCl_3$): δ = 173.5, 159.6, 132.6, 129.7, 128.1, 127.7, 127.3, 126.6, 125.2, 121.3, 109.8, 70.6, 52.9, 37.5, 31.1.

The analytical data were in accordance with the literature.[10]

methyl (1S,5S,6R)-6-phenyl-2-oxabicyclo[3.1.0]hexane-6-carboxylate **(3da)***

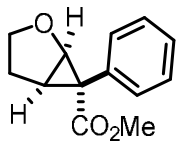

3da

According to GP, 2,3-dihydrofuran (**1d**) (981 mg, 14.0 mmol, 7 equiv) and methyl 2-diazo-2-phenylacetate (**2a**) (352 mg, 2 mmol, 1 equiv) were dissolved in DMC (20 mL). The solution was pumped through the reactor and collected for 20 min (= 11.4 mL). Purification *via* chromatography yielded 152.1 mg of the target compound **3da** (0.70 mmol, 61 %) as a colorless solid.

^{1}H NMR (300 MHz, $CDCl_3$): δ = 7.40 – 7.29 (m, 5H), 4.50 (d, *J* = 5.7 Hz, 1H), 3.77 (ddd, *J* = 10.0, 8.3, 3.6 Hz, 1H), 3.57 (s, 3H), 2.65 (t, *J* = 5.7 Hz, 1H), 2.42 – 2.31 (m, 1H), 2.29 – 2.18 (m, 1H), 1.89 – 1.81 (m, 1H).

^{13}C NMR (75 MHz, $CDCl_3$): δ = 172.1, 132.3, 131.6 (2x), 128.6 (2x), 127.6, 70.2, 70.1, 52.4, 38.1, 32.5, 26.3.

The analytical data were in accordance with the literature.[9]

methyl 7-phenyl-2-oxabicyclo[4.1.0]heptane-7-carboxylate **(3ea)***

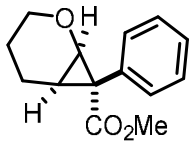

3ea

According to GP, 3,4-dihydro-*2H*-pyran (**1e**) (1177,7 mg, 14 mmol, 7 equiv) and methyl 2-diazo-2-phenylacetate (**2a**) (352 mg, 2 mmol, 1 equiv) were dissolved in DMC (20 mL). The solution was pumped through the reactor and collected for 20 min (= 11.4 mL). Purification *via* chromatography yielded 137 mg of the target compound **3ea** (0.59 mmol, 52%) as a colorless solid.

^{1}H NMR (300 MHz, $CDCl_3$): δ 7.40 – 7.27 (m, 5H), 4.21 (d, J = 7.5 Hz, 1H), 3.56 (s, 3H), 3.44 – 3.38 (m, 1H), 3.30 (ddd, J = 12.0, 10.6, 2.0 Hz, 1H), 2.16 (td, J = 7.2, 1.2 Hz, 1H), 2.01 (ddt, J = 14.0, 11.2, 6.9 Hz, 1H), 1.92 – 1.84 (m, 1H), 1.08 – 0.98 (m, 1H), 0.38 – 0.22 (m, 1H).

^{13}C NMR (101 MHz, $CDCl_3$): δ 173.9, 133.4, 132.7 (2x), 128.2 (2x), 127.2, 64.6, 62.3, 52.5, 35.0, 25.5, 21.3, 17.6.

The analytical data were in accordance with the literature.[9]

methyl (1S,5R,6S)-6-phenylbicyclo[3.1.0]hex-2-ene-6-carboxylate **(3fa)***

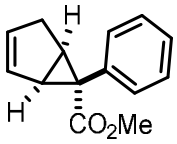

3fa

According to GP, freshly destilled cyclopentadiene (**1f**) (925 mg, 14 mmol, 7 equiv) and methyl 2-diazo-2-phenylacetate (**2a**) (352 mg, 2 mmol, 1 equiv) were dissolved in DMC (20 mL). The solution was pumped through the reactor and collected for 20 min (= 11.4 mL). Purification *via* chromatography yielded 173.4 mg of the target compound **3fa** (0.81 mmol, 71%) as a colorless solid.

^{1}H NMR (300 MHz, $CDCl_3$): δ 7.21 – 7.23 (m, 3H), 7.13 – 7.10 (m, 2H), 5.78 – 5.74 (m, 1H), 5.23 – 5.20 (m, 1H), 3.59 (s, 3H), 2.96 – 2.92 (m, 1H), 2.69 – 2.62 (m, 2H), 2.13 – 2.04 (m, 1H).

^{13}C NMR (101 MHz, $CDCl_3$): δ 174.5, 133.1, 133.0 (2x), 132.9, 129.7, 127.7 (2x), 126.8, 52.5, 40.9, 37.9, 34.2, 32.4.

The analytical data were in accordance with the literature.[58]

methyl (1S,5S,6R)-6-phenyl-2-tosyl-2-azabicyclo[3.1.0]hex-3-ene-6-carboxylate **(3ga)**

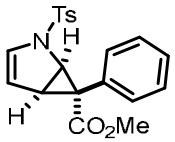

3ga

According to GP, *tert*-butyl 1-pyrrolecarboxylate (**1g**) (3097.8 mg, 14 mmol, 7 equiv) and methyl 2-diazo-2-phenylacetate (**2a**) (352 mg, 2 mmol, 1 equiv) were dissolved in DMC (20 mL). The solution was pumped through the reactor and collected for 20 min (= 11.4 mL). Purification *via* chromatography yielded 205.9 mg of the target compound **3ga** (0.35 mmol, 51%) as a colorless solid.

^{1}H NMR (400 MHz, $CDCl_3$): δ = 7.71 (d, *J* = 8.3 Hz, 2H), 7.33 (d, *J* = 8.5 Hz, 2H), 7.27 – 7.24 (m, 3H), 7.21 – 7.19 (m, 2H), 5.95 (dd, *J* = 3.9 Hz, 1.5 Hz, 1H), 5.28 (dd, *J* = 3.9 Hz, 2.5 Hz, 1H), 4.53 (dd, *J* = 6.5 Hz, 1.4 Hz, 1H), 3.60 (s, 3H), 3.14 (dd, *J* = 6.5 Hz, 2.5 Hz, 1H), 2.45 (s, 3H), 2.45 (s, 3H).

^{13}C NMR (101 MHz, $CDCl_3$): δ = 173.7, 144.5, 135.0, 132.6 (2x), 130.9, 130.5, 130.1 (2x), 127.9, 127.5, 127.3, 127.0, 111.4 (2x), 52.9, 52.3, 38.8, 28.1, 21.7.

The analytical data were in accordance with the literature.[48]

2-(*tert*-butyl) methyl-(1S,5S,6R)-6-phenyl-2-azabicyclo[3.1.0]hex-3-ene-2,6-dicarboxylate **(3ha)**

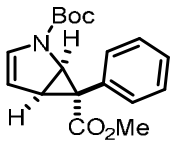

3ha

According to GP, *tert*-butyl 1-pyrrolecarboxylate (**1h**) (813.6 mg, 4.9 mmol, 7 equiv) and methyl 2-diazo-2-phenylacetate (**2a**) (122.5 mg, 0.7 mmol, 1 equiv) were dissolved in DMC (7 mL). The solution was pumped through the reactor and collected. Purification *via* chromatography yielded 111.2 mg of the target compound **3ha** (0.35 mmol, 51%) as a colorless solid.

R$_f$(PE:EA = 9:1) = 0.44.

^{1}H NMR (400 MHz, $CDCl_3$) 2 rotamers: δ = 7.30 – 7.25 (m, 3H), 7.17 – 7.11 (m, 2H), 6.15 (d, *J* = 4.0 Hz, 0.4H), 5.99 (d, *J* = 4.4 Hz, 0.6H), 5.21 (dd, *J* = 4.0 Hz, 2.7 Hz, 0.4H), 5.14 (dd, *J* = 4.0 Hz, 2.7 Hz, 0.6H), 4.72 (d, *J* = 7.9 Hz, 0.6H), 4.62 (d, *J* = 7.9 Hz, 0.4H), 3.65 (s, 1.2H), 3.62 (s, 1.8H), 3.35 – 3.32 (m, 1H), 1.61 (s, 3.6 H), 1.47 (s, 5.4H)

^{13}C NMR (101 MHz, $CDCl_3$) 2 rotamers: δ = 174.2, 173.9, 151.4, 151.3, 132.8, 132.5, 131.3, 131.1, 130.9, 130.6, 128.0, 127.9, 127.5, 127.4, 107.4 (x2), 82.0, 81.7, 52.7, 52.6, 49.5, 49.4, 39.7, 38.4, 29.8, 29.4, 28.5, 28.3.

The analytical data were in accordance with the literature.[29]

dimethyl 7-phenyl-2-azabicyclo[4.1.0]heptane-2,7-dicarboxylate **(3ia)***

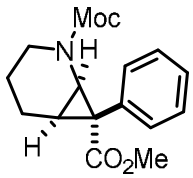

3ia

According to GP, methyl 3,4-dihydro-*2H*-pyridine-1-carboxylate (**1i**) (1779 mg, 14 mmol, 7 equiv) and methyl 2-diazo-2-phenylacetate (**2a**) (352 mg, 2 mmol, 1 equiv) were dissolved in DMC (20 mL). The solution was pumped through the reactor and collected for 20 min (= 11.4 mL). Purification *via* chromatography yielded 185.3 mg of the target compound **3ia** (0.65 mmol, 57%) as a colorless solid.

m.p. 151-154 °C

R$_f$(PE:EA = 4:1) = 0.51.

^{1}H NMR (300 MHz, $CDCl_3$) 2 rotamers: δ 7.31 – 7.09 (m, 5H), 3.83 (s, 1.8H), 3.75 (s, 1.2H), 3.73 (s, 2H, both rotamers), 3.55 (s, 1.9H), 3.52 (s, 1.1H), 3.23 – 3.15 (m, 0.6H), 3.13 – 3.05 (m, 0.4H), 2.76 – 2.66 (m, 1H, both rotamers), 2.37 – 2.24 (m, 1H, both rotamers), 1.96 – 1.73 (m, 2H, both rotamers), 1.19 – 1.11 (m, 1H, both rotamers), 0.42 – 0.28 (m, 1H, both rotamers).

^{13}C NMR (101 MHz, $CDCl_3$) rotamer 1 (rotamer 2): δ = 173.9 (173.7), 157.7 (157.5), 133.4 (133.2), 138.8 (138.5) (2x), 128.7 (128.5) (2x), 127.6 (127.4), 53.1 (53.0), 57.7 (57.7), 42.6 (42.3), 41.5 (41.1), 34.9 (34.7), 25.1 (24.8), 21.1 (20.9), 18.7 (18.6).

HR MS (EI): calcd. for $C_{15}H_{14}O_5$ $(M)^+$, m/z = 289.1309; found 289.1307.

IR (ATR): 2952, 1685, 1439, 1383, 1245, 1197, 1103, 962, 772, 705 cm^{-1}.

2-(tert-butyl) 1-methyl-(1R,1aS,6bS)-1-phenyl-1a,6b-dihydrocyclopropa[b]indole-1,2(1H)-dicarboxylate **(3ja)**

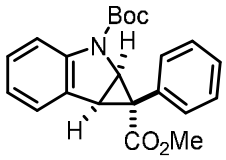

3ja

According to GP, *tert*-butyl 1-indolecarboxylate (**1j**) (1.833 g, 8.4 mmol, 7 equiv) and methyl 2-diazo-2-phenylacetate (**2a**) (212.3 mg, 1.2 mmol, 1 equiv) were dissolved in DMC (11 mL). The solution was pumped through the reactor and collected. Purification *via* chromatography yielded 246.6 mg of the target compound **3ja** (0.7 mmol, 56%) as a yellowish oil.

R_f (PE:EA = 9:1) = 0.47.

^{1}H NMR (400 MHz, $CDCl_3$) 2 rotamers: δ = 7.43 (d, *J* = 8.0 Hz, 1H), 7.38 (d, *J* = 7.2 Hz, 1H), 7.06-7.04 (m, 3H), 7.01-6.96 (m, 3H), 6.92-6.88 (m, 1H), 4.97 (d, *J* = 6.8 Hz, 0.5H), 4.86 (d, *J* = 6.8 Hz, 0.5H), 3.73 (t, *J* = 6.6 Hz, 1H), 3.68 (d, *J* = 10.3, 1.5Hz), 3.65 (s, 1.5H), 1.65 (s, 4.5H), 1.59 (s, 4.5H).

^{13}C NMR (101 MHz, $CDCl_3$): δ = 173.7, 173.5, 153.0, 151.8, 142.5, 141.4, 132.4, 132.1, 130.5, 130.4, 129.3, 128.5, 128.0, 127.8, 127.7, 127.4, 127.3, 125.7, 125.2, 122.5, 122.4, 114.7, 114.5, 82.7, 82.0, 52.9, 52.8, 50.8, 50.7, 35.6, 34.8, 32.2, 31.9, 28.6, 28.4.

The analytical data were in accordance with the literature.[29]

2-*tert*-butyl 1-methyl 5-fluoro-1-phenyl-1,6b-dihydrocyclopropa[b]indole-1,2(1aH)-dicarboxylate **(3ka)***

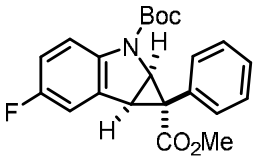

3ka

According to GP, *tert*-butyl 5-fluoroindole-1-carboxylate (**1k**) (1.600 g, 6.8 mmol, 7 equiv) and methyl 2-diazo-2-phenylacetate (**2a**) (0.171 mg, 0.97 mmol, 1 equiv) were dissolved in DMC (9.7 mL). The solution was pumped through the reactor and collected. Purification *via* chromatography yielded 212 mg of the target compound **3ka** (0.55 mmol, 57%) as a yellowish oil.

^{1}H NMR (300 MHz, $CDCl_3$) 2 rotamers: δ = 7.39 – 7.34 (m, 1H), 7.10 – 7.07 (m, 4H), 6.97 – 6.94 (m, 2H), 6.71 – 6.62 (m, 1H), 4.97 (d, *J* = 6.8 Hz, 0.4H), 4.86 (d, *J* = 6.8 Hz, 0.6H), 3.73 – 3.65 (m, 4H), 1.64 (s, 5H), 1.57 (s, 4H).

^{13}C NMR (101 MHz, $CDCl_3$): δ = 173.5, 173.2, 159.9, 157.5, 152.7, 151.7, 138.7, 137.7, 132.3, 132.0, 130.2, 128.0, 127.9, 127.6, 127.4, 115.5, 115.4, 115.3, 115.2, 114.7, 114.4, 114.2, 112.8, 112.6, 112.4, 112.2, 82.9, 82.1, 53.0, 52.9, 51.3, 51.1, 35.2, 34.4, 32.4, 32.1, 28.6, 28.4.

^{19}F NMR (282 MHz, $CDCl_3$): δ = -121.5, -121.9.

The analytical data were in accordance with the literature.[48]

methyl (1S,1aS,6bR)-1-phenyl-1a,6b-dihydro-1H-benzo[b]cyclopropa[d]thiophene-1-carboxylate **(3la)**

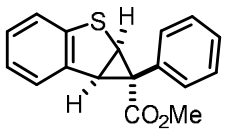

3la

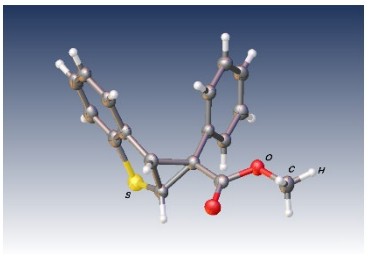

According to GP, 2,3-benzothiophene (**1l**) (2.631 g, 9.3 mmol, 7 equiv) and methyl 2-diazo-2-phenylacetate (**2a**) (234.5 mg, 1.3 mmol, 1 equiv) were dissolved in DMC (11 mL). The solution was pumped through the reactor and collected. Purification *via* chromatography yielded 109 mg of the target compound **3la** (0.4 mmol, 29%) as a yellowish solid.

R_f(PE:EA = 9:1) = 0.42.

^{1}H NMR (400 MHz, $CDCl_3$): δ = 7.50 – 7.48 (m, 1H), 7.10 – 7.05 (m, 3H), 7.04 – 7.02 (m, 3H), 6.98 – 6.94 (m, 1H), 6.79 – 6.77 (m, 1H), 4.08 (d, *J* = 7.8 Hz, 1H), 4.03 (d, *J* = 7.8 Hz, 1H), 3.66 (s, 3H)

^{13}C NMR (101 MHz, $CDCl_3$): δ = 174.4, 142.9, 136.9, 132.9, 130.8, 127.7, 127.3, 127.2, 126.7, 124.4, 121.7, 53.1, 44.3, 39.9, 31.3

The analytical data were in accordance with the literature.[48]

CCDC-Number: 2091948

The crystals were obtained by dissolving the compound in acetone and subsequently slow evaporation of the solvent.

methyl (1S,5S,6R)-6-(4-nitrophenyl)-2-oxabicyclo[3.1.0]hex-3-ene-6-carboxylate **(3ab)**

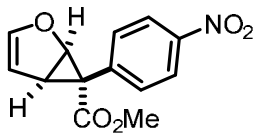

3ab

According to GP but with an residence time of 6.75 min, furan (**1a**) (571.8 mg, 8.4 mmol, 7 equiv) and methyl 2-diazo-2-(4-nitrophenyl)acetate (**2b**) (265.6 mg, 1.2 mmol, 1 equiv) were dissolved in DMC (11.5 mL). The solution was pumped through the reactor and collected. Purification *via* chromatography yielded 84.6 mg of the target compound **3ab** (0.32 mmol, 27%) as a colorless solid.

R_f(PE:EA = 5:1) = 0.39.

^{1}H NMR (300 MHz, $CDCl_3$): δ = 8.15 – 8.12 (m, 2H), 7.38 – 7.33 (m, 2H), 5.91 (dd, *J* = 2.5 Hz, 0.8 Hz, 1H), 5.25 (t, *J* = 2.6 Hz, 1H), 5.20 (dd, *J* =5.6 Hz, 0.8 Hz , 1H), 3.63 (s, 3H), 3.38 (dd, *J* = 5.7, 2.7 Hz, 1H).

^{13}C NMR (75 MHz, $CDCl_3$): δ = 172.5, 147.8, 147.3, 138.6, 133.8 (2x), 123.2 (2x), 104.0, 70.9, 52.9, 39.7, 27.6.

HR MS (EI): calcd. for $C_{12}H_{10}NO_5$ $(M)^+$, m/z = 261.0632; found 261.0627.

IR (ATR): n 3109, 2952, 1700, 1592, 1435, 1249, 1144, 1051, 1018, 977, 954, 689 cm^{-1}.

methyl (1R,5R,6S)-6-(4-chlorophenyl)-2-oxabicyclo[3.1.0]hex-3-ene-6-carboxylate **(3ac)**

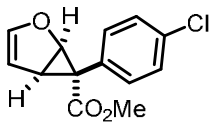

3ac

According to GP but with an residence time of 6.75 min, furan (**1a**) (571.8 mg, 8.4 mmol, 7 equiv) and methyl 2-(4-chlorophenyl)-2-diazoacetate (**2c**) (254.4 mg, 1.2 mmol, 1 equiv) were dissolved in DMC (11.5 mL). The solution was pumped through the reactor and collected. Purification *via* chromatography yielded 144.4 mg of the target compound **3ac** (0.58 mmol, 48%) as a colorless solid.

$\mathbf{R}_f$(PE:EA = 5:1) = 0.31.

^{1}H NMR (400 MHz, $CDCl_3$): δ = 7.29 – 7.28 (m, 2H), 7.15 – 7.12 (m, 2H), 5.95 (d, *J* = 1.8 Hz, 1H), 5.24 (t, *J* = 2.6 Hz, 1H), 5.15 (d, *J* = 5.6, 1H), 3.65 (s, 3H), 3.32 (dd, *J* = 5.6, 2.6, 3.0 Hz, 1H).

^{13}C NMR (101 MHz, $CDCl_3$): δ = 173.6, 147.7, 134.2, 134.2, 133.3, 129.4, 128.3, 128.3, 104.0, 70.9, 52.7, 39.5, 27.3.

HR MS (EI): calcd. for $C_{13}H_{11}O_3Cl$ $(M)^+$, m/z = 250.0391; found 250.0387.

IR (ATR): n 2952, 1696, 1588, 1498, 1435, 1260, 1144, 1088, 988, 854, 691 cm^{-1}.

methyl (1S,5S,6R)-6-(4-methoxyphenyl)-2-oxabicyclo[3.1.0]hex-3-ene-6-carboxylate **(3ad)**

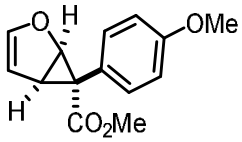

3ad

According to GP, furan (**1a**) (281.6 mg, 4.1 mmol, 7 equiv) and methyl 2-diazo-2-(4-methoxyphenyl)acetate (**2d**) (121.8 mg, 0.6 mmol, 1 equiv) were dissolved in DMC (6 mL). The solution was pumped through the reactor and collected. Purification

via chromatography yielded 100.4 mg of the target compound **3ad** (0.4 mmol, 69%) as a colorless solid.

R_f (PE:EA = 5:1) = 0.25.

^{1}H NMR (400 MHz, $CDCl_3$): δ = 7.10 – 7.06 (m, 2H), 7.82 – 7.80 (m, 2H), 5.93 (d, *J* = 1.8 Hz, 1H), 5.21 (t, *J* = 2.6 Hz, 1H), 5.11 (d, *J* = 5.6, 1H), 3.78 (s, 3H), 3.62 (s, 3H), 3.27 (dd, *J* = 5.6, 2.6 Hz, 1H).

^{13}C NMR (101 MHz, $CDCl_3$): δ = 174.4, 158.8, 147.4, 147.4, 133.9, 133.9, 122.7, 113.4, 104.0, 71.0, 55.2, 52.7, 39.6, 27.2.

HR MS (EI): calcd. for $C_{14}H_{14}O_4$ $(M)^+$, m/z = 246.0887; found 246.0882.

IR (ATR): n 3105, 2952, 2840, 1700, 1517, 1431, 1238, 1141, 1017, 977, 950, 716 cm^{-1}.

3.4.6 NMR Spectra

4-methylbenzenesulfonyl azide **(TsN_3)**

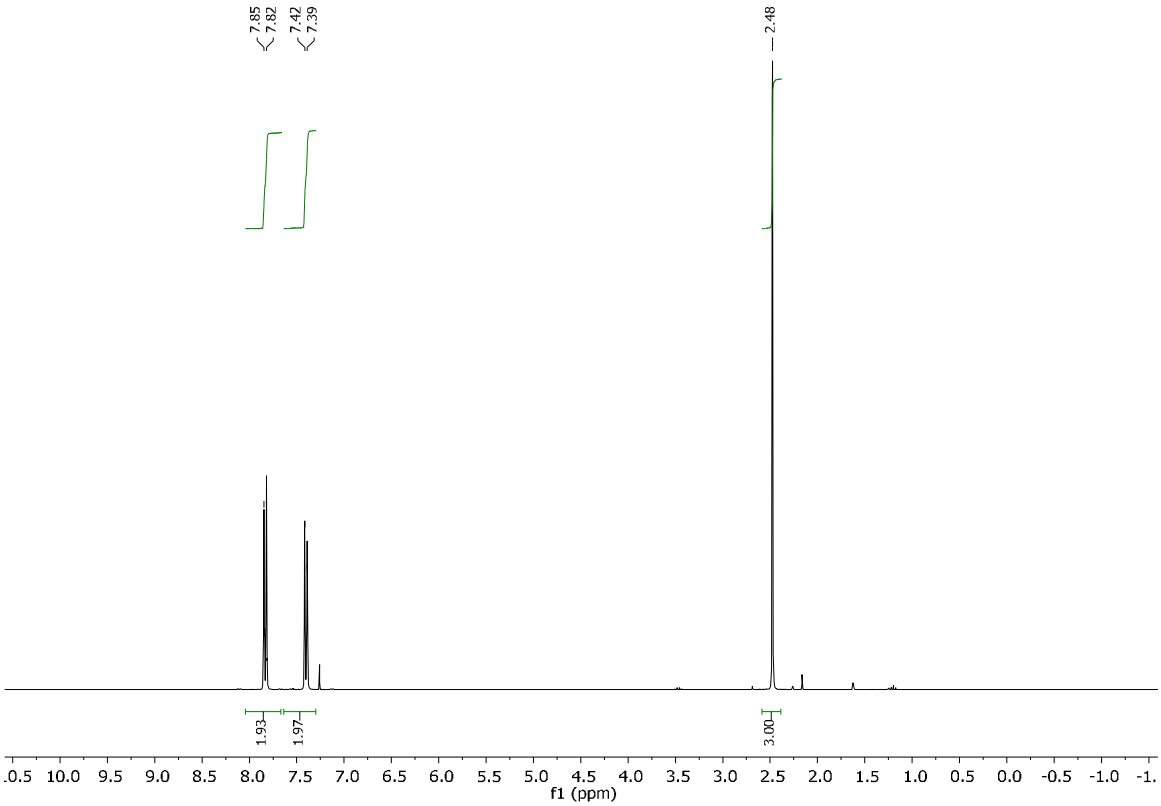

methyl 2-diazo-2-phenylacetate **(2a)**

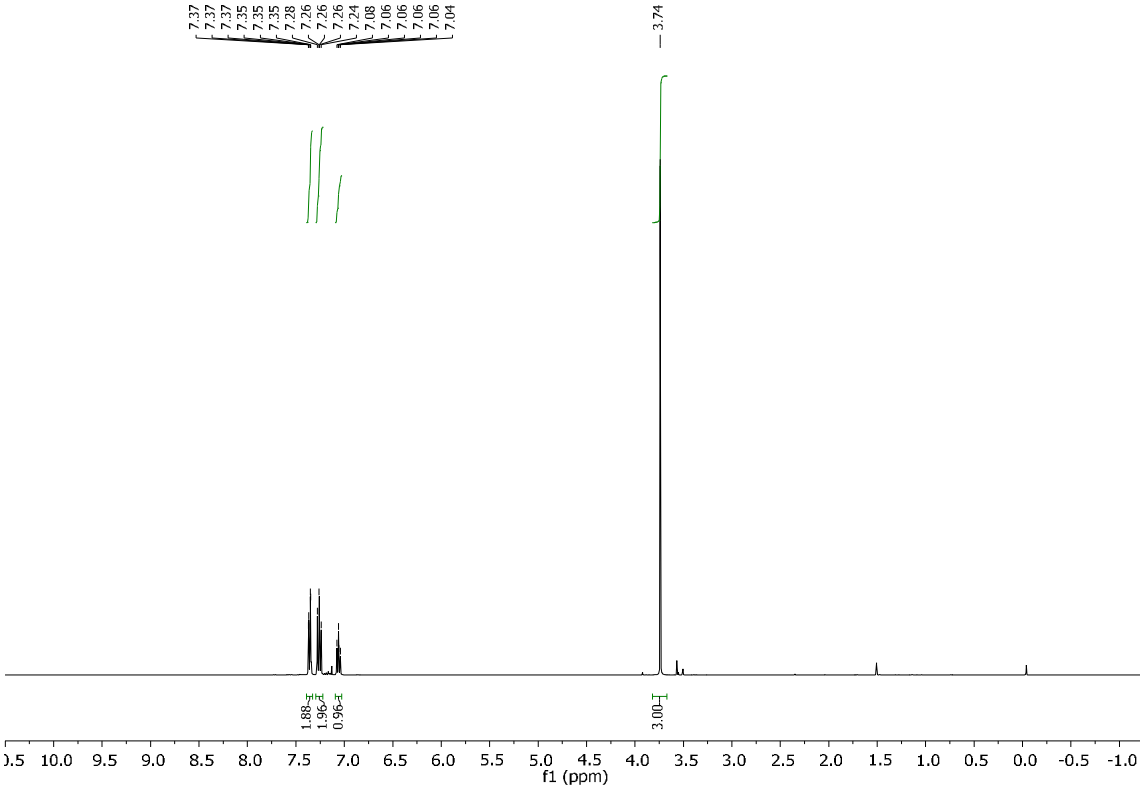

methyl 2-diazo-2-(4-nitrophenyl)acetate **(2b)**

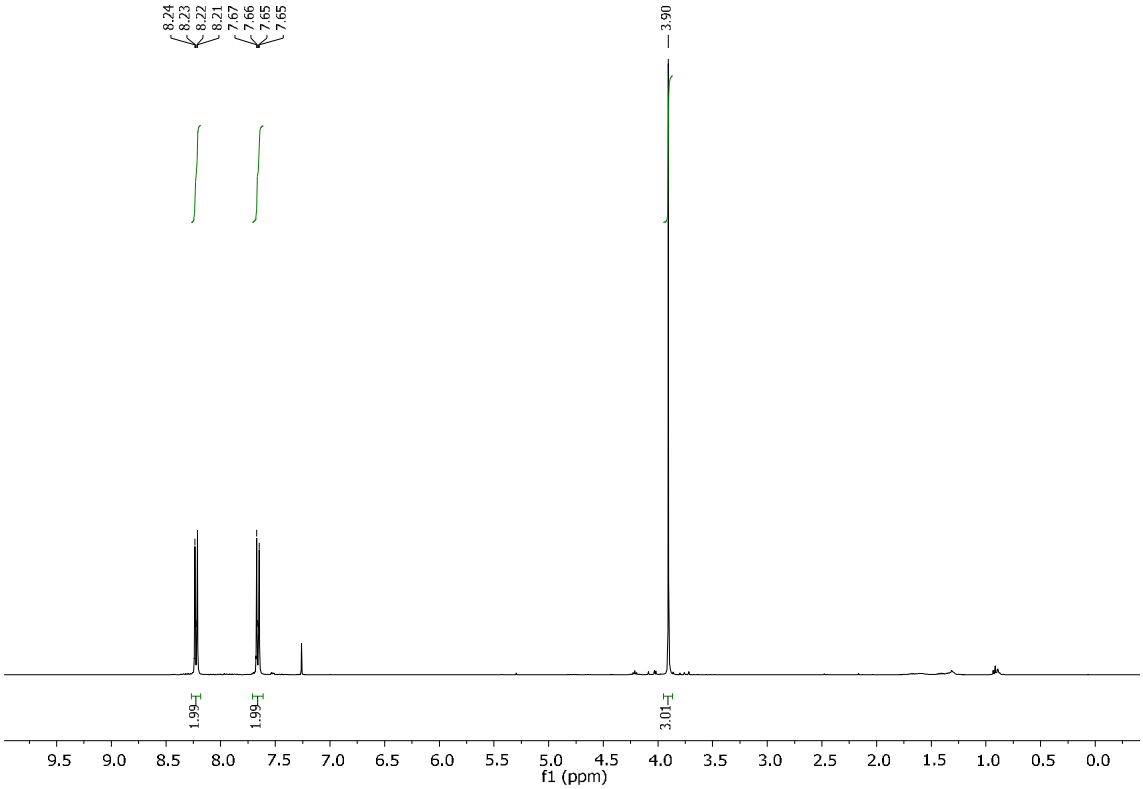

methyl 2-(4-chlorophenyl)-2-diazoacetate **(2c)**

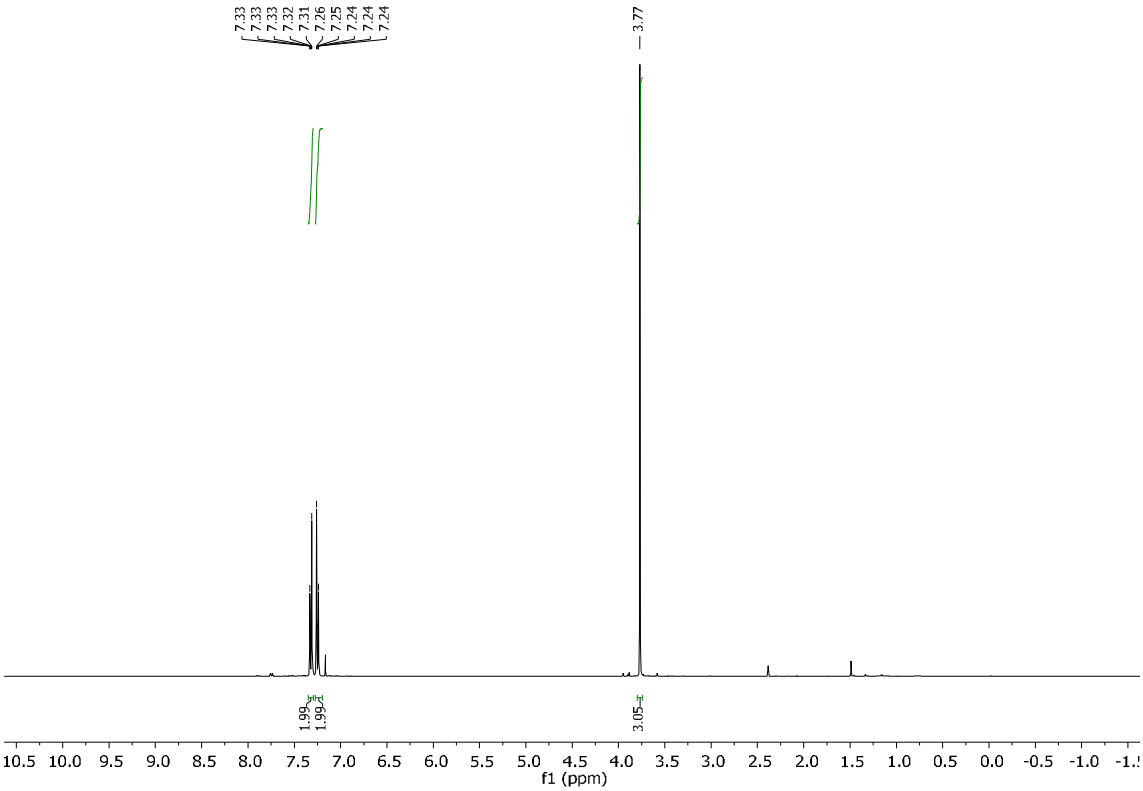

methyl 2-diazo-2-(4-methoxyphenyl)acetate **(2d)**

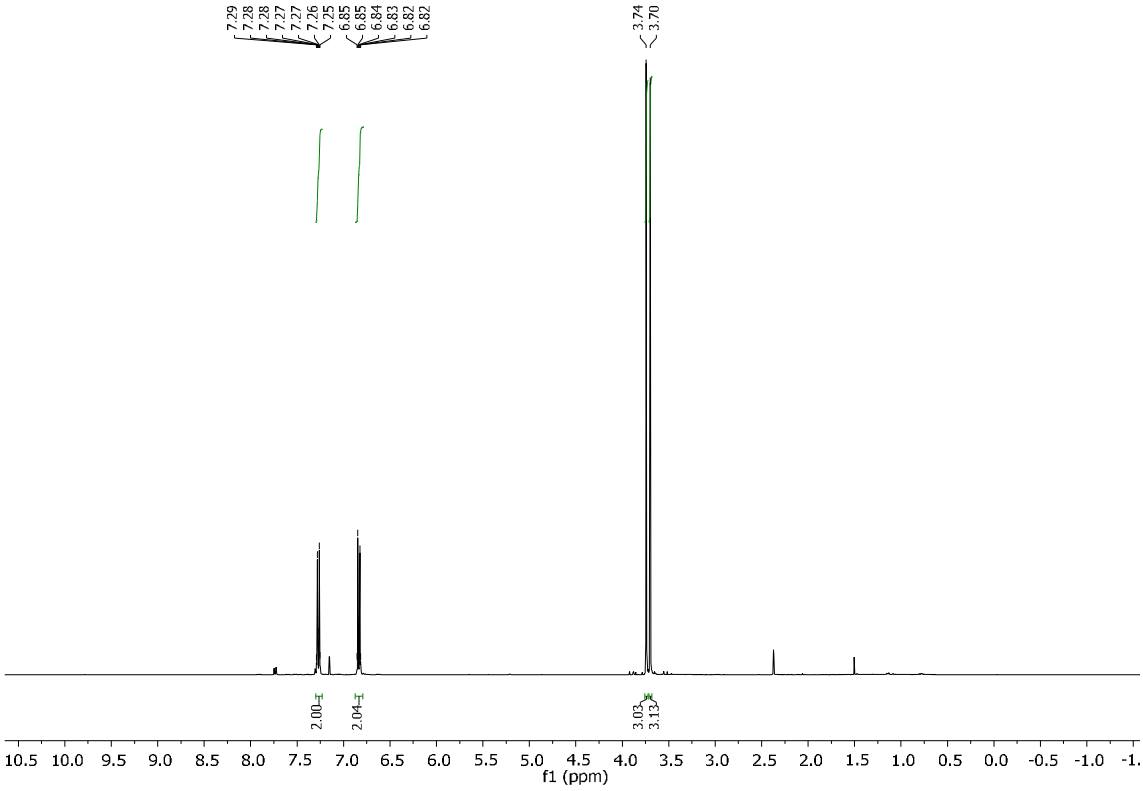

methyl (1S,5S,6R)-6-phenyl-2-oxabicyclo[3.1.0]hex-3-ene-6-carboxylate **(3aa)**

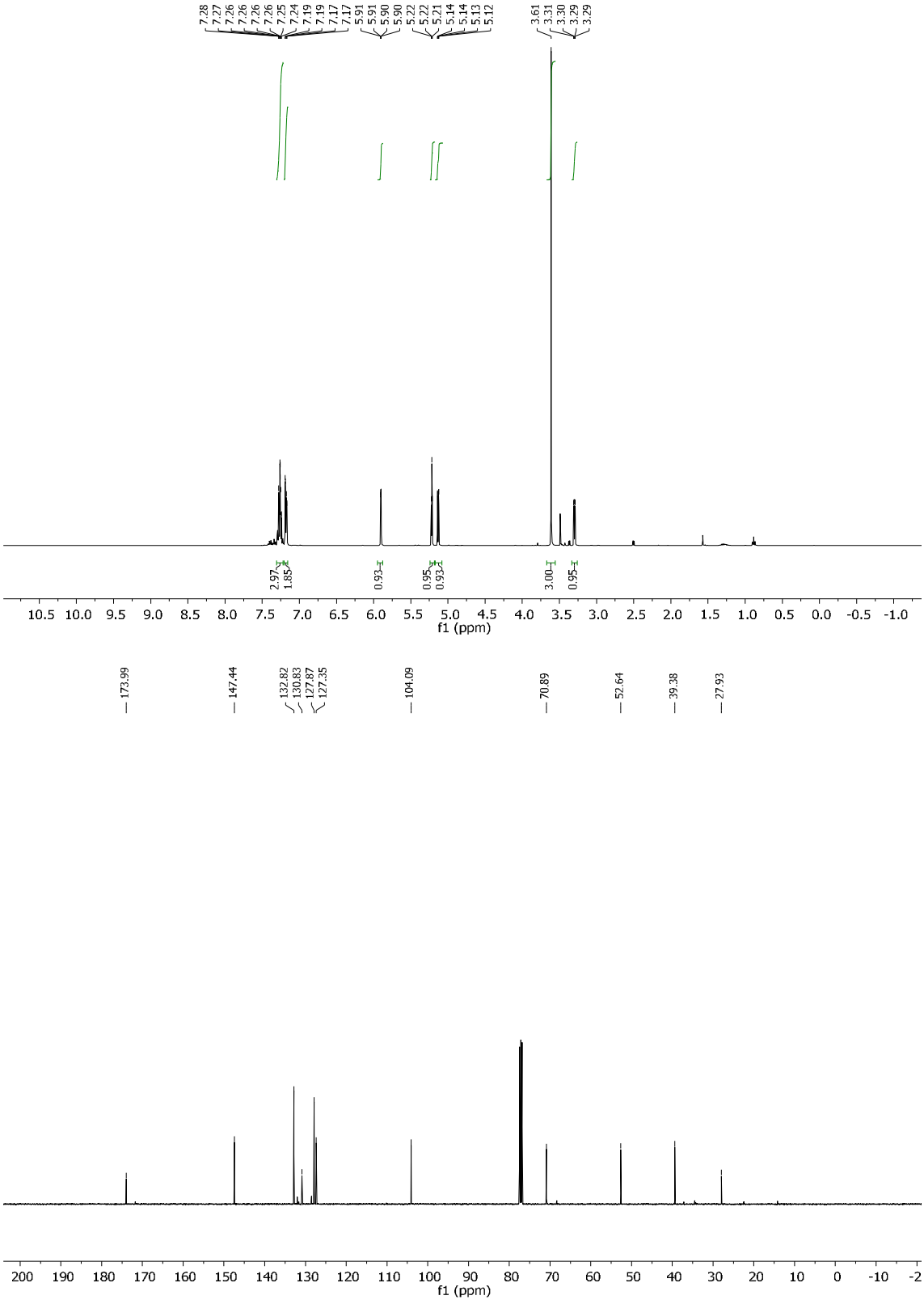

dimethyl (1S,5S,6R)-6-phenyl-2-oxabicyclo[3.1.0]hex-3-ene-3,6-dicarboxylate **(3ba)**

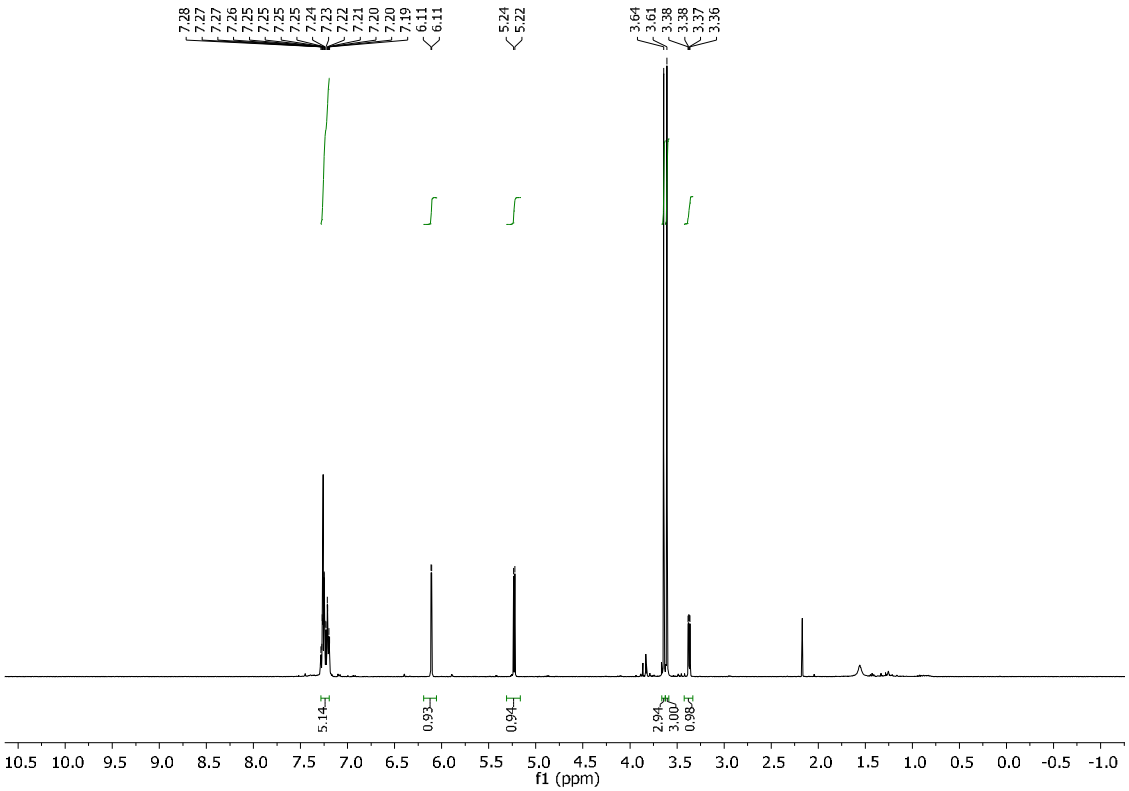

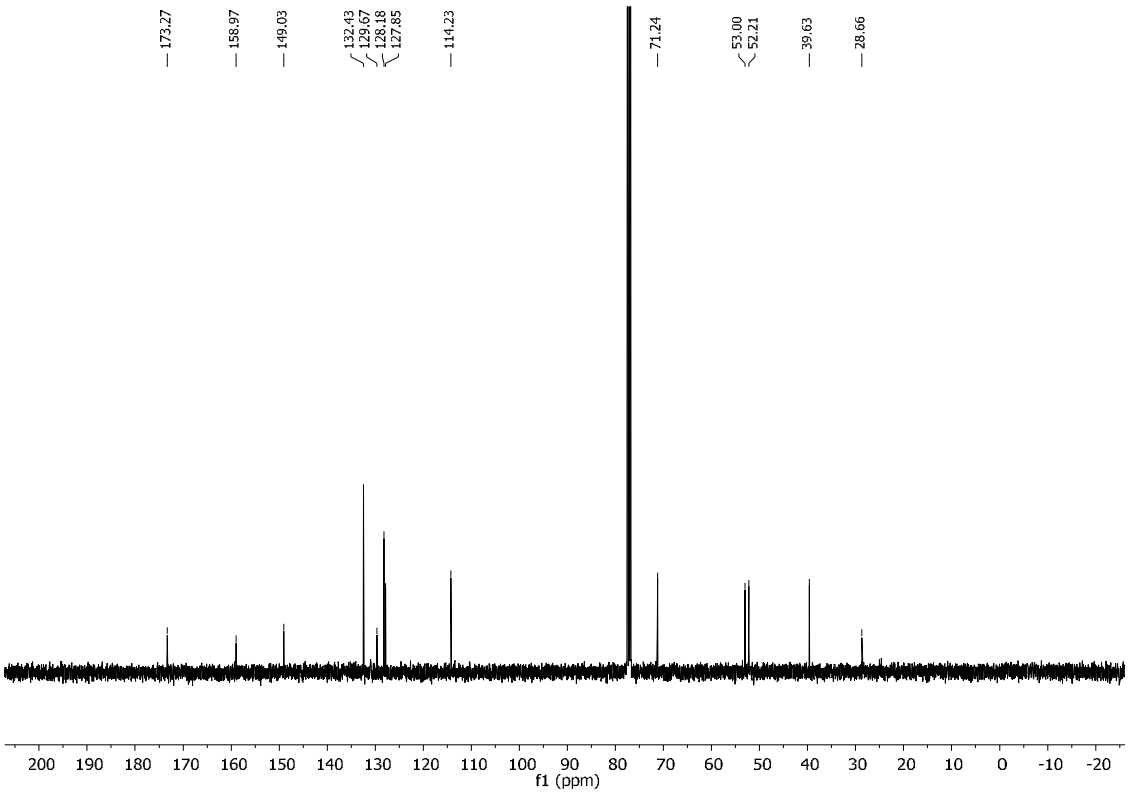

methyl (1R,1aS,6bS)-1-phenyl-1a,6b-dihydro-1H-cyclopropa[b]benzofuran-1-carboxylate **(3ca)**

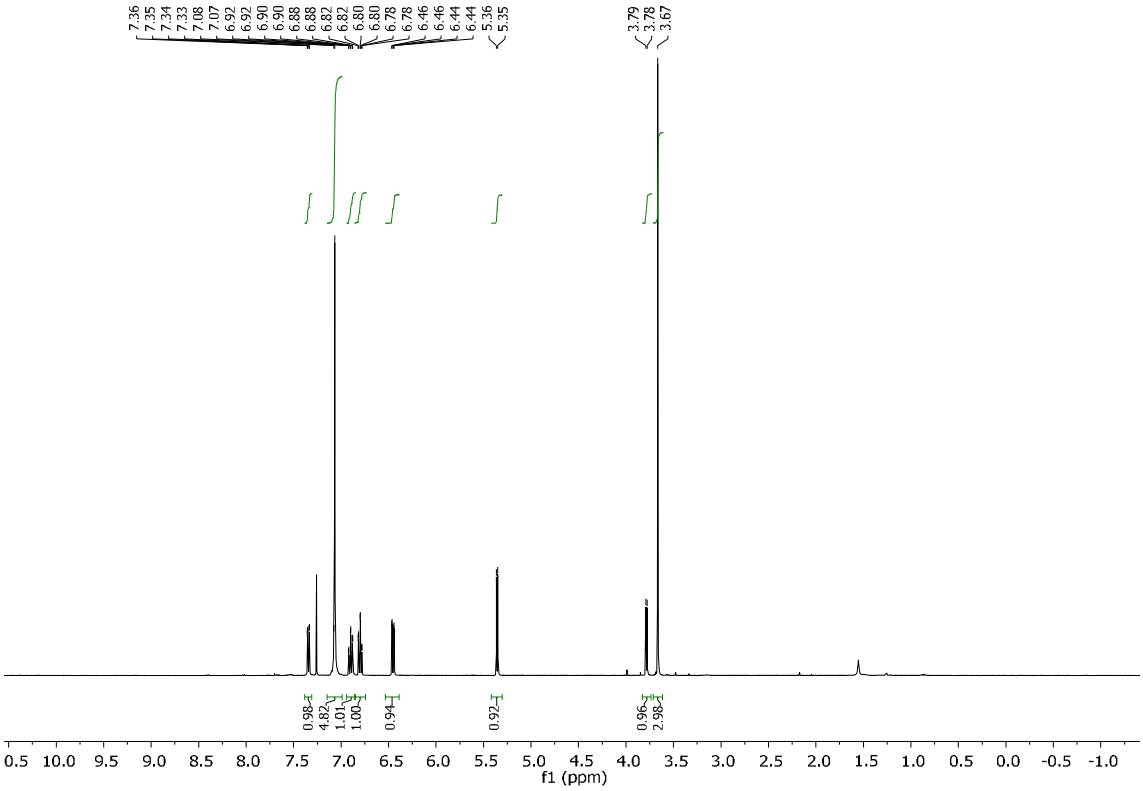

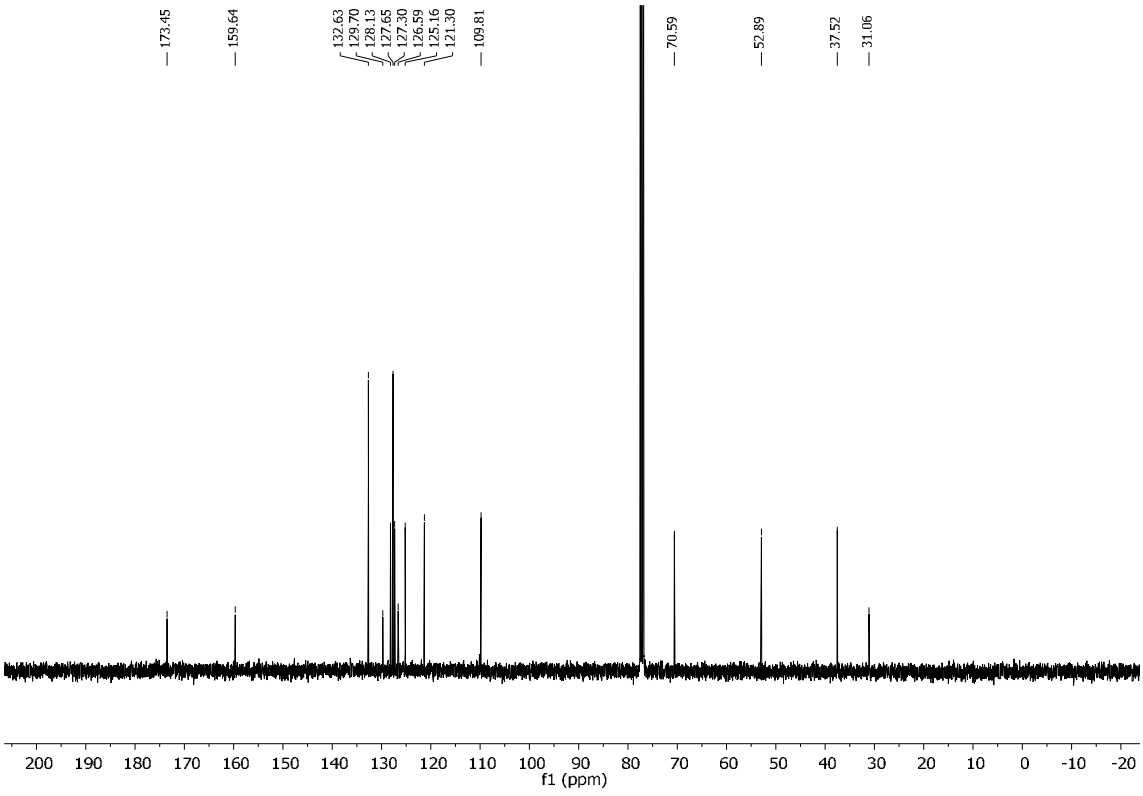

methyl (1S,5S,6R)-6-phenyl-2-oxabicyclo[3.1.0]hexane-6-carboxylate **(3da)***

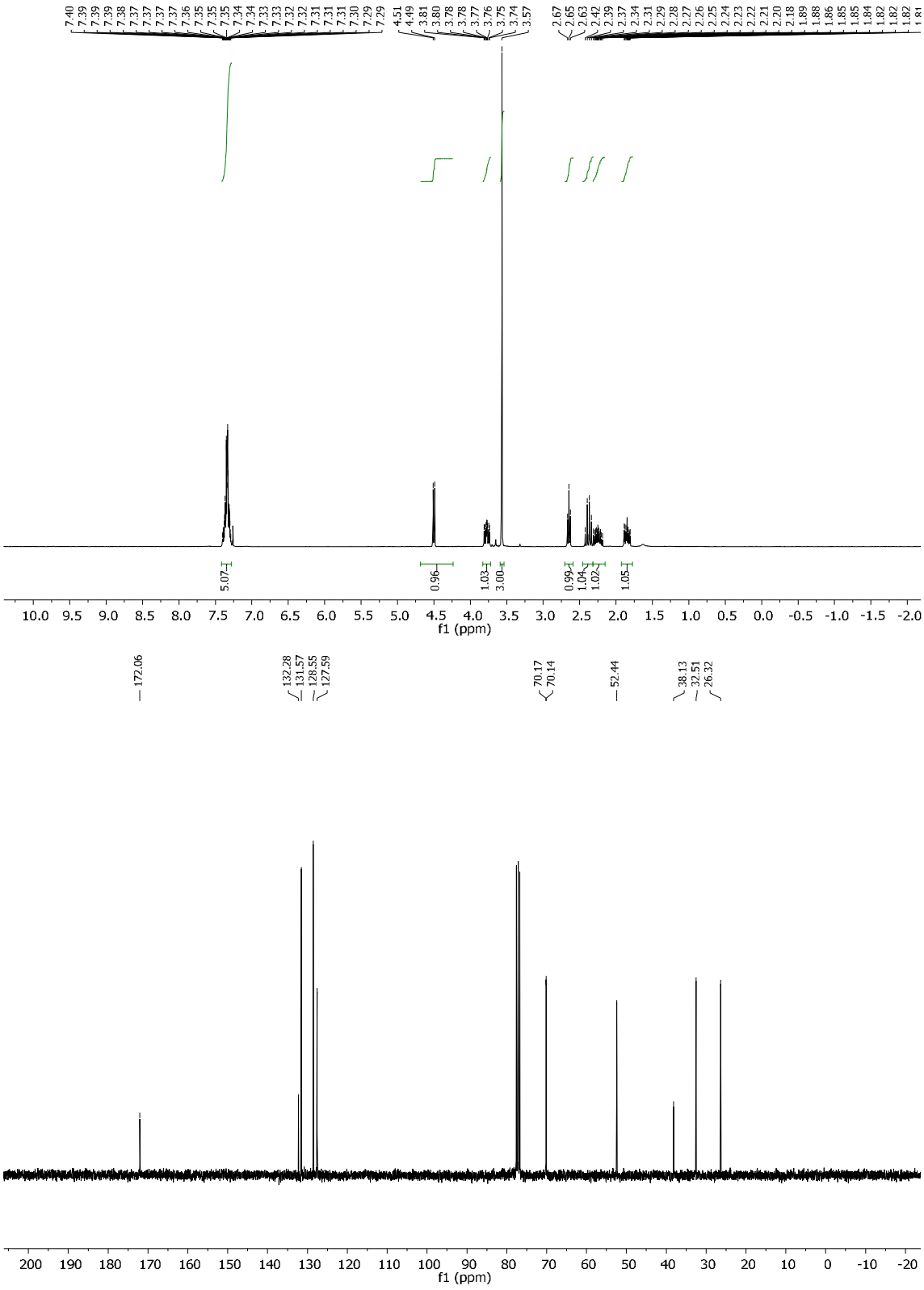

methyl 7-phenyl-2-oxabicyclo[4.1.0]heptane-7-carboxylate **(3ea)***

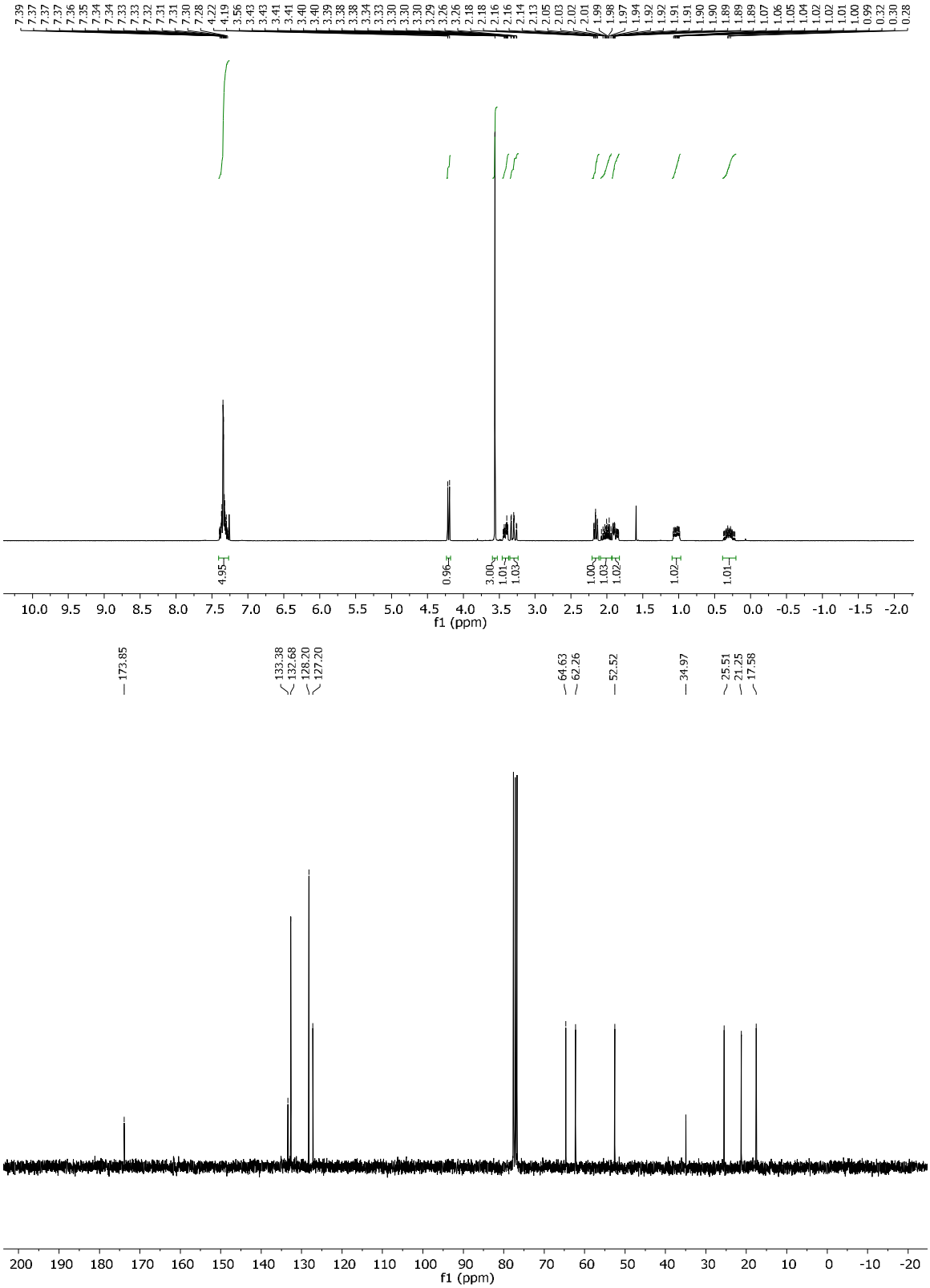

methyl (1S,5R,6S)-6-phenylbicyclo[3.1.0]hex-2-ene-6-carboxylate **(3fa)***

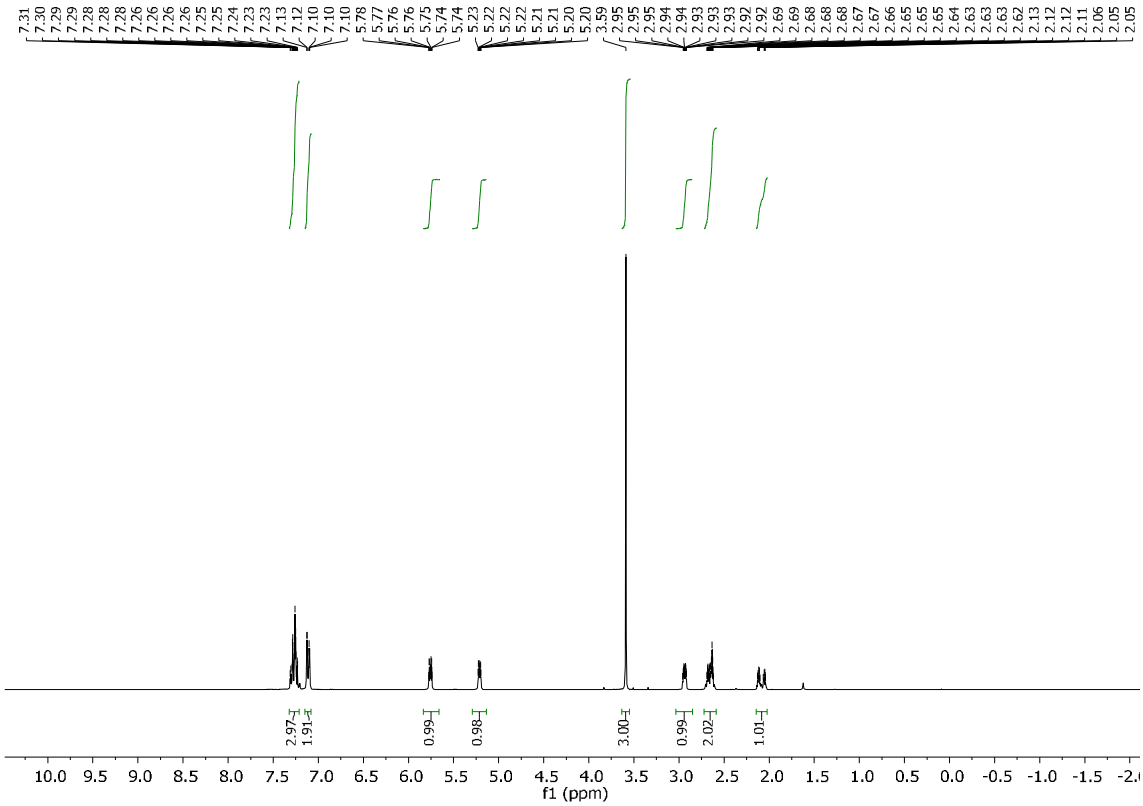

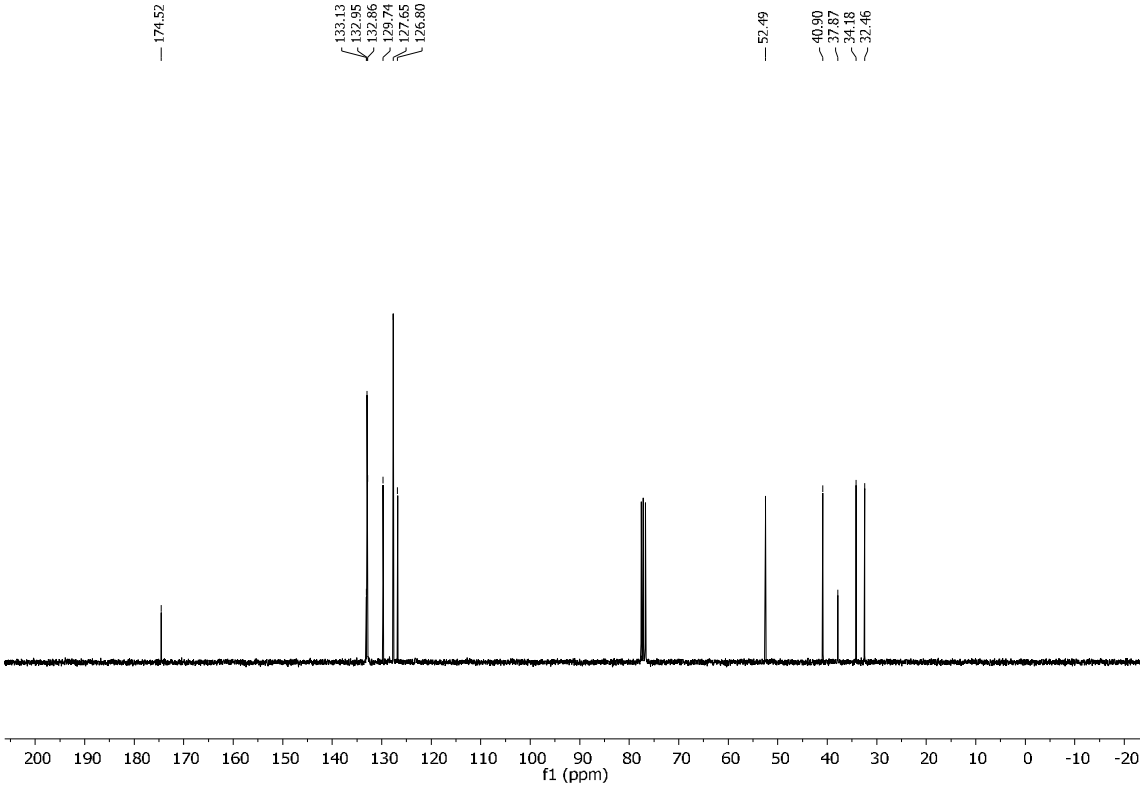

methyl (1S,5S,6R)-6-phenyl-2-tosyl-2-azabicyclo[3.1.0]hex-3-ene-6-carboxylate **(3ga)***

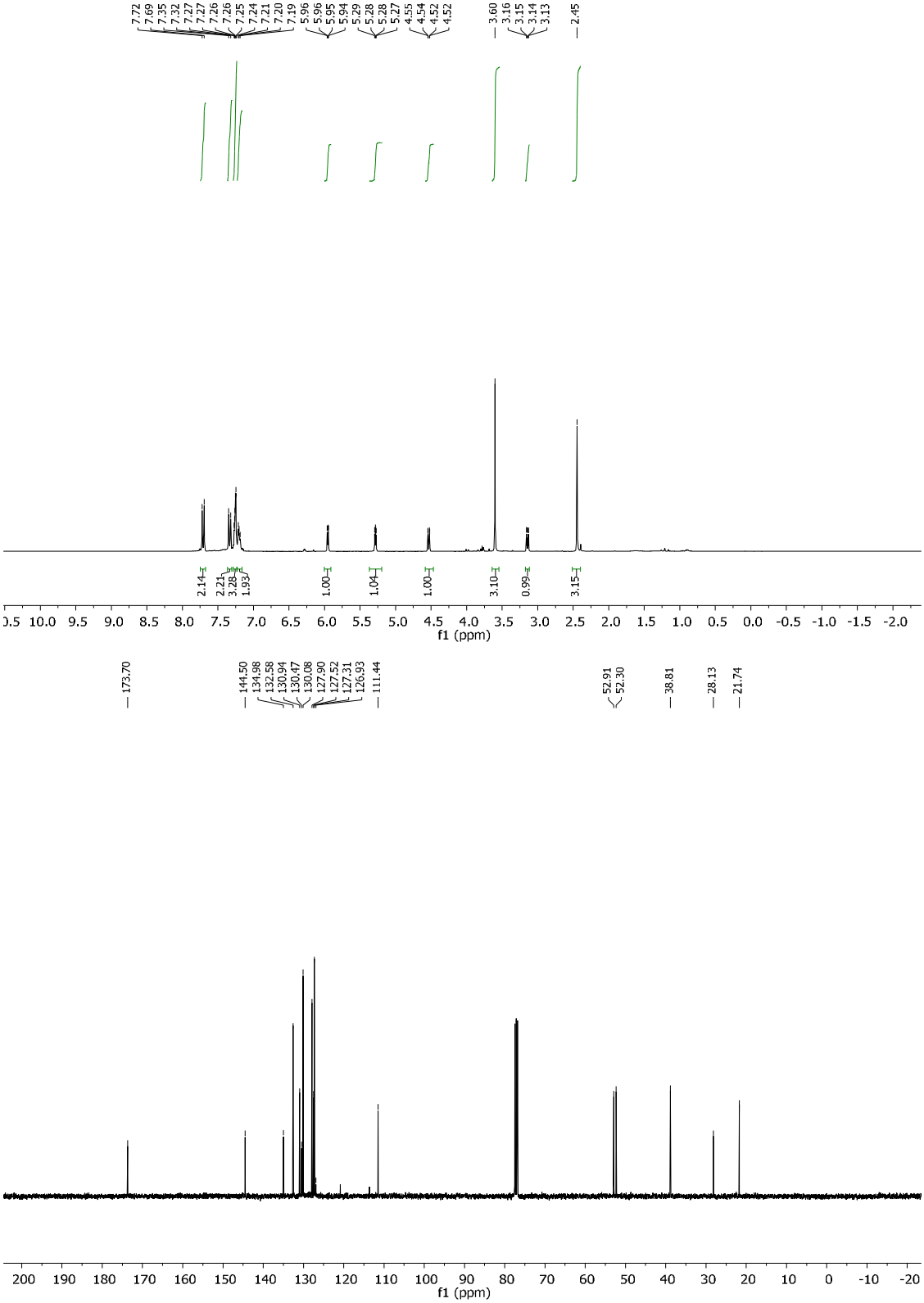

2-(*tert*-butyl) methyl-(1S,5S,6R)-6-phenyl-2-azabicyclo[3.1.0]hex-3-ene-2,6-dicarboxylate **(3ha)**

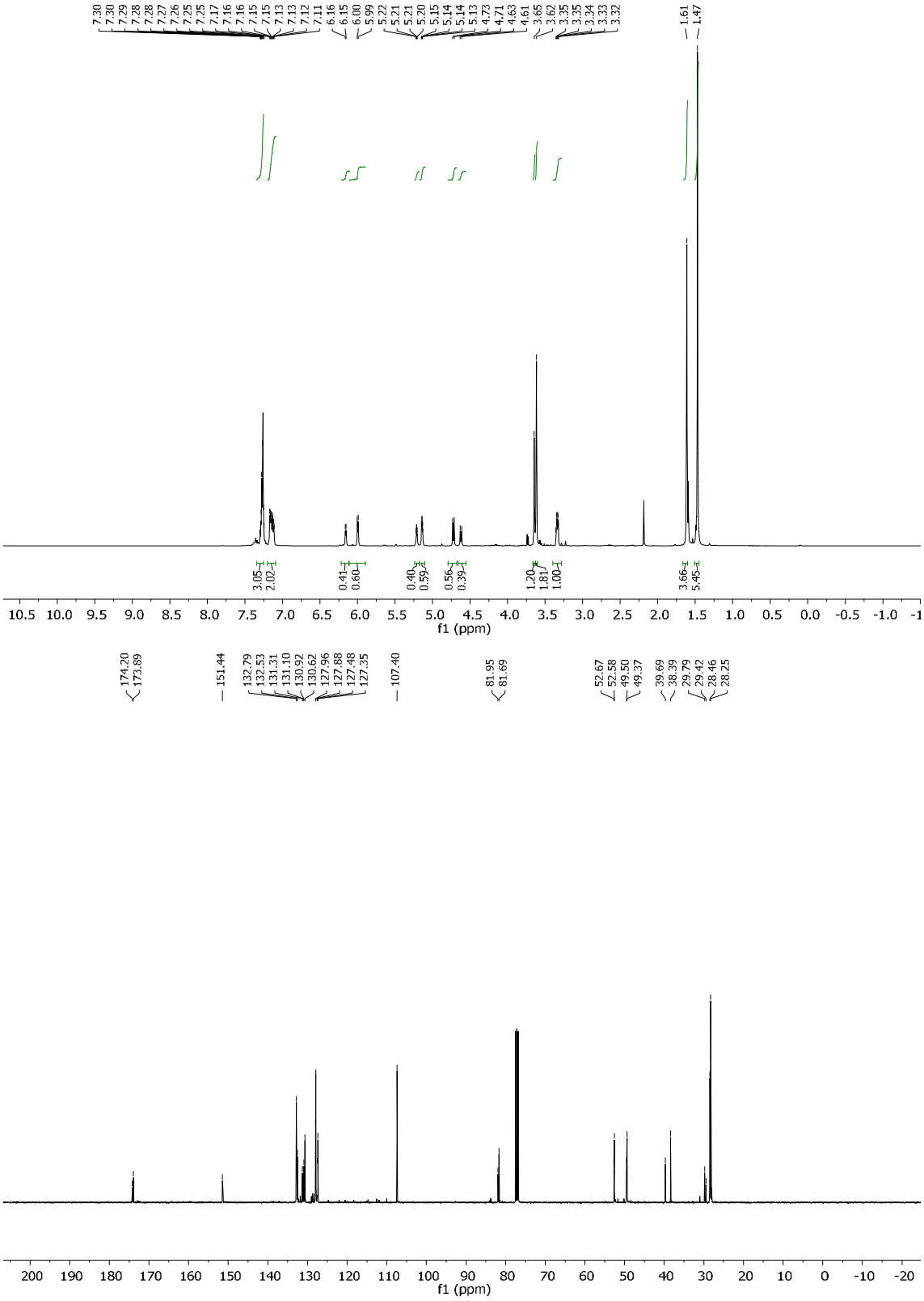

dimethyl 7-phenyl-2-azabicyclo[4.1.0]heptane-2,7-dicarboxylate **(3ia)***

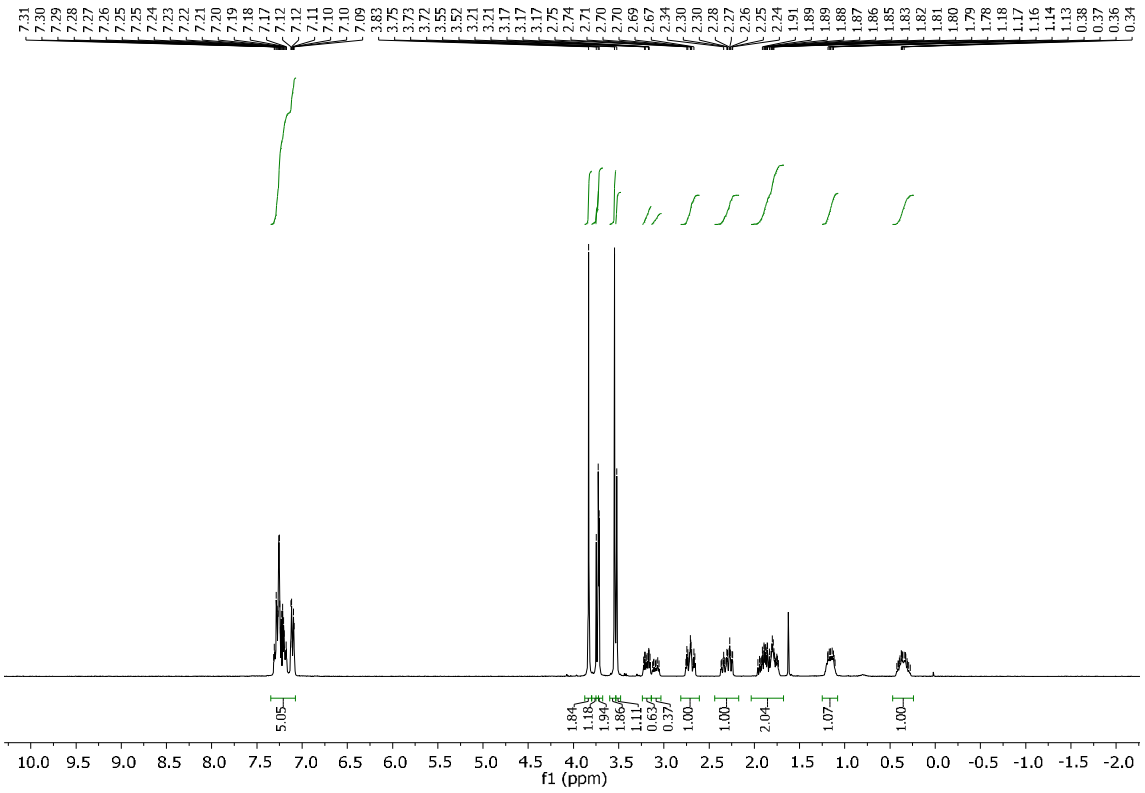

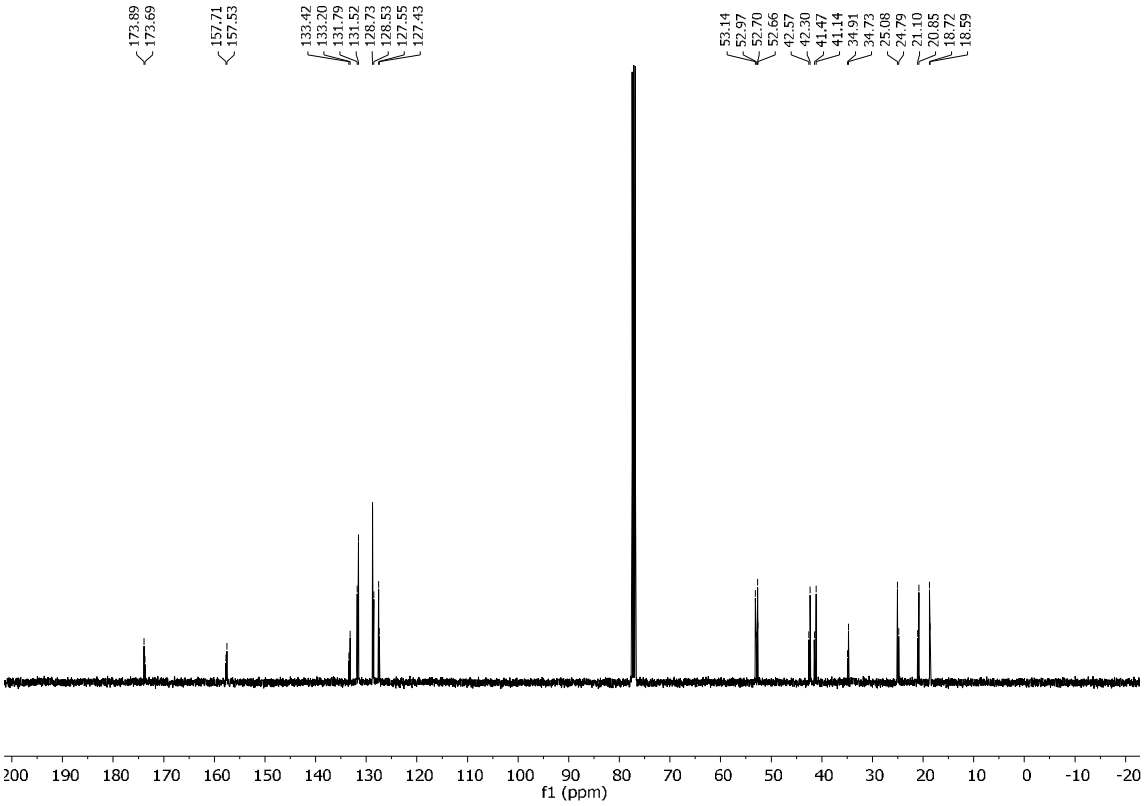

2-(tert-butyl) 1-methyl-(1R,1aS,6bS)-1-phenyl-1a,6b-dihydrocyclopropa[b]indole-1,2(1H)-dicarboxylate **(3ja)**

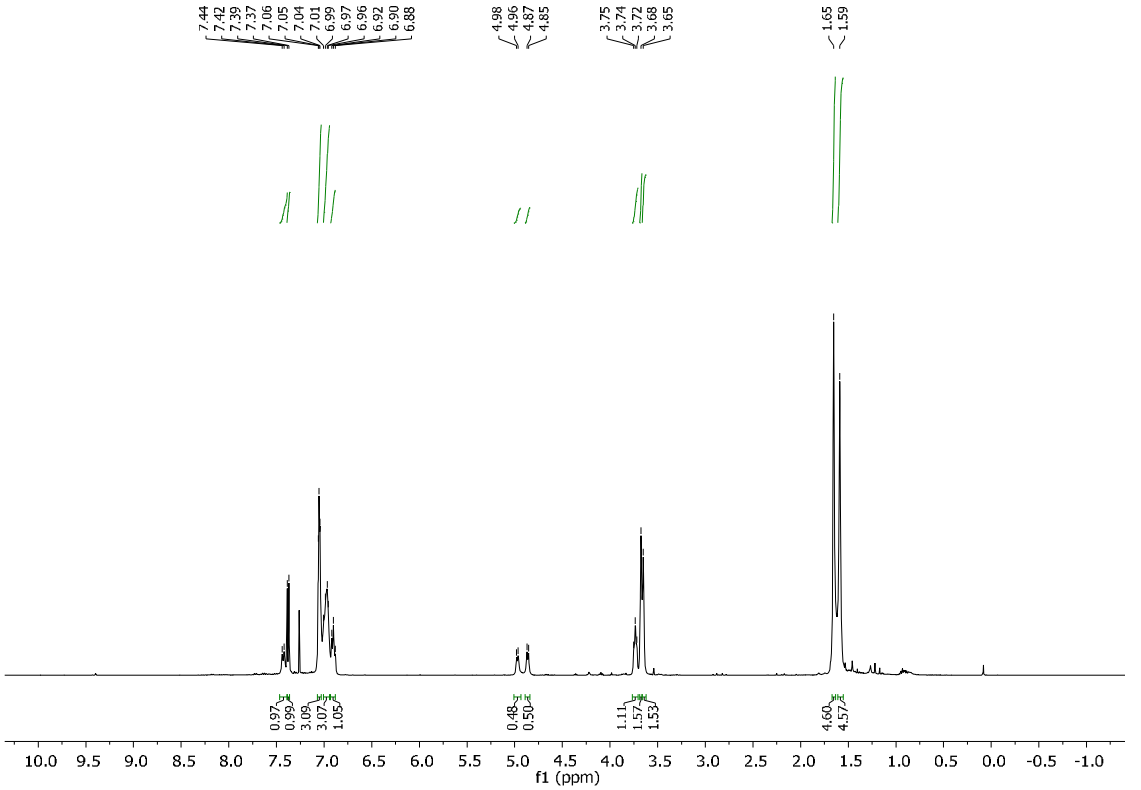

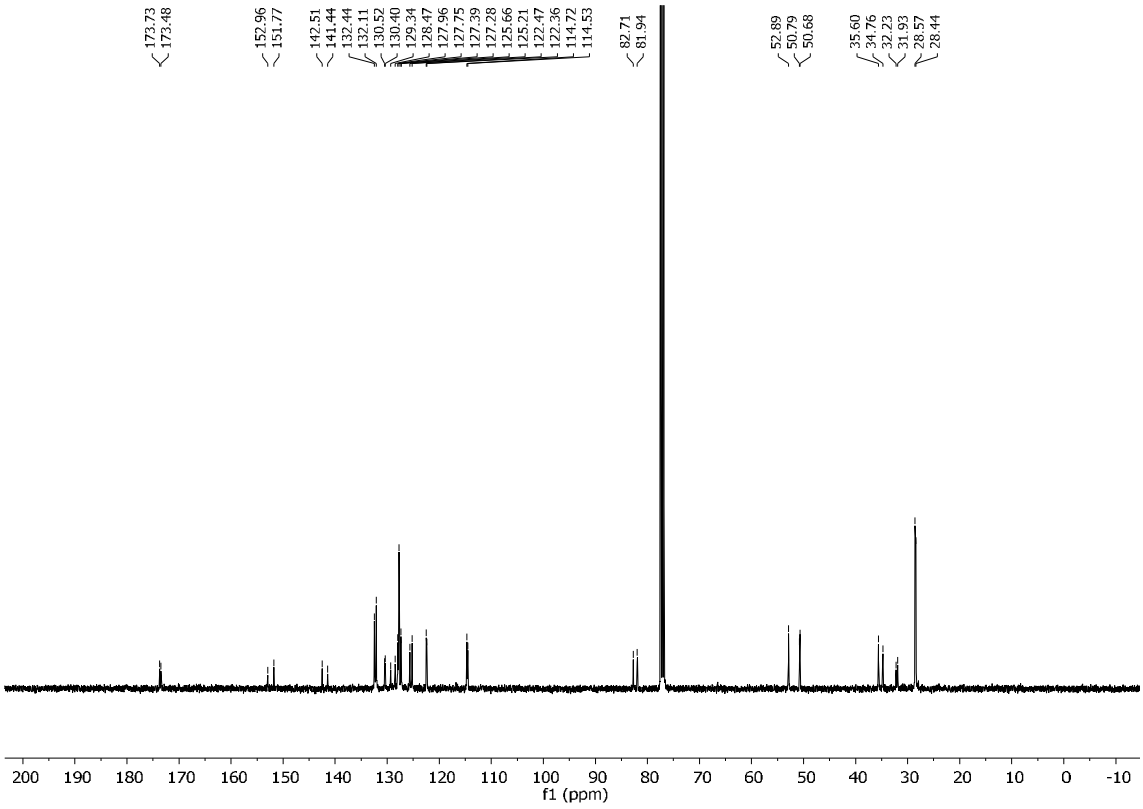

2-*tert*-butyl 1-methyl 5-fluoro-1-phenyl-1,6b-dihydrocyclopropa[b]indole-1,2(1aH)-dicarboxylate **(3ka)***

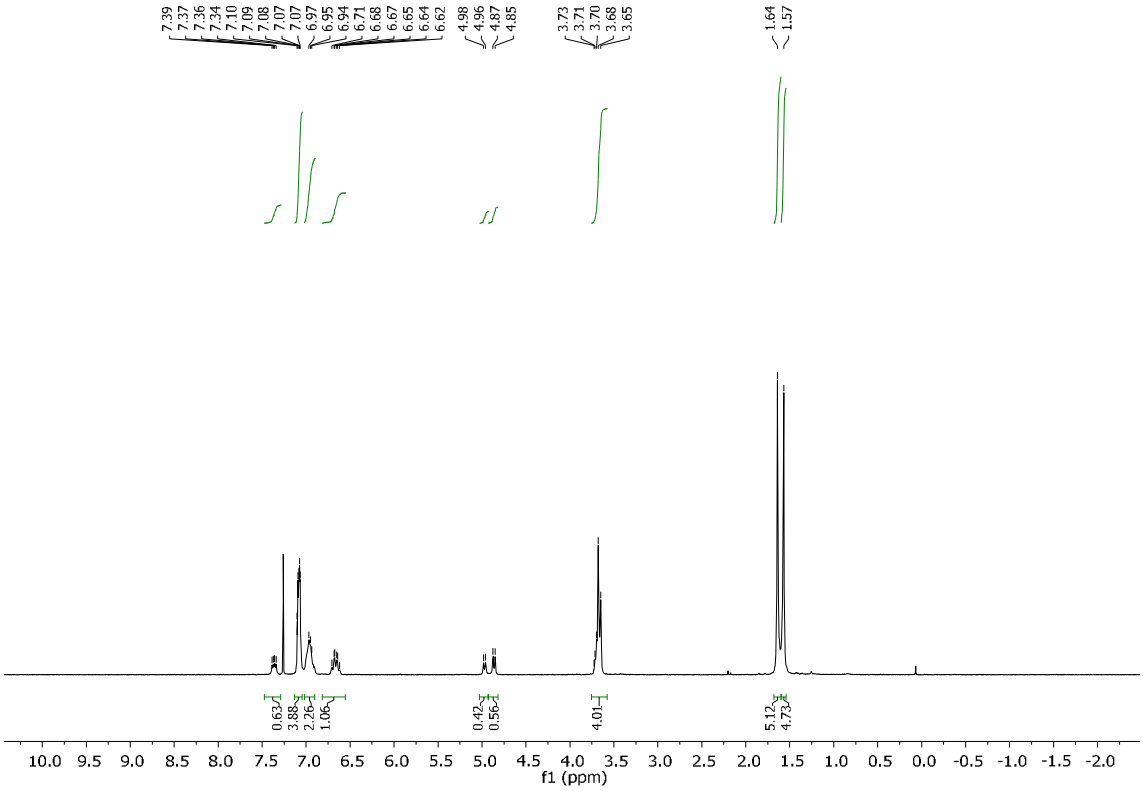

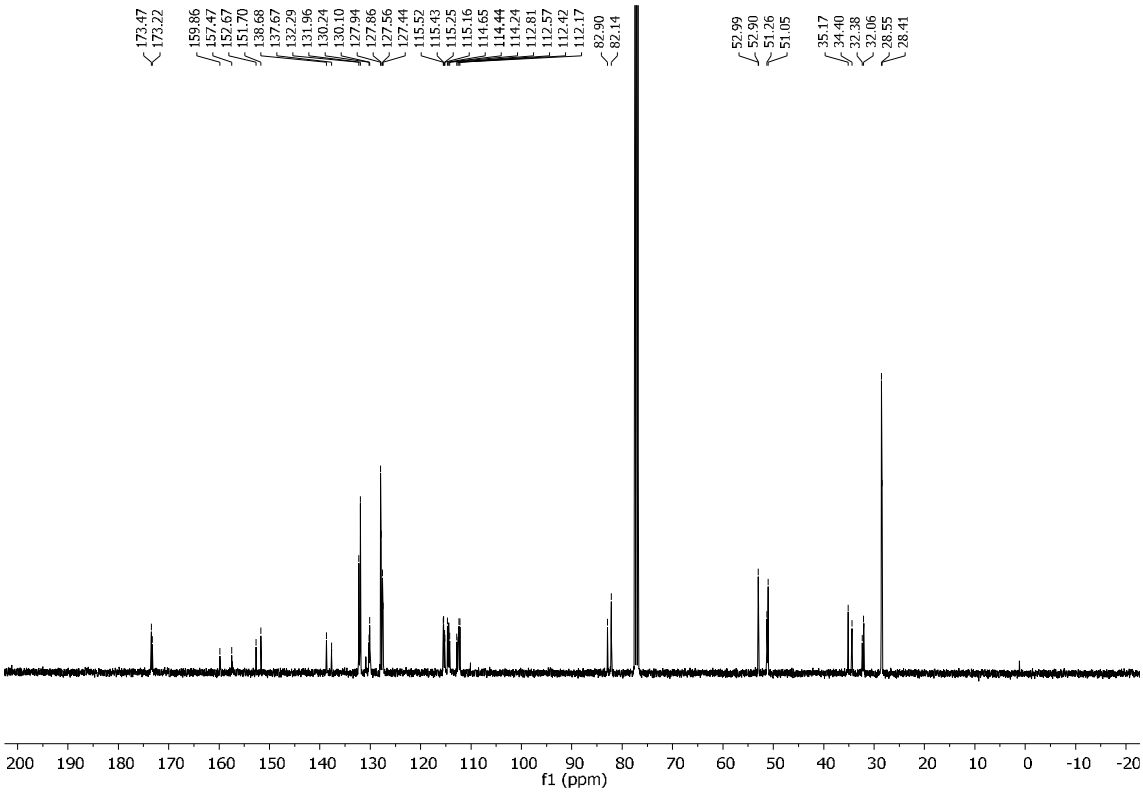

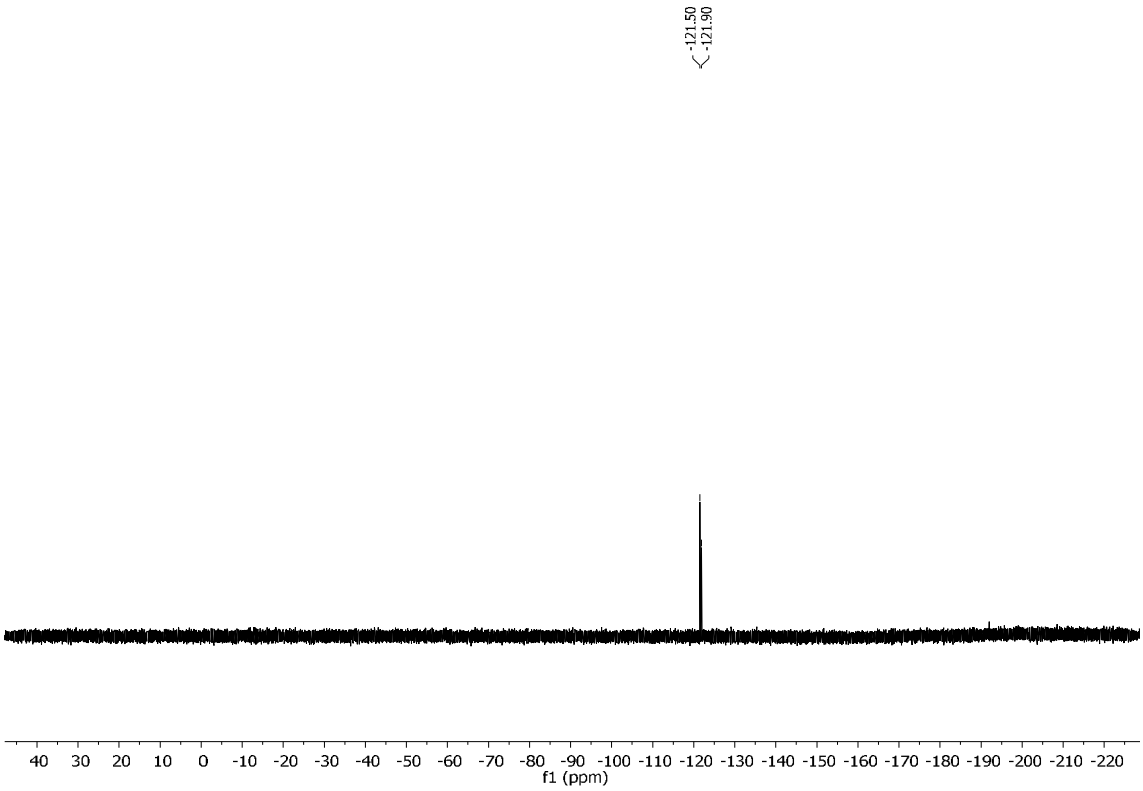

methyl (1S,1aS,6bR)-1-phenyl-1a,6b-dihydro-1H-benzo[b]cyclopropa[d]thiophene-1-carboxylate **(3la)**

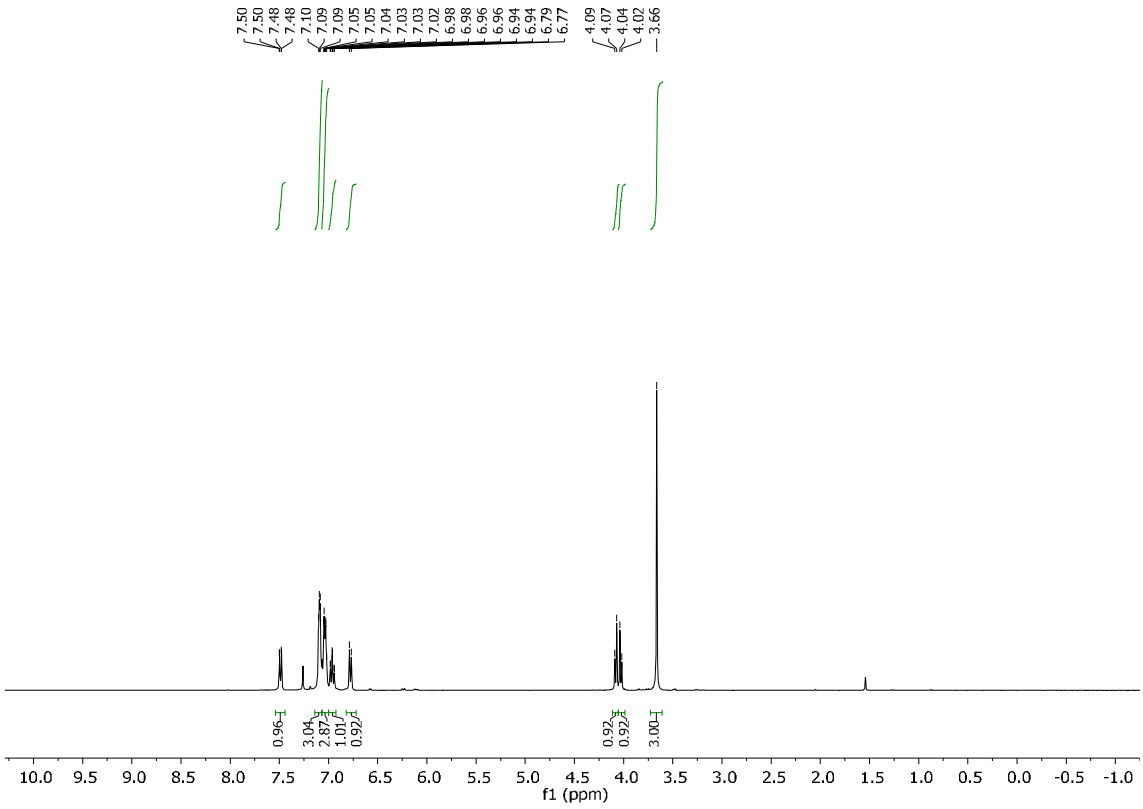

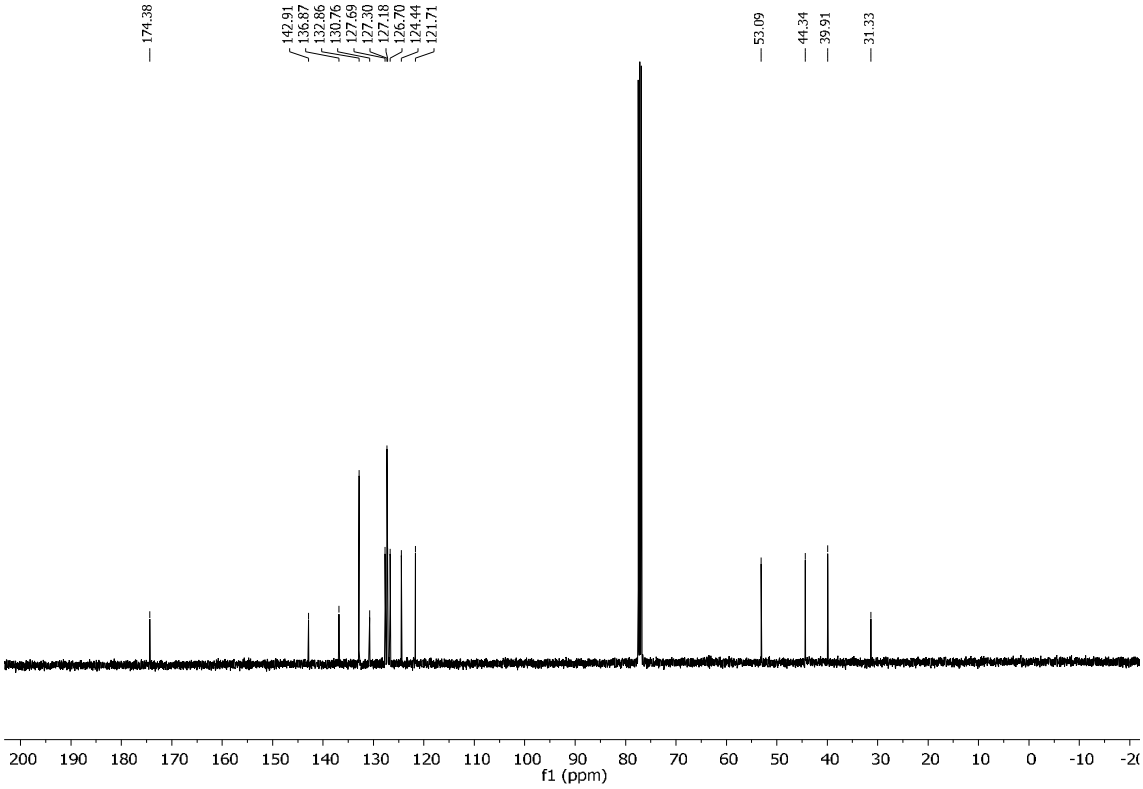

methyl (1S,5S,6R)-6-(4-nitrophenyl)-2-oxabicyclo[3.1.0]hex-3-ene-6-carboxylate **(3ab)**

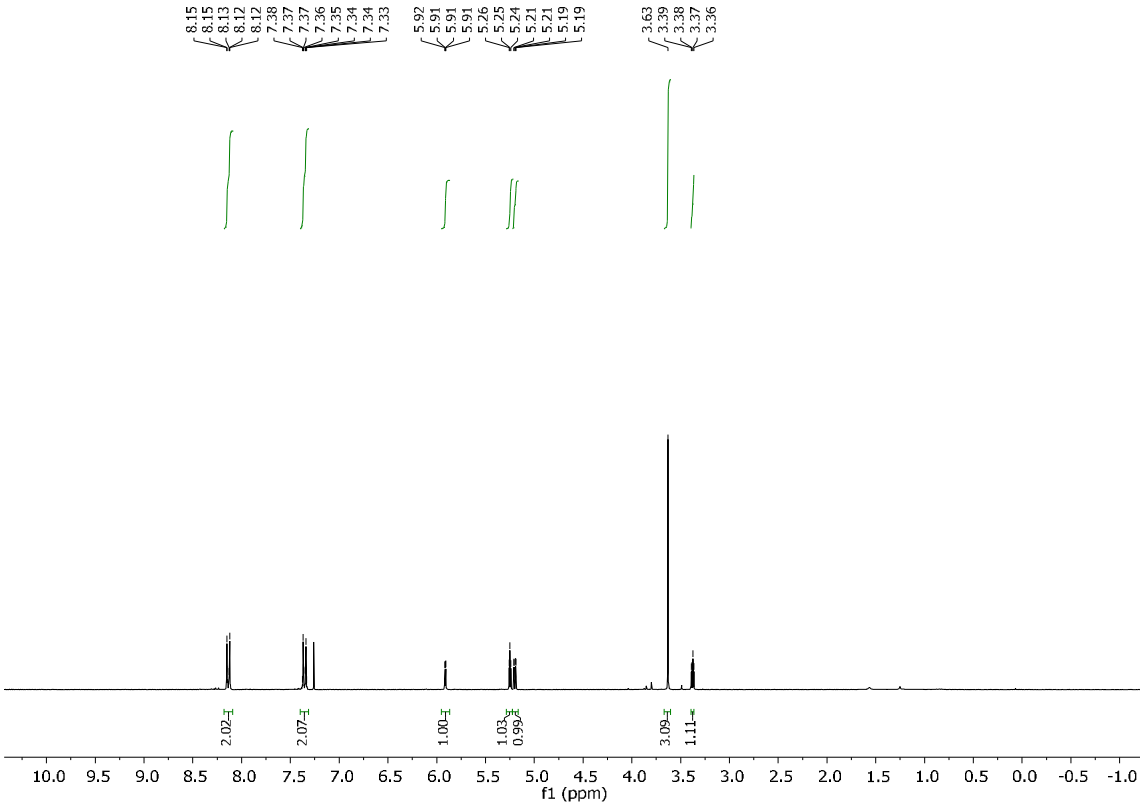

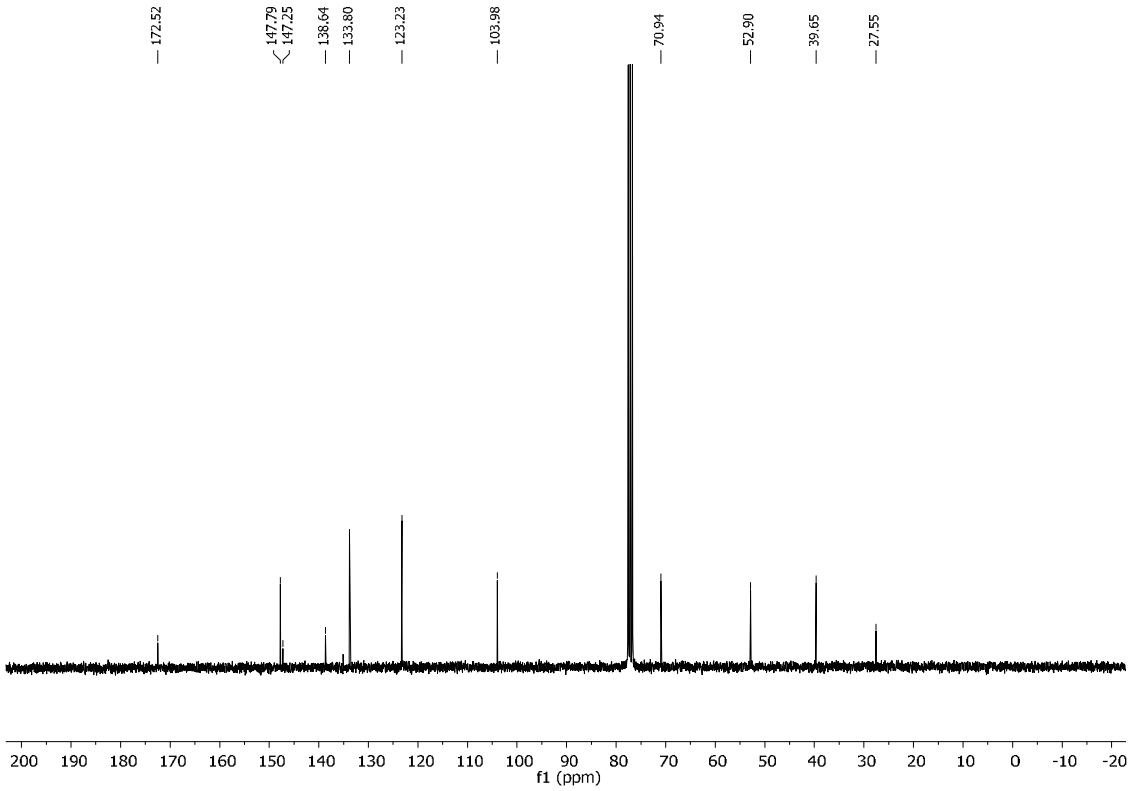

methyl (1R,5R,6S)-6-(4-chlorophenyl)-2-oxabicyclo[3.1.0]hex-3-ene-6-carboxylate **(3ac)**

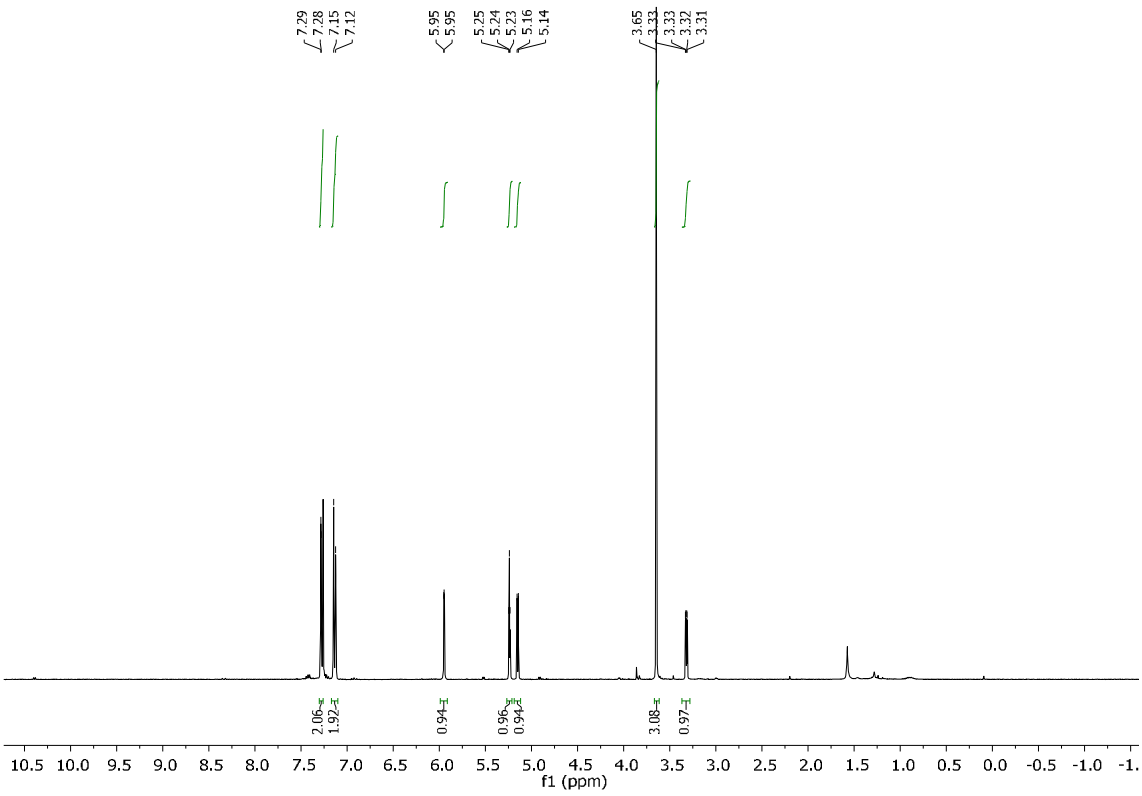

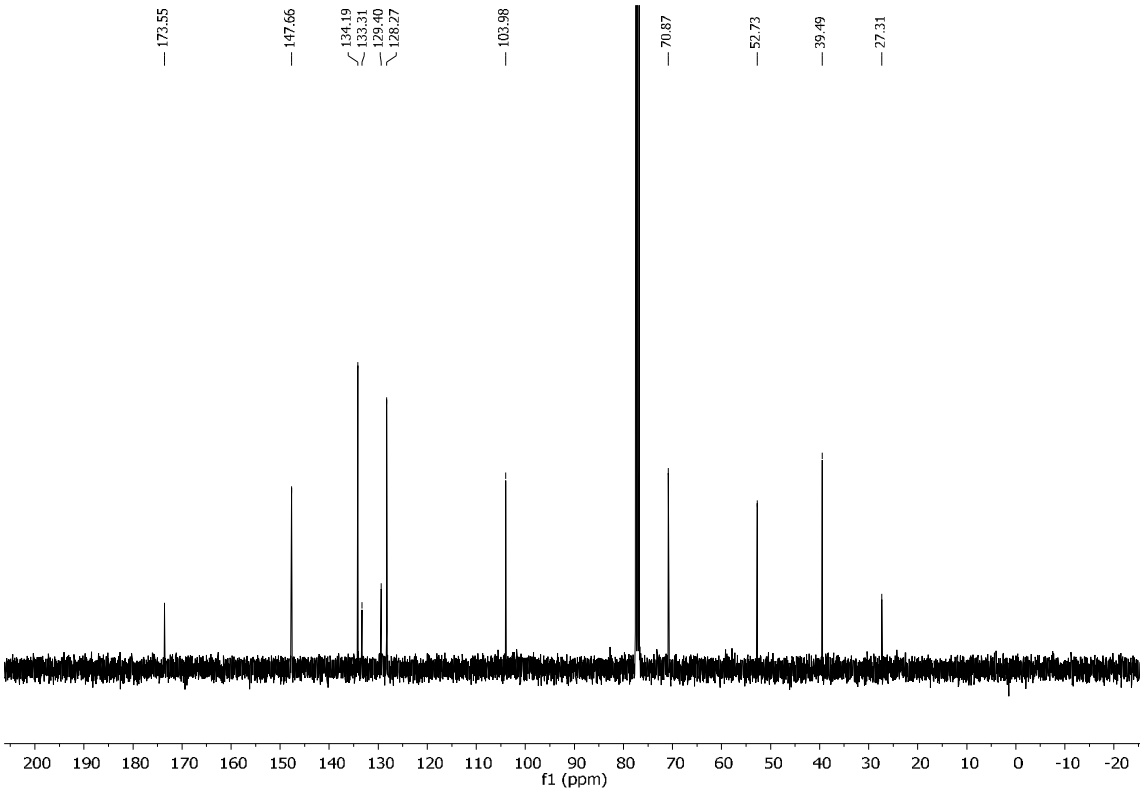

methyl (1S,5S,6R)-6-(4-methoxyphenyl)-2-oxabicyclo[3.1.0]hex-3-ene-6-carboxylate **(3ad)**

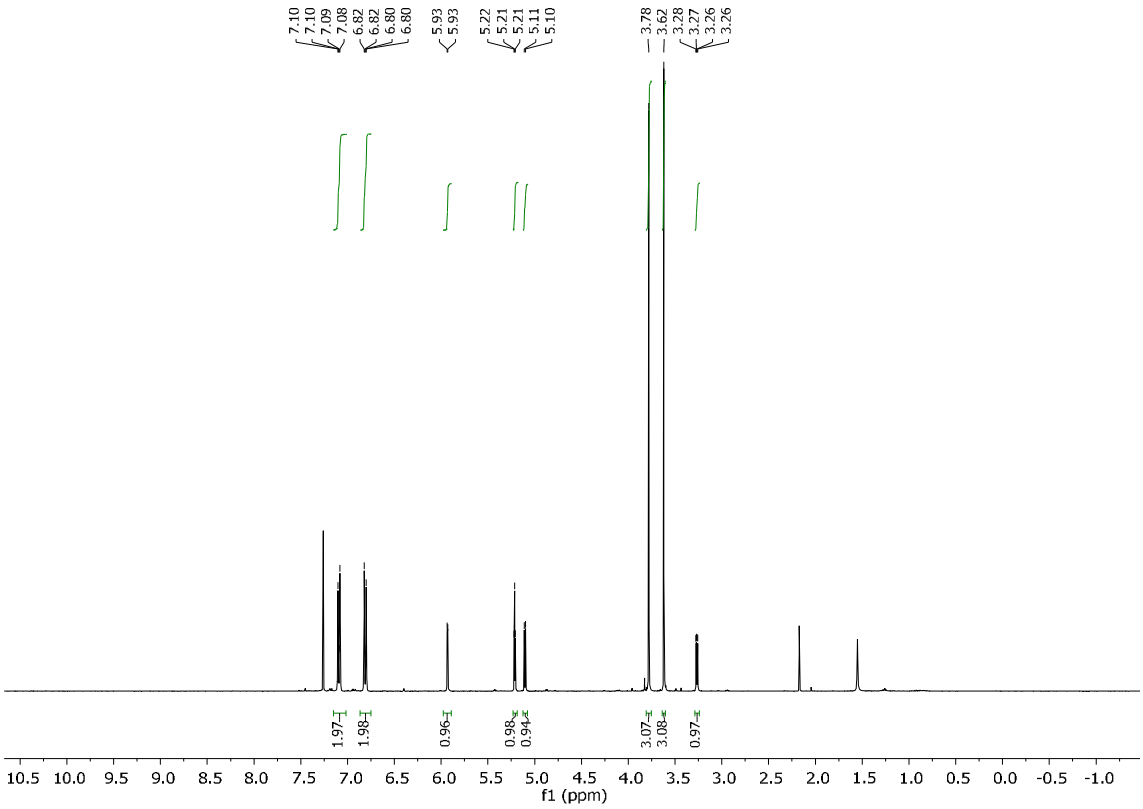

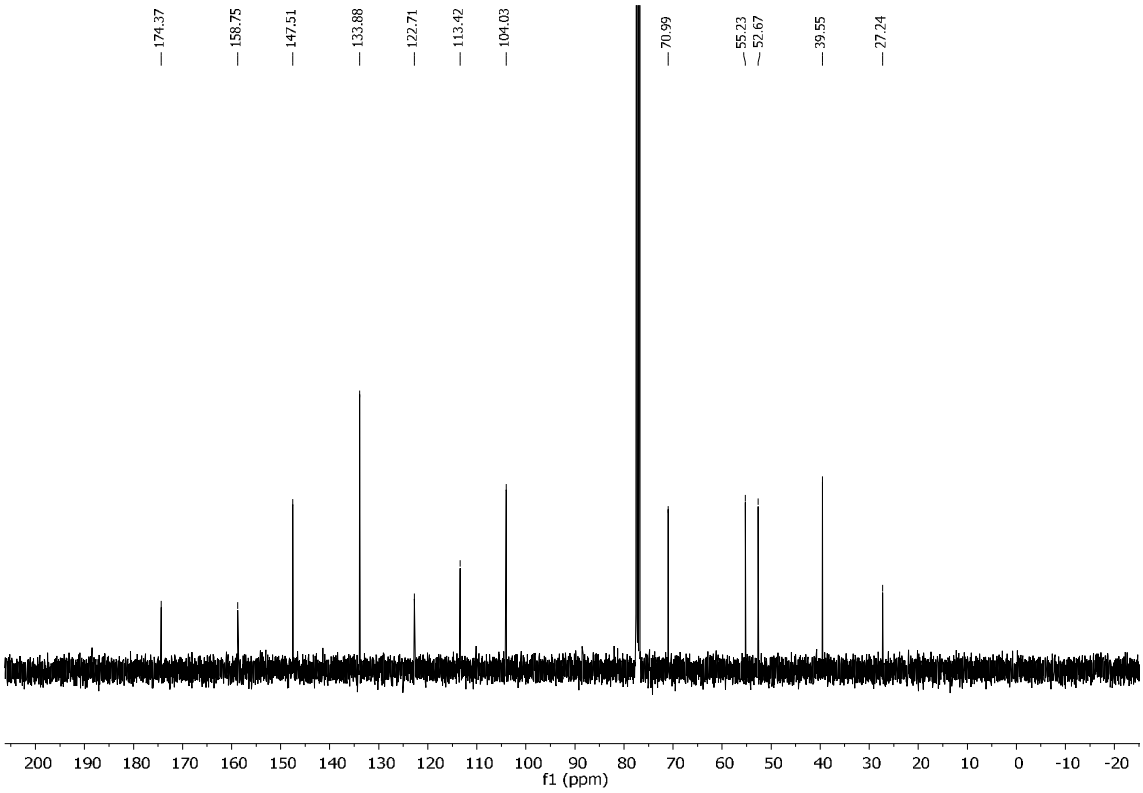

3.4.7 X-Ray Crystallography

Single crystal x-ray diffraction data were recorded for a suitable crystal of **3la**. The crystal was mounted on a MITIGEN holder with inert oil on a XtaLAB Synergy R, DW system, HyPix-Arc 150 diffractometer using Cu-Ka radiation (λ = 1.54184 Å). The crystal was kept at a steady T = 123.00(10) K during data collection. Empirical multi-scan and analytical absorption corrections[59] were applied to the data. Structures were solved using SHELXT[60] using dual methods and Olex2 as the graphical interface,[61] and least-squares refinements on F2 were carried out using SHELXL.[60,62]

All non-hydrogen atoms were refined anisotropically. Hydrogen atom positions were calculated geometrically and refined using the riding model. Most hydrogen atom positions were calculated geometrically and refined using the riding model, but some hydrogen atoms were refined freely.

2091948 (**3la**) contain the supplementary crystallographic data for this paper. These data are provided free of charge by The Cambridge Crystallographic Data Centre.

Table 3-6. Crystallographic data and structure refinement for 3la.

Compound	**3la**
Empirical formular	$C_{17}H_{14}O_2S$
$\rho_{calc}/(g/cm^3)$	1.376
μ/mm^{-1}	2.089
Formular weight	282.34 g mol^{-1}
Crystal colour	Clear colourless
Crystal shape	Block-shaped
Crystal size/mm^3	0.14 x 0.13 x 0.11
Temperature/K	123.00(10)
Crystal system	monoclinic
Space group	$P2_1/c$
a/ Å	11.6106(3)
b/ Å	16.0508(3)
c/ Å	7.5624(2)
α/ Å	90
β/ Å	104.790(2)
γ/ Å	90
Volume/Å³	1362.63(6)
Z	4
Z'	1
Wavelength/Å	1.54184
Radiation	Cu K_α
Θmin (°)	3.938
Θmax (°)	73.823
Reflections collected	15601
Independent reflections	2655
Reflections I≥2 σ(I)	2453
R_{int}	0.0250
Parameters	182
Restraints	0
Largest peak	0.614
Deepest hole	-0.677
GooF	1.077
wR_2 (all data)	0.1274
wR_2	0.1254
R_1 (all data	0.0489
R_1	0.0461

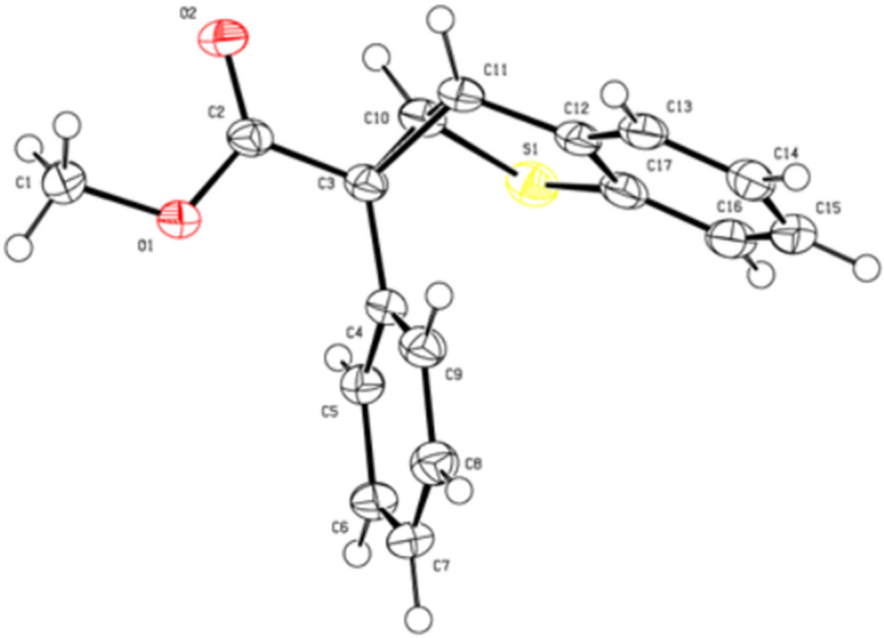

Figure 3-11. Solid-state molecular structure of **3la**, including atom numbering scheme. Thermal ellipsoids are set at the 50% probability level. C atoms shown in grey, S atom in yellow and O atoms in red.

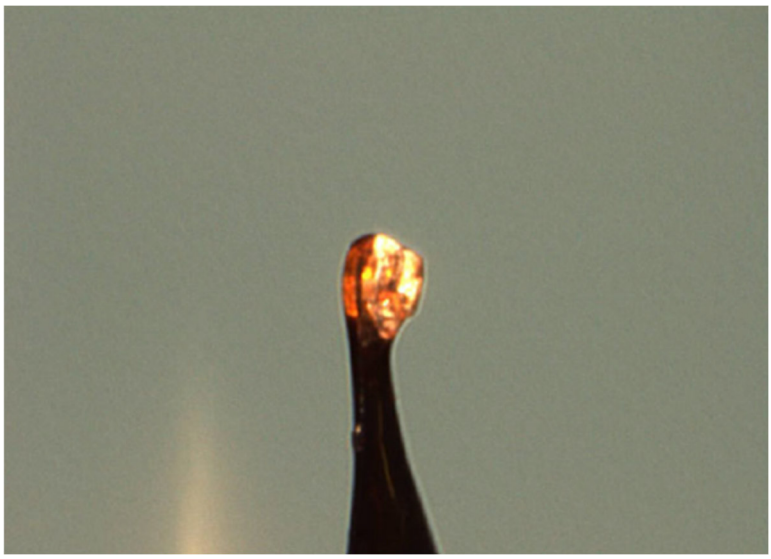

Figure 3-12. Picture of **3la** crystal inside the diffractometer.

Table 3-7. Bond lengths for **3la**.

Atom	Atom	Length/Å
S1	C17	1.773(2)
S1	C10	1.782(2)
O1	C2	1.336(2)
O1	C1	1.455(2)
O2	C5	1.212(2)
C4	C3	1.495(3)
C4	C2	1.496(3)
C4	C9	1.396(3)
C3	C2	1.496(3)
C3	C11	1.547(3)
C3	C10	1.540(3)
C12	C11	1.481(3)
C12	C13	1.408(3)
C12	C17	1.399(3)
C5	C6	1.392(3)
C6	C7	1.390(3)
C11	C10	1.503(3)
C13	C14	1.389(3)
C7	C8	1.384(3)
C9	C8	1.391(3)
C17	C16	1.383(3)
C15	C14	1.398(3)
C15	C16	1.366(3)

Table 3-8. Bond angles for **3la**.

Atom	Atom	Atom	Angle/°
C17	S1	C10	92.01(10)
C2	O1	C1	115.66(15)
C5	C4	C3	120.07(18)
C5	C4	C9	119.13(18)
C9	C4	C3	120.68(18)
C4	C3	C2	117.61(17)
C4	C3	C11	121.08(17)
C4	C3	C10	121.69(17)
C2	C3	C11	112.82(16)
C2	C3	C10	111.87(16)
C10	C3	C11	58.25(13)
C13	C12	C11	126.33(19)
C17	C12	C11	113.73(18)
C17	C12	C13	119.94(19)
O1	C2	C3	112.22(16)
O2	C2	O1	123.75(19)
O2	C2	C3	124.03(18)
C4	C5	C6	120.72(19)
C7	C6	C5	119.64(19)
C12	C11	C3	117.25(16)

C12	C11	C10	109.84(17)
C10	C11	C3	60.66(13)
C14	C13	C12	117.8(2)
C8	C76	C6	120.09(19)
C8	C94	C4	120.19(19)
C12	C17	S1	113.28(16)
C16	C17	S1	125.47(18)
C16	C17	C12	121.2(2)
C3	C10	S1	119.90(14)
C11	C10	S1	110.98(15)
C11	C10	C3	61.10(13)
C7	C8	C9	120.2(2)
C16	C15	C14	121.1(2)
C13	C14	C15	121.0(2)
C15	C16	C17	118.8(2)

The X ray crystal structures of compounds **3aa** and **3ba** have been previously reported (CCDC numbers: 1576359 and 1576357, respectively).[10]

3.5 References

1 S. V. Heines, *J. Chem. Educ.*, 1958, 35, 187.

2 A. Ford, H. Miel, A. Ring, C. N. Slattery, A. R. Maguire and M. A. McKervey, *Chem. Rev.*, 2015, 115, 9981–10080.

3 O. Reiser, *Isr. J. Chem.*, 2016, 56, 531–539.

4 G. Özüduru, T. Schubach and M. M. K. Boysen, *Org. Lett.*, 2012, 14, 4990–4993.

5 J. Kaschel, T. F. Schneider, D. Kratzert, D. Stalke and D. B. Werz, *Angew. Chem. Int. Ed.*, 2012, 51, 11153–11156.

6 M. Waser, E. D. Moher, S. S. K. Borders, M. M. Hansen, D. W. Hoard, M. E. Laurila, M. E. LeTourneau, R. D. Miller, M. L. Phillips, K. A. Sullivan, J. A. Ward, C. Xie, C. A. Bye, T. Leitner, B. Herzog-Krimbacher, M. Kordian and M. Müllner, *Org. Process Res. Dev.*, 2011, 15, 1266–1274.

7 C. M. Sonnleitner, S. Park, R. Eckl, T. Ertl and O. Reiser, *Angew. Chem. Int. Ed.*, 2020, 59, 18110–18115.

8 S. Kalidindi, W. B. Jeong, A. Schall, R. Bandichhor, B. Nosse and O. Reiser, *Angew. Chem. Int. Ed.*, 2007, 46, 6361–6363.

9 S. Budde, F. Goerdeler, J. Floß, P. Kreitmeier, E. F. Hicks, O. Moscovitz, P. H. Seeberger, H. M. L. Davies and O. Reiser, *Org. Chem. Front.*, 2020, 7, 1789–1795.

10 V. Lehner, H. M. L. Davies and O. Reiser, *Org. Lett.*, 2017, 19, 4722–4725.

11 A. Gheorghe, M. Schulte and O. Reiser, *J. Org. Chem.*, 2006, 71, 2173–2176.

12 S. P. Green, K. M. Wheelhouse, A. D. Payne, J. P. Hallett, P. W. Miller and J. A. Bull, *Org. Process Res. Dev.*, 2020, 24, 67–84.

13 R. Anthes, O. Bello, S. Benoit, C.-K. Chen, E. Corbett, R. M. Corbett, A. J. DelMonte, S. Gingras, R. Livingston, J. Sausker and M. Soumeillant, *Org. Process Res. Dev.*, 2008, 12, 168–177.

14 A. P. Colleville, R. A. J. Horan and N. C. O. Tomkinson, *Org. Process Res. Dev.*, 2014, 18, 1128–1136.

15 M. Movsisyan, E. I. P. Delbeke, J. K. E. T. Berton, C. Battilocchio, S. V. Ley and C. V. Stevens, *Chem. Soc. Rev.*, 2016, 45, 4892–4928.

16 F. F. Stoessel, Thermal Safety of Chemical Processes, Wiley- VCH, Weinheim, 2008.

17 B. J. Deadman, S. G. Collins and A. R. Maguire, *Chem. Eur. J.*, 2015, 21, 2298–2308.

18 S. T. R. Müller and T. Wirth, *ChemSusChem*, 2015, 8, 245–250.

19 K. J. Hock and R. M. Koenigs, *Chem. Eur. J.*, 2018, 24, 10571–10583.

20 B. Castano, E. Gallo, D. J. Cole-Hamilton, V. Dal Santo, R. Psaro and A. Caselli, *Green Chem.*, 2014, 16, 3202–3209.

21 M. I. Burguete, A. Cornejo, E. García-Verdugo, J. García, M. J. Gil, S. V. Luis, V. Martínez-Merino, J. A. Mayoral and M. Sokolova, *Green Chem.*, 2007, 9, 1091.

22 L. J. Martin, A. L. Marzinzik, S. V. Ley and I. R. Baxendale, *Org. Lett.*, 2011, 13, 320–323.

23 D. Rackl, C.-J. Yoo, C. W. Jones and H. M. L. Davies, *Org. Lett.*, 2017, 19, 3055–3058.

24 C. Yoo, D. Rackl, W. Liu, C. B. Hoyt, B. Pimentel, R. P. Lively, H. M. L. Davies and C. W. Jones, *Angew. Chem. Int. Ed.*, 2018, 57, 10923–10927.

25 J. P. Knowles, L. D. Elliott and K. I. Booker-Milburn, *Beilstein J. Org. Chem.*, 2012, 8, 2025–2052.

26 Z. J. Garlets, J. D. Nguyen and C. R. J. Stephenson, *Isr. J. Chem.*, 2014, 54, 351–360.

27 D. Cambié, C. Bottecchia, N. J. W. Straathof, V. Hessel and T. Noël, *Chem. Rev.*, 2016, 116, 10276–10341.

28 J. D. Williams and C. O. Kappe, *Curr. Opin. Green Sustain. Chem.*, 2020, 25, 100351.

29 I. D. Jurberg and H. M. L. Davies, *Chem. Sci.*, 2018, 9, 5112–5118.

30 R. Hommelsheim, Y. Guo, Z. Yang, C. Empel and R. M. Koenigs, *Angew. Chem. Int. Ed.*, 2019, 58, 1203–1207.

31 N. Tanbouza, V. Carreras and T. Ollevier, *Org. Lett.*, 2021, 23, 5420–5424.

32 C. Empel and R. M. Koenigs, *J. Flow. Chem.*, 2020, 10, 157–160.

33 C. M. Alder, J. D. Hayler, R. K. Henderson, A. M. Redman, L. Shukla, L. E. Shuster and H. F. Sneddon, *Green Chem.*, 2016, 18, 3879–3890.

34 M. W. Bedore, N. Zaborenko, K. F. Jensen and T. F. Jamison, *Org. Process Res. Dev.*, 2010, 14, 432–440.

35 J. P. Barham, S. Tanaka, E. Koyama, N. Ohneda, T. Okamoto, H. Odajima, J. Sugiyama and Y. Norikane, *J. Org. Chem.*, 2018, 83, 4348–4354.

36 J. P. Barham, S. Tamaoki, H. Egami, N. Ohneda, T. Okamoto, H. Odajima and Y. Hamashima, *Org. Biomol. Chem.*, 2018, 16, 7568–7573.

37 P. Tundo and M. Selva, *Acc. Chem. Res.*, 2002, 35, 706–716.

38 P. Vámosi, K. Matsuo, T. Masuda, K. Sato, T. Narumi, K. Takeda and N. Mase, *Chem. Rec.*, 2019, 19, 77–84.

39 J. P. Barham, E. Koyama, Y. Norikane, N. Ohneda and T. Yoshimura, *Chem. Rec.*, 2019, 19, 188–203.

40 P. Sagmeister, J. Poms, J. D. Williams and C. O. Kappe, *React. Chem. Eng.*, 2020, 5, 677–684.

41 C. J. Taylor, A. Baker, M. R. Chapman, W. R. Reynolds, K. E. Jolley, G. Clemens, G. E. Smith, A. J. Blacker, T. W. Chamberlain, S. D. R. Christie, B. A. Taylor and R. A. Bourne, *J. Flow. Chem.*, 2021, 11, 75–86.

42 H. E. Bonfield, J. D. Williams, W. X. Ooi, S. G. Leach, W. J. Kerr and L. J. Edwards, *ChemPhotoChem*, 2018, 2, 938–944.

43 J. Chen, S. Liu, X. Lv, K. Hong, J. Lei, X. Xu and W. Hu, *J. Org. Chem.*, 2020, 85, 13920–13928.

44 A. F. Da Silva, M. A. S. Afonso, R. A. Cormanich and I. D. Jurberg, *Chem. Eur. J.*, 2020, 26, 5648–5653.

45 T. Xiao, M. Mei, Y. He and L. Zhou, *Chem. Commun.*, 2018, 54, 8865–8868.

46 J. Yang, J. Wang, H. Huang, G. Qin, Y. Jiang and T. Xiao, *Org. Lett.*, 2019, 21, 2654–2657.

47 Z. Yang, Y. Guo and R. M. Koenigs, *Chem. Eur. J.*, 2019, 25, 6703–6706.

48 S. Jana, F. Li, C. Empel, D. Verspeek, P. Aseeva and R. M. Koenigs, *Chem. Eur. J.*, 2020, 26, 2586–2591.

49 G. Xu, K. Liu and J. Sun, *Org. Lett.*, 2018, 20, 72–75.

50 J. Kaschel, T. F. Schneider, P. Schirmer, C. Maaß, D. Stalke and D. B. Werz, *Eur. J. Org. Chem.*, 2013, 2013, 4539–4551.

51 Albert. Padwa and S. F. Hornbuckle, *Chem. Rev.*, 1991, 91, 263–309.

52 W. L. F. Armarego, *Purification of laboratory chemicals*, Butterworth-Heinemann, Kidlington, Oxford, 8th ed., 2017.

53 J. Fu, N. Wurzer, V. Lehner, O. Reiser and H. M. L. Davies, *Org. Lett.*, 2019, 21, 6102–6106.

54 J. E. Jakobsson, G. Grønnevik and P. J. Riss, *Chem. Commun.*, 2017, 53, 12906–12909.

55 T. Jaschinski and M. Hiersemann, *Org. Lett.*, 2012, 14, 4114–4117.

56 H. M. L. Davies, T. Hansen and M. R. Churchill, *J. Am. Chem. Soc.*, 2000, 122, 3063–3070.

57 W.-W. Chan, S.-H. Yeung, Z. Zhou, A. S. C. Chan and W.-Y. Yu, *Org. Lett.*, 2010, 12, 604–607.

58 S. Gratia, K. Mosesohn and S. T. Diver, *Org. Lett.*, 2016, 18, 5320–5323.

59 R. C. Clark and J. S. Reid, *Acta Cryst. A*, 1995, 51, 887–897.

60 G. M. Sheldrick, *Acta Cryst. C*, 2015, 71, 3–8.

61 O. V. Dolomanov, L. J. Bourhis, R. J. Gildea, J. A. K. Howard and H. Puschmann, *J. Appl. Crystallogr.*, 2009, 42, 339–341.

62 G. M. Sheldrick, *Acta Cryst. A*, 2008, 64, 112–122.

Chapter 4

4 Catalyst-Free, Scalable, Green-Light-Mediated Iodoamination, and Further Transformation of Olefins Under Continuous Flow Conditions‡

4.1 Abstract

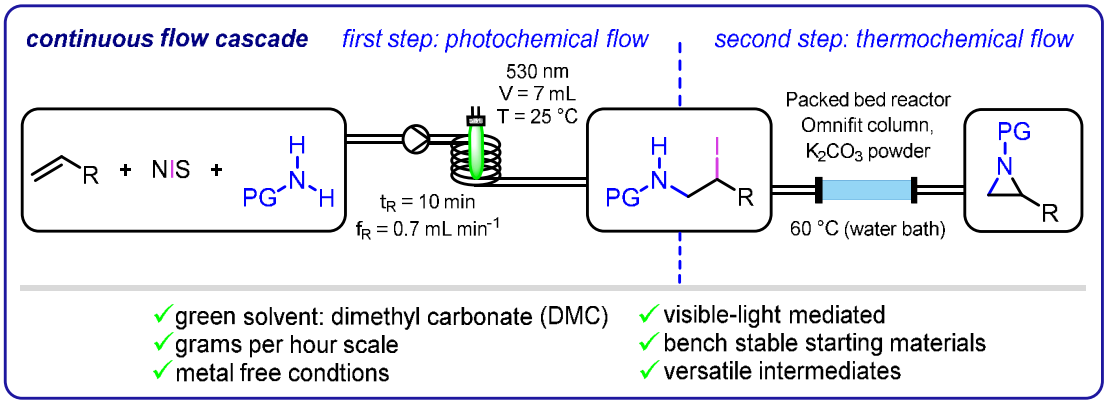

We report the iodoamination of alkenes in continuous flow under metal-free, visible-light-mediated conditions with commercially available N-iodosuccinimide and protected amines. Unactivated and activated alkenes as well as Michael acceptors are amenable substrate classes for this process, allowing the synthesis of 1,2-iodoamines with a broad scope and in high yields (59−94%). The steadiness of the protocol is demonstrated in a continuous flow experiment over 4.5 h for the coupling of styrene, NIS, and N-tosyl-amine, which gave rise to 14 g (91%) of the iodoaminated product, corresponding to a productivity of 3.1 g h^{-1}.Additionally, the direct conversion of the products without prior isolation into aziridines, enamines, amino alcohols, or azidoamines is possible, underscoring the synthetic value of this approach. Variation of the reaction conditions by adding typical impurities in reagents or solvents or changing the irradiation from green to blue light had a minimal effect on the yield, giving credit to the robustness of the process.

‡ This chapter is based on: V. Klöpfer, L. Roithmeier, M. Kobras, P. Kreitmeier, O. Reiser, *Org. Process Res. Dev.* **2025**, *29*, 755-759. L. Roithmeier performed her bachelor's thesis as part of this chapter under the supervision of V. Klöpfer. Optimization of the reaction conditions in flow (**Table 4-1**) was performed by L. Roithmeier. M. Kobras synthesized compound **S1 and 1f**. P. Kreitmeier designed the reactor used in this project and provided technical support. O. Reiser was supervising this project.

4.2 Introduction

Nitrogen-containing compounds are represented in numerous natural products and pharmaceuticals. In fact, 90% of drug molecules bear at least one nitrogen atom.[1] Consequently, the formation of C−N bonds is an ongoing research topic in academia and industry. Haloaminations, first described in the middle of the 20th century, have proven to be a decisive reaction to incorporate an amine and a halogen group into C−C double bonds simultaneously to obtain vicinal haloamines.[1,2] These structural moieties represent key motifs in many bioactive metabolites and are versatile intermediates in pharmaceutical and organic chemistry. Therefore, several protocols for chloro- and bromoamination of unsaturated C−C bonds have been developed in the past decade.[3–14] Inspired by reports on intramolecular iodoaminations,[15–18] we disclosed a photochemical protocol for the intermolecular photochemical iodoamination of unactivated and activated alkenes in 2021.[19] This way, 1,2-iodoamines became broadly accessible, which proved to be valuable for further transformations. Driven by the broad applicability and based on our interest in photo flow reactions,[20] we set out to transfer the developed iodoamination protocol to continuous flow conditions. Kappe *et al.* impressively demonstrated the potential of continuous flow by elaborating a chloroamination of alkenes under photochemical conditions (Scheme 4-1).[21] In a two-step flow cascade setup, they were able first to generate and subsequently incorporate N-chloroamines into various alkenes in an ATRA-type reaction. As an alternative, we herein report the catalyst-free iodoamination of alkenes under continuous photo flow conditions with bench-stable starting materials on a gram-per-hour scale (Scheme 4-1) without first preparing and purifying an N-halogen reagent. Furthermore, we successfully transformed the crude products obtained from the amino-iodination reaction into aziridines (either in a two-step flow setup or in a telescopic batch setup), β-amino alcohols, enamines, or vicinal azidoamines (Scheme 4-3).

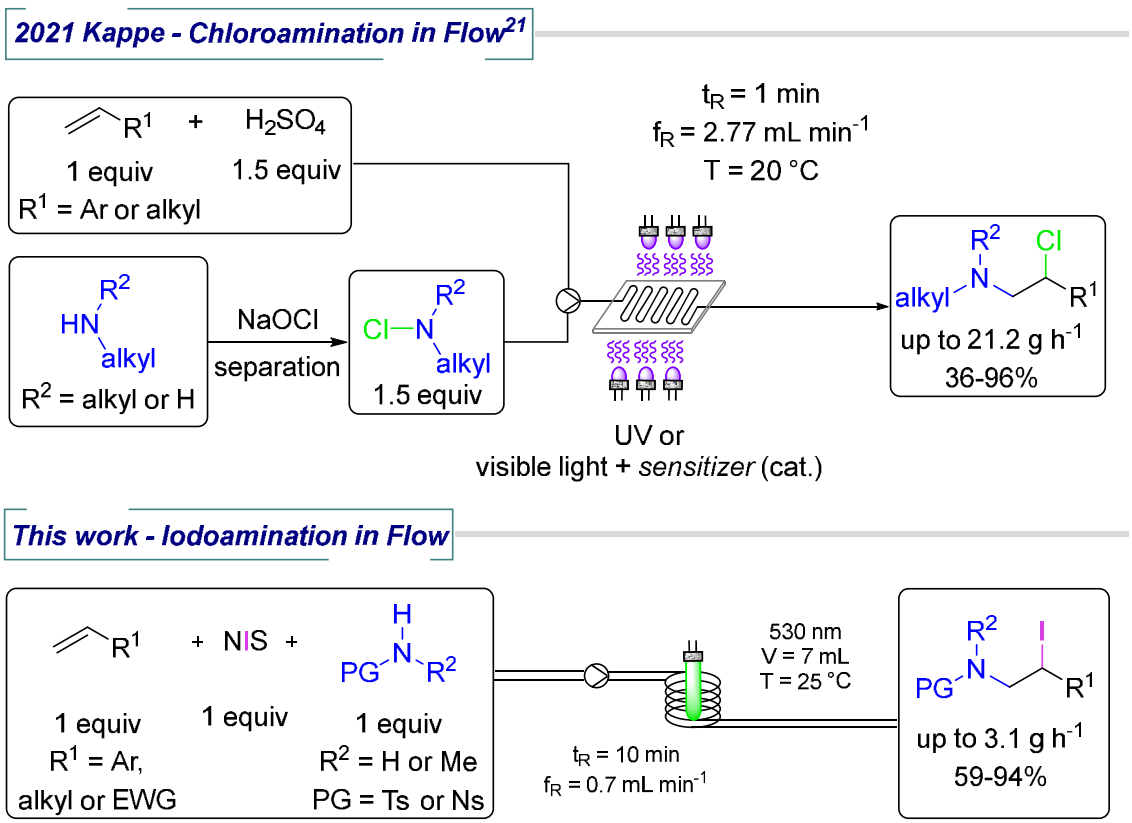

Scheme 4-1. Haloamination of alkenes under continuous photo flow conditions by Kappe et al. (chloroamination)[21] and this work (iodoamination).

4.3 Results and Discussion

4.3.1 Optimization Under Flow Conditions

While batch reactions are not restrained to homogeneity, homogeneous conditions are generally required for trans-formations under continuous flow conditions. Under the batch reaction conditions previously reported by us, the starting materials are not dissolved completely.[19] To maintain the sustainability of the procedure using dimethyl carbonate (DMC) as a solvent, we chose to decrease the concentration to 0.1 M (instead of 0.25 M under batch conditions) rather than change the solvent to obtain complete solubility. Nevertheless, the solvent could be recycled by distillation (90%) at the end of the reaction and reused (robustness scan, see Figure 4-1). Initial attempts converting p-toluene sulfonamide (**3a**, PASAM), N-iodosuccinimide (NIS, **2**), and styrene (**1a**) under continuous photo flow conditions were nevertheless characterized by low conversion and yield (Table 4-1, entry 1). Based on the assumption that traces of hydrogen iodide may be present in NIS (**2**) or formed during the reaction that would affect the reaction negatively, catalytic amounts (10 mol %) of various inorganic bases were added to the stock solution

of the substrates. Initially, potassium carbonate proved to be the most effective, giving rise to **4a** with 85% and perfect regioselectivity at a residence time (t_R) of 10 min (Table 4-1, entry 2). Altering the temperature (Table 4-1,entry 3), flow rate (f_R, Table 4-1, entry 4), or concentration (Table 4-1, entry 5) resulted in lower yields and conversion. Using acetonitrile (MeCN) instead of DMC as a solvent allows a higher concentration, as even at 0.3 M, the reaction solution is homogeneous but proves to be significantly inferior for the process (Table 4-1, entry 6). Finally, we found that the employment of potassium acetate improved the reaction further, resulting in complete conversion and furnishing **4a** in 93% yield (Table 4-1, entry 8), which is equivalent to a productivity of product **4a** of 1.52 g h^{-1} (Scheme 4-2).

Table 4-1. Optimization of the aminoiodination of styrene (**1a**) with NIS (**2**) and N-tosylamine (**3a**) under continuous flow conditions.

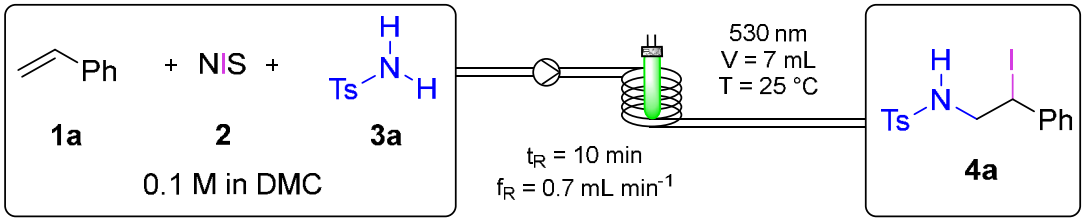

Entry	Variation	Yield % (NMR)[a]
1	No base	35
2	K_2CO_3 / KOH / K_3PO_4 (10 mol%)	85 / 80 / 70
3	T = 10 °C, K_2CO_3 (10 mol %)	75
4	t_R = 5 min (f_R = 1.4 mL min^{-1}) / t_R = 20 min (f_R = 0.35 mL min^{-1}), K_2CO_3 (10 mol %)	37 / 70
5	0.05 M / 0.2 M, K_2CO_3 (10 mol %)	78 / 59
6	0.1 M MeCN, K_2CO_3 (10 mol %)	20
7	0.2 M, t_R = 20 min, K_2CO_3 (10 mol %)	48
8	KOAc (10 mol%)	93

Standard conditions: **1a** (1 equiv, 250 mmol), **2** (1 equiv, 250 mmol), **3a** (1 equiv, 250 mmol) in DMC (0.1 M), KOAc (10 mol%, 25 mmol), collected volume V_C = 2.5 mL (collected in 3 min 34 sec), residence time t_R = 10 min, flow rate f_R = 0.7 mL min^{-1}, reactor volume V_R = 7 mL, T = 25 °C, λ_{max} = 530 nm. [a]Determined by NMR analysis with 1,1,2,2-tetrachlorethane as an internal standard, error ±5 %.

4.3.2 Substrate Scope, Upscaling, and Further Transformations

With the optimized conditions in hand, we evaluated some representative substrates (Scheme 4-2). Activated and unactivated alkenes as well as α,β-unsubstituted alkenes, performed well with similar efficiency − ranging from 59 to 94% of yield − to the previously reported batch setup.[19] Notably, the N-Nosyl product **4c** was generated in 87%

yield, allowing the amine moiety's deprotection under mild conditions. Furthermore, we applied the protocol to N-(2-allylphenyl)-4-methylbenzenesulfonamide (**1f**) to showcase an intramolecular reaction and obtained **4h** in a 73% yield. In addition, we evaluated the ability to boost productivity by increasing the volume of the flow reactor to 14 mL, while the t_R remained the same. No significant decrease in the yield was observed, resulting in an increase in the productivity of **4a** from 1.52 to 3.04 g h^{-1} (Scheme 4-2). Furthermore, the steadiness of the process was demonstrated by performing the reaction in the 14 mL reactor under standard conditions for 4 h and 36min, producing 14.0 g (isolated, 91% yield, 3.04 g h^{-1}) of compound **4a**. To monitor the stability of the process, the output of the reactor was fractionated every 24 min into 2.5 mL aliquots, and the yield of the fractions was determined either by quantitative NMR (in black) or by isolation (in red, for details, see *4.4.2 Synthesis and Analytical Data*, Table 4-4).

The resulting assay yields ranged from 89−94% for all fractions, providing an average yield of 91% (Scheme 4-3, a). While our previously reported batch process proved to be scalable to gram quantities without loss in yield,[19] comparing these conditions with the photo flow process reported here is of limited value due to varied light sources, reaction setup (internal vs external irradiation), and different concentrations (0.25 M vs 0.1 M).[23,24] Therefore, we performed the synthesis of **4a** in a large-scale batch reactor under identical reaction conditions as in flow (180 mmol, 0.1 M, identical light source).

We obtained a good but nevertheless diminished yield of 72% with less than half the productivity (1.15 g h^{-1}, 5.2 g of **4a** after 4.5 h) that is achieved in flow. We attribute this not only to the larger layer thickness in the batch reactor but also to the formation of small quantities of strongly colored byproducts: a color change from yellow to red occurs in the course of the reaction, which deepens in the batch reactor and thereby makes light penetration increasingly difficult over time (for more details, see *4.4.1 General Information*).[25,26] No reactor fouling was observed in either batch or flow, which holds the promise of further upscaling. The robustness of the process was evaluated by modifying the reaction conditions for the synthesis of **4a** from **1a**, **2**, and **3a** by adding typical contaminants that could be detrimental for the title reaction (Figure 4-1, for more details, see *4.4.2 Synthesis and Analytical Data*, Table 4-3). Additional succinimide that could stem from low-grade NIS (**2**), undistilled styrene (**1a**), and 0.5% water (v/v) had no significant effect on the yield. In turn, running the reaction under a nitrogen atmosphere by degassing the solution and purging the reactor with nitrogen prior to operation did not

increase the yield. Likewise, reusing the solvent upon recycling was possible without a loss of yield. In contrast, using blue (455 nm) instead of green (530 nm) LEDs for irradiation of the solution resulted in a reduced yield of 83% (10% difference from the standard conditions), which might be due to an increased iodine production with higher energy light, which is known to be an effective quencher and thus a poison for photocatalytic processes.[27,28]

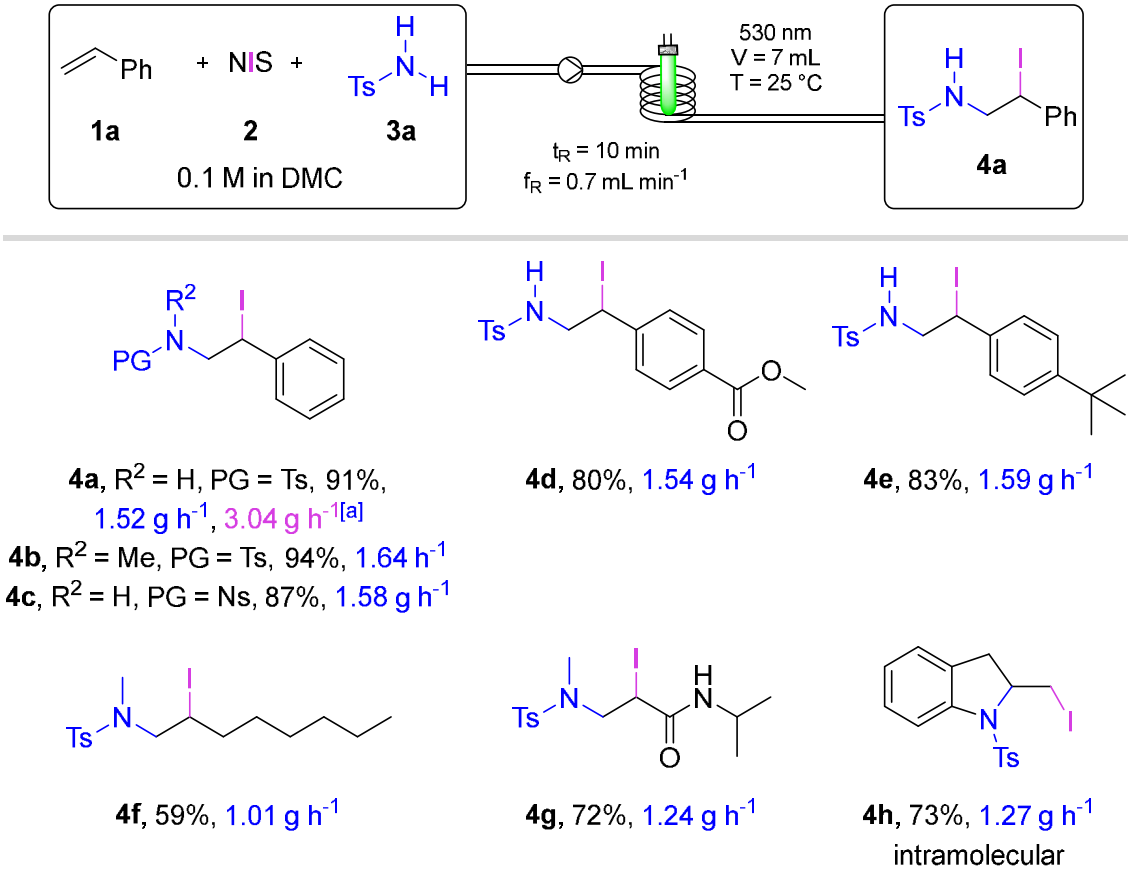

Scheme 4-2. Substrate Scope of the Iodoamination of Olefins Under Continuous Photo-Flow Conditions. *Standard conditions*: **1** (1 equiv, 250 mmol), **2** (1 equiv, 250 mmol), **3** (1 equiv, 250 mmol) in DMC (0.1 M), KOAc (10 mol%, 25 mmol), collected volume V_C = 2.5 mL (collected in 3 min 34 sec), residence time t_R = 10 min, flow rate f_R = 0.7 mL min^{-1}, reactor volume V_R = 7 mL, T = 25 °C, λmax = 530 nm. Isolated yields. [a]Increased productivity, reaction conditions: *standard conditions* but V_R = 14 mL, f_R = 1.4 ml min^{-1}, collected volume V_C = 2.5 mL (collected in 1 min 47 sec).

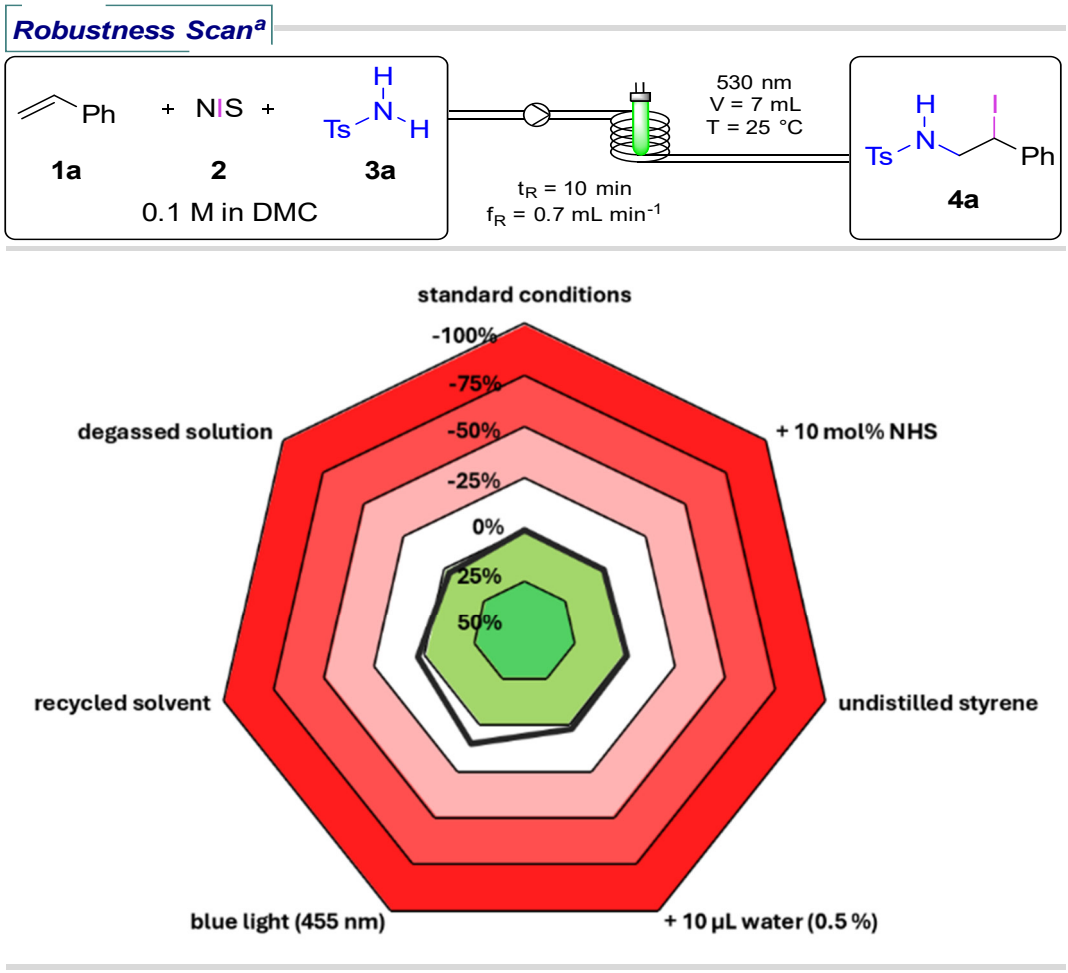

Figure 4-1. Robustness Scan. [a]Radar chart of the robustness scan[22] showing the deviation of yields from the benchmark (standard conditions) at modified reaction conditions. Negative values (red area) show a lower yield compared to the benchmark. Positive values (green area) show a higher yield compared to the benchmark. Yields were determined by quantitative NMR analysis with 1,1,2,2-tetrachlorethane as an internal standard, error ±5 %.

As we have already demonstrated a number of trans-formations of product **4** in our previous work,[19] we performed further functionalizations directly from the crude products, aiming for economical and operationally facile procedures. Since the products **4a** and **4c** serve as precursors for aziridine **5**, representing privileged structural motifs in organicchemistry,[29] we elaborated a flow-batch cascade for the direct synthesis of these three-membered heterocycles. While the conversion of **4** to aziridine **5** was described in chlorinatedsolvents,[19] it was also possible to achieve the ring closure without changing the solvent or isolation of the iodoamination product **4** by treating the crude reaction solution with an excess of K_2CO_3 for 3 h at ambient temperature.

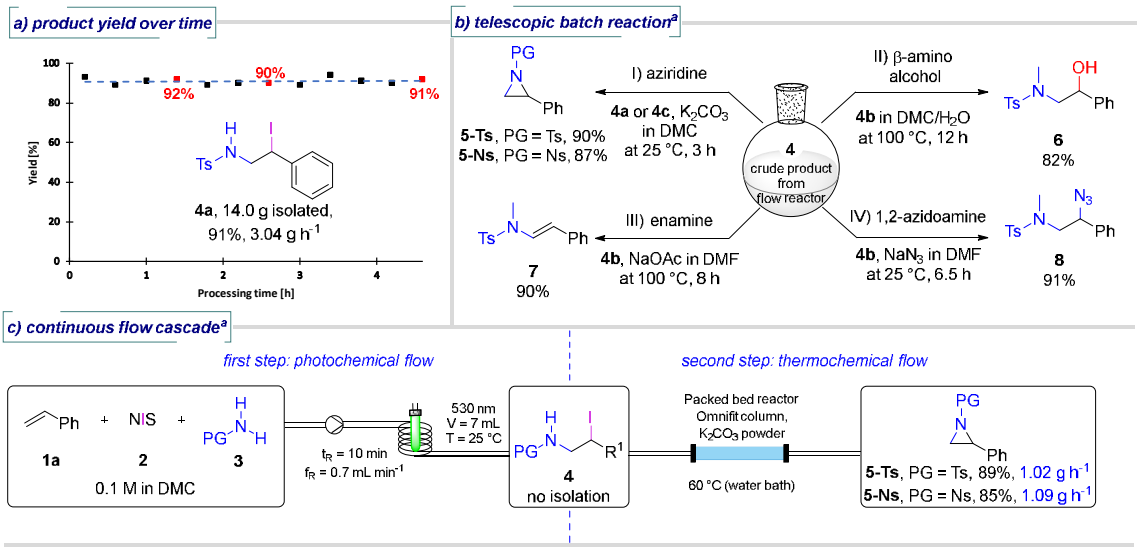

Scheme 4-3. Extended Operation Experiment and Further Transfromations. a) Product yield over time experiment under standard conditions, but V_R = 14 mL, f_R = 1.4 mL min^{-1}, and V_C = 386 mL in 4 h 36 min. The spots represent analyzed aliquots (V = 2.5 mL), the yield was determined either by NMR (black) or by isolation (red). b) Further transformations of the crude product in a telescopic manner without prior isolation: I) **4a** or **4c** (1 equiv, 250 mmol) and K_2CO_3 (3.0 equiv, 750 mmol) in DMC (0.1M) for 3 h at 25 °C, II) **4b** (1 equiv, 250 mmol) DMC/water (1:1, 0.05 M) for 12 h at 100 °C, III) **4b** (1 equiv, 250 mmol) and NaOAc (10 equiv,2.5 mol) in DMF (0.1 M) for 8 h at 100 °C, and IV) **4b** (1 equiv, 250 mmol) and NaN_3 (5 equiv, 1.25 mol) in DMF (0.1 M) for 6.5 h at 25 °C. c) Further transformations of the crude product in a two-step flow cascade: first step was performed under standard conditions: **1** (1 equiv, 250mmol), **2** (1 equiv, 250 mmol), **3** (1 equiv, 250 mmol) in DMC (0.1 M), KOAc (10 mol %, 25 mmol), residence time t_R = 10 min, reactor volumeV_R = 7 mL, T = 25 °C, λmax = 530 nm. Conditions of the second step: the crude reaction mixture from the first step was submitted directly to an Omnifit column packed with K_2CO_3 powder and heated by a water bath, t_R = 3.4 min, T = 60 °C, V(K_2CO_3) = 2.4 cm^3. Collected volume V_C = 2.5 mL (collected in 3 min 34 s). [a]Yields given are isolated yields over two steps.

The desired products **5-Ts** and **5-Ns** were obtained in yields of 90% and 87%, respectively, over two steps. In addition, the β-aminoalcohol **6** was obtained in an overall yield of 82% by heating the iodoaminated product **4b** in a mixture of DMC and water(1:1, 0.05 M) for 12 h at 100 °C. Furthermore, enamine **7** was accessible in a total yield of 91% by removing the solvent, redissolving the obtained crude **4b** in DMF, followed by heating for 8 h in the presence of sodium acetate. Alternatively, evaporation of the solvent, dissolving the residue in DMF, and addition of NaN_3 gave rise to 1,2-azidoamine **8** in overall 91% yield (Scheme 4-3, b).The ability to perform the second step of the aziridine **5** synthesis also in DMC offers the possibility to carry out this transformation in a two-step flow cascade starting from olefin **1**, NIS (**2**), and amine **3**. Therefore, we connected

the outlet of the photo flow reactor to an Omnifit column, which was packed with K_2CO_3 and placed in a 60 °C water bath (see more details in *4.4.1 General Information*, Figure 4-4). The desired aziridines **5-Ts** and **5-Ns** were successfully synthesized with an overall yield of 89% and 85%, respectively, over two flow steps, resulting in a productivity of 1.02 g h^{-1} for **5-Ts** and 1.09 g h^{-1} for **5-Ns** (Scheme 4-3, c).

4.4 Conclusion

In conclusion, we developed an economical and environmentally attractive process for synthesizing vicinal iodoamine **4** under continuous flow conditions. Furthermore, value-added products **5**−**8** were subsequently obtained in a telescopic flow-batch fashion or a two-step flow cascade with a g h^{-1} productivity starting from commercially available compounds without the need for isolation of intermediate **4**.

4.5 Experimental Part

4.5.1 General Information

Reagents, Solvents and Working Methods

Commercially available chemical materials were purchased in high quality and were used without further purification. Potassium carbonate K_2CO_3 , which was used for the aziridination of compound **4a** and **4c**, respectively, to form **5-Ts** and **5-Ns**, was purchased from Fisher Scientific (for specification certificate: Code-number: P/4080/60, LOT-number: 1543367) and was used as purchased. Solvents for reaction mixtures were used in p.a. quality or dried according to common procedures.[30] EtOAc and hexanes (40-60 °C) for chromatography were distilled prior to use. The reported yields are referred to isolated compounds unless otherwise stated. Reactions were monitored by thin layer chromatography (TLC).

NMR-Spectroscopy

NMR spectra were recorded on Bruker Avance 300 (^{1}H: 300 MHz, ^{13}C: 75 MHz, T = 295 K), Bruker Avance 400 (^{1}H: 400 MHz, ^{13}C: 101 MHz, T = 295 K). All chemical

shifts are reported in δ[ppm] (multiplicity, coupling constant *J*, number of protons, assignment of the proton) relative to the solvent residual peak as the internal standard. All spectra were recorded in $CDCl_3$ (δ = 7.26 ppm in 1H-NMR, δ = 77.0 ppm in 13C-NMR). Spectra were evaluated in first order and coupling constants *J* are reported in Hertz (Hz). Abbreviations used for signal multiplicity: s = singlet, bs = broad singlet, d = doublet, t = triplet, q = quartet, p = pentet, sex = sextet, hept = heptet, m = multiplet and combinations thereof.

UV/Vis Spectroscopy

UV/Vis spectroscopy was carried out on an Analytik jena Specord® 200Plus. As we observed a color change from yellow to red (Figure 4-2) while performing the reaction in both, batch and flow, we performed a UV/Vis measurement of the reaction solution (prior to irradiation) and of the crude product solution (after irradiation). The results are shown in Figure 4-2. Measurement range was from 300 nm to 700 nm. Both solutions were measured in dimethylcarbonate (DMC) in a 10 x 10 quartz cuvette.

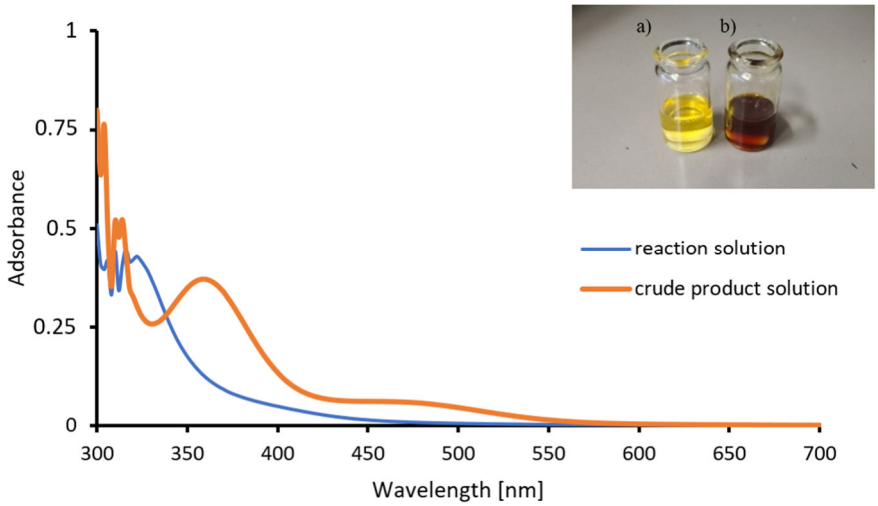

Figure 4-2. UV/Vis spectra of a) reaction solution prior to irradiation (measured solution obtained 60 µL of reaction solution in 3 mL pure DMC, which is equal to a concentration of 0.0019 M regarding all reactants), b) crude product solution after irradiation (measured solution obtained 20 µL of reaction solution in 3 mL pure DMC, which is equal to a concentration of 0.00066 M regarding all reactants).

Chromatography

Thin-layer chromatography (TLC) was performed with TLC precoated aluminum sheets (Machery-Nagel GmbH & Co. KG, TLC sheets ALUGRAM® Xtra SIL G/UV254, thickness 0.2 mm) and visualized by a dual short (λ = 254 nm) / long (λ = 366 nm) wavelength UV lamp. Staining was done with Seebach`s Magic Stain (2.5 g phosphomolybdic acid, 1.0 g cerium(IV) sulfate tetrahydrate, 94.0 mL distilled water and 6.0 mL conc. sulfuric acid), vanillin (6.0 g vanillin, 100.0 mL ethanol (95%) and 1.0 mL conc. sulfuric acid) or potassium permanganate (1.0 g KMnO4, 2.0 g Na2CO3 and 100.0 mL distilled water) followed by heating. Column chromatography was performed with silica gel (Merck, 0.063-0.200 mm particle size) and flash silica gel (Merck, 0.040-0.063 mm particle size).

IR-Spectroscopy

FTIR spectroscopy was carried out on a Cary 630 FTIR Spectrometer. Solid and liquid compounds were measured neatly, and the wave numbers are reported as cm^{-1}.

Mass Spectrometry

Mass spectra were recorded by the Central Analytic Department of the University of Regensburg using Jeol AccuTOF GCX and Agilent Q-TOF 6540 UHD Spectrometer. High-resolution mass spectra were measured using atmospheric pressure chemical ionization (APCI), electron ionization (EI) or electrospray ionization (ESI) with a quadrupole time-of-flight (Q-TOF) detector.

Light Source

All photochemical reactions were performed using a monochromatic light emitting diodes (LED) as irradiation source. Green light irradiation was performed using an Osram OSLON® SSL 80 green (3 W, 700 mA, dominant wavelength λ_{dom} = 530 nm, spectral bandwidth at 50% I_{max} = 30 nm, luminous flux at 25 °C and 700 mA ~ 250 lum). Information was taken from the official data sheets provided by Osram, which are available free of charge via the internet at the Osram web page. The LEDs were placed on a metal construction (in total 36 LEDs, six rows, six LEDs per row).

Photochemical Flow Setup and Flow Cascade Setup

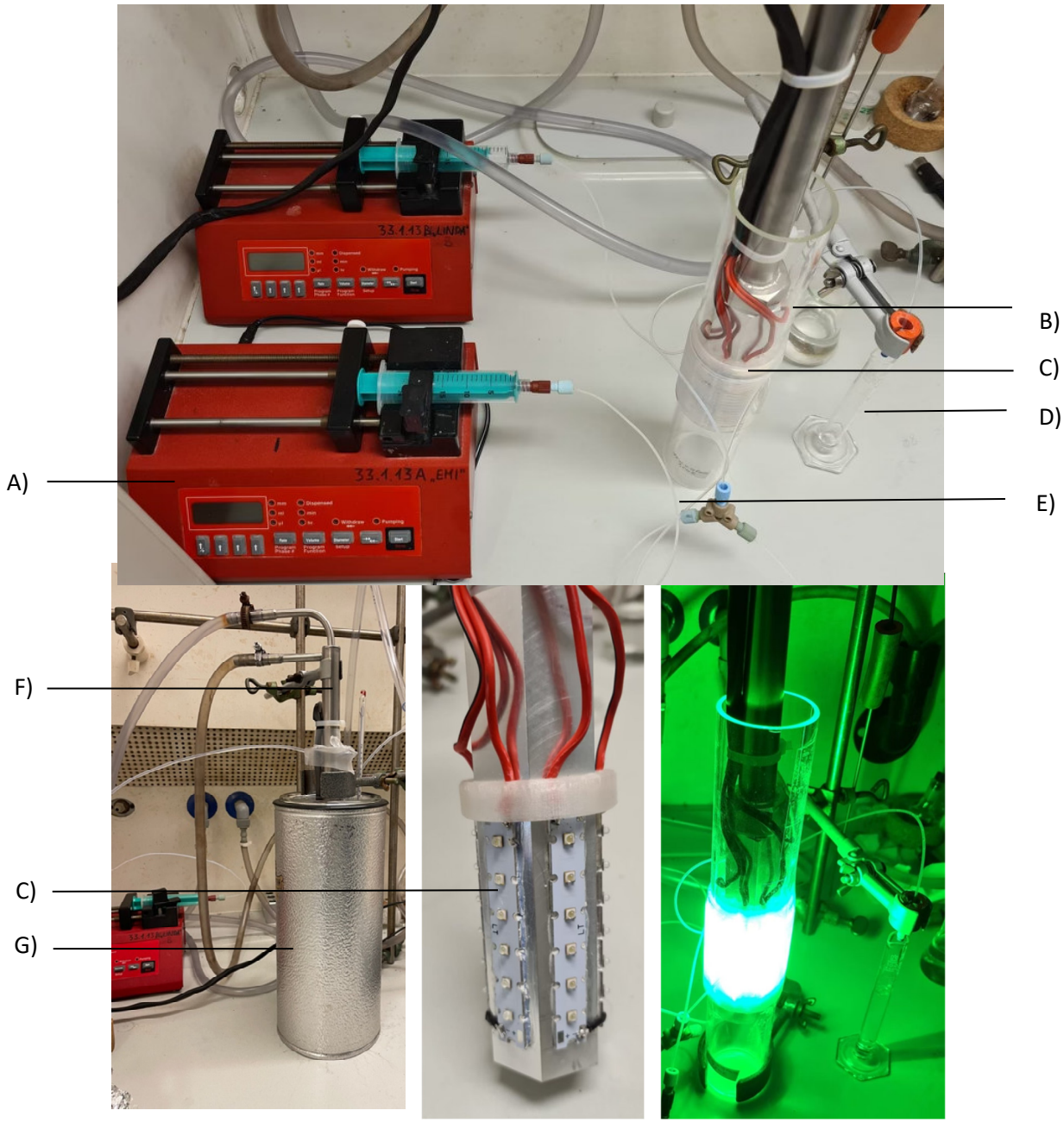

Figure 4-3. Irradiation setup for photochemical reactions: (A) single channel syringe pump; (B) glass cylinder; (C) LEDs; (D) graduated cylinder (10.0 mL size); (E) reaction tube; (F) cooling unit for LEDs; (G) KGW isotherm dewar vessel.

Photochemical flow reactions were performed in a tube (with an irradiated volume of 7 mL for the standard reactor and 14 mL for the reactor used during the scale-up experiment, Figure 4-3, E) wrapped around a glass cylinder with closed bottom (Figure 4-3, B) in which monochromatic immersion LEDs (λ= 530, Figure 4-3, C) were placed. The LED unit was cooled by directing water through its inside (Figure 4-3, F). The glass

cylinder with the reactor tube and the LEDs were placed in a KGW isotherm dewar vessel (Figure 4-3, G) filled with water to guarantee constant temperature. A single channel syringe pump (Figure 4-3, A) was used to flow the solution into the reactor system with desired flow rate (f_R), where it was irradiated as it flowed through the reactor tube. The outlet was collected in a graduated cylinder (Figure 4-3, D). This setup was expanded by a thermochemical flow setup (Figure 4-4). The outlet of the photo flow reactor was directly connected to an omnifit column (Figure 4-4, H), which was placed in a water bath (60 °C, Figure 4-4, I) and packed with K_2CO_3 (V = 2.4 cm^3). The outlet of the omnifit column was directed into a graduated cylinder (10.0 mL size).

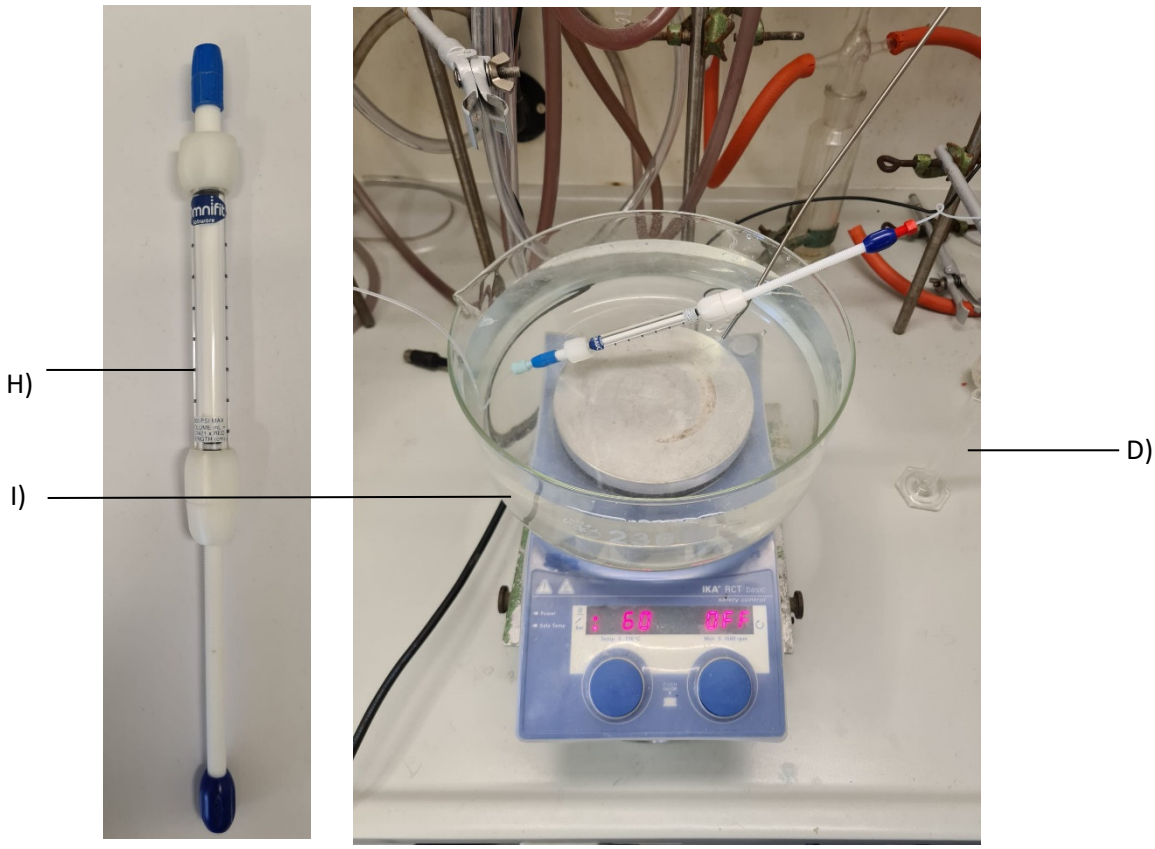

Figure 4-4. Setup for thermochemical reactions of the continuous flow cascade: (H) omnifit column filled with K_2CO_3; (I) water bath (heated to 60°C); (D) graduated cylinder (10.0 mL size).

4.5.2 Synthesis and Analytical Data

Reaction Optimization

Table 4-2. Results of the iodoamination under optimized conditions.

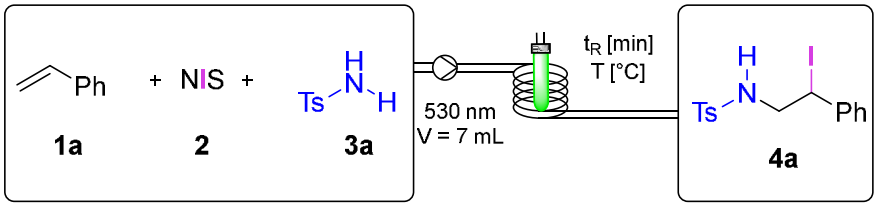

Entry	Concentration of Reactants [M]	Base	Solvent	Temperature [°C]	t_R [min]	Conversion[a] of **1a**	Yield[a] of **4a**
1	0.1	K_2CO_3	DMC	10	10	82%	75%
2	0.1	K_2CO_3	DMC	25	10	85%	85%
3	0.1	K_2CO_3	DMC	25	20	79%	70%
4	0.1	K_2CO_3	DMC	25	5	68%	37%
5	0.1	K_2CO_3	MeCN	25	10	n.d.	20%
6[b]	0.1	---	DCM	---	---	---	---
7	0.05	K_2CO_3	DMC	25	10	85%	78%
8	0.2	K_2CO_3	DMC	25	10	78%	59%
9	0.2	K_2CO_3	DMC	25	20	65%	48%
10	0.1	KOH	DMC	25	10	100%	80%
11	0.1	K_3PO_4	DMC	25	10	91%	70%
12	**0.1**	**CH_3COOK**	**DMC**	**25**	**10**	**100%**	**93%**

[a]determined by quantitative NMR analysis by addition of 1,1,2,2-tetrachlorethane as an internal standard after running the experiments, error ±5 %. [b]heterogeneous solution.

Robustness Scan

The robustness scan was conducted as reported by *Glorius et al.*[22] using modified conditions from GP. The ^{1}H NMR yield (93%) obtained during the optimization of the reaction (Table 4-1, entry 8) was taken as the benchmark. Recycling of the solvent was performed by transferring 20 mL of DMC to a round bottom flask, evaporating the solvent on the rotavap, addition of $Na_2S_2O_3$ (25 mg per 5 mL of solvent), stirring until the red color disappears and finally distilling the solvent again to obtain 18 mL of DMC. The distilled solvent was used without any further purification.

Table 4-3. Robustness scan of the iodoamination in flow under unmodified and modified standard conditions from GP.

Entry	Deviation from standard conditions from GP	Yield[a] of **4a**	Deviation from benchmark
1	No deviation	93%	0%
2	Additional 10 mol% succinimide	94%	1%
3	Undistilled styrene was used	92%	-1%
4	Additional 10 µL H_2O per 2.0 mL of DMC (0.5% v/v)	91%	-2%
5	Blue LEDs (455 nm)	83%	-10%
6	Recycled solvent	90%	-3%
7	Degassed solution	96%	3%

[a]determined by quantitative NMR analysis by addition of 1,1,2,2-tetrachlorethane as an internal standard after running the experiments, error ±5 %.

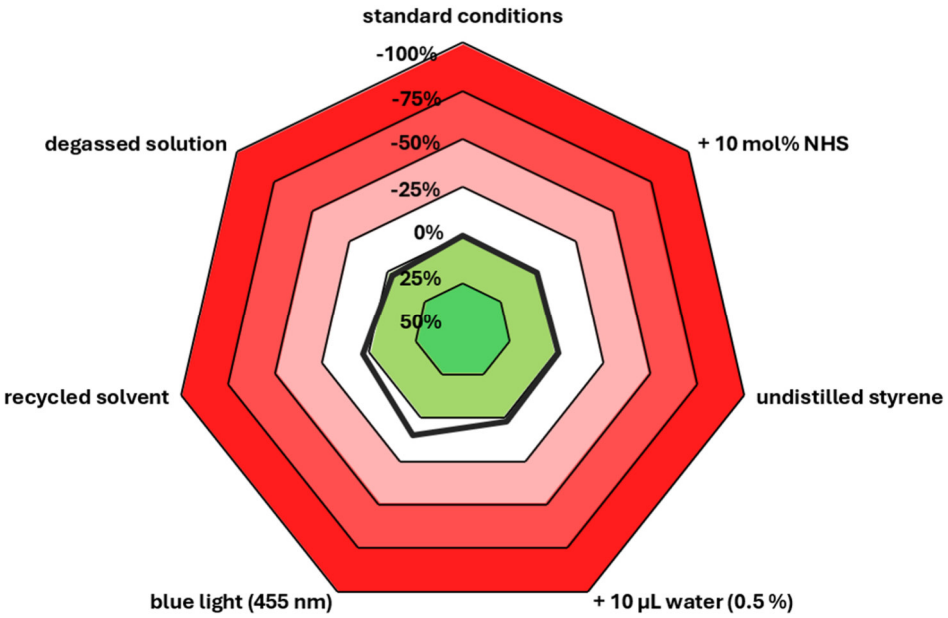

Figure 4-5. Radar chart of the robustness scan showing the deviation of yields from the benchmark (standard condition) at changed reaction conditions. Negative values (red area) show a lower yield compared to the benchmark. Positive values (green area) show a higher yield compared to the benchmark.

General Procedure (GP) for the Photoinduced Iodoamination in Flow

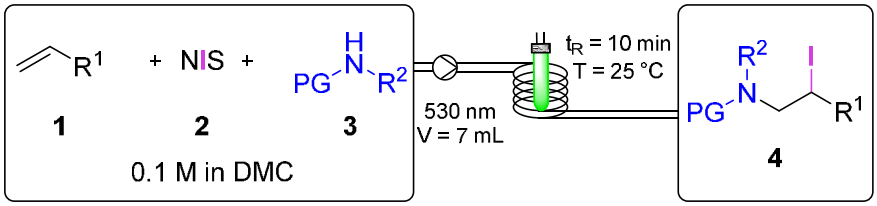

A flame-dried Schlenk flask (50.0 mL size) equipped with a magnetic stirring bar was charged with alkene **1** (1.0 equiv), NIS (**2**, 1.0 equiv), amine **3** (1.0 equiv), potassium acetate (0.1 equiv) and dissolved in DMC to form a homogenous feedstock solution. The stock solution was prepared and kept in the dark during the experiment. A single channel syringe pump was used to pump the solution into the reactor system with a flow rate f_R of 0.7 mL min^{-1} (t_R = 10 min), where it was irradiated (λ_{max} = 530) as it was pumped through the reactor tube (7 ml reactor volume). To ensure constant flow rates, the outlet was collected in a graduated cylinder while measuring the time of collection for all samples to calculate the t_R. Aliquots of 2.5 mL (=0.25 mmol) were collected for the isolation of the product, the determination of the yield and the characterization of the compounds. The crude reaction mixture was concentrated under reduced pressure at a temperature of 40°C (as the product decomposes at higher temperatures) and product was isolated by silica gel chromatography.

N-(2-iodo-2-phenylethyl)-4-methylbenzenesulfonamide **(4a)**

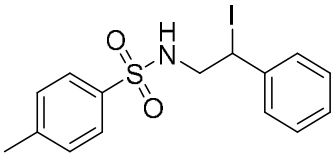

Following general procedure ***GP*** using styrene (**1a**, 286 µL, 260 mg, 2.50 mmol, 1.0 equiv), *N*-iodosuccinimide (**2**, 562 mg, 2.50 mmol, 1.0 equiv), 4-methylbenzenesulfonamide (**3a**, 428 mg, 2.50 mmol, 1.0 equiv), DMC (25.0 mL, 0.25 M) and potassium acetate (24.5 mg, 0.250 mmol, 0.1 equiv) at room temperature (25 °C) with t_R = 10 min (f_R = 0.7 mL min^{-1}). A volume of 2.5 mL (= 0.250 mmol) was collected in 3 min 34 sec. The solvent was evaporated under reduced pressure, and product **4a** was isolated by silica gel column chromatography using hexanes/ethylacetate (9:1 to 3:1) as eluent to obtain 91.5 mg (1.52 g h^{-1}, 0.228 mmol, 91%).

The analytical data are consistent with the literature.[19]

R_f (hexanes/ethylacetate 5:1 on silica) = 0.28

^{1}H NMR (400 MHz, $CDCl_3$) δ 7.71 (d, *J* = 7.9 Hz, 2H), 7.33 – 7.26 (m, 7H), 5.02 (t, *J* = 7.8 Hz, 1H), 4.80 (t, *J* = 6.62 Hz, 1H), 3.69 (dt, *J* = 14.3, 7.2 Hz, 1H), 3.51 (ddd, *J* = 14.2, 8.2, 6.1 Hz, 1H), 2.45 (s, 3H).

^{13}C NMR (101 MHz, $CDCl_3$) δ 143.98, 140.02, 137.15, 130.02, 129.23, 128.90, 127.69, 127.17, 51.45, 30.04, 21.72.

Scale-Up Experiment and Product Yield Over Time Experiment

Following general procedure ***GP*** using styrene (**1a**, 4.57 mL, 4.16 g, 40.0 mmol, 1.0 equiv), *N*-iodosuccinimide (**2**, 9 g, 40.0 mmol, 1.0 equiv), 4-methylbenzenesulfonamide (**3a**, 6.85 g, 40.0 mmol, 1.0 equiv), DMC (400 mL, 0.1 M) and potassium acetate (392 mg, 4.00 mmol, 0.1 equiv) at room temperature (25 °C) with t_R = 10 min (f_R = 1.4 mL). The reaction was performed for 4 h 36 min with the 14 mL reactor (see *4.4.1 General Information*, Figure 4-3) resulting in a collected volume of 386 mL (= 38.6 mmol). The solvent of the crude reaction mixture was evaporated, and the residue was dissolved in 200 mL $CHCl_3$. The organic phase was washed twice with 100 mL water, once with 50% aqueous $Na_2S_2O_3$ solution and dried with brine and over $NaSO_4$. After filtration the organic phase was evaporated on the rotavap to give 14.0 g of the desired product **4a** (3.04 g h^{-1}, 34.9 mmol, 90%).

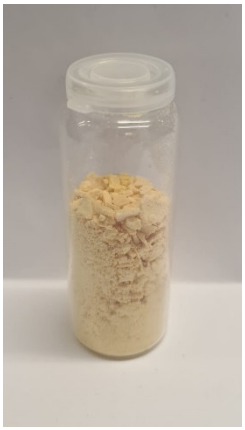

14.0 g of isolated product **4a**

For determination of the yield during the reaction in order to monitor the steadiness of the process, twelve aliquots with a volume of 2.5 mL each were collected separately in 24 min intervals and the yield was determined either by quantitative NMR (using $C_2H_2Cl_4$ as internal standard) or by isolation of the product by silica gel column chromatography using hexanes/ethylacetate (9:1 to 3:1) as eluent (Table 4-4).

Table 4-4. Yield over time experiment.

Entry	Time [min]	Yield [%]	Yield determined by[a]
1	12	93	NMR
2	36	89	NMR
3	60	91	NMR
4	84	92	Isolation
5	108	89	NMR
6	132	90	NMR
7	156	90	Isolation
8	180	89	NMR
9	204	94	NMR
10	228	91	NMR
11	252	90	NMR
12	276	92	Isolation

[a]1,1,2,2-tetrachlorethane was used to determine the product yield *via* quantitative NMR, error ±5 %.

Big Scale Batch Experiment

Up-scaling to gram quantities was carried out in a batch photo reactor (180 mL size, Figure 4-6) using styrene (**1a**) (2.06 mL, 1.87 g, 18.0 mmol, 1.0 equiv), 4-methylbenzenesulfonamide (**2a**) (3.08 g, 18.0 mmol, 1.0 equiv), N-iodosuccinimide (**3**) (4.05 g, 18.0 mmol, 1.0 equiv), potassium acetate (177 mg, 1.80 mmol, 0.1 equiv) and dissolved in DMC (180.0 mL, 0.1 M). The solution was irradiated for 4.5 h (monitored by TLC) at room temperature (25 °C). The solvent of the crude reaction mixture was evaporated, and the residue was dissolved in 200 mL $CHCl_3$. The organic phase was washed twice with 100 mL water, once with 50% aqueous $Na_2S_2O_3$ solution and dried with brine and over $NaSO_4$. Further purification was performed by silica gel column chromatography using hexanes/ethylacetate (9:1 to 3:1) as eluent to obtain 5.20 g (1.15 g h^{-1}, 13.0 mmol, 72%) of product **4a**.

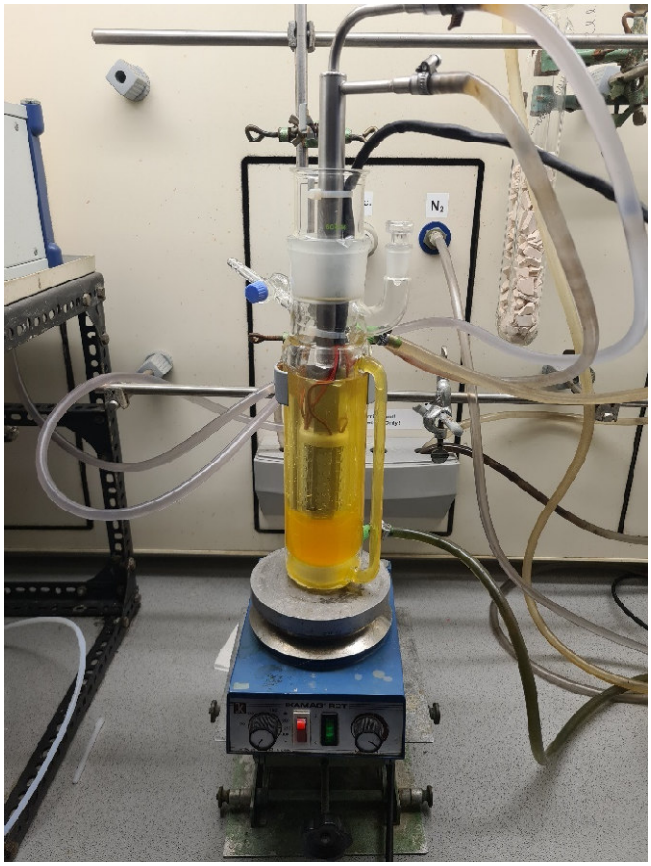

Figure 4-6. Big scale batch photoreactor (180 mL size, water cooled by outer shell) using the identical light source as shown in Figure 4-3, C.

N-(2-iodo-2-phenylethyl)-*N*,4-dimethylbenzenesulfonamide **(4b)**

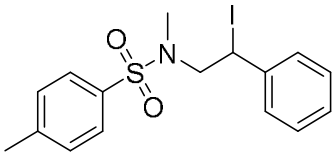

Following general procedure ***GP*** using styrene (**1a**, 286 µL, 260.4 mg, 2.50 mmol, 1.0 equiv), *N*-iodosuccinimide (**2**, 562 mg, 2.50 mmol, 1.0 equiv), *N*,4-dimethylbenzenesulfonamide (**3b**, 463 mg, 2.50 mmol, 1.0 equiv), DMC (25.0 mL, 0.25 M) and potassium acetate (24.5 mg, 0.250 mmol, 0.1 equiv) at room temperature (25 °C) with t_R = 10 min (f_R = 0.7 mL min^{-1}). A volume of 2.5 mL (= 0.250 mmol) was collected in 3 min 34 sec. The solvent was evaporated under reduced pressure, and product **4b** was isolated by silica gel column chromatography using hexanes/ethylacetate (9:1, 3:1) as eluent to obtain 97.6 mg (1.64 g h^{-1}, 0.235 mmol, 94%). The analytical data are consistent with the literature.[19]

R_f (hexanes/ethylacetate 5:1 on silica) = 0.37

^{1}H NMR (300 MHz, $CDCl_3$) δ 7.66 – 7.57 (m, 2H), 7.47 – 7.39 (m, 2H), 7.34 – 7.25 (m, 5H), 5.28 (dd, *J* = 9.5, 6.5 Hz, 1H), 3.79 (dd, *J* = 14.4, 6.5 Hz, 1H), 3.59 (dd, *J* = 14.4, 9.4 Hz, 1H), 2.55 (s, 3H), 2.42 (s, 3H).

^{13}C NMR (75 MHz, $CDCl_3$) δ 143.73, 140.64, 134.53, 129.86, 128.90, 128.57, 128.12, 127.40, 58.97, 36.47, 29.93, 21.61.

N-(2-iodo-2-phenylethyl)-4-nitrobenzenesulfonamide **(4c)**

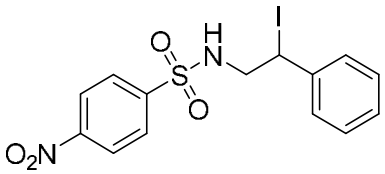

Following general procedure ***GP*** using styrene (**1a**, 286 µL, 260 mg, 2.50 mmol, 1.0 equiv), *N*-iodosuccinimide (**2**, 562 mg, 2.50 mmol, 1.0 equiv), 4-nitrobenzenesulfonamide (**3c**, 505 mg, 2.50 mmol, 1.0 equiv), DMC (25.0 mL, 0.25 M) and potassium acetate (24.5 mg, 0.250 mmol, 0.1 equiv) at room temperature (25 °C) with t_R = 10 min (f_R = 0.7 mL min^{-1}). A volume of 2.5 mL (= 0.250 mmol) was collected in 3 min 34 sec. The solvent was evaporated under reduced pressure, and product **4c** was isolated by silica gel column chromatography using hexanes/ethylacetate (9:1 to 3:1) as eluent to obtain 93.8 mg (1.58 g h^{-1}, 0.217 mmol, 87%).

R_f (hexanes/ethylacetate 3:1 on silica) = 0.38

^{1}H NMR (300 MHz, $CDCl_3$) δ 8.37 – 8.35 (m, 2H), 8.02 – 7.99 (m, 2H), 7.29 (m, 5H), 5.06 (t, *J* = 7.7 Hz, 1H), 4.92 (t, *J* = 6.5 Hz, 1H), 3.81 – 3.71 (m, 1H), 3.65 – 3.55 (m, 1H).

^{13}C NMR (75 MHz, $CDCl_3$) δ 150.33, 146.01, 139.63, 129.38, 129.15, 128.37, 127.70, 124.66, 51.62, 29.46.

IR (neat): 3280, 2922, 2851, 1528, 1349, 1312, 1159, 1092, 857, 734 cm^{-1}

HRMS (ESI) m/z calculated for the fractionated product of **4c**: $C_{14}H_{13}N_2O_4SNa$ $(M+Na)^+$ 454.9535, found 454.9533.

Methyl 4-(2-((*N*,4-dimethylphenyl)sulfonamido)-1-iodoethyl)benzoate **(4d)**

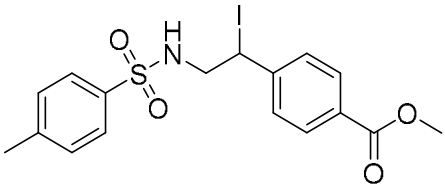

Following general procedure ***GP*** using methyl 4-vinylbenzoate (**1b**, 405 mg, 2.50 mmol, 1.0 equiv), *N*-iodosuccinimide (**2**, 562 mg, 2.50 mmol, 1.0 equiv), 4-methylbenzenesulfonamide (**3a**, 428 mg, 2.50 mmol, 1.0 equiv), DMC (25.0 mL, 0.25 M) and potassium acetate (24.5 mg, 0.250 mmol, 0.1 equiv) at room temperature (25 °C) with t_R = 10 min (f_R = 0.7 mL min^{-1}). A volume of 2.5 mL (= 0.250 mmol) was collected in 3 min 34 sec. The solvent was evaporated under reduced pressure, and product **4d** was isolated by silica gel column chromatography using hexanes/ethylacetate (9:1 to 3:1) as eluent to obtain 91.8 mg (1.54 g h^{-1}, 0.200 mmol, 80%).

R_f (hexanes/ethylacetate 3:1 on silica) = 0.30

^{1}H NMR (400 MHz, DMSO-d6) δ 8.07 (t, *J* = 6.0 Hz, 1H), 7.87 – 7.84 (m, 2H), 7.64 – 7.61 (m, 2H), 7.52 – 7.49 (m, 2H), 7.37 – 7.34 (m, 2H), 5.18 (t, *J* = 7.1 Hz, 1H), 3.85 (s, 3H), 3.49 – 3.45 (m, 2H), 2.37 (s, 3H).

^{13}C NMR (101 MHz, DMSO-d6) δ 165.77, 146.30, 142.83, 137.50, 129.68, 129.42, 129.08, 128.17, 126.43, 52.22, 50.19, 28.99, 20.96.

IR (neat): 3291, 2926, 2855, 1710, 1606, 1528, 1453, 1349, 1162, 1092, 853, 697 cm^{-1}

HRMS (ESI) m/z calculated for the fractionated product of **4d**: $C_{17}H_{17}NO_4S$ $(M+H)^+$ 332.0951, found 332.0947.

N-(2-(4-(tert-butyl)phenyl)-2-iodoethyl)-*N*,4-dimethylbenzenesulfonamide **(4e)**

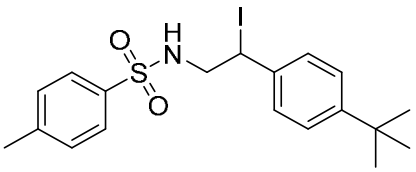

Following general procedure ***GP*** using methyl 4-*tert*-butylstyrene (**1c**, 458 µL, 401 mg, 2.50 mmol, 1.0 equiv), *N*-iodosuccinimide (**2**, 562 mg, 2.50 mmol, 1.0 equiv), 4-methylbenzenesulfonamide (**3a**, 428 mg, 2.50 mmol, 1.0 equiv), DMC (25.0 mL, 0.25

M) and potassium acetate (24.5 mg, 0.250 mmol, 0.1 equiv) at room temperature (25 °C) with t_R = 10 min (f_R = 0.7 mL min^{-1}). A volume of 2.5 mL (= 0.250 mmol) was collected in 3 min 34 sec. The solvent was evaporated under reduced pressure, and product **4e** was isolated by silica gel column chromatography using hexanes/ethylacetate (9:1 to 3:1) as eluent to obtain 95.1 mg (1.59 g h^{-1}, 0.208 mmol, 83%).

R_f (hexanes/ethylacetate 5:1 on silica) = 0.40

^{1}H NMR (300 MHz, $CDCl_3$) δ 7.73 – 7.71 (m, 2H), 7.35 – 7.28 (m, 4H), 7.19 – 7.17 (m, 2H), 5.01 (t, J = 7.8 Hz, 1H), 4.67 (t, J = 6.7 Hz, 1H), 3.74 – 3.65 (m, 1H), 3.56 – 3.46 (m, 1H), 2.46 (s, 3H), 1.30 (s, 9H).

^{13}C NMR (75 MHz, $CDCl_3$) δ 152.17, 144.00, 137.21, 136.83, 130.04, 127.35, 127.21, 126.24, 51.49, 34.86, 31.33, 30.26, 21.74.

IR (neat): 3283, 2963, 2870, 1696, 1603, 1461, 1409, 1334, 1163, 1096, 816, 705, 663 cm^{-1}

HRMS (ESI) m/z calculated for the fractionated product of **4e**: $C_{19}H_{23}NO_2SNa$ $(M+Na)^+$ 330.1522, found 330.1522.

N-(2-iodooctyl)-*N*,4-dimethylbenzenesulfonamide **(4f)**

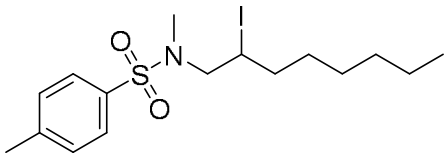

Following general procedure ***GP*** using 1-octene (**1d**, 391 µL, 280 mg, 2.50 mmol, 1.0 equiv), *N*-iodosuccinimide (**2**, 562 mg, 2.50 mmol, 1.0 equiv), *N*,4-dimethylbenzenesulfonamide (**3b**, 463 mg, 2.50 mmol, 1.0 equiv), DMC (25.0 mL, 0.25 M) and potassium acetate (24.5 mg, 0.250 mmol, 0.1 equiv) at room temperature (25 °C) with t_R = 10 min (f_R = 0.7 mL min^{-1}). A volume of 2.5 mL (= 0.250 mmol) was collected in 3 min 34 sec. The solvent was evaporated under reduced pressure, and product **4f** was isolated by silica gel column chromatography using hexanes/ethylacetate (9:1 to 3:1) as eluent to obtain 62.7 mg (1.01 g h^{-1}, 0.148 mmol, 59%). The analytical data are consistent with the literature.[19]

R_f (hexanes/ethylacetate 5:1 on silica) = 0.67

^{1}H NMR (400 MHz, $CDCl_3$) δ 7.67 (d, J = 8.3 Hz, 2H), 7.33 (d, J = 8.0 Hz, 2H), 4.19 (dq, J = 9.3, 2.9, 2.5 Hz, 1H), 3.47 (dd, J = 14.0, 9.0 Hz, 1H), 3.26 (dd, J = 14.0, 6.0 Hz, 1H), 2.77 (s, 3H), 2.44 (s, 3H), 1.88 – 1.84 (m, 1H), 1.75 – 1.69 (m, 1H), 1.62 – 1.57 (m, 1H), 1.37 – 1.28 (m, 7H), 0.91 – 0.88 (m, 3H).

^{13}C NMR (101 MHz, $CDCl_3$) δ 143.81, 134.41, 129.94, 127.60, 59.02, 36.64, 36.51, 33.65, 31.80, 29.62, 28.61, 22.74, 21.68, 14.20.

3-((*N*,4-dimethylphenyl)sulfonamido)-2-iodo-*N*-isopropylpropanamide **(4g)**

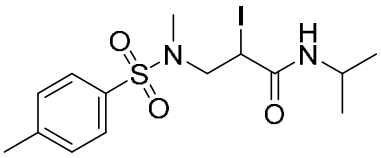

Following general procedure ***GP*** using *N*-isopropylacrylamide (**1e**, 283 mg, 2.50 mmol, 1.0 equiv), *N*-iodosuccinimide (**2**, 562 mg, 2.50 mmol, 1.0 equiv), *N*,4-dimethylbenzenesulfonamide (**3b**, 463 mg, 2.50 mmol, 1.0 equiv), DMC (25.0 mL, 0.25 M) and potassium acetate (24.5 mg, 0.250 mmol, 0.1 equiv) at room temperature (25 °C) with t_R = 10 min (f_R = 0.7 mL min^{-1}). A volume of 2.5 mL (= 0.250 mmol) was collected in 3 min 34 sec. The solvent was evaporated under reduced pressure, and product **4g** was isolated by silica gel column chromatography using hexanes/ethylacetate (9:1 to 3:1) as eluent to obtain 76.3 mg (1.24 g h^{-1}, 0.180 mmol, 72%). The analytical data are consistent with the literature.[19]

R_f (hexanes/ethylacetate 5:1 on silica) = 0.2

^{1}H NMR (400 MHz, $CDCl_3$) δ 7.67 (d, J = 8.3 Hz, 2H), 7.35 – 7.33 (m, 2H), 5.83 (d, J = 7.9 Hz, 1H), 4.54 (dd, J = 9.2, 6.2 Hz, 1H), 4.11 – 4.03 (m, 1H), 3.47 – 3.44 (m, 2H), 2.82 (s, 3H), 2.44 (s, 3H), 1.18 (dd, J = 13.5, 6.6 Hz, 6H).

^{13}C NMR (101 MHz, $CDCl_3$) δ 168.36, 144.11, 133.72, 130.05, 130.05, 127.57, 127.57, 55.52, 42.51, 38.02, 22.85, 22.69, 21.88, 21.69

2-(iodomethyl)-1-tosylindoline **(4h)**

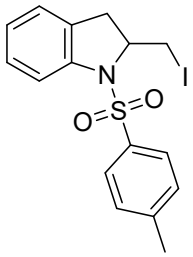

Synthesis of 2-allylaniline (**S1**)

To a solution of *N*-allyl aniline (530 mg, 4.00 mmol, 1 equiv) in *m*-xylene (6 mL) $BF_3{\cdot}OEt_2$ (48% solution, 4.80 mmol, 1.2 equiv) was added dropwise at a temperature of -78°C. The mixture was stirred for 10 min at 25°C. Subsequently, the reaction mixture was transferred to a Schlenk tube and then stirred for 17 h at 190°C. After the mixture cooled to room temperature, the reaction was quenched by the addition of 2N NaOH. The resulting mixture was extracted three times with 1.5 mL Et_2O and the organic phase was washed with brine, dried and concentrated under reduced pressure. The desired product 2-allylaniline (**S1**) was isolated by silica gel column chromatography using hexanes/ethylacetate (15:1) as eluent to give 2-allylaniline (**S1**) (350 mg, 2.60 mmol, 66%). The product was subsequently used to synthesis the starting material **1f**.

Synthesis of *N*-(2allylphenyl)-4-methylbenzenesulfonamide (**1f**):

To a solution of **S1** (350 mg, 2.60 mmol, 1 equiv) in Chloroform (9 mL) were added pyridine (1 mL, 13 mmol, 5 equiv) and *p*-toluenesulfonyl chloride (760 mg, 4.00 mmol, 1.5 equiv) at a temperature of 0 °C. The resulting mixture was stirred for 30 min at ambient temperature. Afterwards 5 mL of brine was added and the organic compounds were three times with 5 mL of $CHCl_3$. The combine organic phase was dried and the solvent was evaporated under reduced pressure. The desired product **1f** was obtained after isolation *via* silica gel chromatography using hexanes/ethylacetate (8:1) as eluent to give 747 mg (2.60 mmol, 99%) of product **1f**. The analytical data are consistent with the literature.[31]

^{1}H NMR (400 MHz, $CDCl_3$) δ 7.62 – 7.60 (m, 2H), 7.38 (dd, J = 8.0, 1.3 Hz, 1H), 7.22 – 7.18 (m, 3H), 7.13 – 7.06 (m, 2H), 6.74 (s, 1H), 5.77 (ddt, J = 17.2, 10.1, 6.1 Hz, 1H),

5.08 (dq, J = 10.1, 1.6 Hz, 1H), 4.93 (dq, J = 17.2, 1.7 Hz, 1H), 3.05 (d, J = 6.1 Hz, 2H), 2.38 (s, 3H).

^{13}C NMR (101 MHz, $CDCl_3$) δ 143.84, 136.79, 135.69, 134.93, 132.42, 130.49, 129.65, 127.62, 127.16, 126.34, 124.63, 116.99, 36.04, 21.58.

Following general procedure ***GP*** using *N*-(2allylphenyl)-4-methylbenzenesulfonamide (**1f**, 283 mg, 2.50 mmol, 1.0 equiv), *N*-iodosuccinimide (**2**, 718 mg, 2.50 mmol, 1.0 equiv), DMC (25.0 mL, 0.25 M) and potassium acetate (24.5 mg, 0.250 mmol, 0.1 equiv) at room temperature (25 °C) with t_R = 10 min (f_R = 0.7 mL min^{-1}). A volume of 2.5 mL (= 0.250 mmol) was collected in 3 min 34 sec. The solvent was evaporated under reduced pressure, and product **4h** was isolated by silica gel column chromatography using hexanes/ethylacetate (9:1 to 3:1) as eluent to obtain 75.6 mg (1.27 g h^{-1}, 0.183 mmol, 73%). The analytical data are consistent with the literature.[32]

R$_f$ (hexanes/ethylacetate 5:1 on silica) = 0.3

^{1}H NMR (400 MHz, $CDCl_3$) δ 7.64 (d, J = 8.1 Hz, 1H), 7.56 (d, J = 8.3 Hz, 2H), 7.17 – 7.07 (m, 3H), 7.07 – 7.02 (m, 2H), 4.36 (ddt, J = 10.1, 9.3, 3.5 Hz, 1H), 3.66 (dd, J = 9.7, 3.5 Hz, 1H), 3.26 (t, J = 9.9 Hz, 1H), 2.97 – 2.81 (m, 2H), 2.35 (s, 3H).

^{13}C NMR (101 MHz, $CDCl_3$) δ 144.38, 141.30, 134.59, 130.51, 129.86, 128.12, 127.16, 125.36, 125.00, 116.91, 62.64, 34.96, 21.68, 11.52.

Further Transformations

2-phenyl-1-tosylaziridine **(5-Ts)**

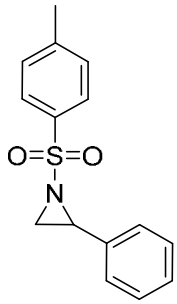

Telescopic Batch Reaction

Following general procedure ***GP*** using styrene (**1a**, 286 µL, 260 mg, 2.50 mmol, 1.0 equiv), *N*-iodosuccinimide (**2**, 562 mg, 2.50 mmol, 1.0 equiv), 4-

methylbenzenesulfonamide (**3a**, 428 mg, 2.50 mmol, 1.0 equiv), DMC (25.0 mL, 0.25 M) and potassium acetate (24.5 mg, 0.250 mmol, 0.1 equiv) at room temperature (25 °C) with t_R = 10 min (f_R = 0.7 mL min^{-1}). A volume of 2.5 mL (= 0.250 mmol) was collected in 3 min 34 sec in a round bottom flask, potassium carbonate (104 mg, 0.750 mmol, 3 equiv in respect to the collected amount of substance) was added and the resulting mixture was stirred for 3h at 25°C. The solvent was evaporated under reduced pressure, and product **5-Ts** was isolated by silica gel column chromatography using hexanes/ethylacetate (9:1 to 3:1) as eluent to obtain 61.5 mg (0.225 mmol, 90%).

Continuous Flow Cascade

Following general procedure ***GP*** using styrene (**1a**, 286 µL, 260 mg, 2.50 mmol, 1.0 equiv), *N*-iodosuccinimide (**2**, 562 mg, 2.50 mmol, 1.0 equiv), 4-methylbenzenesulfonamide (**3a**, 428 mg, 2.50 mmol, 1.0 equiv), DMC (25.0 mL, 0.250 M) and potassium acetate (24.5 mg, 0.250 mmol, 0.1 equiv) at room temperature (25 °C) with t_R = 10 min (f_R = 0.7 mL min^{-1}). The outlet of the photoflow reactor was directly connected to an omnifit column filled with K_2CO_3 (2.4 cm^{-3}, t_R = 3.4 min at f_R = 0.7 min), which was placed in a 60 °C water bath. After the crude reaction mixture passed the omnifit column, 2.5 mL was collected in 3 min 34 sec. The solvent was evaporated under reduced pressure, and product **5-Ts** was isolated by silica gel column chromatography using hexanes/ethylacetate (9:1 to 3:1) as eluent to obtain 61.0 mg (1.02 g h^{-1}, 0.223 mmol, 89%).

The analytical data are consistent with the literature.[19]

R_f (hexanes/ethylacetate 5:1 on silica) = 0.4

^{1}H NMR (300 MHz, $CDCl_3$) δ 7.89 – 7.85 (m, 2H), 7.35 – 7.20 (m, 7H), 3.78 (dd, J = 7.2, 4.5 Hz, 1H), 2.98 (d, J = 7.2 Hz, 1H), 2.43 (s, 3H), 2.39 (d, J = 4.4 Hz, 1H).

^{13}C NMR (75 MHz, $CDCl_3$) δ 144.77, 135.13, 135.05, 129.86, 128.66, 128.40, 128.04, 126.65, 41.14, 36.05, 21.76.

1-((4-nitrophenyl)sulfonyl)-2-phenylaziridine **(5-Ns)**

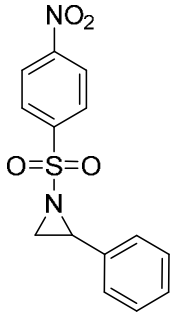

Telescopic Batch Reaction

Following general procedure ***GP*** using styrene (**1a**, 286 µL, 260 mg, 2.50 mmol, 1.0 equiv), *N*-iodosuccinimide (**2**, 562 mg, 2.50 mmol, 1.0 equiv), 4-nitrobenzenesulfonamide (**3c**, 505 mg, 2.50 mmol, 1.0 equiv), DMC (25.0 mL, 0.250 M) and potassium acetate (24.5 mg, 0.250 mmol, 0.1 equiv) at room temperature (25 °C) with t_R = 10 min (f_R = 0.7 mL min^{-1}). A volume of 2.5 mL (= 0.250 mmol) was collected in 3 min 34 sec in a round bottom flask, potassium carbonate (104 mg, 0.750 mmol, 3 equiv in respect to the collected amount of substance) was added and the resulting mixture was stirred for 3h at 25°C. The solvent was evaporated under reduced pressure, and product **5-Ns** was isolated by silica gel column chromatography using hexanes/ethylacetate (9:1 to 3:1) as eluent to obtain 66.3 mg (0.218 mmol, 87%).

Continuous Flow Cascade

Following general procedure ***GP*** using styrene (**1a**, 286 µL, 260 mg, 2.50 mmol, 1.0 equiv), *N*-iodosuccinimide (**2**, 562 mg, 2.50 mmol, 1.0 equiv), 4-nitrobenzenesulfonamide (**3c**, 505 mg, 2.50 mmol, 1.0 equiv), DMC (25.0 mL, 0.25 M) and potassium acetate (24.5 mg, 0.250 mmol, 0.1 equiv) at room temperature (25 °C) with t_R = 10 min (f_R = 0.7 mL min^{-1}). The outlet of the photoflow reactor was directly connected to a omnifit column filled with K_2CO_3 (2.4 cm^{-3}, t_R = 3.4 min at f_R = 0.7 min), which was placed in a 60 °C water bath. After the crude reaction mixture passed the omnifit column, 2.5 mL was collected in 3 min 34 sec. The solvent was evaporated under reduced pressure, and product **5-Ts** was isolated by silica gel column chromatography using hexanes/ethylacetate (9:1 to 3:1) as eluent to obtain 64.8 mg (1.05 g h^{-1}, 0.213 mmol, 85%).

The analytical data are consistent with the literature.[33]

R_f (hexanes/ethylacetate 5:1 on silica) = 0.35

^{1}H NMR (300 MHz, $CDCl_3$) δ 8.40 – 8.36 (m, 2H), 8.21 – 8.18 (m, 2H), 7.33 – 7.31 (m, 3H), 7.23 – 7.20 (m, 2H), 3.91 (dd, J = 7.2, 4.6 Hz, 1H), 3.12 (d, J = 7.3 Hz, 1H), 2.51 (d, J = 4.6 Hz, 1H).

^{13}C NMR (75 MHz, $CDCl_3$) δ 150.81, 144.11, 134.28, 129.32, 128.9, 126.59, 124.49, 42.05, 36.71.

N-(2-hydroxy-2-phenylethyl)-*N*,4-dimethylbenzenesulfonamide **(6)**

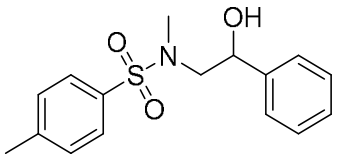

Following general procedure ***GP*** using styrene (**1a**, 286 µL, 260.4 mg, 2.50 mmol, 1.0 equiv), *N*-iodosuccinimide (**2**, 562 mg, 2.50 mmol, 1.0 equiv), *N*,4-dimethylbenzenesulfonamide (**3b**, 463 mg, 2.50 mmol, 1.0 equiv), DMC (25.0 mL, 0.25 M) and potassium acetate (24.5 mg, 0.250 mmol, 0.1 equiv) at room temperature (25 °C) with t_R = 10 min (f_R = 0.7 mL min^{-1}). A volume of 2.5 mL (= 0.250 mmol) was collected in 3 min 34 sec in a schlenk tube, diluted with 2.5 mL of water and heated to 100°C for 12 h. The reaction mixture was extracted three times with 3 mL EtOAc. The organic layer was collected, washed with brine, the solvent was evaporated under reduced pressure, and product **6** was isolated by silica gel column chromatography using hexanes/ethylacetate (9:1 to 3:1) as eluent to obtain 62.6 mg (205 mmol, 82%). The analytical data are consistent with the literature.[19]

R_f (hexanes/ethylacetate 5:1 on silica) = 0.2

^{1}H NMR (400 MHz, $CDCl_3$) δ 7.66 (d, J = 8.3 Hz, 2H), 7.39 – 7.29 (m, 7H), 4.92 (dd, J = 8.9, 3.4 Hz, 1H), 3.28 (dd, J = 14.2, 8.9 Hz, 1H), 3.02 (dd, J = 14.2, 3.4 Hz, 1H), 2.99 (br, 1H), 2.80 (s, 3H), 2.41 (s, 3H).

^{13}C NMR (101 MHz, $CDCl_3$) δ 143.81, 141.16, 134.32, 129.91, 128.67, 128.11, 127.53, 126.12, 72.24, 58.44, 36.90, 21.62

N,4-dimethyl-*N*-styrylbenzenesulfonamide **(7)**

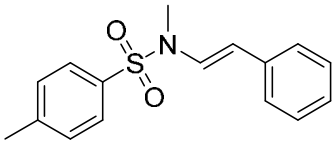

Following general procedure ***GP*** using styrene (**1a**, 286 µL, 260.4 mg, 2.50 mmol, 1.0 equiv), *N*-iodosuccinimide (**2**, 562 mg, 2.50 mmol, 1.0 equiv), *N*,4-dimethylbenzenesulfonamide (**3b**, 463 mg, 2.50 mmol, 1.0 equiv), DMC (25.0 mL, 0.25 M) and potassium acetate (24.5 mg, 0.250 mmol, 0.1 equiv) at room temperature (25 °C) with t_R = 10 min (f_R = 0.7 mL min^{-1}). A volume of 2.5 mL (= 0.250 mmol) was collected in 3 min 34 sec in a round bottom flask. After evaporating the solvent under reduced pressure, dissolving the residue in 2.5 mL DMF and adding NaOAc (205 mg, 2.50 mmol, 10 equiv in respect to the collected amount of substance), the resulting mixture was heated to 100°C for 8 h. The crude product was diluted with 5 mL and extracted five times with 5 mL EtOAc. The combined organic phase was washed with brine and the solvent was evaporated under reduced pressure. The product **7** was isolated by silica gel column chromatography using hexanes/ethylacetate (9:1 to 3:1) as eluent to obtain 64.7 mg (225 mmol, 90%). The analytical data are consistent with the literature.[19]

R_f (hexanes/ethylacetate 5:1 on silica) = 0.45

^{1}H NMR (300 MHz, $CDCl_3$) δ 7.61 – 7.57 (m, 2H), 7.44 (d, J = 14.4 Hz, 1H), 7.23 – 7.07 (m, 7H), 5.60 (d, J = 14.4 Hz, 1H), 2.92 (s, 3H), 2.33 (s, 3H).

^{13}C NMR (75 MHz, $CDCl_3$) δ 142.93, 135.26, 133.49, 128.83, 127.66, 127.13, 125.97, 125.42, 124.44, 109.80, 31.17, 20.52.

N-(2-azido-2-phenylethyl)-*N*,4-dimethylbenzenesulfonamide **(8)**

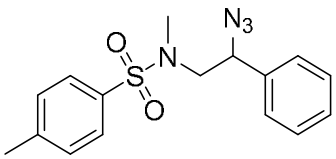

Following general procedure ***GP*** using styrene (**1a**, 286 µL, 260.4 mg, 2.50 mmol, 1.0 equiv), *N*-iodosuccinimide (**2**, 562 mg, 2.50 mmol, 1.0 equiv), *N*,4-dimethylbenzenesulfonamide (**3b**, 463 mg, 2.50 mmol, 1.0 equiv), DMC (25.0 mL, 0.25

M) and potassium acetate (24.5 mg, 0.250 mmol, 0.1 equiv) at room temperature (25 °C) with t_R = 10 min (f_R = 0.7 mL min^{-1}). A volume of 2.5 mL (= 0.250 mmol) was collected in 3 min 34 sec in a round bottom flask. After evaporating the solvent under reduced pressure, dissolving the residue in 2.5 mL DMF and adding NaN_3 (98 mg, 1.25 mmol, 5 equiv in respect to the collected amount of substance), the resulting mixture was stirred for 8h at 6.5 h. The crude product was diluted with 5 mL and extracted five times with 5 mL EtOAc. The combined organic phase was washed with brine and the solvent was evaporated under reduced pressure. The product **8** was isolated by silica gel column chromatography using hexanes/ethylacetate (9:1 to 3:1) as eluent to obtain 75.3 mg (0.228 mmol, 91%). The analytical data are consistent with the literature.[19]

R_f (hexanes/ethylacetate 3:1 on silica) = 0.5

^{1}H NMR (400 MHz, $CDCl_3$) δ 7.57 – 7.55 (m, 2H), 7.32 – 7.17 (m, 7H), 4.74 (dd, J = 8.3, 5.7 Hz, 1H), 3.17 – 3.07 (m, 2H), 2.68 (s, 3H), 2.32 (s, 3H).

^{13}C NMR (101 MHz, $CDCl_3$) δ 143.84, 136.79, 135.69, 134.93, 132.42, 130.49, 129.65, 127.62, 127.16, 126.34, 124.63, 116.99, 36.04, 21.58

4.5.3 NMR Spectra

N-(2-iodo-2-phenylethyl)-4-methylbenzenesulfonamide **(4a)**

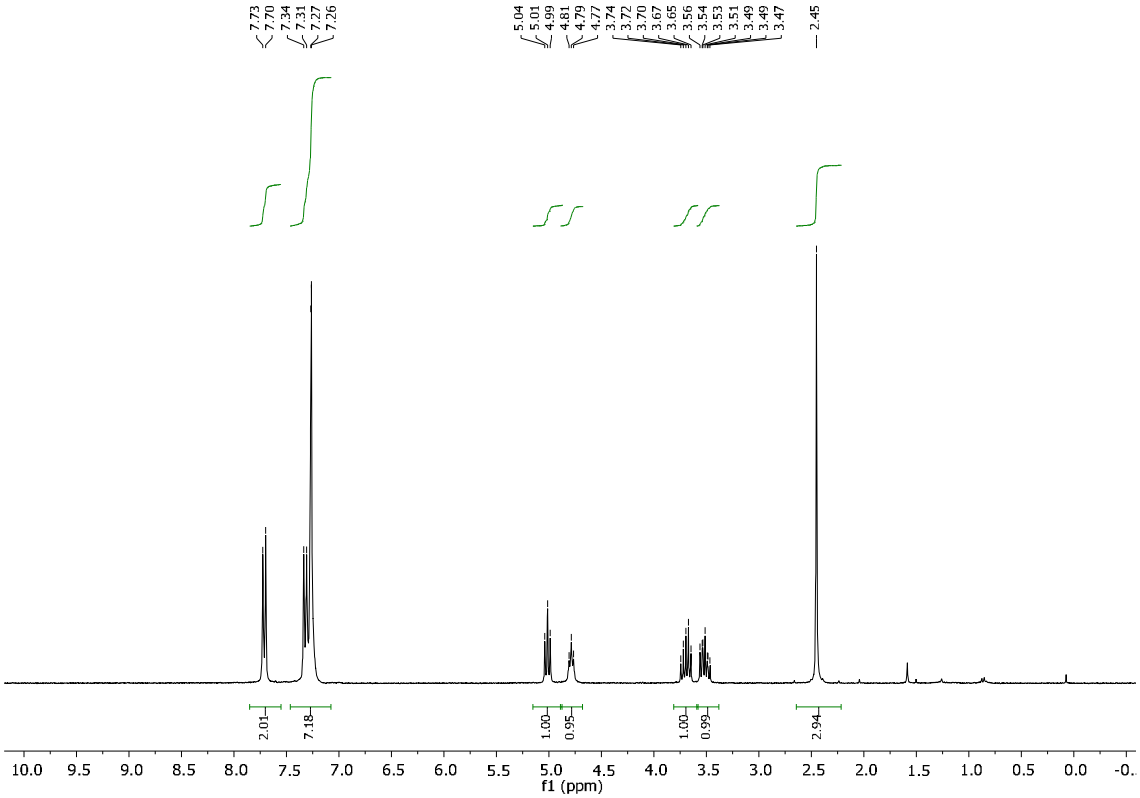

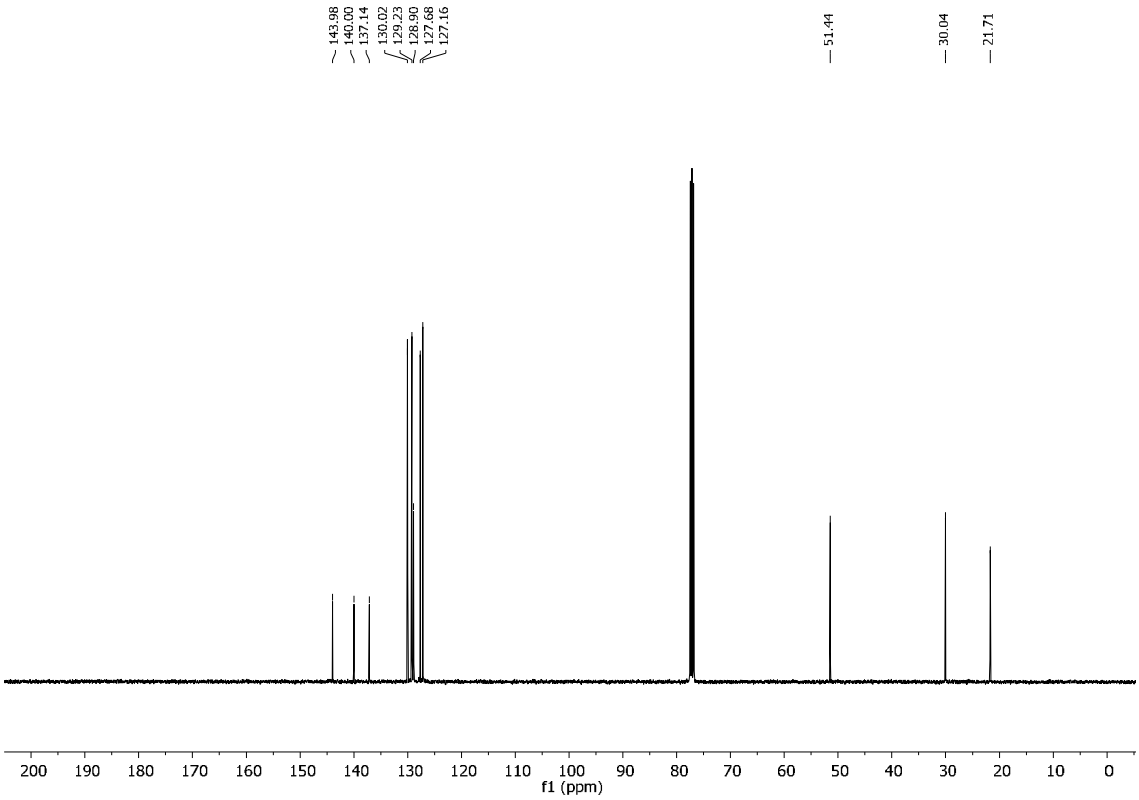

N-(2-iodo-2-phenylethyl)-*N*,4-dimethylbenzenesulfonamide **(4b)**

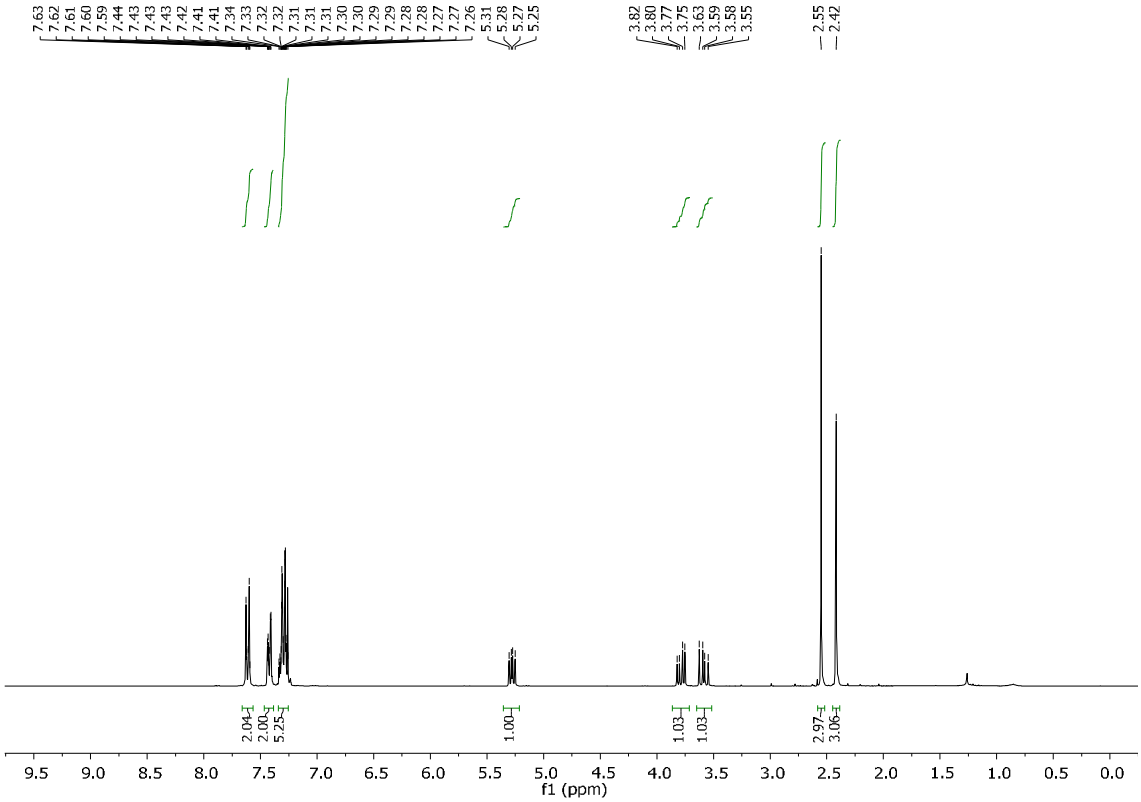

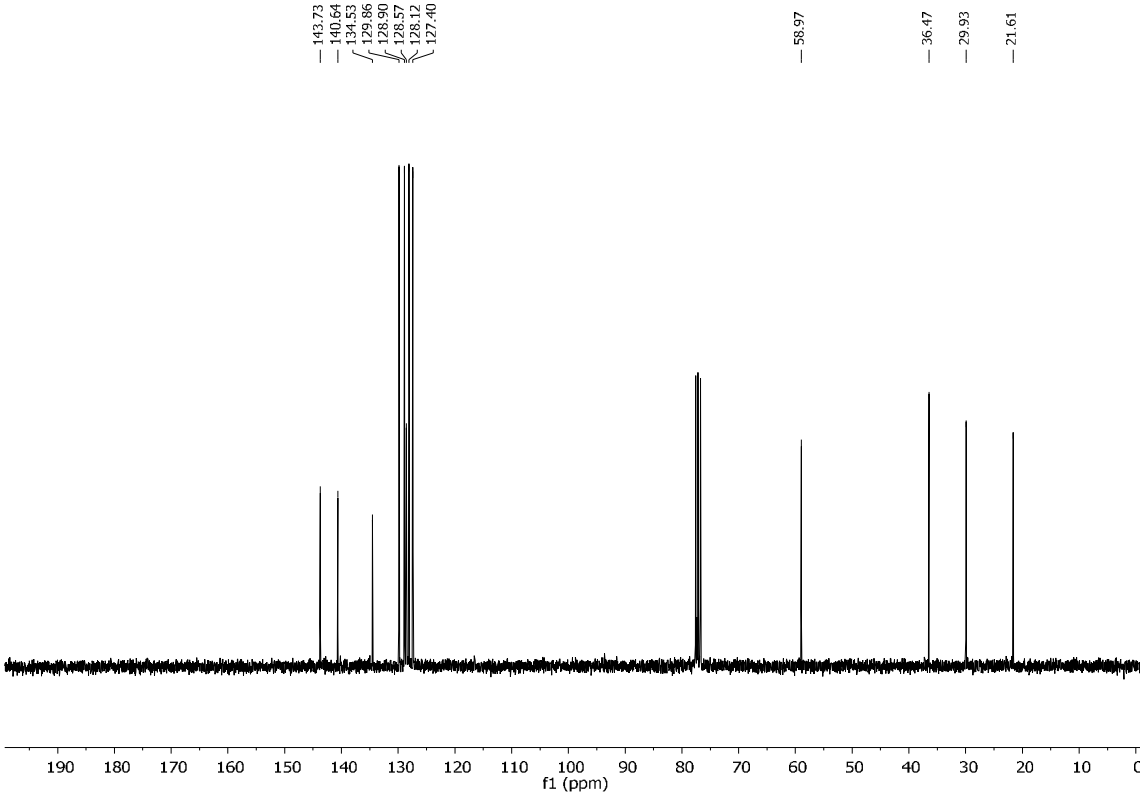

N-(2-iodo-2-phenylethyl)-4-nitrobenzenesulfonamide **(4c)**

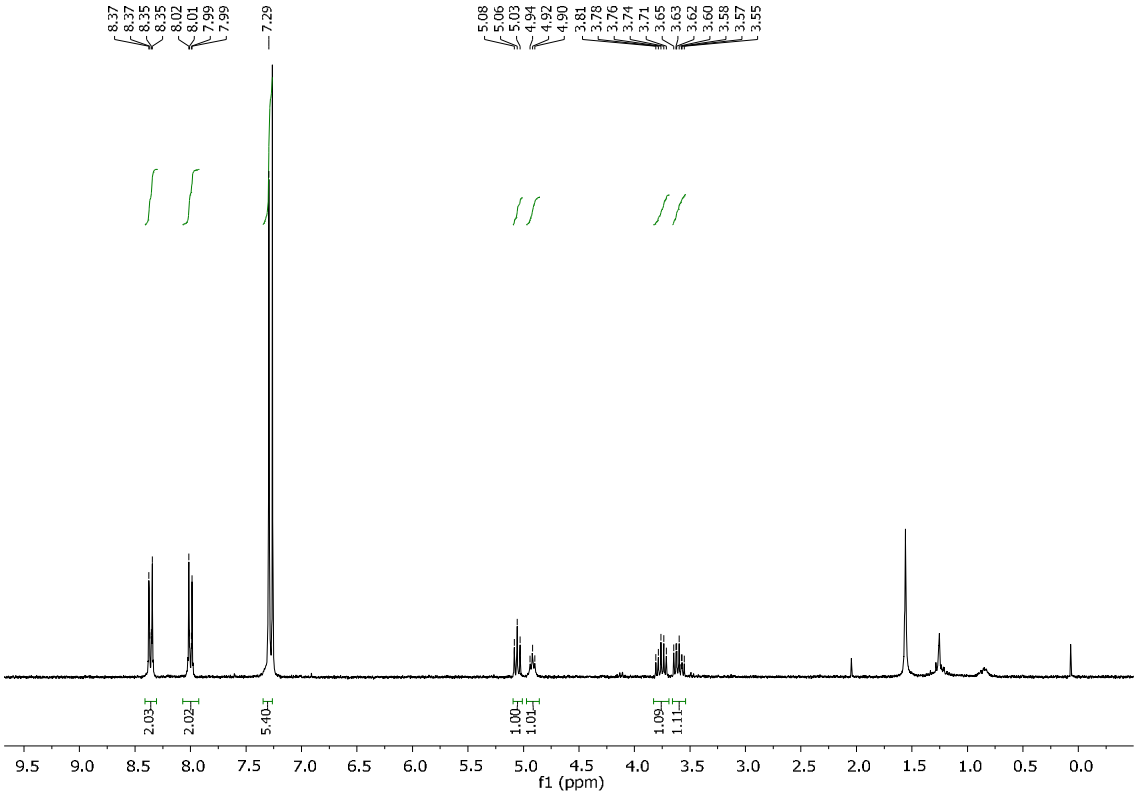

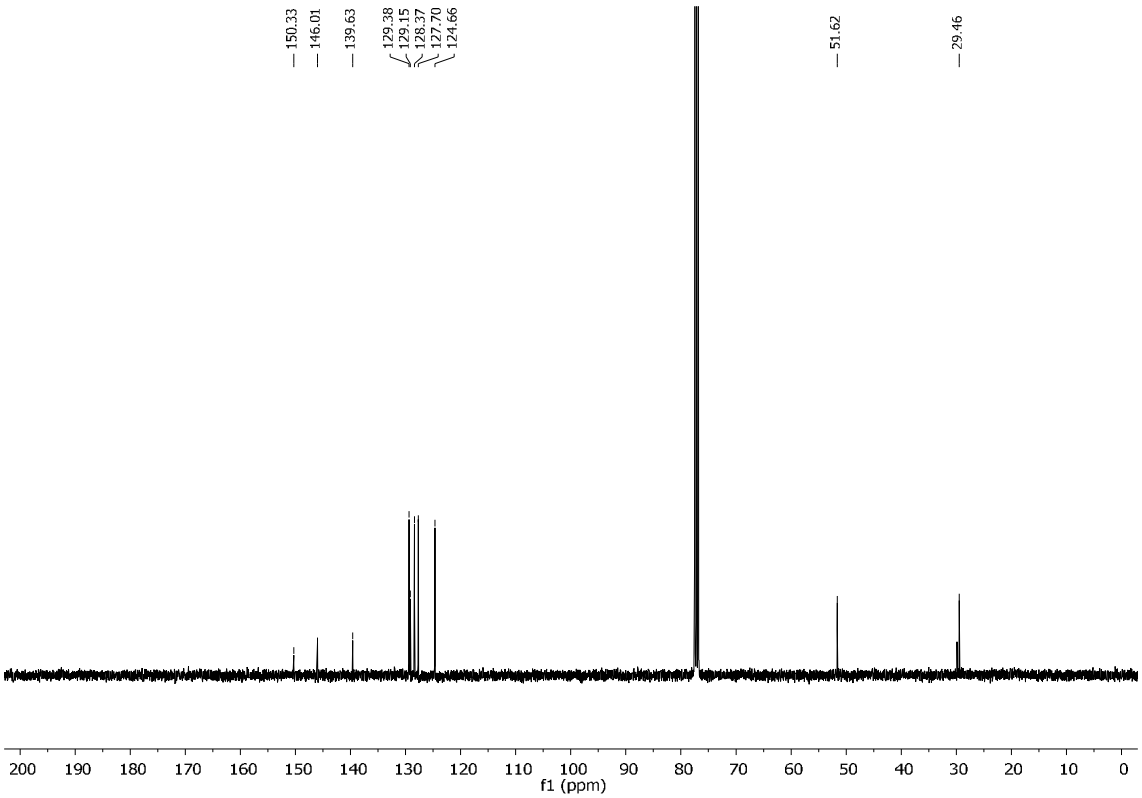

Methyl 4-(2-((*N*,4-dimethylphenyl)sulfonamido)-1-iodoethyl)benzoate **(4d)**

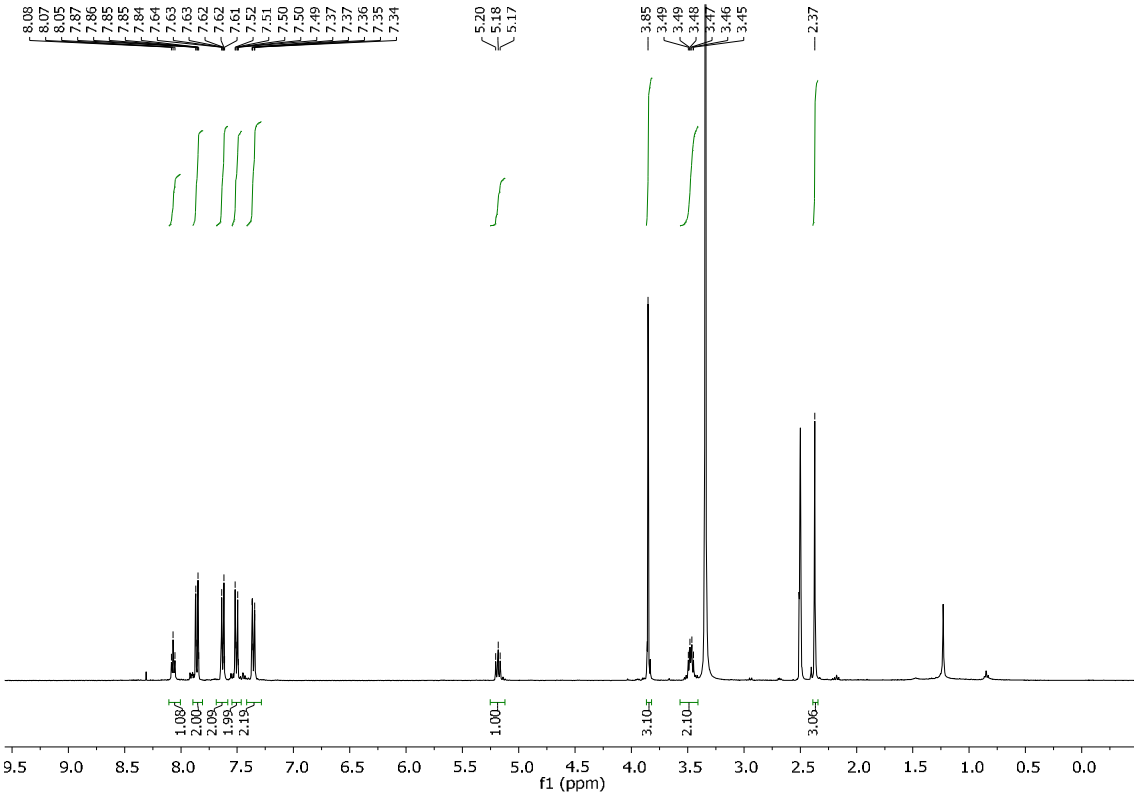

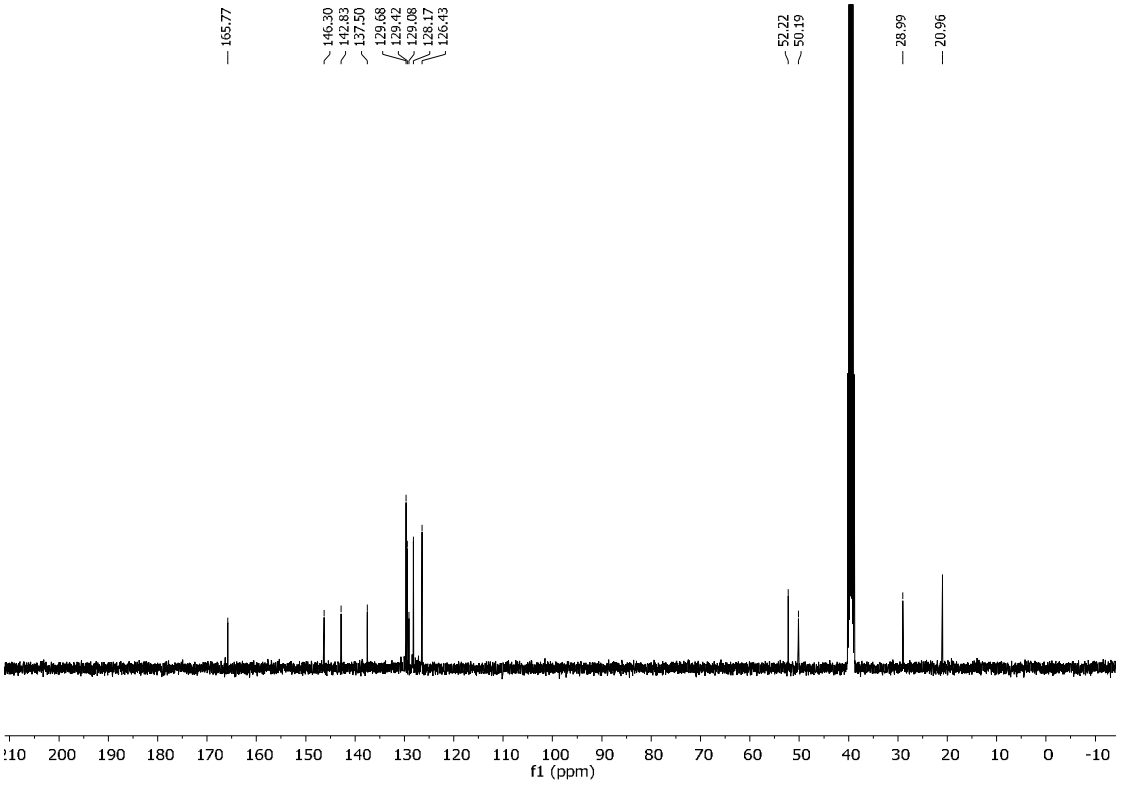

N-(2-(4-(tert-butyl)phenyl)-2-iodoethyl)-*N*,4-dimethylbenzenesulfonamide **(4e)**

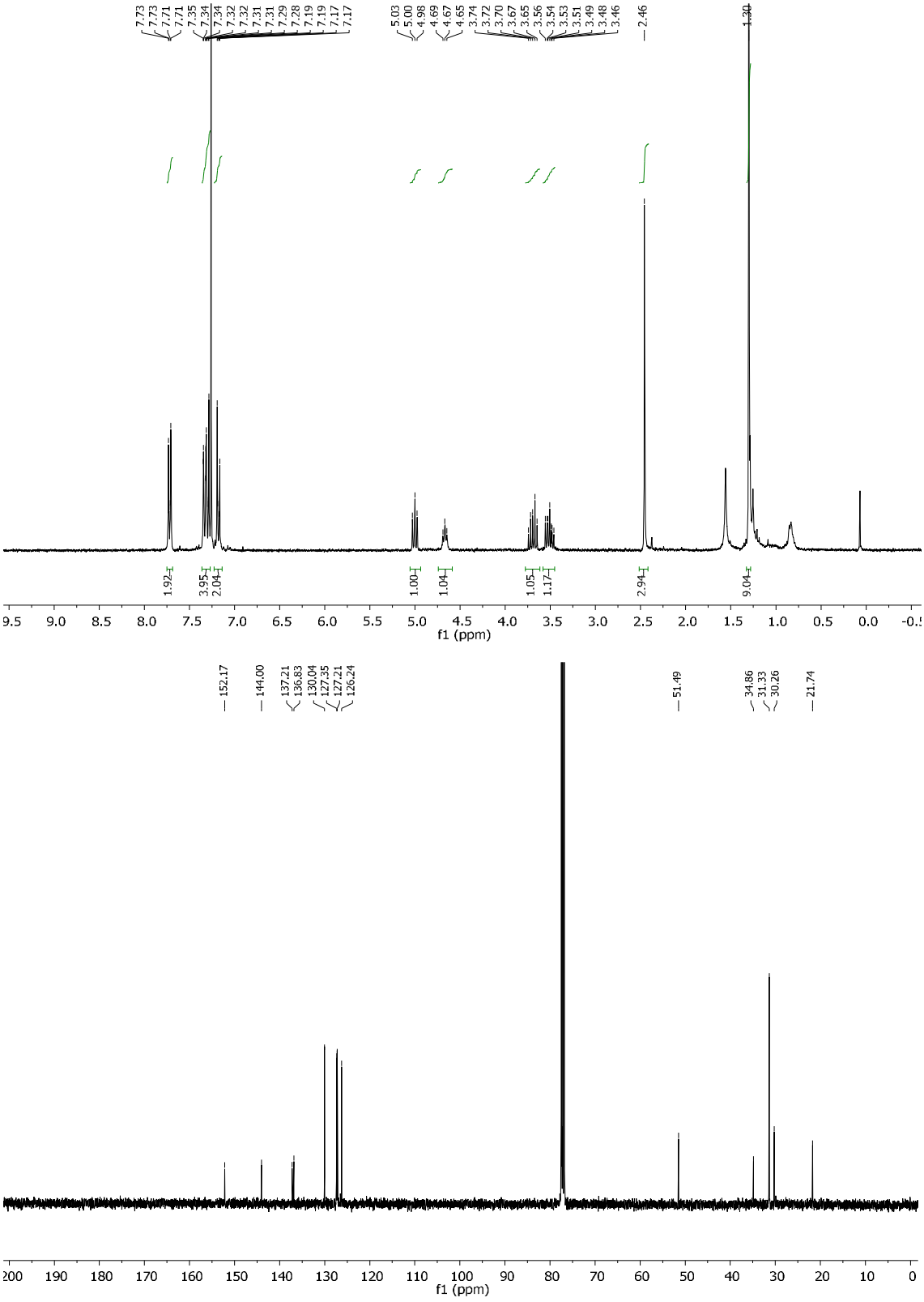

N-(2-iodooctyl)-*N*,4-dimethylbenzenesulfonamide **(4f)**

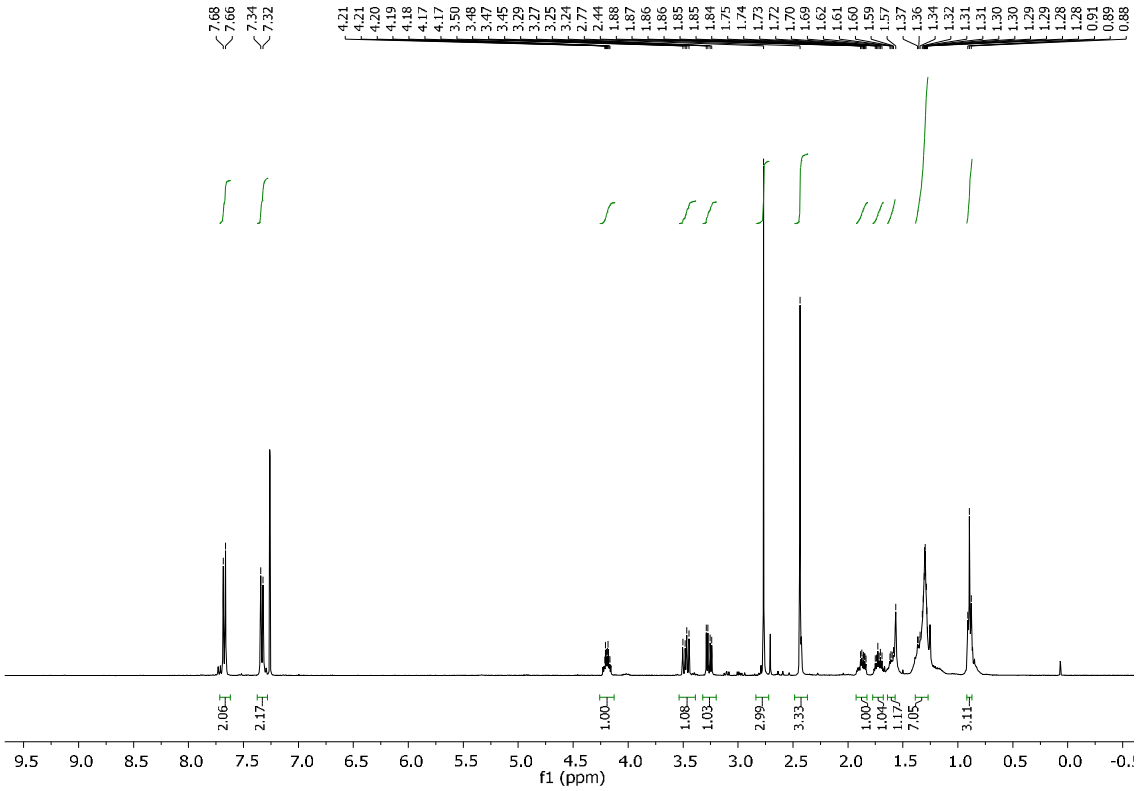

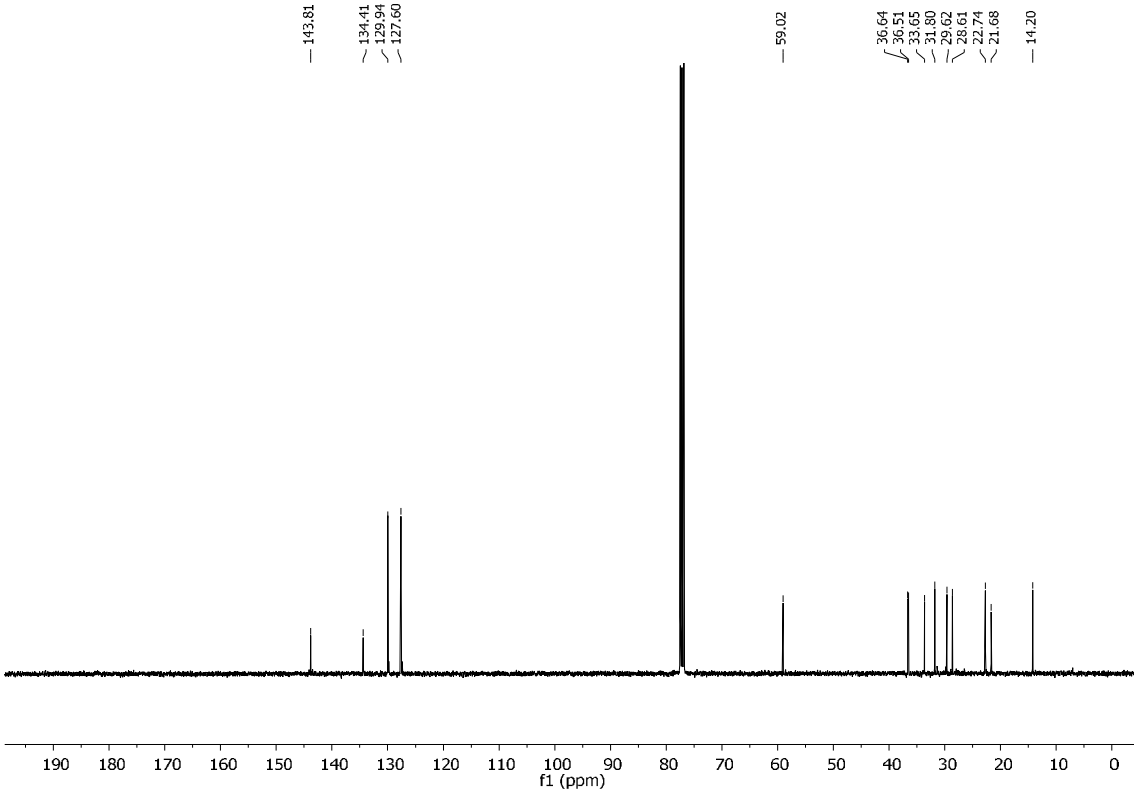

3-((*N*,4-dimethylphenyl)sulfonamido)-2-iodo-*N*-isopropylpropanamide **(4g)**

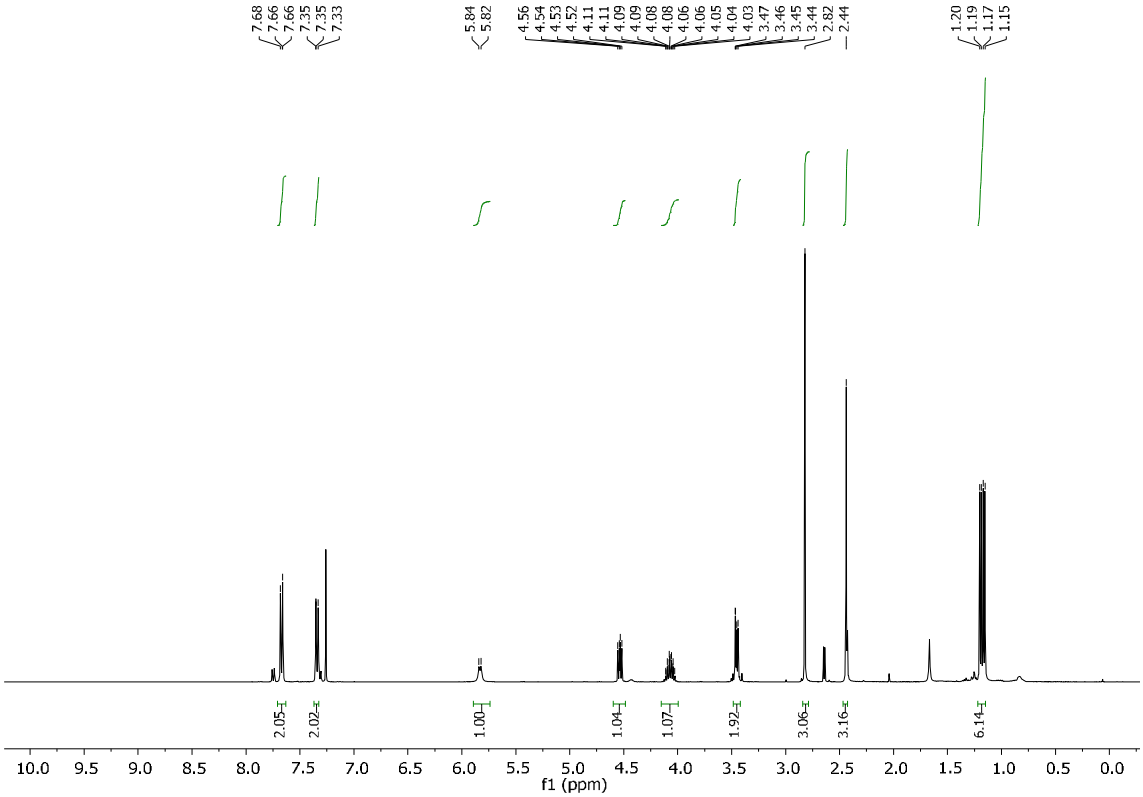

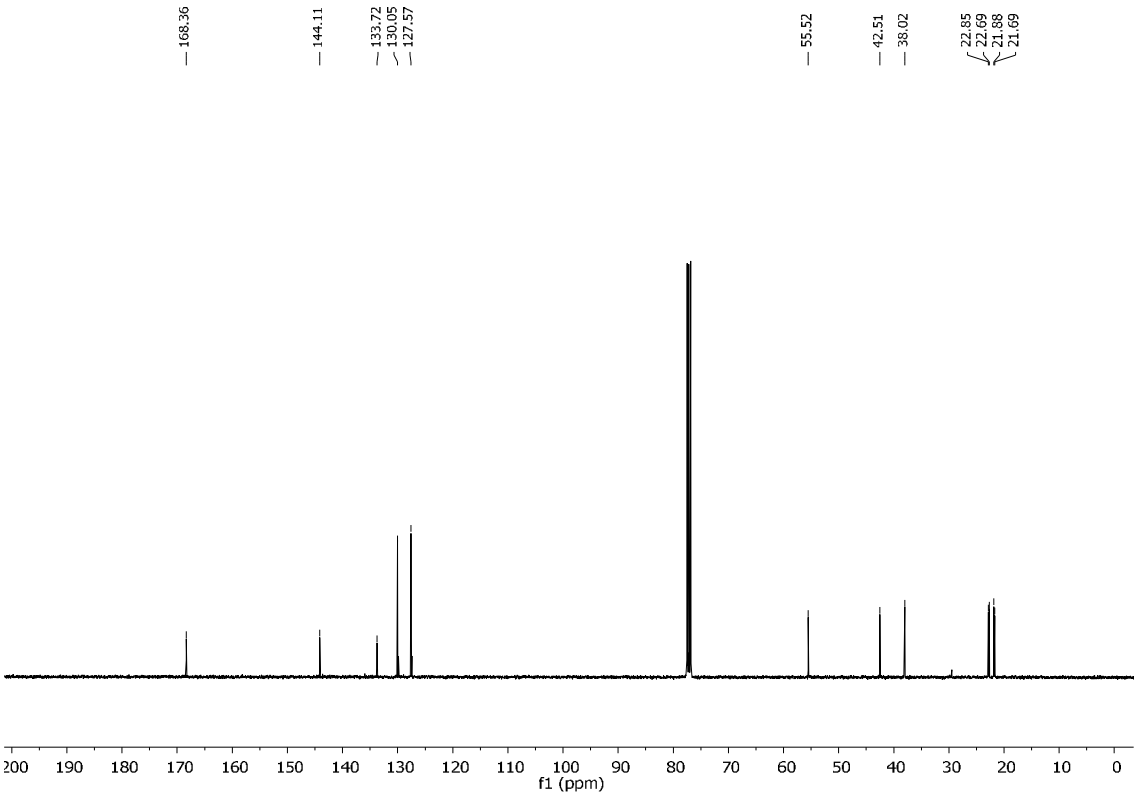

2-(iodomethyl)-1-tosylindoline **(4h)**

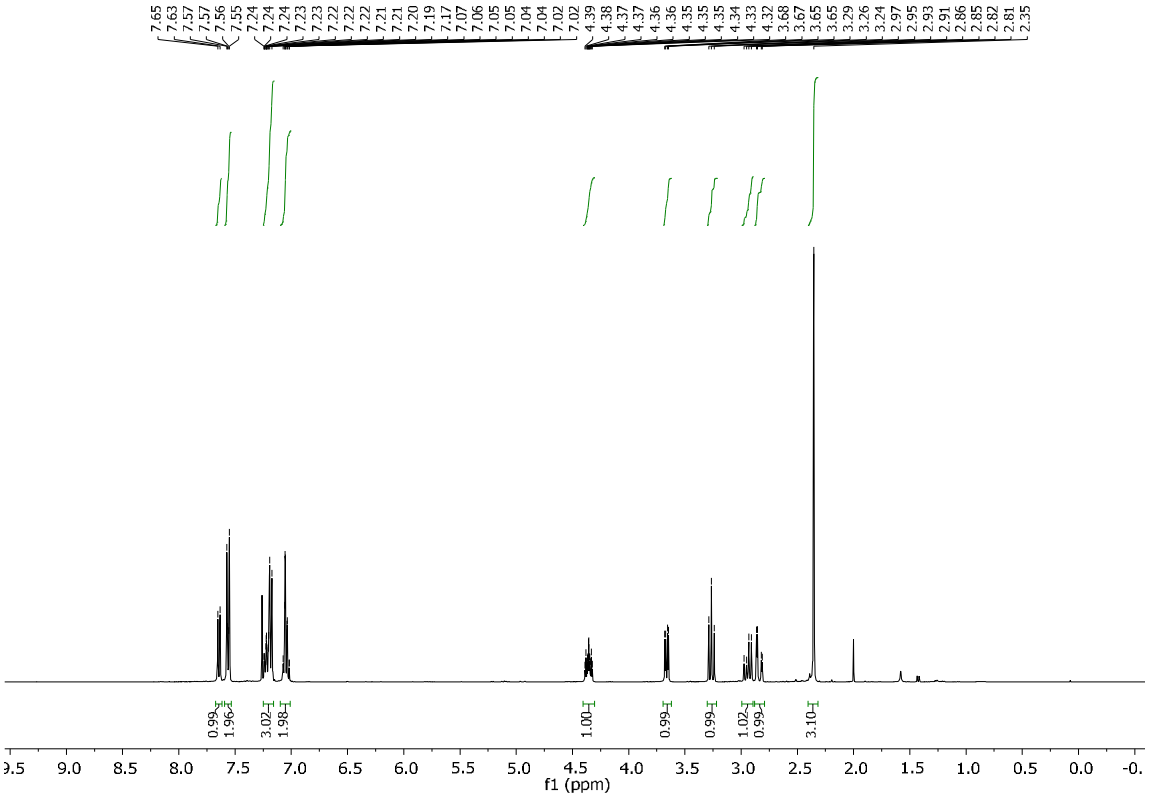

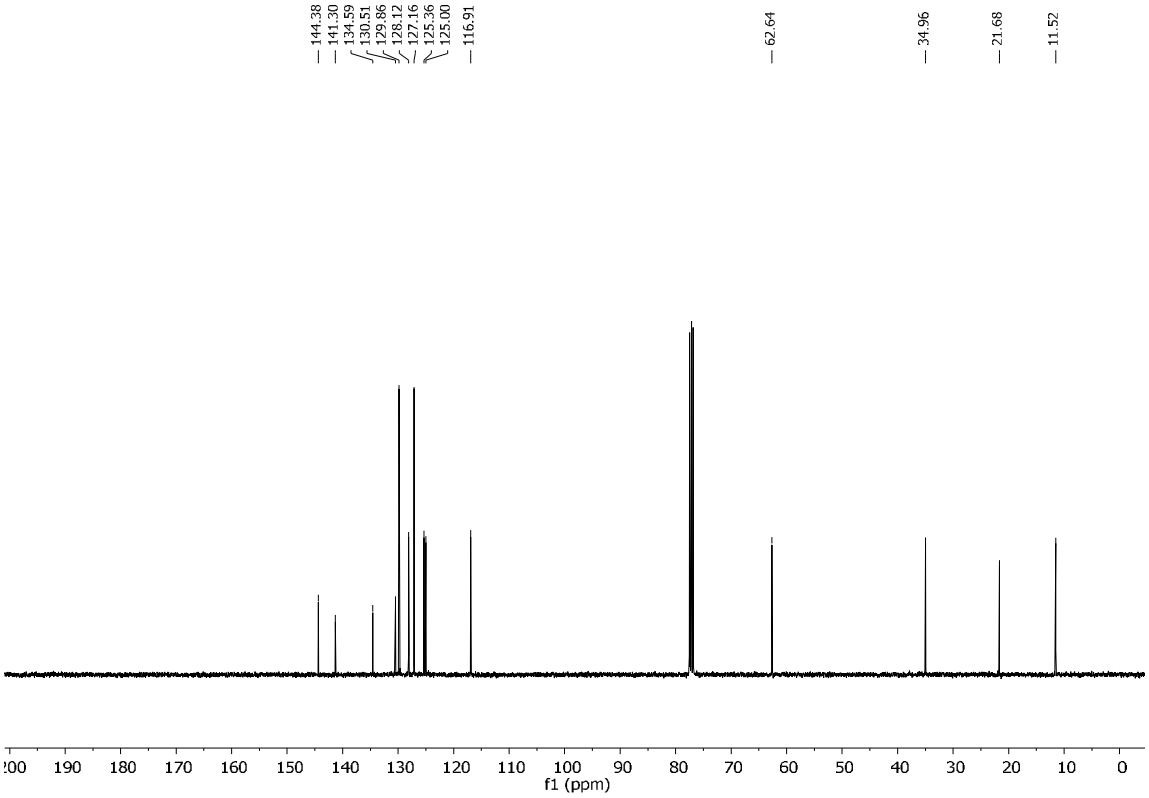

2-phenyl-1-tosylaziridine **(5-Ts)**

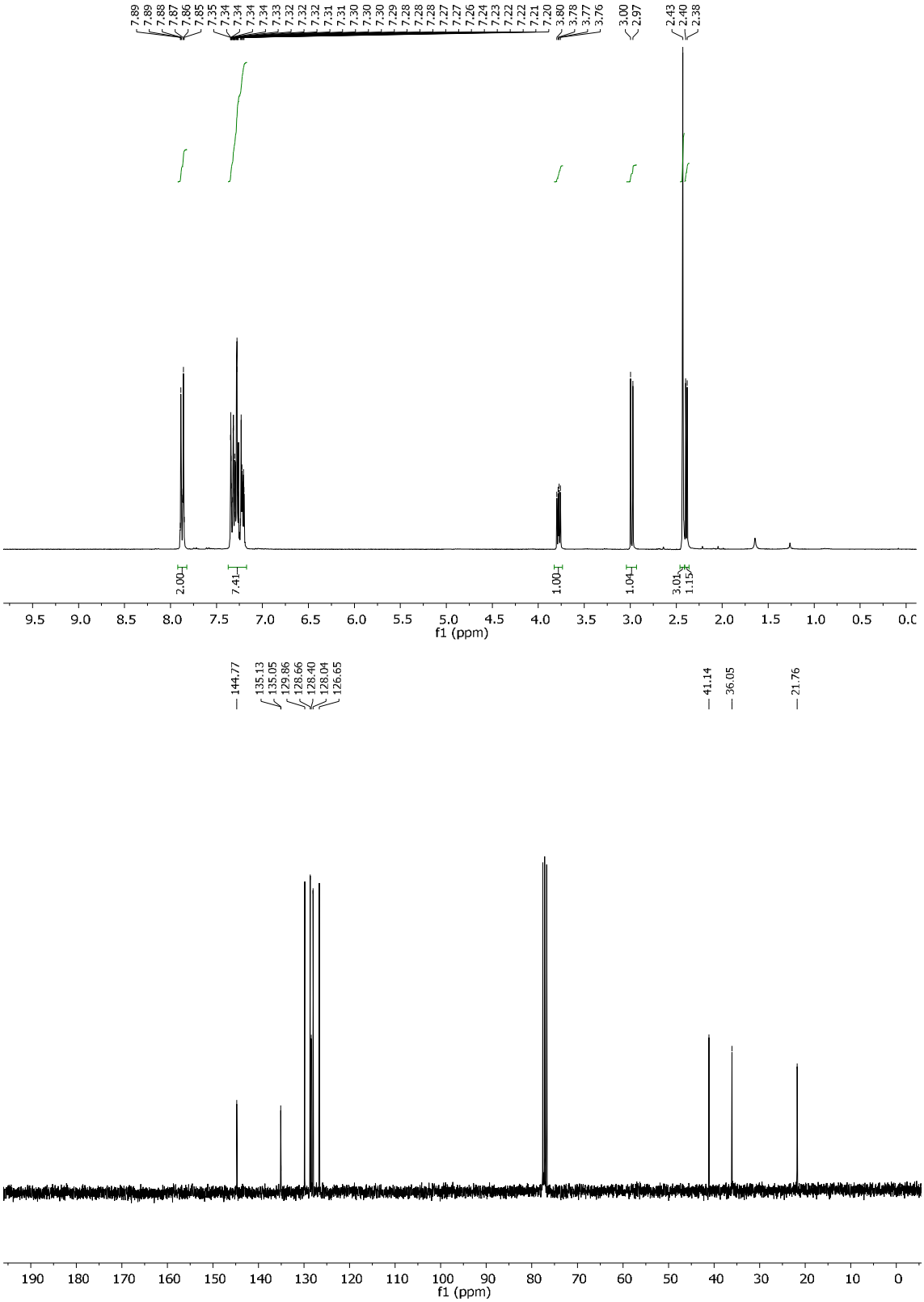

1-((4-nitrophenyl)sulfonyl)-2-phenylaziridine **(5-Ns)**

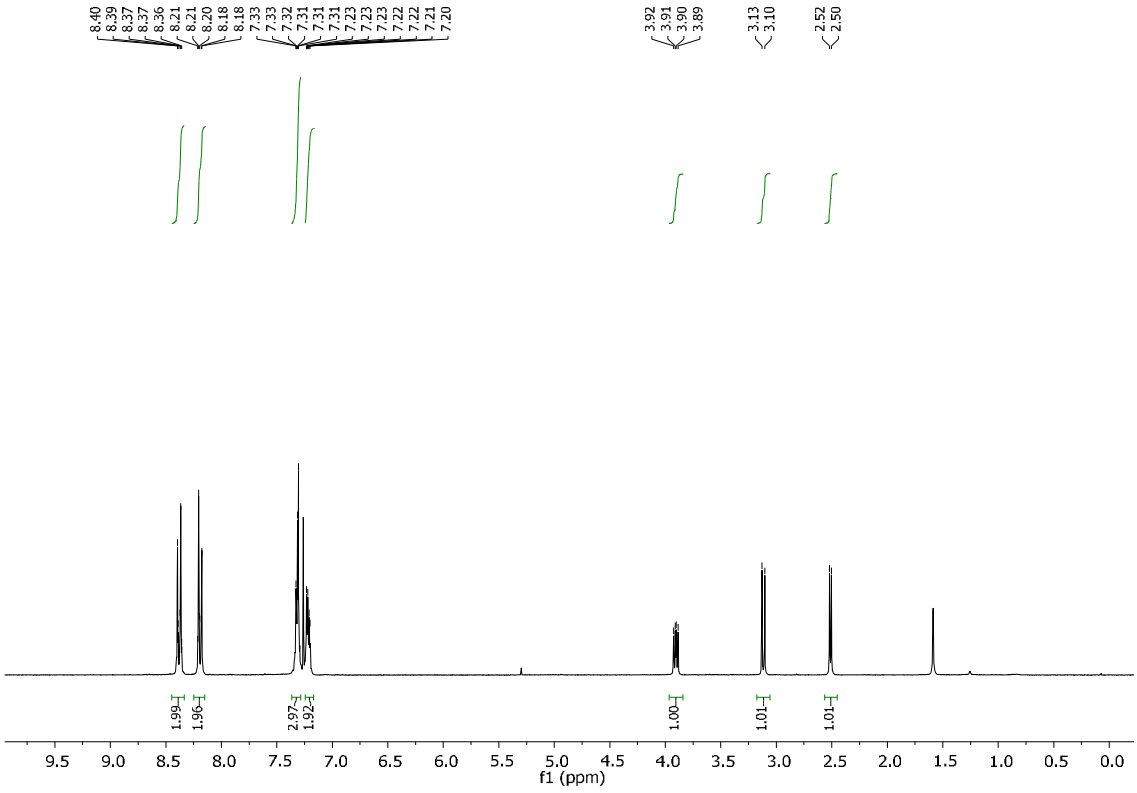

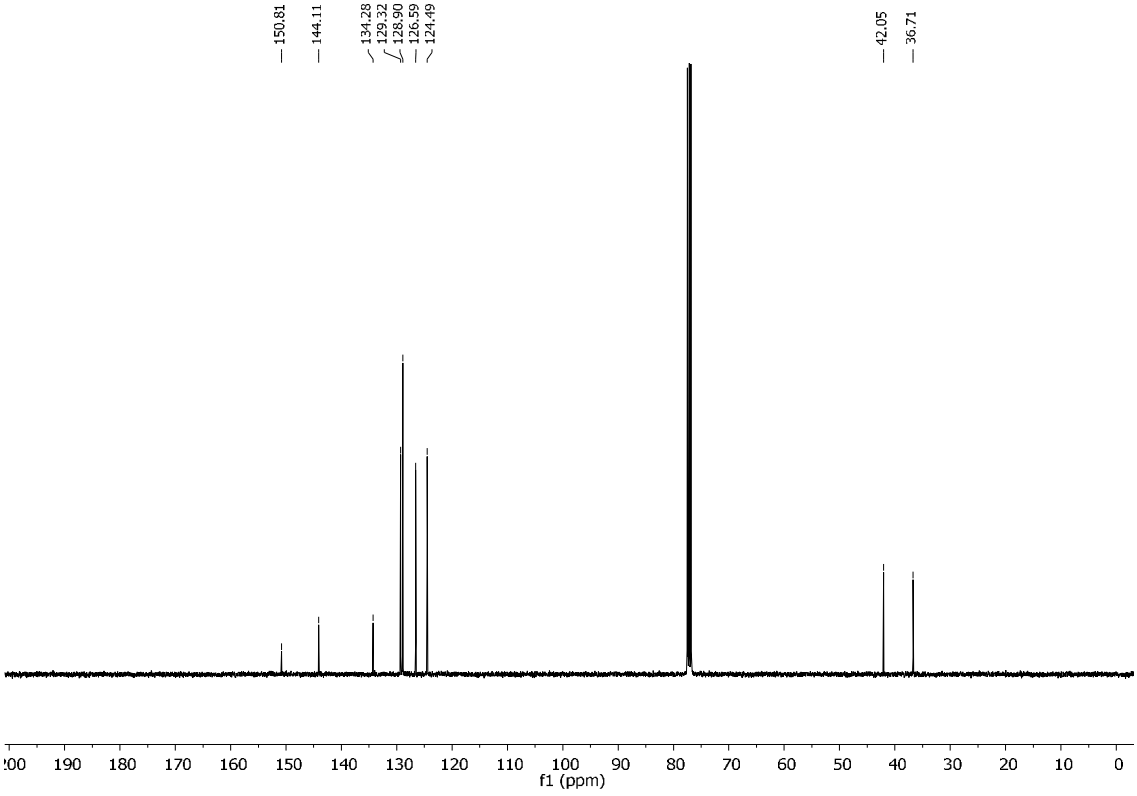

N-(2-hydroxy-2-phenylethyl)-*N*,4-dimethylbenzenesulfonamide **(6)**

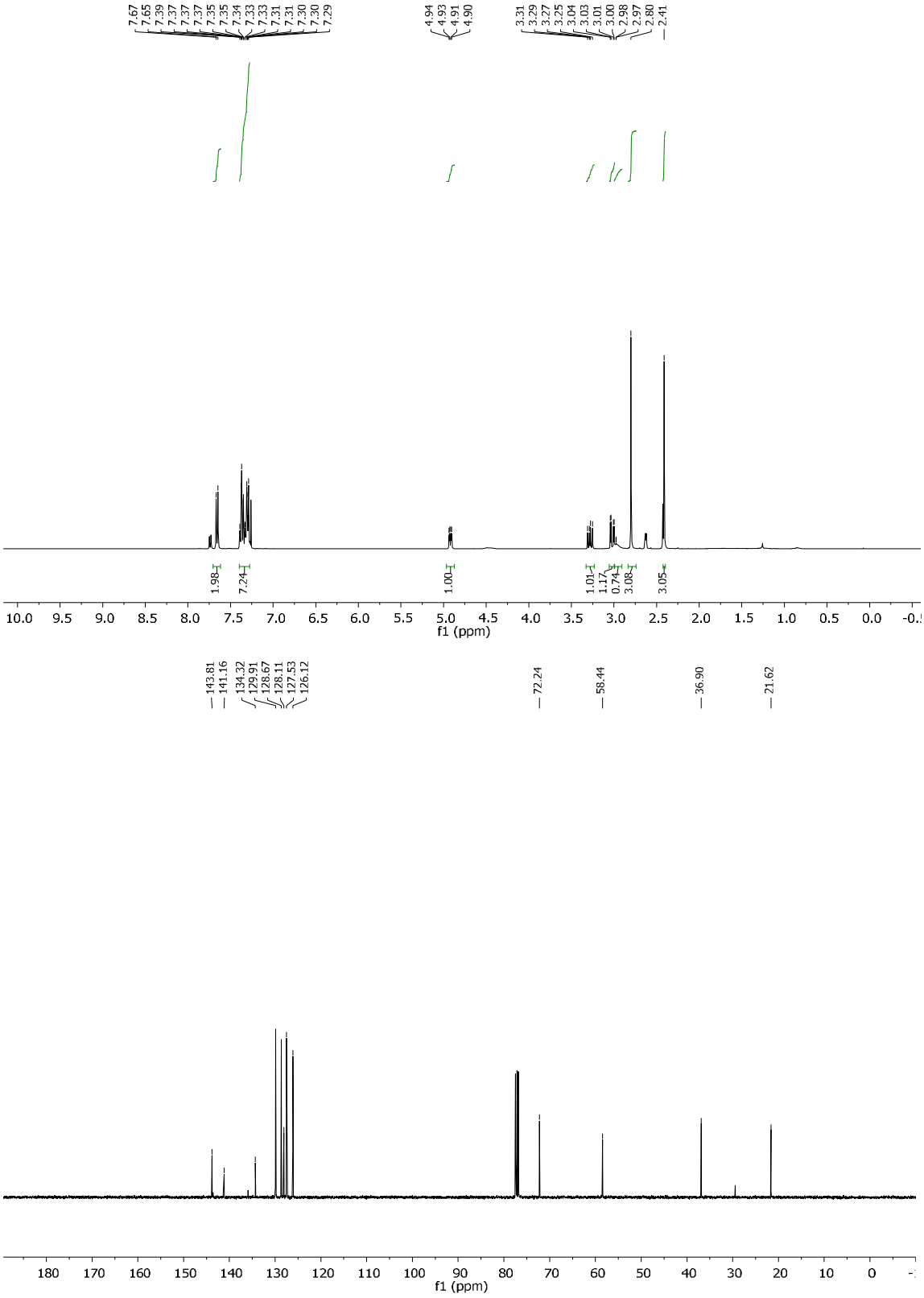

N,4-dimethyl-*N*-styrylbenzenesulfonamide **(7)**

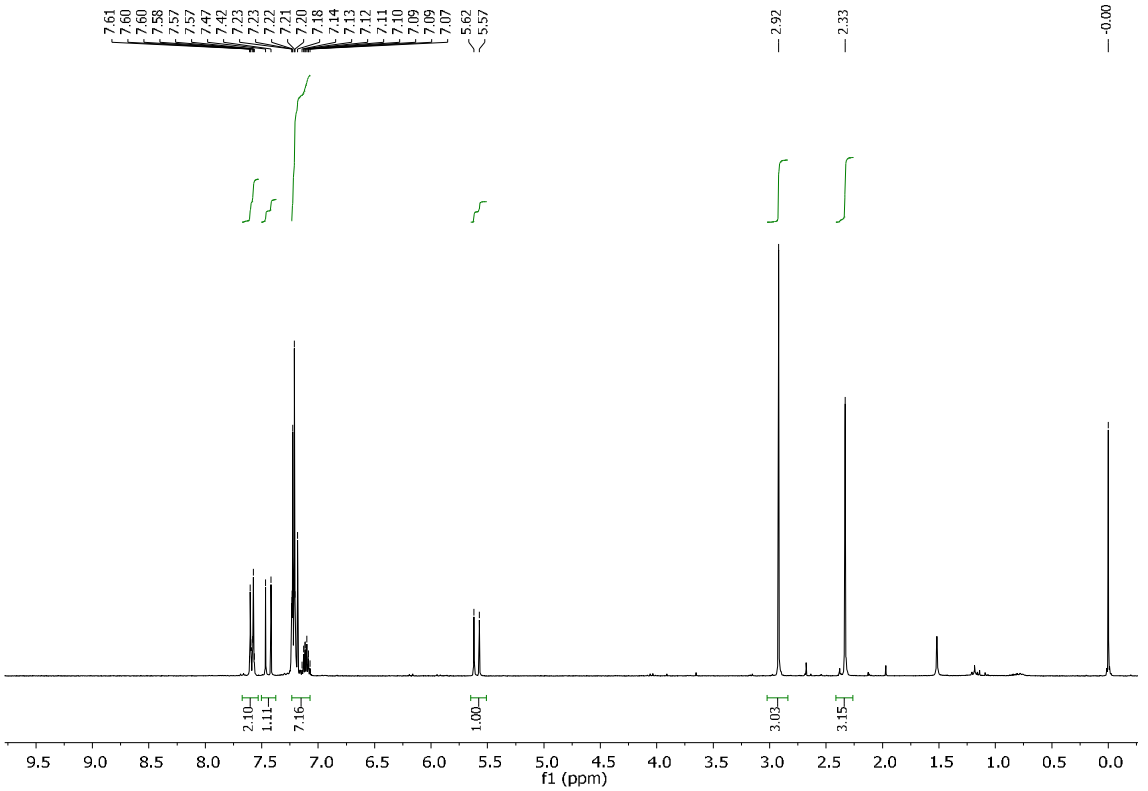

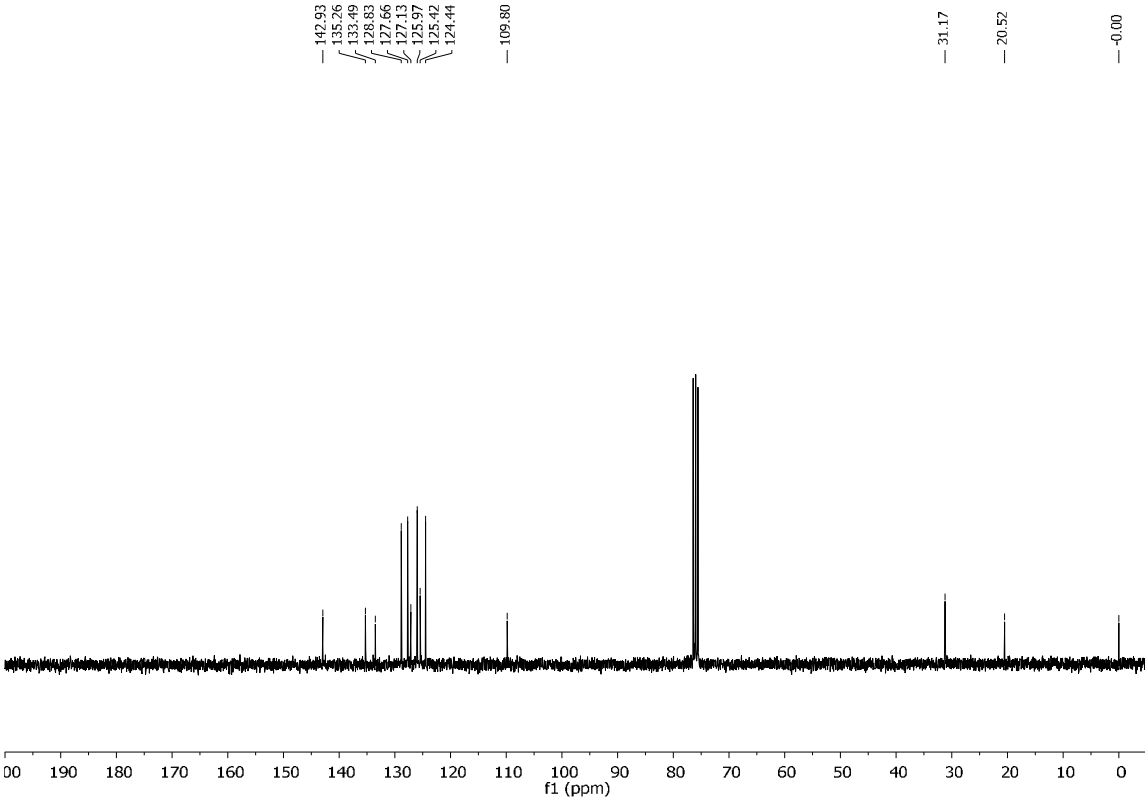

N-(2-azido-2-phenylethyl)-*N*,4-dimethylbenzenesulfonamide **(8)**

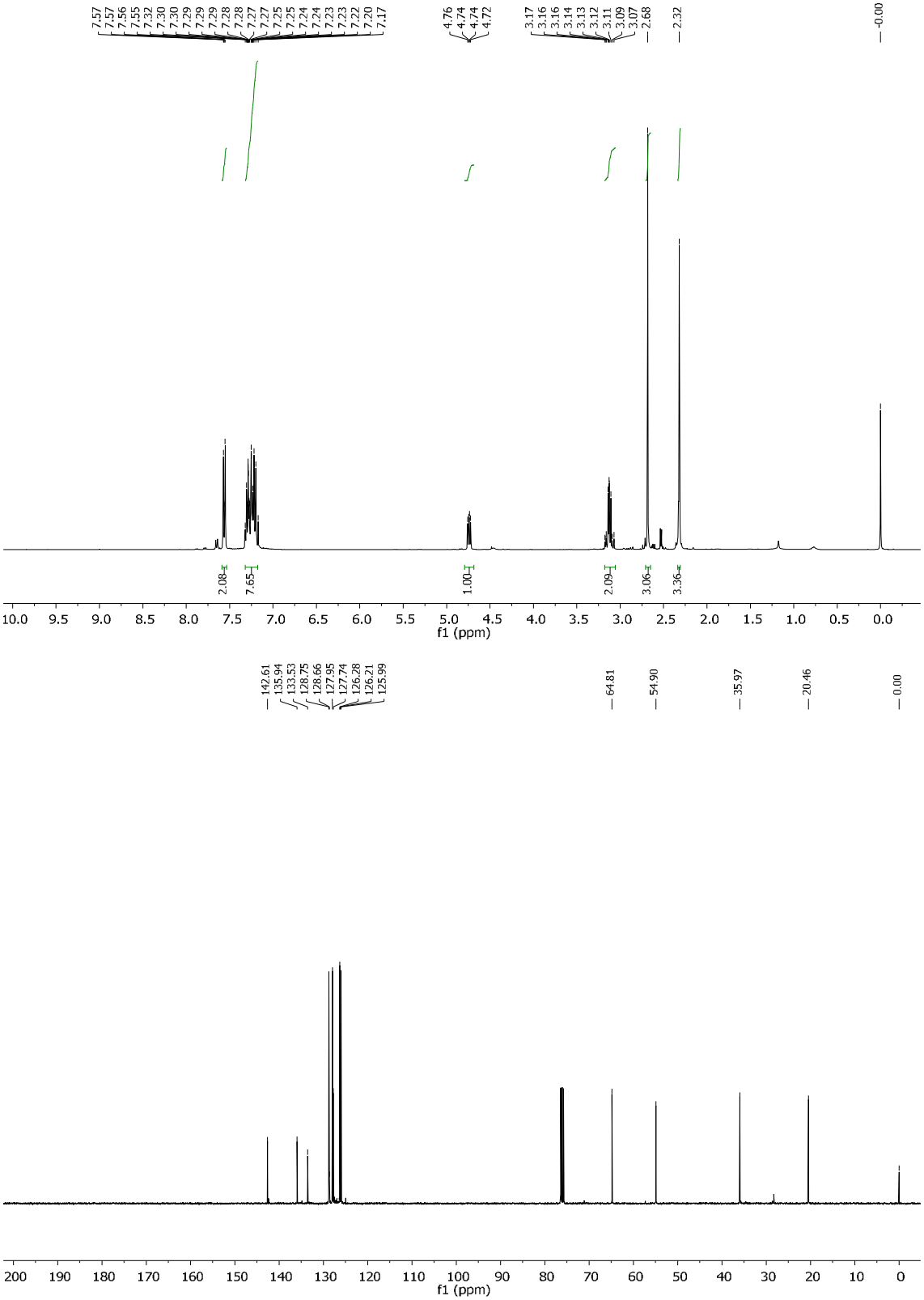

N-(2allylphenyl)-4-methylbenzenesulfonamide (**1f**)

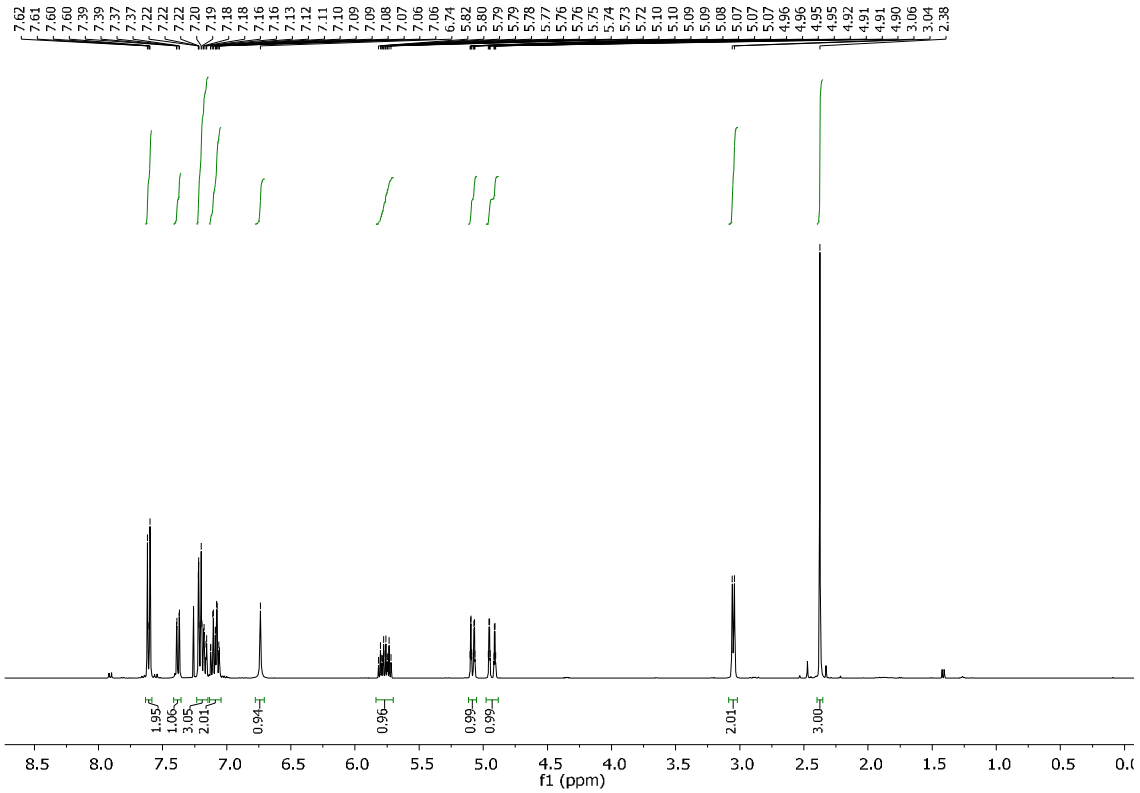

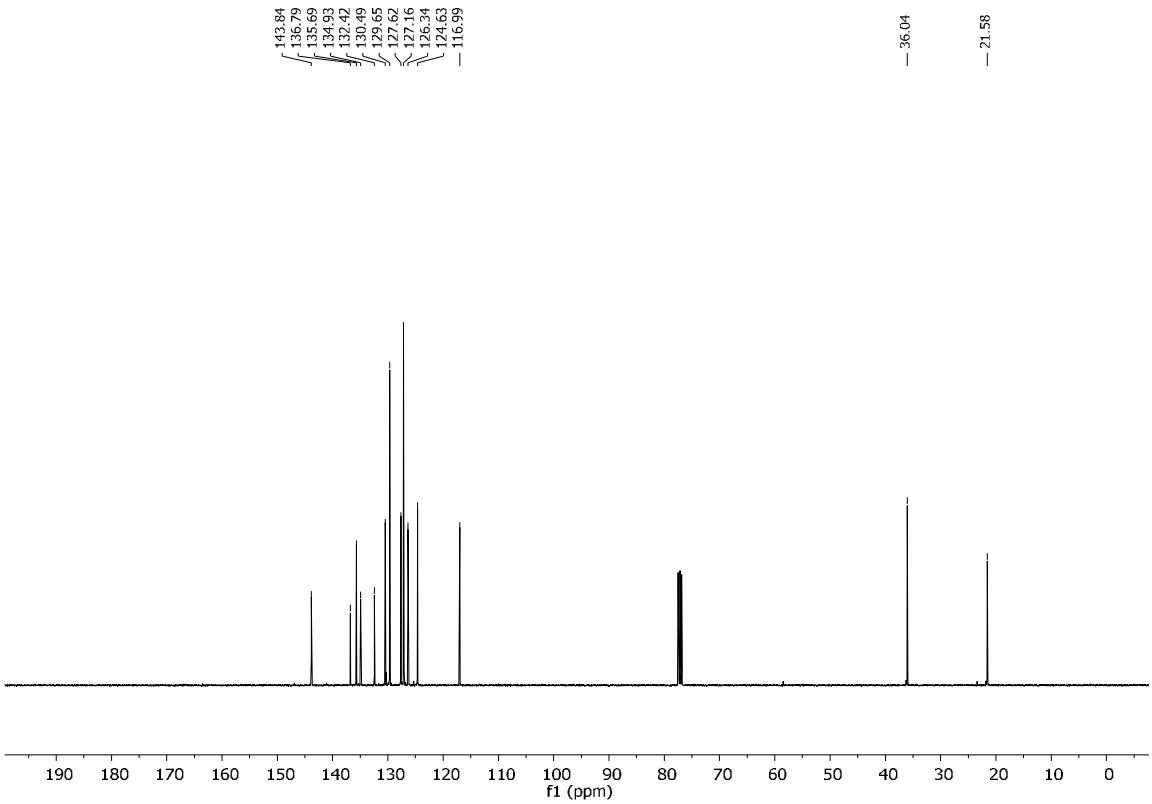

4.6 References

1 Z. Wu, M. Hu, J. Li, W. Wu and H. Jiang, *Org. Biomol. Chem.*, 2021, **19**, 3036–3054.

2 S. R. Chemler and M. T. Bovino, *ACS Catal.*, 2013, **3**, 1076–1091.

3 G. Li, H.-X. Wei and S. H. Kim, *Tetrahedron*, 2001, **57**, 8407–8411.

4 S. Minakata, Y. Yoneda, Y. Oderaotoshi and M. Komatsu, *Org. Lett.*, 2006, **8**, 967–969.

5 Q. Qin, D. Ren and S. Yu, *Org. Biomol. Chem.*, 2015, **13**, 10295–10298.

6 K. E. Jolley, M. R. Chapman and A. J. Blacker, *Beilstein J. Org. Chem.*, 2018, **14**, 2220–2228.

7 C. Martínez and K. Muñiz, *Adv. Synth. Catal.*, 2014, **356**, 205–211.

8 E. Falk, S. Makai, T. Delcaillau, L. Gürtler and B. Morandi, *Angew. Chem. Int. Ed.*, 2020, **59**, 21064–21071.

9 Y. Li, Y. Liang, J. Dong, Y. Deng, C. Zhao, Z. Su, W. Guan, X. Bi, Q. Liu and J. Fu, *J. Am. Chem. Soc.*, 2019, **141**, 18475–18485.

10 L. Legnani, G. Prina-Cerai, T. Delcaillau, S. Willems and B. Morandi, *Science*, 2018, **362**, 434–439.

11 A. Śliwińska and A. Zwierzak, *Tetrahedron Lett.*, 2003, **44**, 9323–9325.

12 G. Zhang, G. An, J. Zheng, Y. Pan and G. Li, *Tetrahedron Lett.*, 2010, **51**, 987–989.

13 T. M. Shaikh, P. U. Karabal, G. Suryavanshi and A. Sudalai, *Tetrahedron Lett.*, 2009, **50**, 2815–2817.

14 V. V. Thakur, S. K. Talluri and A. Sudalai, *Org. Lett.*, 2003, **5**, 861–864.

15 S. Giofrè, R. Sala, E. M. Beccalli, L. L. Presti and G. Broggini, *Helv. Chim. Acta*, 2019, **102**, e1900088.

16 P. Mizar, A. Burrelli, E. Günther, M. Söftje, U. Farooq and T. Wirth, *Chem. Eur. J.*, 2014, **20**, 13113–13116.

17 H. Sun, B. Cui, G.-Q. Liu and Y.-M. Li, *Tetrahedron*, 2016, **72**, 7170–7178.

18 T. J. Struble, H. M. Lankswert, M. Pink and J. N. Johnston, *ACS Catal.*, 2018, **8**, 11926–11931.

19 S. Engl and O. Reiser, *Org. Lett.*, 2021, **23**, 5581–5586.

20 V. Klöpfer, R. Eckl, J. Floß, P. M. C. Roth, O. Reiser and J. P. Barham, *Green Chem.*, 2021, **23**, 6366–6372.

21 A. Steiner, O. De Frutos, J. A. Rincón, C. Mateos, J. D. Williams and C. O. Kappe, *React. Chem. Eng.*, 2021, **6**, 2434–2441.

22 F. Schäfer, L. Lückemeier and F. Glorius, *Chem. Sci.*, 2024, **15**, 14548–14555.

23 L. D. Elliott, J. P. Knowles, P. J. Koovits, K. G. Maskill, M. J. Ralph, G. Lejeune, L. J. Edwards, R. I. Robinson, I. R. Clemens, B. Cox, D. D. Pascoe, G. Koch, M. Eberle, M. B. Berry and K. I. Booker-Milburn, *Chem. Eur. J.*, 2014, **20**, 15226–15232.

24 L. Buglioni, F. Raymenants, A. Slattery, S. D. A. Zondag and T. Noël, *Chem. Rev.*, 2022, **122**, 2752–2906.

25 T. H. Rehm, *Chem. Eur. J.*, 2020, **26**, 16952–16974.

26 L. Candish, K. D. Collins, G. C. Cook, J. J. Douglas, A. Gómez-Suárez, A. Jolit and S. Keess, *Chem. Rev.*, 2022, **122**, 2907–2980.

27 T. Rawner, E. Lutsker, C. A. Kaiser and O. Reiser, *ACS Catal.*, 2018, **8**, 3950–3956.

28 G. Filippini, M. Silvi and P. Melchiorre, *Angew. Chem. Int. Ed.*, 2017, **56**, 4447–4451.

29 M. K. Ghorai, A. Bhattacharyya, S. Das and N. Chauhan, in *Synthesis of 4- to 7-membered Heterocycles by Ring Expansion*, eds. M. D'hooghe and H.-J. Ha, Springer International Publishing, Cham, 2015, vol. 41, pp. 49–142.

30 W. L. F. Armarego, *Purification of laboratory chemicals*, Butterworth-Heinemann, Kidlington, Oxford, 8th ed., 2017.

31 H. Yamamoto, E. Ho, K. Namba, H. Imagawa and M. Nishizawa, *Chem. Eur. J.*, 2010, **16**, 11271–11274.

32 G.-Q. Liu and Y.-M. Li, *J. Org. Chem.*, 2014, **79**, 10094–10109.

33 N. Hsueh, G. J. Clarkson and M. Shipman, *Org. Lett.*, 2015, **17**, 3632–3635.

Curriculum Vitae

Personal Data

Name	Viktor Klöpfer
Date of birth	05.12.1995
Place of birth	Chromtau, Kazakhstan
Nationality	German

Education

06/2021 – 03/2025	**PhD**, Institute of Organic Chemistry, University of Regensburg, Prof. Dr. Oliver Reiser. *"Sustainable Photochemical Approaches: Dual Iron-Photocatalysis and Transformations under Continuous Photo-Flow Conditions"*
11/2023 – 12/2023	**Research Stay**, Institute of Organic Chemistry, Indian Institute of Technology, Prof. Dr. Debayan Sarkar
10/2019 – 04-2021	**Master of Science – Applied Chemistry**, Technische Hochschule Nürnberg Georg-Simon Ohm
10/2015 – 05/2019	**Bachelor of Science – Applied Chemistry**, Technische Hochschule Nürnberg Georg-Simon Ohm
09/2006 – 06/2014	**Allgemeine Hochschulreife (A-level)**, Martin-Behaim-Gymnasium, Nürnberg

Conferences & Presentations

06/2023	**23rd Tetrahedron Symposium**, Gothenburg, Sweden

Publications

V. Klöpfer, A. Chinchole, O. Reiser, *Tetrahedron Chem.* 2024, **10**, 100073–100077.

V. Klöpfer, R. Eckl, J. Floß, P. M. C. Roth, O. Reiser, J. P. Barham, *Green Chem* 2021, **23**, 6366–6372.

V. Klöpfer, L. Roithmeier, M. Kobras, P. Kreitmeier, O. Reiser, *Org. Process Res. Dev.* 2025, **29**, 755-759.

Declaration

Herewith I declare that this present thesis is a presentation of my original work prepared single-handed. Wherever contributions from others are involved, all of them are marked, clearly, with reference to the literature, license, and acknowledgment of collaborative research.

Regensburg, January 2026

_____

Viktor Klöpfer